MEASURING AND MODELING RAINFALL WITH TERRESTRIAL SENSORS AND RADAR: IMPLICATIONS FOR RAINFALL HETEROGENEITY AND DISCHARGE

A Dissertation

presented to

the Faculty of the Graduate School

at the University of Missouri

In Partial Fulfillment

of the Requirements for the Degree

Doctor of Philosophy

---

by

MICHEAL JOSEPH SIMPSON

Dr. Neil Fox, Dissertation Supervisor

DECEMBER 2017

The undersigned, appointed by the dean of the Graduate School, have examined the dissertation entitled

MEASURING AND MODELING RAINFALL WITH TERRESTRIAL SENSORS AND RADAR: IMPLICATIONS FOR RAINFALL HETEROGENEITY AND DISCHARGE

presented by Micheal Simpson,

a candidate for the degree of doctorate of philosophy,

and hereby certify that, in their opinion, it is worthy of acceptance.

Professor Neil Fox

Professor Patrick Market

Professor Rebecca North

Professor Kathleen Trauth

This dissertation would not have been possible without the love and support of my family. The countless hours spent on developing this material is a direct result of their continued support.

ACKNOWLEDGEMENTS

Thanks are due to my advisors throughout my academic career: Dr. Scott Rochette, Dr. Patrick Market, Dr. Jason Hubbart, and Dr. Neil Fox.

I would also like to thank Dr. Kathleen Trauth and Dr. Rebecca North for their helpful comments throughout their service on my dissertation committee.

Thanks are also in order to Dr. Baxter and Jean Vieux, of Vieux Inc. for their support and assistance with the hydrologic model, Vflo, which encompasses the fourth chapter of this dissertation.

Special thanks are due to the National Science Foundation's Experimental Project to Stimulate Competitive Research (EPSCoR) program, who have provided funding throughout this research.

Finally, thanks are extended to all former and current members of the Atmospheric Science department who contributed their time and effort either physically, or emotionally, to the completion of this work.

TABLE OF CONTENTS

LIST OF FIGURES

Figure Page

LIST OF TABLES

Table Page

MEASURING AND MODELING RAINFALL WITH TERRESTRIAL SENSORS AND RADAR: IMPLICATIONS FOR RAINFALL HETEROGENEITY AND DISCHARGE

Micheal Joseph Simpson
Dissertation Advisor: Neil I. Fox, Ph.D.

ABSTRACT

Quantitative precipitation estimates are fundamental for hydrometeorological analyses. Radars provide a superior spatiotemporal advantage over terrestrial-based precipitation gauges to provide such measures of rainfall. However, many regions of the Continental US (CONUS) reside outside of the optimal range of weather radar surveillance (i.e., 100 km), with few studies analyzing the performance of radar rain rate estimates beyond this range. Several years' worth of radar rain rate estimates were analyzed from distant S-band Weather Surveillance Radars – 1988 Doppler (WSR-88D) series, demonstrating poor performance in quantitative precipitation estimates (QPE's) at distances beyond 150 km. Furthermore, these S-band radar rain rates were determined to be significantly ($p < 0.10$) less accurate in Quantitative Precipitation Estimates (QPE's) when compared to a locally-sited X-band dual polarimetric radar. In general, S-band radars were best utilized when implementing R(Z,ZDR) algorithms, with the bulk of QPE errors due to missed precipitation, whereas the X-band radar was superior overall with either R(Z,ZDR) or R(ZDR,KDP) with errors primarily due to false alarms. These radar QPE's were then used as input to a physically-based hydrologic model, Vflo, which showed superior performance over spatially-averaged rain gauges, which sometimes missed precipitation events. The results presented demonstrate the importance of choosing the proper radar QPE datasets for hydrometeorological studies.

CHAPTER I
INTRODUCTION

BACKGROUND

For urban hydrologic applications, rain gauge data represents the main input of the rainfall-runoff simulation models (Habib et al., 2001). The uncertainties that may be associated with the recorded data of rainfall intensity and duration have an important and significant effect on the design of urban drainage systems (Schilling 1991). Rain gauge observations are also used in the calibration of radar rainfall estimation algorithms (Anagnostou and Krajewski, 1998). However, the development of such algorithms seldom account for the sampling properties of the rain gauge and its associated measurement errors (Ciach and Krajewski, 1999). Several studies have been conducted that reveal the sensitivity of the tipping bucket (TB) rain-gauge data, both in terms of random and systematic errors (Sevruk and Lapin, 1993). The systematic errors account for the most significant of errors in the TB analysis, involving losses due to wind, wetting, evaporation, and splashing (Sevruk and Harmon, 1984). Tipping bucket gauges also suffer from mechanical and electrical problems, occasionally failing to tip during a rain event, especially during the beginning and ending of an event (Nystuen and Proni, 1996; Frankhauser 1997). Although these errors exist for the TB gauges, many hydrological models use 30-min to 1-h precipitation data assumed from the reflectivity from a nearby radar. However, TB's do not provide an accurate distribution of the actual rainfall in terms of drop size distribution (DSD); devices, such as disdrometers, and radars, are capable of measuring such distributions.

Hydrological models are helpful tools to analyze current conditions to predict future values within a catchment (Niehoff et al., 2002). A relatively common challenge in modelling watershed hydrology is obtaining accurate weather input data (Mehta et al., 2004; Kouwen et al., 2005). Significant advancements in the resolution of disdrometers, spatially and temporally, have provided better estimations for accurate rainfall rates (Bodtmann and Ruthroff, 1976; Habib et al., 2001). In general, disdrometers are primarily used to measure the DSD for a given precipitation event, for a specific location, which is an integral part of measuring the reflectivity from a given radar within the region (Zrnic and Ryzhkov, 1996; Ryzhkov et al., 2005). However, weather tends to be monitored at locations outside the watershed of study (Fuka et al., 2014), with point source disdrometer measurements representing precipitation poorly across an entire watershed (Ciach 2003). To remedy this solution of spatially distributed point source measurements, some researches have utilized radar data to provide precipitation inputs to hydrological modelling studies (Ogden and Julien, 1994; Habib et al., 2008a).

Rainfall rates during convective rainstorms, or long-lived stratiform events, often exceed maximum infiltration rates of even well-drained soils (Sadler and Busscher, 1989). High rainfall rates also have a major impact on agricultural processes, including erosion, degrading radio communications (Ruthroff 1970), flooding, and possible hydrologic structure failure. Recent advances in the field of weather radars present unprecedented opportunities for improving hydrological predictions and forecasting (Habib et al., 2008b). A fundamental step in radar-rainfall estimation is through the estimation of converting radar reflectivity values (Z) into surface rainfall rates (R). Since the advent of a relationship between Z and R, a Z-R relationship, work pioneered by

Marshall and Palmer (1948) yielded power-laws in the form of $Z = aR^b$ estimated the best distribution between Z and R, where a and b are numerical constants. Battan (1973) expanded upon this work to include a total of 69 power-law relationships reflecting different rainfall rates dependent upon climatological variability and geographic locations. Despite early advancements of Z-R relationships in measuring precipitation amounts near the surface, it has been recognized the variability of Z-R relations for not only geographic locations, but also storm types (convective versus stratiform), storm origin (continental versus maritime), and time of day (Atlas et al., 1999; Tokay et al., 2001; Bringi et al., 2003). Several of these studies, including countless more, demonstrated that accounting for temporal variability in DSD and the corresponding Z-R relationships has a significant impact on the overall accuracy of rainfall estimates.

Steiner and Smith (2000) demonstrated that storm-to-storm variability in Z-R parameters, especially the numerical constant a, can be significant, signifying the use of a single Z-R relationship for a specific region is problematic. Bringi et al. (2003) would later show that variability in continental versus maritime, as well as convective versus stratiform rains have a major impact on the multiplicative constant a in the standard Marshall-Palmer relation. Lee and Zawadzki (2005) performed an extensive study to show that different temporal scales (climatologically, day to day, within a day) yielded DSD variability, namely in the origin within a storm or between storms within a given day.

Dual-polarization technology have several distinct advantages of improving quantitative precipitation estimation (QPE). They are beneficial due to the fact they reduce the impact of drop size distribution (DSD) variability on the quality of rainfall

estimation. Differential reflectivity, ZDR, is a good measure of the mean drop diameter and should be taken into account for more accurate rain measurements (Zrnic and Ryzhkov, 1996). Dual-polarized radars show promise in retrieving rain rates using a physical basis as opposed to an engineering/statistical approach (Gorgucci et al., 2001). Gamma distributions are utilized to model the DSD within a region, with an implementation and usage of surface disdrometers to study the variability of the DSD for a specific region (Bringi et al., 2003). It has also been noted (Ryzhkov et al., 2005) that different polarimetric algorithms for rainfall tend to perform better than the standard Z-R relationship, including Z (reflectivity), ZDR (differential reflectivity), and KDP (specific differential phase). A new "synthetic" algorithm was developed for rainfall estimation, resulting in significant reduction in the root mean square errors (RMSE) of hourly precipitation estimates when compared with the conventional Z-R relation: 1.7 times for point measurements, and 3.7 times for areal rainfall measurements. These relations consisted of the following forms:

$$R(Z) = aZ^b \tag{1.1}$$

$$R(K_{DP}) = a|KDP|^b sign(KDP) \tag{1.2}$$

$$R(Z, ZDR) = aZ^b ZDR^C \tag{1.3}$$

$$R(KDP, ZDR) = a|KDP|^b ZDR^c sign(KDP) \tag{1.4}$$

where a, b, and c are all numerical constants. It is desired to model the difference between the use of the WSR-88D's in KEAX and KLSX compared to an upgraded dual-polarized X-band radar in Columbia, MO (KCOU). The outcome is also desired to be compared to studies that measure DSD from local disdrometers within the Hinkson Creek watershed.

Columbia MO, located approximately 140 km between St. Louis (LSX) to the east and 170 km from Kansas City (KEAX) to the west, resides in a region termed the cone of silence. This region, indicated by Figures 1 and 2, lies beneath a radars beam when scanning the atmosphere; the lower-levels of the atmosphere near Columbia are entirely void under 3km. This leaves the region with an enormous gap in radar coverage that must be met by less-powerful radars run by local news stations. Recently, due to the enhancement of disdrometer resolutions, studies have been conducted to measure the relative error of the radar's algorithmic calculation of a regions DSD in comparison to localized disdrometers (Bringi et al., 2001; Gorgucci et al., 2001), analyzing different rainfall rate estimations in the process.

Numerous studies have focused on the effects of radar-rainfall estimation errors on runoff simulations (Sun et al., 2000; Borga 2002; among others). Due to the variability in DSD's discussed above, and the effects these have on the Z-R temporal variability, it has been shown that these different Z-R relationships result in significantly different simulated runoff hydrographs (Pessoa et al., 1993). The authors also concluded that a proper relationship between radar reflectivity and surface rainfall is the most crucial factor in obtaining accurate flood hydrographs. Other researchers (Vieux and Bedient, 1998) found a better agreement between measured and simulated runoff response during an extreme precipitation event when different Z-R relationships were used instead of the NWS default relationship ($Z = 300R^{1.4}$). Habib et al. (2008b) focused on the sensitivity of streamflow simulations to temporal variations in radar reflectivity-rainfall relations.

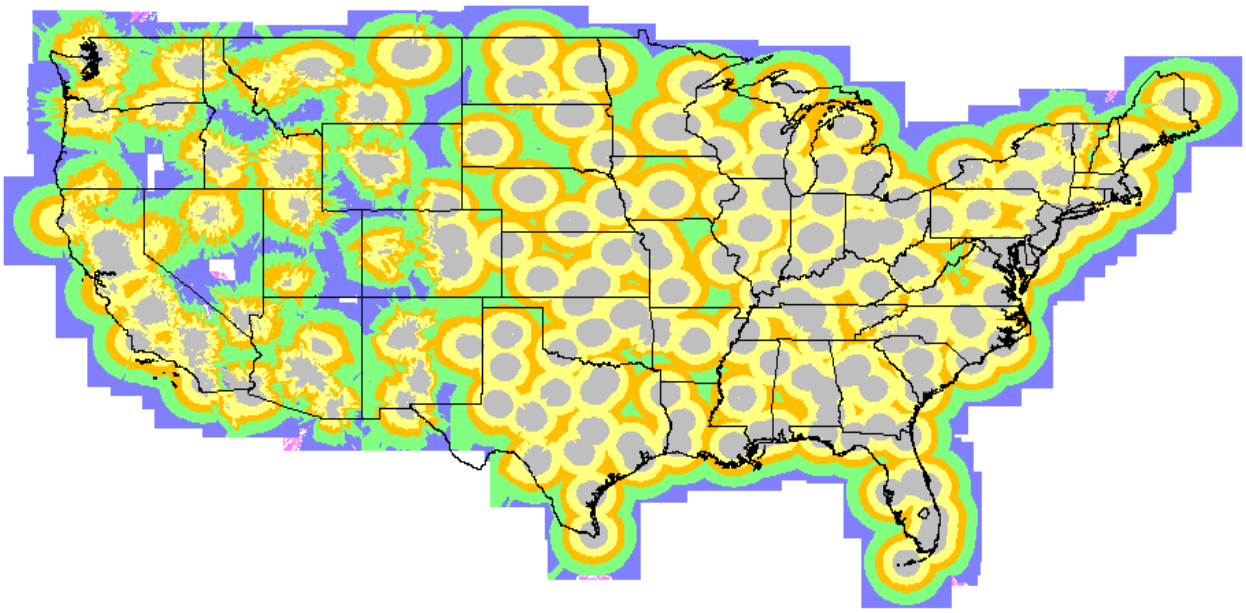

Figure 1: Continental United States (CONUS) Weather Surveillance Radar 1988 Doppler (WSR-88D) radar coverage. Concentric circle coloring represent average beam height above ground level. Grey, 0-1km; yellow, 1-2km; orange, 2-3km; and green, 3-5km. Adopted from National Weather Service (NWS) Supplemental Product Generator (SPG) for Terminal Doppler Weather Radar (TDWR) Data.

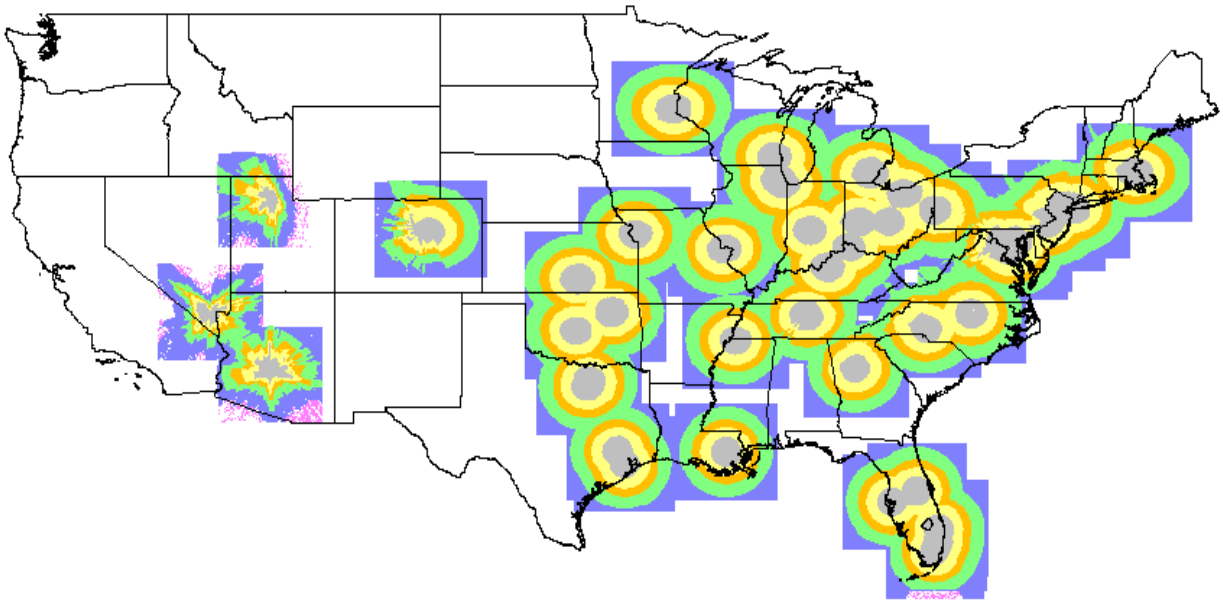

Figure 2: CONUS TDWR radar coverage. Color scheme is consistent with that of Figure 1.

Z-R relations were derived at a series of temporal scales ranging from climatological scale (i.e. interstorm Z-R relations are ignored), down to subevent scales, where the rainfall type are taken into account (i.e. convective versus stratiform). The analysis was first performed using Z and R data pairs derived from disdrometer DSD measurements, then repeated using WSR-88D reflectivity data. The authors found that using event specific Z-R relations resulted in accurate hydrographs when the parameters were derived based on bias removal and minimization of random errors of rainfall estimates. Srivastava et al. (2014) explored the performance of rainfall and evapotranspiration data from the global European Centre for Medium Range Weather Forecasts (ECMWF) for discharge prediction, and downscaled Weather Research and Forecasting (WRF) mesoscale modelling for hydro-meteorological variables. The authors found good agreement using the WRF downscaled evapotranspiration compared to observed ground-based observation datasets, yielding a promise for discharge predictions. However, WRF precipitation revealed poor performance, so much so that the authors concluded that further research is necessary for improvement on precipitation estimation.

Despite the wide usage of precipitation data as input for watershed modelling, many authors have expressed one of the main difficulties in modelling watershed hydrology is that of obtaining accurate weather input data (Mehta et al., 2004; Kouwen et al., 2005; Fuka et al., 2014). The weather is often monitored at locations outside of a watershed, sometimes at long distances from the watershed. Authors such as Fabry et al. (1992) and Smith et al. (1996) describe that significant underestimation of rainfall occurs within 40 km of the radar. Mean rainfall was found at 30 km is less than half the mean rainfall at 100 km range for southern plains radars. Not only is spatial resolution an issue

with radar rainfall accuracy, but seasonality is important as well; beyond 150 km in spring-summer and beyond 100 km in winter-fall, underestimation of precipitation is pronounced. Due to this spatial discrepancy, available records may not meaningfully represent the weather actually occurring over the region of interest. Additionally, disdrometers and TB's, effectively, are point source measurements, which may represent precipitation rather poorly across a selected area of interest. Therefore, most researchers have upgraded the spatial resolution of data from point source measurements of rainfall (Manguerra and Engel, 1998) to using either downscaled rainfall models (Nam et al., 2014), or reanalysis data (Fuka et al., 2014; Srivastava et al., 2014). Most of the studies within the literature appears to model hydrological processes in the past; after an event has occurred with modelled precipitation is when the authors conduct the study. Thus, there appears to be a lack of research in the literature using the most updated weather radars (equipped with dual-polarized technology) to model rainfall within a localized watershed, and modelling the input in real time.

STATEMENT OF NEED

The Hinkson Creek watershed, roughly 17,317.42 ha in area, resides in the eastern portion of Boone County, which is located in central Missouri. The largest river within the watershed, Hinkson Creek, is considered a Missouri Ozark border stream, and can be characterized as a transitional zone between the Glaciated Plains and Ozark Natural Divisions. This watershed encompasses important cities to Missouri, including the capital, Jefferson City, and Columbia, where the largest university in Missouri is located. In 1998, the Missouri Department of Natural Resources (DNR), Water Protection

Program (WPP) placed a 14-mile segment of the main river within the Hinkson watershed (Hinkson Creek) for "unspecified pollutants" due to urban runoff. The amount of pollutants that reach the Hinkson Creek will, ultimately, be impacted by the amount of runoff that occurs, as well as the amount of infiltration of precipitation that will convert to baseflow.

This study will 1) assess the accuracy of estimating rainfall from the nearest Next Generation Radar (NEXRAD) system to Boone County (i.e., KLSX and KEAX), 2) determine whether the installation of a nearby X-band dual-polarimetric radar to Boone County is significantly better at estimating precipitation than KLSX or KEAX, and 3) model streamflow using precipitation data from the three aforementioned radars against terrestrial-based precipitation gauges (i.e., tipping buckets). It is pertinent to determine which method produces the most realistic values of runoff and streamflow to help determine the actual amount of pollutants within the Hinkson Creek so that the necessary actions can be implemented. Gauging the correct amount of precipitation, whether by point source measurements or by areal estimation from radar, will be able to accurately assess streamflow characteristics within the Hinkson Creek watershed. Although point source measurements are the most commonly used inputs of hydrologic modelling, using real-time radar data would assist in not only the temporal, but also the spatial resolution of flood forecasting. Temporally, hydrologic models, such as the Soil Water and Assessment Tool (SWAT) could input real-time radar data to model streamflow characteristics, and, other variables related to streamflow (e.g. sediment loading, pollutant transport, etc.). However, the “lumping” of similar watershed characteristics does not allow for the spatial heterogeneity to be similar to the spatial resolution of radar

data. Therefore, a physically-based hydrologic model, Vflo®, would provide a more accurate means of estimating runoff and streamflow. Furthermore, this would reduce the amount of time needed to make decisions within the watershed. Spatially, radars cover a much larger area than tipping buckets, which will aid in the overall coverage of precipitation. If the accuracy of radar rainfall-rate is modelled such that it accurately describes precipitation measurements near the surface and streamflow measurements, better hydrologic models could be used to effectively simulate the actual environmental responses to precipitation input in real time.

OBJECTIVES AND DISSERTATION STRUCTURE

This dissertation is presented in five chapters. Within chapter one, "Introduction", the pertinent information necessary to justify the current research is presented. In chapter two, "S-band Dual-Polarimetric Radar Performance", the overarching objective is to:

Objective 1: Determine the relative error in using Kansas City (KEAX) and St. Louis (KLSX) radars on localized rain rates using ground-truthed tipping buckets within the state of Missouri.

This statement will be assessed through three studies, the first of which is entitled "Multi Radar Performances in the Midwestern United States at Large Ranges" which analyzes the performance of three S-band dual-polarimetric radars at varying ranges from ground-truthed rain gauges. The second study, entitled "Yearly Analyses of Two Distant Dual-Polarized Radar Performances Part I: Overall Analyses" assesses the performance of KLSX and KEAX based on over 7,000 hours of radar rainfall data compared to several

rain gauges. The last of the studies in chapter two, "Yearly Analyses of Two Distant Dual-Polarized Radar Performances Part II: Seasonal Analyses" determines the variability in radar performance as a function of seasonality.

Chapter three, "X-band Dual-Polarimetric Radar Performance", presents data from a newly installed X-band dual-polarimetric weather radar in Boone County, MO as part of the National Science Foundation (NSF) funded project, the Missouri Transect of the Experimental Project to Stimulate Competitive Research (EPSCoR) program. This data will be compared to the distant S-band radar rainfall estimates such in order to:

Objective 2: Analyze whether the implementation of a dual-polarized X-band radar within Columbia MO will be better at estimating rainfall rates as opposed to KEAX and/or KLSX.

The first study assesses the overall performance of the X-band radar, MZZU by analyzing one-years' worth of data from February 2016 through February 2017, entitled "X-band Polarized Radar Performance Analyses in the Midwestern United States". The second study, "Quantitative Improvement of Nearby X-band Radar Rainfall Estimates Versus Distant S-band Radar Rainfall Estimates", compares the X-band and S-band performances via several different ground-truthed tipping buckets at varying ranges from MZZU, KLSX, and KEAX.

Chapter four, entitled "Assessing Performance of Rainfall Estimates from Rain Gauges and Local X-band and Distant S-band Radars for Hydrologic Simulations", will determine whether a physically based hydrologic model is more accurate in estimating observed streamflow values when precipitation data from either MZZU, KLSX, or

several different tipping buckets are implemented. The overarching syntheses will be derived from a study to:

Objective 3: Model streamflow in the Hinkson Creek Watershed using a physically based hydrologic model, Vflo, to determine comparisons between observed streamflow and precipitation-gauge, X-band, and S-band radar rainfall data.

Chapter five, "Conclusions and Synthesis", will address key findings with potential future research.

Literature Cited

Anagnostou, E. N., and Krajewski, W. F., 1998: Calibration of WSR-88D Precipitation Processing Subsystem. *Wea. Forecasting,* **13**, 396–406.

Atlas, D., C. W. Ulbrich, F. D. Marks Jr., E. Amitai, and C. R. Williams, 1999: Systematic variation of drop size and radar-rainfall relations. *J. Geophys. Res*., **104**, 6155–6169.

Battan, L.J., 1973: Radar Observations of the Atmosphere. The University of Chicago Press, Chicago.

Bodtmann, W.F., and Ruthroff, C.L., 1976: The measurement of 1 min rain rates from weighing raingage recordings. *J. Appl. Meteor.*, **15**, 1160-1166.

Borga, M., 2002: Accuracy of Radar Rainfall Estimates for Stream Flow Simulation. *J. Hydrol.*, **267**, 26-39.

Bringi, V. N., G. Huang, V. Chandrasekar, and T. D. Keenan, 2001: An Aerial Rainfall Estimator Using Differential Propagation Phase: Evaluation Using a C-band Radar and a Dense Gauge Network in the Tropics. *J. Atmos. Oceanic Technol.,* **18,** 1810–1818.

Bringi, V.N., Chandrasekar, V., Hubbert, J., Gorgucci, E., Randeu, W., and Schoenhuber, M., 2003: Raindrop size Distribution in Different Climate Regimes from Disdrometer and Dual-Polarized Radar Analysis. *J. Atmos. Sci.,* **60,** 354–365.

Ciach, G.J., and Krajewski, W.F., 1999: On the Estimation of Radar Rainfall Error Variance. *Adv. Water Res.*, **22**, 585-595.

Ciach, G.J., 2003: Local Random Errors in Tipping-Bucket Rain Gauge Measurements. *J. Atmos. Oceanic Technol*., **20**, 752-759.

Fabry, F., Austin, G.L., and Tees, D., 1992: The Accuracy of Rainfall Estimates by Radar as a Function of Range. *Q. J. R. Meteorol. Soc.*, **118**, 435-453.

Frankhauser, R., 1997: Influence of Systematic Errors from Tipping Bucket Gauges on Urban Runoff Simulation. Use of Historical Rainfall Series for Hydrological Modeling. *Preprints, 3rd Int. Workshop on Rainfall in Urban Areas*, 37-44.

Fuka, D.R., Walter, T., MacAlister, C., Degaetano, A.T., Steenhuis, T.S., and Easton, Z.M., 2014: Using the Climate Forecast System Reanalysis as Weather Input Data for Watershed Models. *Hydrol. Process*, **28**, 5613-5623.

Gorgucci, E., G. Scarchilli, V. Chandrasekar, and V. N. Bringi, 2001: Rainfall Estimation from Polarimetric Radar Measurements: Composite Algorithms Independent of Raindrop Shape-Size Relation. *J. Atmos. Oceanic Technol.,* **18,** 1773–1786.

Habib, E., Krajewski, W.F., and Kruger, A., 2001: Sampling errors of Tipping-Bucket Rain Gauge Measurements. *J. Hydrol. Eng.*, **6**, 159-166.

Habib, E., Aduvala, A.V., and Meselhe, E.A., 2008a: Analysis of Radar-Rainfall Error Characteristics and Implications for Streamflow Simulation Uncertainty. *Hydrol. Sci. Jour*., **53**, 568–587.

Habib, E., Malakpet,G., Tokay, A., and Kucera, P.A., 2008b: Sensitivity of Streamflow Simulations to Temporal Variations and Estimation of Z-R Relationships. *J. Hydrol. Eng*., **13**, 1177-1186.

Kouwen, N., Danard, M., Bingeman, A., Luo, W., Seglenieks, FR., and Soulis, ED., 2005: Case Study: Watershed Modeling with Distributed Weather Model Data. *J. Hydrol. Eng.*, **10**, 23–38.

Lee, G.W., and Zawadski, I., 2005: Variability of Drop Size Distributions: Noise and Noise Filtering in Disdrometric Data. *J. Appl. Meteorol.*, **44**, 634-652.

Manguerra, H.B. and Engel, B.A., 1998: Hydrologic Parameterization of Watersheds for Runoff Prediction using SWAT. *Jour. Amer. Water Res.*, **34**, 1149-1162.

Marshall, J. S., and Palmer, W., 1948: The Distribution of Raindrops with Size. *J. Meteor.* **5**, 165–166.

Mehta, V.K., Walter, M.T., Brooks, E.S., Steenhuis, T.S., Walter, M.F., Johnson, M., Boll, J., and Thongs, D., 2004: Evaluation and application of SMR for watershed modeling in the Catskill Mountains of New York State. *Environmental Modeling and Assessment*, **9**, 77–89.

Nam, D.H., Mai, T.D., Udo, K., and Mano, A., 2014: Short-term Flood Inundation Prediction using Hydrologic-Hydraulic Models Forced with Downscaled Rainfall from Global NWP. *Hydrol. Process.*, **28**, 5844-5859.

Niehoff, D., Fritsch, U., Bronstert, A., 2002: Land-use impacts on stormrunoff generation: scenarios of land-use change and simulation of hydrological response in a meso-scale catchment in SW Germany. *Journal of Hydrology*., **267**, 80–93.

Nystuen, J.A., and Proni, J.R., 1996: A Comparison of Automatic Rain Gauges. *J. Atmos. And Oceanic Tech.*, **13**, 62-73.

Ogden, F.L., Julien, P.Y., 1994: Runoff Model Sensitivity to Radar Rainfall Resolution. *Journal of Hydrology,* **158**, 1–18.

Pessoa, M.L., Bras, R.L., and Williams, E.R., 1993: Use of Weather Radar for Flood Forecasting in the Sieve River Basin: A Sensitivity Analysis. *J. Appl. Meteo.*, **32**, 462-475.

Ruthroff, C.L., 1970: Rain attenuation and radio path design. *Bell Teleph. Tech. J.*, **49**, 121-135.

Ryzhkov, A.V., S. E. Giangrande, and T. J. Schuur, 2005. Rainfall Estimation with a Polarimetric Prototype of WSR-88D. *J. Appl. Meteor*., **44**. 502-515.

Sadler, E. J., and Busscher, W. J., 1989: High-intensity Rainfall Rate Determination from Tipping-Bucket Rain Gauge Data. *Agronomy J.*, **68**, 126–129.

Schilling, W., 1991: Rainfall Data for Urban Hydrology: What do we need? *Atmospheric Res.*, **27**, 5-21.

Sevruk, B., and Harmon, W.R., 1984: International Comparison of National Precipitation Gauges with a Reference Pit Gauge, Instruments and Observing Methods. *Rep. No. 17*, WMO, Geneva.

Sevruk, B., and Lapin, M., 1993: Precipitation Measurement and Quality Control. *Int. Symp. On Precip and Evap*, **1**, Slovak Hydrometeorological Institute, Bratislava, Slovakia.

Smith, J.A., Seo, D.J., Baeck, M.L., and Hudlow, M.D., 1996: An Intercomparison Study of NEXRAD Precipitation Estimates. *Water Resour. Res.*, **32**, 2035-2045.

Srivastava, P.K., Han, D., Rico-Ramirez, A., and Islam, T., 2014: Sensitivity and Uncertainty Analysis of Mesoscale Model Downscaled Hydro-meteorological Variables for Discharge Prediction. *Hydrol. Process.*, **28**, 4419-4432.

Steiner, M., and Smith, J.A., 2000: Reflectivity Rain Rate and Kinetic Energy Flux Relationships based on Raindrop Spectra. *J. Appl. Meteorol*., **39**, 1923-1940.

Sun, S., Mein, R G., Keenan, T.D., and Elliot, J.F., 2000: Flood Estimation using Radar and Raingauge Data. *J. Appl. Meteorol.*, **239**, 4-18.

Tokay, A., Kruger, A., and Krajewski, W., 2001: Comparison of Drop Size Distribution Measurements by Impact and Optical Disdrometers. *J. Appl. Meteor.* **40**, 2083-2097.

Vieux, B. E., and Bedient, P. B., 1998: Estimation of rainfall for flood prediction from WSR-88D reflectivity: A case study, 17–18 October 1994." *Weather Forecasting*, **13**, 407–415.

Zrnic, D., and A. Ryzhkov, 1996: Advantages of Rain Measurements Using Specific Differential Phase. *J. Atmos. Oceanic Technol.,* **13,** 454–464.

CHAPTER II
MULTI RADAR PERFORMANCE IN THE MIDWESTERN UNITED STATES AT LARGE RANGES

In Revision:
Simpson, M.J., and Fox, N.I., 2017: Multi Radar Performance in the Midwestern United States at Large Ranges. *Hydrol. Earth Syst. Sci.*

Abstract. Since the advent of dual-polarized technology, many studies have been conducted to determine the extent to which the differential reflectivity (ZDR) and specific differential phase shift (KDP) add benefits to estimating rain rates (R) to reflectivity (Z). It has been previously noted that this new technology provides significant improvement to rain rate estimation, but only for ranges within 125 km from the radar. Beyond this range, it is unclear as to whether the National Weather Service conventional R(Z)-Convective algorithm is superior, as little research has investigated radar precipitation estimate performance at large ranges. The current study investigates the performance of three radars, St. Louis (KLSX), Kansas City (KEAX), and Springfield (KSGF), MO, with respect to range, with 15 terrestrial-based tipping bucket gauges served as ground-truth to the radars. Over 1100 hours of precipitation data were analyzed for the current study. It was found that, in general, performance degraded with range beyond, approximately, 150 km from the radar. Probability of detection in addition to bias values decreased, while the false alarm ratios increased as range increased. Bright-band contamination was observed to play a potential role as large increases in the absolute bias and overall error values were near 120 km for the cool season, and 150 km in the warm season. Results within further our understanding in the strengths and limitations of the Next Generation Radar system overall, and from a seasonal perspective.

Introduction

In 2012, the National Weather Service (NWS) began upgrading the Next Generation Radar (NEXRAD) system from single- to dual-polarization. The potential benefits of this upgrade were investigated by the National Severe Storms Laboratory (NSSL) and the Cooperative Institute for Mesoscale Meteorological Studies. These advantages include, but are not limited to, (1) significant improvement in radar rainfall estimation (Ryzhkov et al., 2005; Gourley et al., 2010) through better representation of precipitation shape (Brandes et al., 2002; Gorgucci et al., 2000, 2006), (2) discrimination between solid and liquid precipitation (Zrnic and Ryzhkov, 1996), allowing for better distinction between areas of heavy rain and hail (Park et al., 2009; Giangrande and Ryzhkov, 2008; Cunha et al., 2013), (3) identifying the melting layer position in the radar field (Straka et al., 2000; Park et al., 2009), and (4) calculating drop-size distributions retrieved from measurements of reflectivity (Z), differential reflectivity (ZDR), and specific differential phase shift (KDP) as opposed to using ground-based point located disdrometers (Zhang et al., 2001; Brandes et al., 2004; Anagnostou et al., 2008).

Despite the advantages listed above, there are several sources of uncertainty and challenges that meteorologists and hydrometeorologists currently endure. For example, in order to ensure accuracy in rain-rate (R) estimates, Ryzhkov et al. (2005) stated the (mis)calibration effects should be limited between $\pm$1 dBZ in reflectivity, and $\pm$0.2 dB for differential reflectivity. The specific differential phase has been shown to be unaffected by beam blockage and other absolute calibration issues (Zrnic and Ryzhkov, 1999), yet attenuation effects may be amplified at X-band radars where the wavelength of the radar

signal is more affected by the size of the hydrometeors (Delrieu et al., 2000; Berne and Uijlenhoet, 2005).

Rain rate retrieval by weather radars is an estimation based upon the dielectric properties of the hydrometeors encountered in the atmosphere. Therefore, there is no direct measurement of rainfall, and this inherently introduces error. Although dual-polarized technology allows for the measurements of not only Z, but also ZDR and KDP, conflicting studies have been conducted as to whether dual-polarized radar rain rate algorithms have improved estimates over single-polarized radar rain rate algorithms. For example, Gourley et al. (2010) and Cunha et al. (2015) reported that conventional R(Z) algorithms have significantly better bias than algorithms containing ZDR and/or KDP, while others (e.g., Ryzhkov et al., 2013; Simpson et al., 2016) report the opposite. This could be due, at least in part, to the fact that hydrometeor types (e.g., rain versus hail) vary on spatial scales that cannot be easily resolved by even densely gauged networks.

Multiple studies have found that, in general, the performance of radar rain rate estimates decrease as range increases (Smith et al., 1996; Ryzhkov et al., 2003) which is caused by degradation of beam quality and broadening of the beam with range. Furthermore, the researchers also discuss how the probability of detection at larger ranges decreases, as the radar beam overshoots shallow, stratiform precipitation, including winter storms. Bright-banding can also play a crucial role in significantly increasing the amount of precipitation estimated by the radar.

Despite these overall disadvantages, studies have shown that radar rainrate algorithms seldom exceed absolute errors on the order of 10 mm h^{-1}. However, many of these studies have looked at a small sample of rain events (on the order of 10-50 hours)

(Kitchen and Jackson, 1993; Smith et al., 1996; Ryzhkov et al., 2003; Gourley et al., 2010; Cunha et al., 2013). Additionally, few studies (e.g., Smith et al., 1996; Cunha et al., 2015; Simpson et al., 2016) quantified meteorologically significant statistical measures including the probability of detection and false alarm ratio. In order to get a better understanding of the performance of weather radars on rain rate estimates, more data must be collected over a broad range of precipitation regimes in addition to an overall broad region of interest.

The overarching objective of the current study was to assess the overall performance of three different radars within the state of Missouri at various ranges from the radar, using terrestrial-based tipping bucket gauges as ground-truth data. Radar rain rate estimation algorithms include 55 algorithms encompassing standard R(Z) relations, in addition to algorithms containing dual-polarization variables including ZDR and KDP. A rain rate echo classification algorithm was also tested for performance in correctly identifying the suitable rain rate algorithm to choose based on the Z, ZDR, and KDP radar fields. The current work expands upon that of Simpson et al. (2016) such that a larger sample of data were analyzed (over 1000 hours of rainfall data from forty-six separate days in 2014) to encompass multiple different precipitation regimes for both summer and winter, with several ground-truth tipping buckets to analyze the performance of three separate radars as a function of range, and further expanding upon the effects of erroneous precipitation estimates on the overall radar error. Objectives for this study included, (1) statistically analyze the performance of each radar at various ranges (compared against the terrestrial-based gauges), (2) compute (a) the amount of precipitation incorrectly estimated by the radar (quantifying the probability of false

detection) and (b) the amount of precipitation incorrectly missed by the radar but measured by the rain gauge, (3) test the overall best radar rain rate algorithm, and (4) perform objectives (1), (2), and (3) while the data is separated into warm and cool seasons.

Study area and methods

Study area

National Weather Service radars from St. Louis (KLSX), Kansas City (KEAX), and Springfield (KSGF), MO are able to scan the majority of the state of Missouri. Because of this, the three aforementioned radars were used to assess overall performance in estimating precipitation for this study. Each radar covered a 200-km radius for which a different number of gauges were within the domain: KLSX, KEAX, and KSGF covered 9, 8, and 5 gauges, respectively (Figure 2A.1).

Missouri is characterized as a continental type of climate, marked by relatively strong seasonality. Furthermore, Missouri is subject to frequent changes in temperature, primarily due to its inland location and its lack of proximity to any large lakes. All of Missouri experiences below-freezing temperatures on a yearly-basis. For example, the majority of the state experiences, on average, 110 days with temperatures below freezing, while the Bootheel (i.e., southeast region) registers, on average, 70 days of below freezing days. This elaborates upon the typical northwest to southeast warming pattern of temperatures observed in the state. Because of the large variability in temperature, the warm and cool seasons were defined from an agronomic perspective, primarily taking

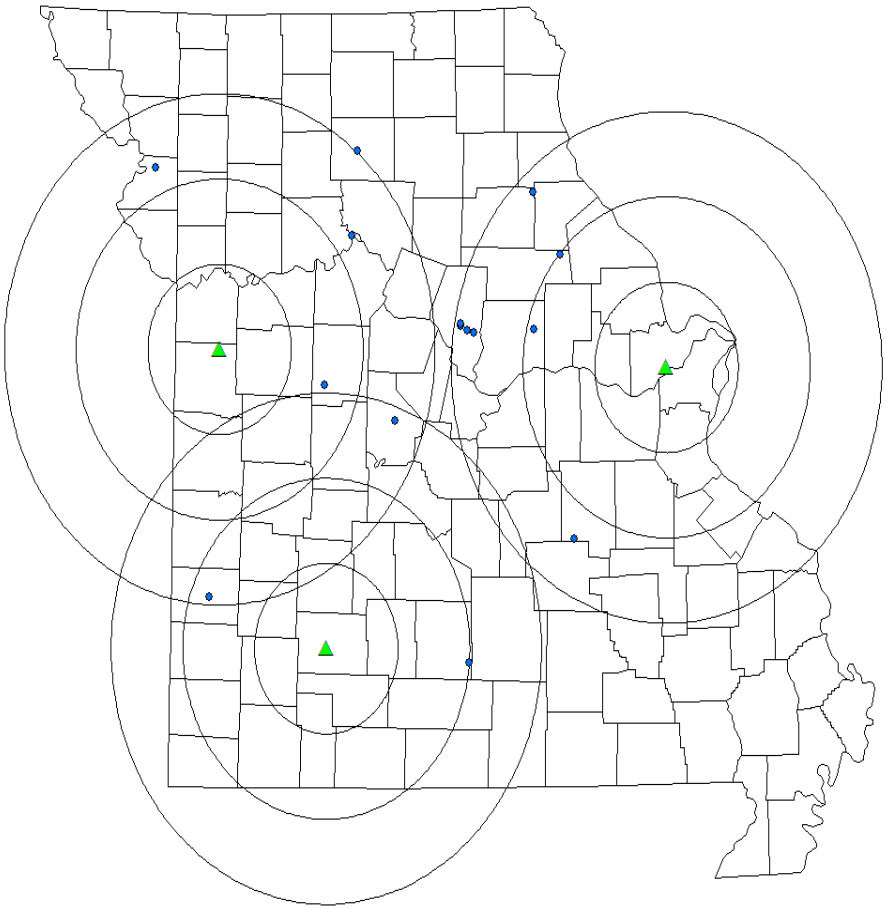

Figure 2A.1. Study location (Missouri) with St. Louis (KLSX), Kansas City (KEAX), and Springfield (KSGF), MO radars (triangles) overlaid with 50-, 100-, and 150-km range rings in addition to the 15 terrestrial-based precipitation gauges utilized as ground-truthed data.

probabilities of freezing into account. Based on the climatological averages of Missouri, from 1983 to 2013, November through April registered average minimum temperatures below freezing, and was considered the cool season, while May through October's minimum average temperature were above freezing and constituted the warm season.

Rainfall data

Terrestrial-based (ground-truthed) precipitation gauge data were collected from 15 separate weather stations within the Missouri Mesonet, established by the Commercial Agriculture Program of University Extension (Table 2A.1). All precipitation data were recorded in hourly intervals which, ultimately, were aggregated to daily totals from 0 to 0 CST for each day used in the study. Forty-six days for the year of 2014 were analyzed for a total of 1,104 hours for each radar which converts to, approximately, 33,000 radar scans in all. The days were chosen based on availability of data from the National Climate Data Center's (NCDC) Hierarchal Data Storage System (HDSS) for all three radars, in addition to error-free performance notes from each of the gauges used. The dates analyzed were split near evenly between warm (May – October) and cool (November – April), therefore encompassing an overall performance of each of the radars throughout the year with no preferential bias towards rain or snow. Additionally, days were distributed evenly during the summer between convective and stratiform events with a threshold of 38 dBZ (Gamache and Houze, 1982).

Observed precipitation data were collected using Campbell Scientific TE525 tipping buckets located at each of the locations for the study (Table 2A.1). The precipitation gauges have a 15.4 cm orifice which funnels to a fulcrum which registers 0.01 mm of rainfall per tip. The performance of each gauge is maximized between 0 and 50°C, for which each day of the study's temperature did not exceed. Accuracy in gauge measurements range between -1 to 1%, -3 to 0%, and -5 to 0% for precipitation up to 25.4 mm h^{-1}, 25.4 to 50.8 mm h^{-1}, and 50.8 to 76.2 mm h^{-1}, respectively, which are, primarily, associated with local random errors and errors in tip-counting schemes

(Kitchen and Blackall, 1992; Habib et al., 2001). Each tipping bucket is located, approximately, 1 m above the ground in areas clear of buildings and properly maintained vegetation height to mitigate turbulence effects (Habib et al., 1999). These errors were assumed negligible and, therefore, allowed for the gauges to be representative of the true rainfall rate.

Radar data and radar-rainfall algorithms

Next Generation Radar (NEXRAD) level-II data were retrieved from the NCDC's HDSS. Files were analyzed using the Weather Decision Support System – Integrated Information (WDSS-II) program (Lakshmanan et al., 2007) to assess reflectivity (Z) in addition to dual-polarized radar variables including differential reflectivity (ZDR) and specific differential phase shift (KDP). Three other variables were also generated based an R(Z), R(KDP), R(Z,ZDR), or R(ZDR, KDP) algorithm was implemented in estimating rain rates based on the radar fields of Z, ZDR, and KDP (Kessinger et al., 2003). All seven variables (Z, ZDR, KDP, DSMZ, DZDR, DKDP, and RREC) were converted from their native polar grid to 256 x 256 1-km Cartesian grids, where the lowest radar elevation scans (0.5°) were used to mitigate uncalculated effects from evaporation and wind drift. An average of 5-minute scans were used for each of the variables, which were aggregated to hourly totals to be compared to the hourly tipping-bucket accumulations. The latitude and longitude of each of the 15 gauges were matched with the radar pixel that corresponds to the Cartesian grid such that each quantitative value of the seven radar variables were able to be extracted and used in rain rate calculations. Post-processing rain-rate calculations were conducted using the equations presented by Ryzhkov et al. (2005) (Table 2A.2), which were gathered from multiple studies using disdrometers to

Table 2A.1. Terrestrial-based precipitation gauge locations used for the study in addition to the National Weather Service Radars Springfield, MO (KSGF), Kansas City, MO (KEAX), and St. Louis, MO (KLSX) used in conjunction with each gauge.

Gauge Location	Latitude (°N)	Longitude (°W)	Radar(s) Used
Bradford	38.897236	-92.218070	KLSX, KEAX
Brunswick	39.412667	-93.196500	KEAX
Capen Park	38.929237	-92.321297	KLSX, KEAX
Cook Station	37.797945	-91.429645	KLSX, KSGF
Green Ridge	38.621147	-93.416652	KEAX, KSGF
Jefferson Farm	38.906992	-92.269976	KLSX, KEAX
Lamar	37.493366	-94.318185	KSGF
Linneus	39.856919	-93.149726	KEAX
Monroe City	39.635314	-91.725370	KLSX
Mountain Grove	37.153865	-92.268831	KSGF
Sanborn Field	38.942301	-92.320395	KLSX, KEAX
St. Joseph	39.757821	-94.794567	KEAX
Vandalia	39.302300	-91.513000	KLSX
Versailles	38.434700	-92.853733	KEAX, KSGF
Williamsburg	38.907350	-91.734210	KLSX

derive a relationship between reflectivity, differential reflectivity, and specific differential phase (Bringi and Chandrasekar, 2001; Brandes et al., 2002; Illingworth and Blackman,

Table 2A.2. List of single- and dual-polarimetric algorithms used for radar rainfall estimates.

$R(Z) = aZ^b$			
Precipitation type	a	b	c
Stratiform	200	1.6	-
Convective	300	1.4	-
Tropical	250	1.2	-
$R(KDP) = a \mid KDP \mid^b sign(KDP)$			
Algorithm number			
1	50.7	0.85	-
2	54.3	0.81	-
3	51.6	0.71	-
4	44.0	0.82	-
5	50.3	0.81	-
6	47.3	0.79	-
$R(Z, ZDR) = aZ^b ZDR^c$			
Algorithm number			
7	6.70×10^{-3}	0.927	-3.43
8	7.46×10^{-3}	0.945	-4.76
9	1.42×10^{-2}	0.770	-1.67
10	1.59×10^{-2}	0.737	-1.03
11	1.44×10^{-2}	0.761	-1.51

$R(ZDR, KDP) = a \mid KDP \mid^{b} ZDR^{c} sign(KDP)$			
Algorithm number			
12	90.8	0.930	-1.69
13	136	0.968	-2.86
14	52.9	0.852	-0.53
15	63.3	0.851	-0.72

2002; Ryzhkov et al., 2003). Standard R(Z) algorithms were also included to test whether the addition of dual-polarized technology to rainfall estimates produced improvement.

With the use of both Z, ZDR, KDP, and DSMZ, DZDR, and DKDP fields produced by WDSS-II, the numberof algorithms tested was 55. This includes the three standard single-polarized algorithms (stratiform, convective, and tropical) which were calculated using reflectivity R(Z), and then calculated as R(DSMZ), while algorithms 1-6 (R(KDP)) were also calculated as R(DKDP). Algorithms 7-11 (R(Z, ZDR)) were additionally calculated as R(Z, DZDR), R(DSMZ, ZDR), and R(DSMZ, DZDR), while the same four combinations of non- and KDP-smoothed fields were applied to the R(KDP, ZDR) algorithms (12-15).

Statistical analyses

To test the performance of each algorithm, several statistical analyses were calculated. The average difference (Bias) was calculated as

$$Bias = \frac{\sum (R_i - G_i)}{N} \tag{2A.1}$$

where R_i is each hourly aggregated radar estimated rainfall amount calculated from one of the 55 algorithms, G_i is the hourly aggregated gauge (observed) measurement, and N is the total number of observations which, for this study, was 1,104 hours. A second statistical parameter, the normalized mean bias (NMB), was calculated as

$$NMB = \frac{1}{N} \frac{\sum (R_i - G_i)}{\sum G_i} \tag{2A.2}$$

The normalized mean bias is included in the analyses due to the fact that overestimations (i.e., radar estimates larger than gauge measurements) and underestimations (i.e., radar estimates smaller than gauge measurements) are treated proportionately. This is directly analogous to choosing the mean absolute error (MAE) opposed to the standard deviation as the MAE does not penalize smaller or larger errors, obscuring the overall results (Chai and Draxler, 2014). Bias measurements (Bias and NMB) were calculated to determine whether radar derived rain rates were over- or under-estimated in comparison to the gauges. However, to calculate the overall magnitude of error associated with the performance of the radars, the absolute values of (2A.1) and (2A.2) were performed to yield the mean absolute error (MAE), and normalized standard error (NSE), respectively.

Several other meteorological parameters were calculated, including probability of detection (PoD) which was calculated as

$$PoD = \frac{\sum | R_i \bullet G_i > 0 \,\&\, R_i > 0 |}{\sum | G_i |} \tag{2A.3}$$

where the bullet ($\bullet$) indicates "if", to determine how accurate the radars were at correctly detecting precipitation. The probability of detection values range between 0.0 (radar did not detectany precipitation correctly) and 1.0 (radar detected the occurrence of all

precipitation 100% correctly). The probability of false detection takes into account the amount of precipitation the radars incorrectly estimated when the gauges recorded zero values, and was calculated as

$$PoFD = \frac{\sum R_i \bullet (G_i = 0 \,\&\, R_i > 0)}{\sum G_i} \tag{2A.4}$$

Conversely, the missed precipitation amount (MPA) is the opposite of the PoFD, such that

$$MPA = \sum R_i \bullet (G_i > 0 \,\&\, R_i = 0) \tag{2A.5}$$

Equations 3, 4, and 5 are scaled by the amount of precipitation measured by the gauges. The total amount of rainfall missed and falsely detected (i.e., numerator) of (2A.3), (2A.4), and (2A.5) were also quantified and reported.

Results and discussion

Individual radar performance: All data

To test the overall performance of each radar, it was necessary to determine the overall best algorithm for each statistical measure. Furthermore, the algorithm that performed the best and worst for each gauge and for each radar was assessed.

Kansas City (KEAX)

The overall bias showed that there was a positive bias, peaking near 5.5 mm hr^{-1} at the second gauge for KEAX, approximately 115 km from the radar for both the best and worst performing algorithms (Figure 2A.2). This could correspond to a bright-band signature which caused overestimation in precipitation from the algorithms. The overall

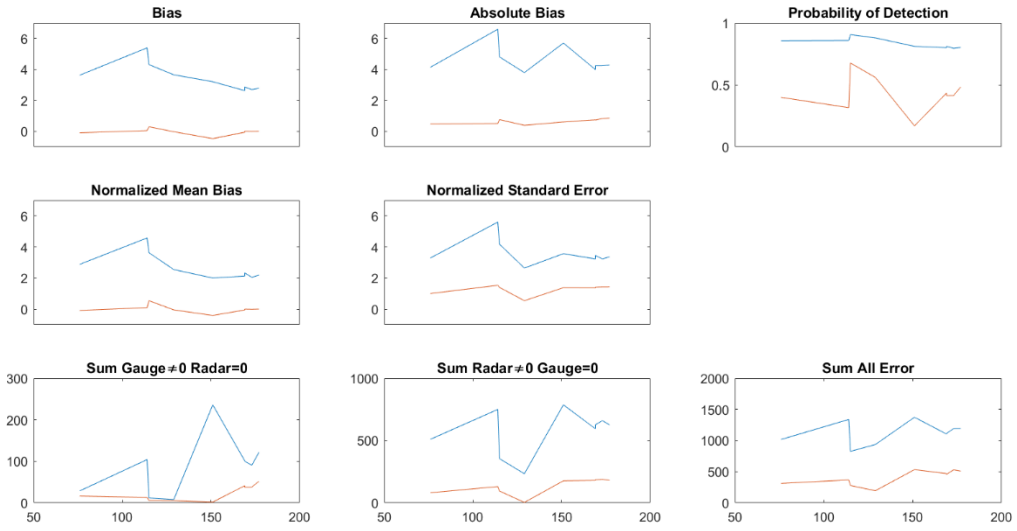

Figure 2A.2. Overall statistical analyses for the nine gauges used for Kansas City, MO. The blue line represents the weakest performing rain rate estimation algorithm, while the red line represents the overall best performing algorithm for all graphs, with the exception of the probability of detection. All units are in mm hr^{-1} with the exclusion of the probability of detection (unitless).

worst algorithm, equation 13, an R(ZDR,KDP) relationship, revealed a decreasing trend in bias as the distance from the radar increased. This could be due, at least in part, to the algorithm's utilization of KDP, which performs poorly in frozen precipitation (Zrnic and Ryzhkov, 1996), causing the underestimation. Conversely, the algorithm with the lowest bias was an R(Z,ZDR) algorithm (equation 11). There was a maximum in the bias calculations while utilizing equation 11 near 120 km, similar to equation 13, however, there was a more pronounced minimum in the data near 150 km. Furthermore, it appears the data oscillates around a bias value of 0 mm hr^{-1} when using equation 13. This could

be due to ZDR's capability to respond to precipitation shape (Kumjian 2013a, b), which helps to scale the reflectivity portion of the rainfall estimation algorithm to a more accurate value. The normalized mean bias (NMB) reveals the same trend in values for bias but with a decrease in magnitude. It is important to note, however, that the algorithms that tend to perform the worst (e.g., algorithms containing KDP) result in anomalous range responses which would be due, at least in part, to a stronger response to precipitation type.

The absolute bias and normalized standard error (NSE) shows the same maxima in the data at the second gauge (Brunswick) that was present in the bias data. However, a second maxima is located at the fifth gauge at, approximately, 150 km (Linneus), which could be a second bright-band present in the summer data, whereas the first maxima is a bright-band in the winter data. There was also a more pronounced minimum in the NSE results at the fourth gauge, indicating the effects of stratiform as opposed to convective precipitation.

The probability of detection (PoD) results show a large difference in algorithm choice for correctly detecting precipitation. The KDP-smoothed R(Z) convective algorithm, R(DSMZ) convective, performed the best in terms of correctly detecting precipitation, whereas algorithm 1 (KDP1) performed the worst, despite its advantages at large ranges (Zrnic and Ryzhkov, 1996). The increased PoD at the second gauge indicates the definite presence of a bright-band, while the low PoD at, approximately 150 km, indicates overshooting of the beam. This is further aided by the MPA results, as about 225 mm of precipitation was missed by the radar at 150 km, whereas only 100 mm of precipitation was missed by the radar at the second gauge at 120 km. Although

equation 11, an R(Z,ZDR) algorithm was superior in terms of the bias, the same algorithm with a KDP-smoothed reflectivity value, R(DSMZ,ZDR) revealed the overall least amount of falsely missed precipitation. However, the summation of the amount of precipitation falsely detected (PoFD) by KEAX showed a larger source of error than the MPA in terms of magnitude. For example, at the second (fifth) gauge, only 100 (225) mm of precipitation was missed by the radar, but over 700 (725) mm of precipitation was incorrectly estimated by the radar.

St. Louis (KLSX)

Unlike the KEAX data, the gauges used for analyses for the KLSX radar span between 90 – 150 km. Furthermore, 5 out of the 8 gauges were located within 10 km of range from one-another, near 140 km from the radar, limiting the data available for analyses between 100 and 140 km (Figure 2A.3).

The bias and NMB show a relatively modest peak in values near the second gauge of 5 mm hr^{-1}, which decreases to approximately 3.6 mm hr^{-1} at the third gauge, 120 km from the radar. The worst performing algorithm, equation 13, was the same R(ZDR,KDP) relation as the worst KEAX bias and NMB data. Additionally, the overall trend of decreasing bias and NMB as distance from the radar increases was noted, presumably due to overshooting effects similar to the KEAX data. Furthermore, the overall negative bias displayed by the best-performing algorithm, equation 11, was similar to the KEAX data as well.

The double maxima in the absolute bias graph are present as with the KEAX data, but are not as pronounced. Additionally, the overall minima in the absolute bias for both

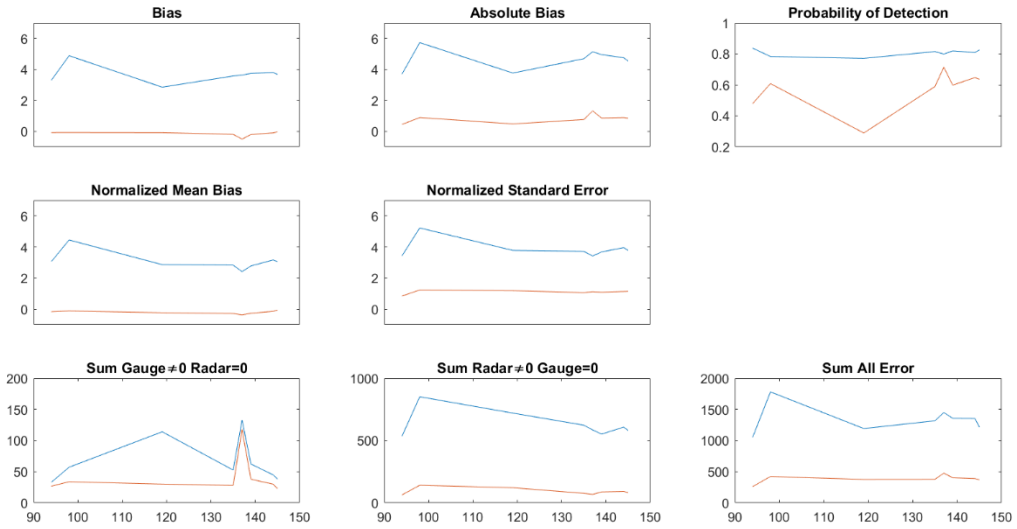

Figure 2A.3. Overall statistical analyses for the nine gauges used for St. Louis, MO. The blue line represents the weakest performing rain rate estimation algorithm, while the red line represents the overall best performing algorithm for all graphs, with the exception of the probability of detection. All units are in mm hr^{-1} with the exclusion of the probability of detection (unitless).

KEAX and KLSX are at, approximately, 125 km from the radar. However, the relative distance from the radars are the same, where the two maxima for KEAX were at 115 and 150 km, while the maxima were at, approximately, 100 and 140 km. The overall best and worst performing algorithms for the absolute bias and NSE were equations 11 and 13, the R(Z,ZDR) and R(ZDR,KDP) algorithms, respectively.

One of the main differences between the KLSX and KEAX data was the decreased probability of detection at 120 km for KLSX, while there was an increased probability of detection for KEAX. In general, the PoD values were worse for KLSX

when compared to KEAX. There was also a trend of increasing PoD values as distance from the St. Louis radar increased and, at one point near 140 km, the best algorithm, R(DSMZ) convective and the worst algorithm, KDP1, were not significantly different (10% difference in detection). Additionally, the maxima in the PoD while utilizing KDP1 corresponds to a minima in the R(DSMZ) detection percentage, which is well correlated by the similarly valued MPA results.

Another difference between the KEAX and KLSX data was the overall decrease in the PoFD as distance from the radar increased. Because of this, the maxima in the amount of falsely identified precipitation is only 100 km from the radar, which may be effects from bright-banding. Furthermore, this resulted in the overall error in precipitation for algorithm 13 to be in excess of 1,500 mm, while algorithm 11 did not exceed 500 mm for the 1,104-hour dataset for KLSX.

Springfield (KSGF)

Although the KLSX and KEAX data strongly suggests bright-banding signatures near approximately 100 km and 150 km from the radar, the KSGF results reveal an overall increase of error with range (Figure 2A.4). One of the main reasons for this could be due to the fact that the gauge furthest from any radar analyzed is Cook Station, 185 km from KSGF, which is the range where Ryzhkov et al. (2003, 2005) reported significant fallout in radar performance in rainfall estimation.

Overall, the absolute bias values for KLSX, KEAX, and KSGF were within $\pm$ 2 from 6 mm hr^{-1} for the worst performing algorithm, equation 13. However, the radar at Springfield, MO revealed the maximum absolute bias was the furthest gauge at,

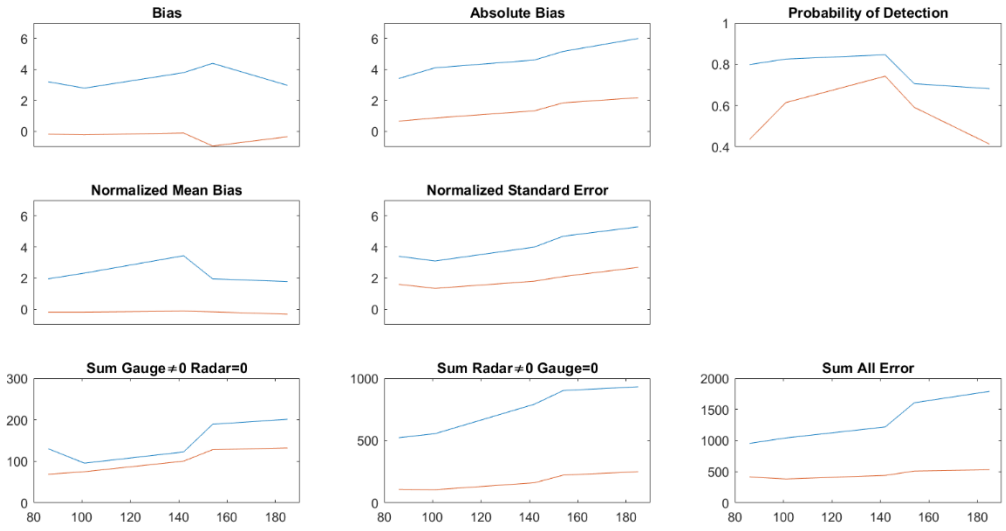

Figure 2A.4. Overall statistical analyses for the nine gauges used for Springfield, MO. The blue line represents the weakest performing rain rate estimation algorithm, while the red line represents the overall best performing algorithm for all graphs, with the exception of the probability of detection. All units are in mm hr^{-1} with the exclusion of the probability of detection (unitless).

approximately, 185 km (Cook Station). Although a slight bright-band effect is evident at the second gauge, 100 km from KSGF, the first bright-band is not as evident when compared to the KEAX and KLSX data. However, the overshooting of the beam is more pronounced between 140- and 160-km from KSGF. For example, there is a sharp decrease in the probability of detection within this range, correlating with a decrease in the bias and NMB. Furthermore, there is an increase in the magnitude of the FAR, indicating a large portion of precipitation was no captured by the radar beam.

Individual radar performance: Seasonal data

In order to achieve a better understanding of the minimum and maximum values portrayed by the data, all of the radar scans and gauge data were divided into summer (May – October) and winter (November – April) months based on the average climatology of Missouri. This resulted in 652 hours of data for summer, and 452 hours for winter (59 and 41% of the entire data, respectively). Because of this, the overall error is more weighted towards the summer data than the winter data.

The Kansas City bias and absolute bias summer data (Figure 2A.5) shows a similarity to the overall data (Figure 2.2) in terms of both trend and magnitude. Also, the best performing algorithm for the probability of detection (equation 11) was the same for the summer and overall data. However, the R(Z) Tropical algorithm showed the least reliability in correctly detecting precipitation for the summer, resulting in a more pronounced decrease in the PoD percentage overall. For the NMB and NSE data, the same algorithms that performed best and worse for the overall data (equations 11 and 13) were the best and worst for summer, respectively, and showed similar magnitudes and trends. Conversely, the winter data (Figure 2A.6) showed a pronounced overestimation in the NMB and NSE at the third gauge (125 km) from the radar, with values exceeding 30 mm hr^{-1} compared to values below 6 mm hr^{-1} for the combined seasonal data. This could be due, at least in part, to the large amount of precipitation overestimated by the radar relative to the total amount of precipitation. For example, winter precipitation amounts are significantly lower than convective summertime amounts and, thus, result in a small denominator in (2A.2), leading to an increase in bias. These trends in the KEAX higher

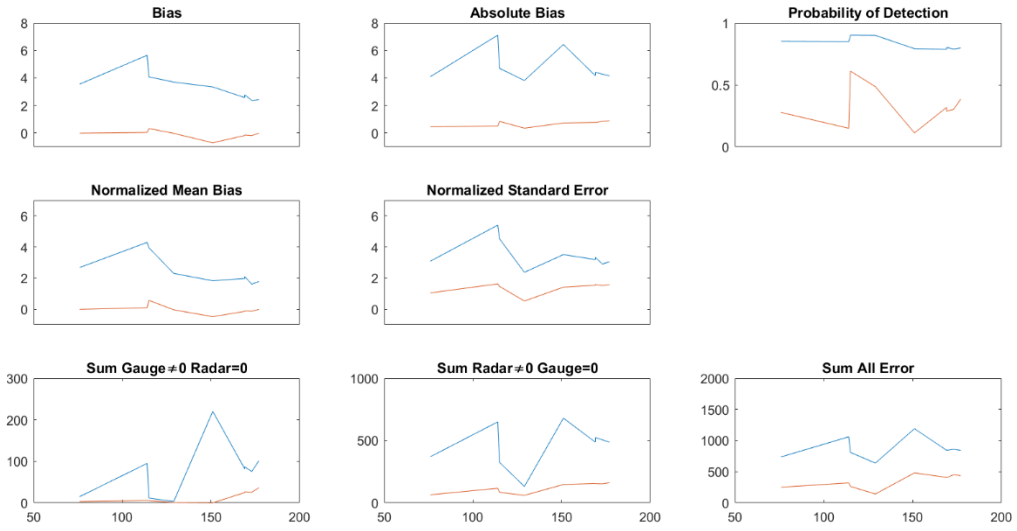

Figure 2A.5. Statistical analyses for the nine gauges used for Kansas City, MO for warm season data, only. The blue line represents the weakest performing rain rate estimation algorithm, while the red line represents the overall best performing algorithm for all graphs, with the exception of the probability of detection. All units are in mm hr^{-1} with the exclusion of the probability of detection (unitless).

NMB and NSE values can be observed for the KLSX and KSGF data as well (Figures 2A.7 and 2A.8, respectively). However, the magnitudes of NMB and NSE were smaller for KSGF in comparison to KLSX and KEAX.

Summing the amount of precipitation not recorded by the radar but recorded by the gauge (MPA) showed similar results when compared between summer and the overall data, but also revealed little contribution of the overall amount from the winter data. Additionally, the best and worst algorithms for the MPA (equations 10 and 14, respectively) were not significantly different ($p = 0.05$). Furthermore, the relatively small

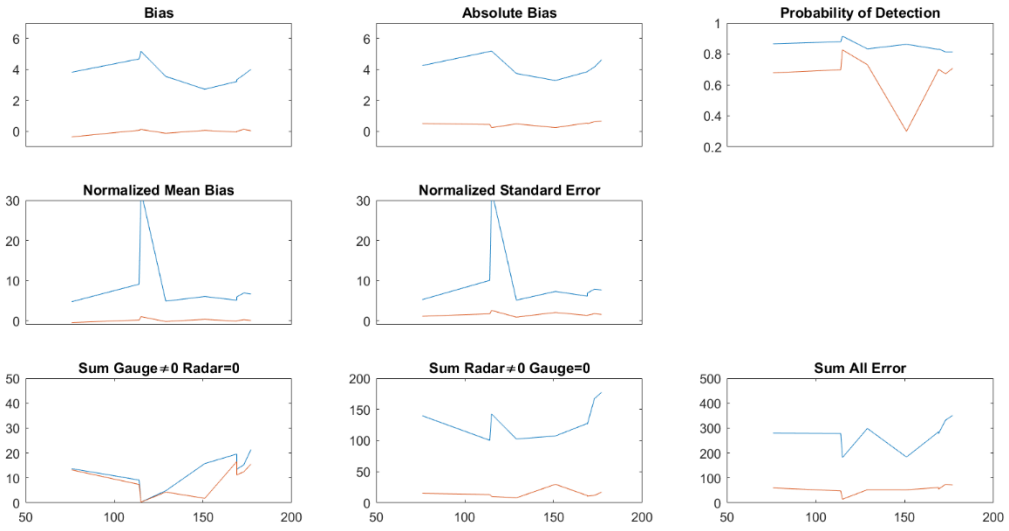

Figure 2A.6. Statistical analyses for the nine gauges used for Kansas City, MO for cool season analyses, only. The blue line represents the weakest performing rain rate estimation algorithm, while the red line represents the overall best performing algorithm for all graphs, with the exception of the probability of detection. All units are in mm hr^{-1} with the exclusion of the probability of detection (unitless).

contribution from the winter data to the amount of precipitation not estimated by the gauge but estimated by the radar (30 and 40 mm for KLSX and KSGF, respectively) was similar to the KEAX data. The contributions of winter MPA to the overall MPA for all three radars were, approximately, 20%. Conversely, the total amount of precipitation recorded by the radar but not recorded by the gauge (PoFD) showed a relatively large portion from the winter data as opposed to the summer data, with the noticeable exception of the bright-banding effects at the second and fifth gauges (120 and 150 km, respectively) for KEAX. Overall, the winter contribution to the PoFD was about 50%.

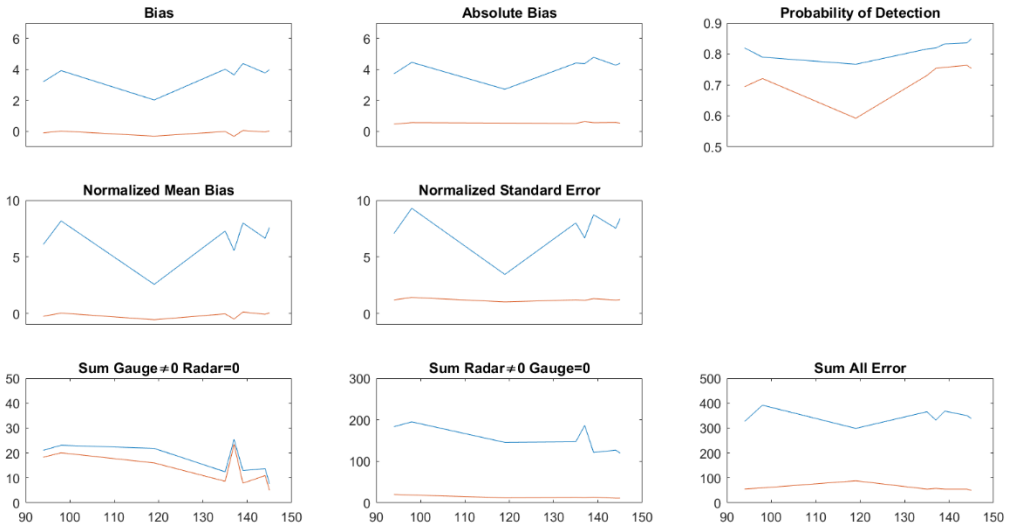

Figure 2A.7. Statistical analyses for the nine gauges used for St. Louis, MO for cool season analyses, only. The blue line represents the weakest performing rain rate estimation algorithm, while the red line represents the overall best performing algorithm for all graphs, with the exception of the probability of detection. All units are in mm hr^{-1} with the exclusion of the probability of detection (unitless).

Overall, the summation of all errors from the radar, including MPA, PoFD, and the absolute bias reveals that, approximately, 20-30% of the error was due to the winter data while comprising 41% of the entire dataset for all three radars. Conversely, the bulk of the error (80%) was due to the 59% total summer results, primarily due to the overall larger magnitudes in rainfall from convective storms. This is further exemplified via Figure 2A.9, showing a scatterplot of all gauge versus radar comparisons. With the exception of a few data points for KEAX, seldom does the winter radar estimated precipitation exceed 10 mm hr^{-1}, while no gauge recorded precipitation exceeding this.

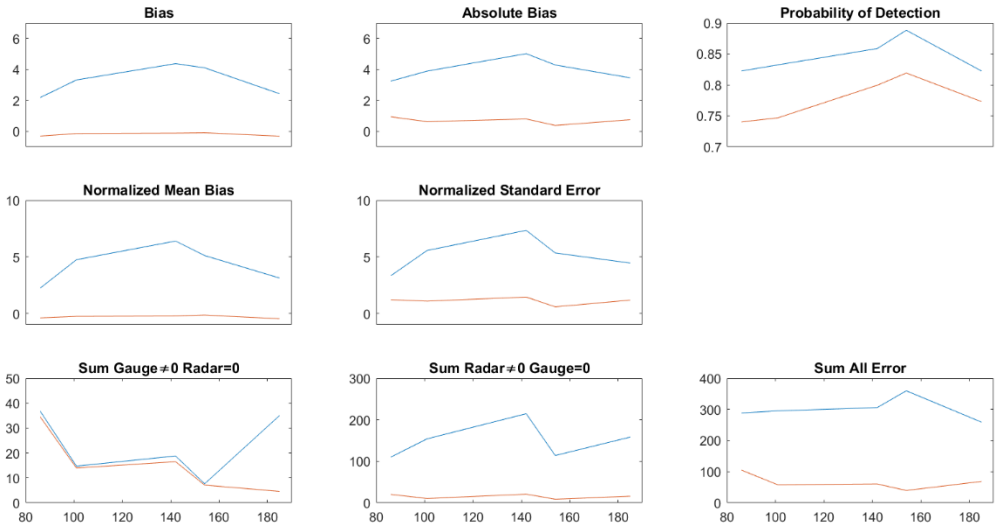

Figure 2A.8. Statistical analyses for the nine gauges used for Springfield, MO for cool season analyses, only. The blue line represents the weakest performing rain rate estimation algorithm, while the red line represents the overall best performing algorithm for all graphs, with the exception of the probability of detection. All units are in mm hr^{-1} with the exclusion of the probability of detection (unitless).

It is interesting to note that, with the exception of the KLSX data, the winter correlation coefficient values exceed the summer. This could be due, at least in part, to local random errors (Ciach and Krajewski, 1999a) and the excessive (i.e., convective) rainfall that the tipping buckets are unable to accurately measure (Ciach and Krajewski, 1999b; Ciach 2002). Furthermore, because the magnitude of precipitation in the winter is less than the summer, smaller variance and absolute error values are common, causing the correlation coefficient values to be larger than the frequent summertime showers where precipitation values can range from 0 mm hr^{-1} to, in extreme cases, 100 mm hr^{-1}.

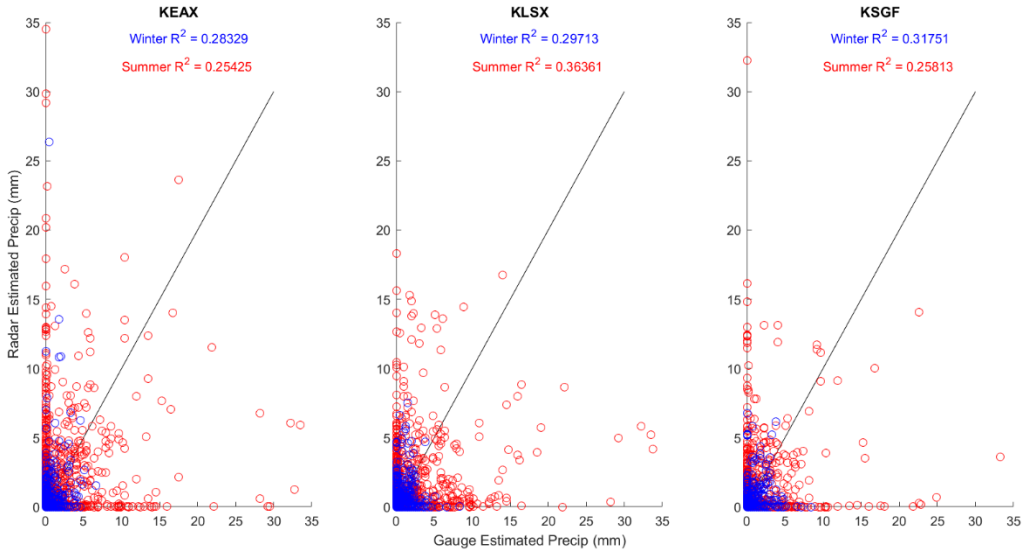

Figure 2A.9. Scatterplot of gauge estimation precipitation versus radar estimated precipitation with their respective correlation coefficient values for warm and cool seasons.

Radar performance: Hits only

From the results presented thus far, the majority of the error has resulted from either the PoFD or MPA. Therefore, an analysis into how accurate each algorithm was in comparison to a one-to-one ratio for a correct hit (i.e., gauge and radar recorded precipitation) is presented. This will, in turn, determine whether algorithm 11, an R(Z,ZDR) equation, is still most accurate and whether algorithm 13, an R(ZDR,KDP) equation, is least accurate.

From the 55 algorithms possible, the first gauge from each of the three radars (Greenridge, Williamsburg, and Lamar for KEAX, KLSX, and KSGF, respectively), all within 100 km from the radar, showed that either an R(Z) or R(DSMZ) convective

algorithm was most accurate with correlation coefficient values around 0.70 (Figures 2A.10-2A.12). Additionally, the second gauge from KEAX (Brunswick) also revealed that an R(Z) convective R^2 value was superior to all other algorithms. For the intermediate gauges from each radar, the rain rate echo classification (RREC) algorithm had the highest correlation coefficient value. For example, for KEAX, St. Joseph (115 km) and Versailles (129 km) had some of the highest R^2 values of 0.62 and 0.88, respectively. For KLSX, the fourth gauge (Bradford, at 135 km from the radar), the RREC correlation coefficient value was 0.55. Beyond, approximately, 140 km from the radar, the KDP3 equation was superior. In fact, the furthest two gauges from each radar showed KDP3 R^2 values exceeding 0.40. This could be due, at least in part, to the fact that the specific differential phase does not degrade quality with range, resulting in more accurate results at larger distances (Zrnic and Ryzhkov, 1999; Ryzhkov et al., 2003).

For the vast majority of scenarios, DZDRDKDP2 or the R(Z) Tropical algorithms were the worst performing equations. Because the R(Z) Tropical equation was designed for maritime precipitation while this study was conducted in the Midwest, it was not surprising that it was one of the poorest performing algorithms. From the scatterplots of gauge versus radar precipitation (Figures 2A.10-12A.2), when the R(Z) Tropical equation was the worst correlation correlation-valued algorithm, there was, generally, underestimation of precipitation estimated by the radar. Conversely, for the DZDRDKDP algorithm, overestimation of radar estimated precipitation was observed. This could be due to over-smoothing of the ZDR and KDP fields, causing overestimation in rain estimates (Simpson et al., 2016).

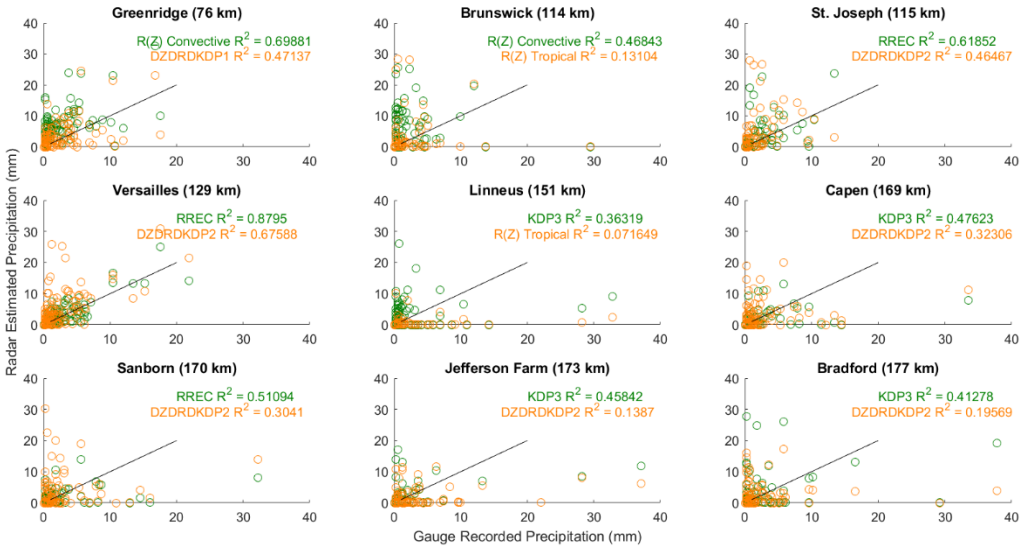

Figure 2A.10. Scatterplots of the best (green) and worst (orange) performing radar rain rate estimation algorithms at each terrestrial based gauge location. Distance from the Kansas City (KEAX) radar is labeled in parenthesis next to the gauge name.

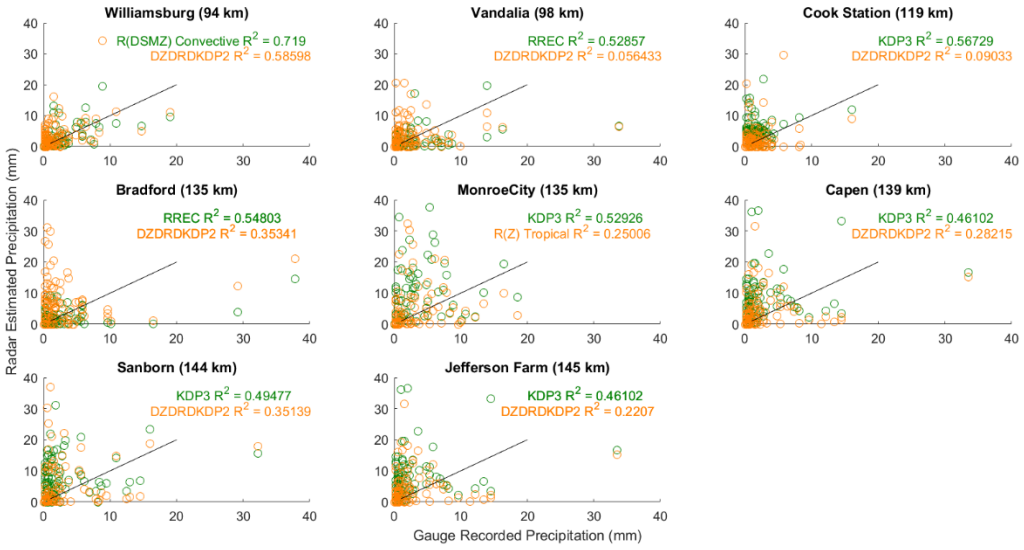

Figure 2A.11. Scatterplots of the best (green) and worst (orange) performing radar rain rate estimation algorithms at each terrestrial based gauge location. Distance from the St. Louis (KLSX) radar is labeled in parenthesis next to the gauge name.

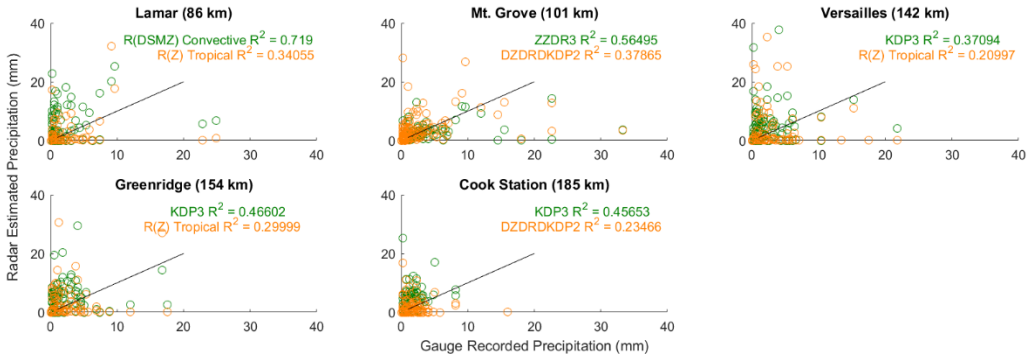

Figure 2A.12. Scatterplots of the best (green) and worst (orange) performing radar rain rate estimation algorithms at each terrestrial based gauge location. Distance from the Springfield (KSGF) radar is labeled in parenthesis next to the gauge name.

Conclusions

Dual-polarization technology was implemented to the National Weather Service Next Generation Radar network in the Spring of 2012 to, primarily, improve precipitation estimation and hydrometeor classification. Since this time, a number of studies have been conducted to determine whether this upgrade has improved radar performance in a meteorological, and hydrometeorological sense. Many studies have observed an improvement of radar-based precipitation estimation compared to terrestrial-based precipitation monitors (e.g., Ryzhkov et al., 2003, 2005; Simpson et al., 2016), while other studies show ambiguity between whether there is improvement (e.g., Gourley et al., 2010; Cunha et al., 2015). This study observed over 1,100 hours of precipitation data with three separate radars in Missouri using 55 algorithms including the three conventional R(Z) radar rain-rate estimation algorithms (stratiform, convective, and tropical) along with a myriad of R(KDP), R(Z,ZDR), and R(ZDR,KDP) algorithms

which can be found in Ryzhkov et al. (2005). Additionally, a KDP-smoothing field of reflectivity, differential reflectivity, and the specific differential phase shift (DSMZ, DZDR, and DKDP, respectively) were measured and used for analyses. Unlike previous studies, the current work emphasizes the amount of precipitation correctly and incorrectly estimated by the radar in comparison to the terrestrial based precipitation gauges through measurements of the probability of detection, probability of false detection, and missed precipitation amount.

For all three radars, Kansas City, St. Louis, and Springfield, MO (KEAX, KLSX, and KSGF, respectively), the vast majority of precipitation error (over 60%) was contributed by the amount of precipitation falsely detection by the radar (up to 725 mm), while 20% was due to the radar missing the precipitation (up to 225 mm) for KEAX. Similar magnitudes of error were reported for KLSX and KSGF, with an overall error in precipitation for each radar ranging between 250 mm for the best performing of the 55 algorithms, equation 11 (an R(Z,ZDR) algorithm), and up to 2000 mm for the worst performing algorithms, R(ZDR,KDP) equation 13.

Radar performance in different seasons has been shown to be significantly different, therefore, the data was divided into summer (May – October) and winter (November – April) months resulting in 652 hours for summer, and 452 hours for winter (59 and 41% of the entire data, respectively). Despite the winter data contributing less than the summertime data, it accounted for 20% of the overall MPA, and 40% to the overall PoFD. The best and worst performing algorithms were the same for the summer and winter data as the overall data, R(Z,ZDR) equation 11 and R(ZDR,KDP) equation 13, respectively.

The overall data was further subdivided into correct radar hits (radar correctly estimated precipitation to be present while the terrestrial based gauge recorded precipitation) for the 1,100-hour dataset. It was found that within 100 km from each of the three radars, the R(Z) or R(DSMZ) convective algorithm revealed the best correlation coefficient values of, approximately, 0.70. Further from the radar, beyond 135 km, RKDP3 generally performed the best due to the algorithms non-degrading capabilities and immunity to beam blockage, whereas at intermediate distances (between 100 and 135 km from the radars), the rain rate echo classification algorithm performed the best. Overall, the worst performing equations were either the R(Z) tropical, or DZDRDKDP2.

These results help our understanding in the possibilities for hydrometeorological studies. Although a mixture of R(Z) convective and R(KDP) algorithms performed the best when precipitation was correctly estimated by the radar, nearly 50% of the 1,100 hours analyzed for the study consisted of either falsely estimated precipitation by the radar, or missed by the radar. Furthermore, these errors accumulate between 500 to 2,000 mm of precipitation depending on the algorithms chosen. Because of this, a significant source of error and uncertainty must be overcome before radar data can be fully implemented into hydrologic models, especially on a continuous, operational basis.

Acknowledgements. This material is based upon work supported by the National Science Foundation under Award Number IIA-1355406. Any opinions, findings, and conclusions or recommendations expressed in this material are those of the authors and do not necessarily reflect the views of the National Science Foundation.

Literature Cited

Anagnostou, M.N., Anagnostou, E.N., Vulpiani, G., Montopoli, M., Marzano, F.S., and Vivekanandan, J., 2008: Evaluation of X-band polarimetric-radar estimates of drop-size distributions from coincident S-band polarimetric estimated and measured raindrop spectra. *IEEE Trans. Geosci. Remote Sens.*, **46**, 3067-3075.

Berne, A., and Uijlenhoet, R., 2005: A stochastic model of range profiles of raindrop size distributions: application to radar attenuation correction. *Geophys. Res. Lett.*, **32**, doi:10.1029/2004GL021899.

Berne, A., and Krajewski, W.F., 2013: Radar for hydrology: Unfulfilled promise or unrecognized potential? *Adv. Water Resour.*, **51**, 357-366.

Bringi, V.N., and Chandrasekar, V., 2001: Polarimetric Doppler weather radar, principles and applications. Cambridge University Press: Cambridge, UK, 636.

Brandes, E.A., Zhang, G., and Vivekanandan, J., 2002: Experiments in rainfall estimation with a polarimetric radar in a subtropical environment. *J. Appl. Meteor.*, **41**, 674–685.

Brandes, E.A., Zhang, G., and Vivekanandan, J., 2004: Drop size distribution retrieval with polarimetric radar: model and application. *J. Appl. Meteor.*, **43**, 461-475.

Chai, T., and Draxler, R.R., 2014: Root mean square error (RMSE) or mean absolute error (MAE)? – Arguments against avoiding RMSE in the literature. *Geosci. Model Dev.*, **7**, 1247-1250.

Ciach, G.J., and Krajewski, W.F., 1999a: On the Estimation of Radar Rainfall Error Variance. *Adv. Water Res.*, **22**, 585-595.

Ciach, G.J. and Krajewski, W.F. 1999b: Radar-raingage comparisons under observational uncertainties. *J. Appl. Meteor.*, **38**, 1519-1525.

Ciach, G.J., 2002: Local Random Errors in Tipping-Bucket Rain Gauge Measurements. *J. Atmos. Oceanic Technol*., **20**, 752-759.

Cunha, L.K., Smith, J.A., Baeck, M.L., and Krajewski, W.F., 2013: An early performance of the NEXRAD dual-polarization radar rainfall estimates for urban flood applications. *Wea. Forecasting*, **28**, 1478-1497.

Cunha, L.K., Smith, J.A., Krajewski, W.F., Baeck, M.L., and Seo, B., 2015: NEXRAD NWS polarimetric precipitation product evaluation for IFloods. *J. Appl. Meteor.*, **16**, 1676-1699.

Delrieu, G., Andrieu, H., and Creutin, J.D., 2000: Quantification of path-integrated attenuation for X- and C-band weather radar systems operating in Mediterranean heavy rainfall. *J. Appl. Meteor.*, **39**, 840-850.

Kitchen, M. and Blackall, M., 1992: Representativeness errors in comparisons between radar and gauge measurements of rainfall. *J. Hydrol.*, **134**, 13–33.

Gamache, J.F. and Houze, R.A., 1982: Mesoscale air motions associated with a tropical squall line. *Mon. Weather Rev.*, **110**, 118–135.

Giangrande, S.E. and Ryzhkov, A.V., 2008: Estimation of rainfall based on the results of polarimetric echo classification. *J. Appl. Meteor.*, **47**, 2445-2460.

Gorgucci, E., Scarschilli, G., Chandrasekar, V., and Bringi, V.N., 2000: Measurement of mean raindrop shape from polarimetric radar observations. *J. Atmos. Sci.*, **57**, 3406-3413.

Gorgucci, E., Baldini, L., and Chandrasekar, V., 2006: What is the shape of a raindrop? An answer from radar measurements. *J. Atmos. Sci.*, **63**, 3033-3044.

Gourley, J.J., Giangrande, S.E., Hong, Y., Flamig, Z., Schuur, T., and Vrugt, J., 2010: Impacts of polarimetric radar observations on hydrologic simulation. *J. Hydrometeorol.*, **11**, 781-796.

Habib, E., Krajewski, W.F., Nespor, V., and Kruger, A., 1999: Numerical simulation studies of rain gauge data correction due to wind effect. *J. Geophys. Res.*, **104**, 723–734.

Habib, E., Krajewski, W.F., and Kruger, A., 2001: Sampling errors of Tipping-Bucket Rain Gauge Measurements. *J. Hydrol. Eng.*, **6**, 159-166.

Illingworth, A. and Blackman, T.M., 2002: The need to represent raindrop size spectra as normalized gamma distributions for the interpretation of polarization radar observations. *J. Appl. Meteor.*, **41**, 286–297.

Kessinger, C., Ellis, S., and Van Andel, J., 2003: The radar echo classifier: a fuzzy logic algorithm for theWSR-88D. 19th Conf. on Inter. Inf. Proc. Sys. (IIPS) for Meteor., Ocean., and Hydr., Amer. Meteor. Soc., Long Beach, CA.

Kitchen, M. and Jackson, P.M., 1993: Weather radar performance at long range – simulated and observed. *J. Appl. Meteor.*, **32**, 975-985.

Kumjian, M.R., 2013a: Principles and applications of dual-poarization weather radar. Part 1: Description of the polarimetric radar variables. *J. Operational Meteor.*, **1**, 226-242.

Kumjian, M.R., 2013b: Principles and applications of dual-poarization weather radar. Part 2: Warm and cold season applications. *J. Operational Meteor.*, **1**, 243-264.

Kumjian, M.R., 2013c: Principles and applications of dual-poarization weather radar. Part 3: Artifacts. *J. Operational Meteor.*, **1**, 265-274.

Lakshmanan, V., Smith, T., Stumpf, G., and Hondl, K., 2007: The warning decision support system—integrated information. *Wea. Forecasting*, **22**, 596–612.

Park, H.S., Ryzhkov, A.V., and Zrnic, D.S., 2009: The hydrometeor classification algorithm for the polarimetric WSR-88DL Description and application to an MCS. *Wea. Forecasting*, **24**, 730-748.

Ryzhkov, A.V., Giangrande, S., and Schurr, T., 2003: Rainfall measurements with the polarimetric WSR-88D radar. National Severe Storms Laboratory Rep. Norman: OK, 98 pg.

Ryzhkov, A.V., Giangrande, S., and Schurr, T., 2005: Rainfall estimation with a polarimetric prototype of WSR-88D. *J. Appl. Meteor.*, **44**, 502–515.

Simpson, M.J., Hubbart, J.A., and Fox, N.I., 2016: Ground truthed performance of single and dual-polarized radar rain rates at large ranges. *Hydrol. Process.*, **30**, 3692-3703.

Smith, J.A., Seo, D.J., Baeck, M.L., and Hudlow, M.D., 1996: An intercomparison study of NEXRAD precipitation estimates. *Water Resour. Res.*, **32**, 2035-2045.

Straka, J.M., Zrnic, D.S., and Ryzhkov, A.V., 2000: Bulk hydrometeor classification and quantification using polarimetric radar data: Synthesis of relations. *J. Appl. Meteor.*, **39**, 1341-1372.

Zhang, G., Vivekanandan, J., and Brandes, E.A., 2001: A method for estimating rain rate and drop size distribution from polarimetric radar measurements. *IEEE Trans. Geosci. Remote Sens.*, **39**, 830-841.

Zrnic, D.S., and Ryzhkov, A.V., 1996: Advantages of rain measurements using specific differential phase. *J. Atmos. Oceanic Tech.*, **13**, 454-464.

Zrnic, D.S., and Ryzhkov, A.V., 1999: Polarimetry for weather surveillance radars. *Bull. Amer. Meteor. Soc.*, **80**, 389-406.

YEARLY ANALYSES OF TWO DISTANT DUAL-POLARIZED RADAR PERFORMANCES PART I: OVERALL ANALYSES

Abstract. Long-term analyses of radar performance, especially at large distances (i.e., greater than 125-km) are not well documented. Research, typically, exists over relatively small domains and temporal scales, leading to a discussion such that radar is a superior tool for estimating precipitation than terrestrial-based precipitation sensors. The current study implements parameter-based methods to radar data from St. Louis (KLSX) and Kansas City (KEAX), MO to test the overall performance of conventional and dual-polarized radar rain rate algorithms in the vicinity of the Hinkson Creek watershed, located in Boone County, MO, at a distance of up to 175-km from the radars. One year's worth or 7464 hours, of radar data were processed and compared to four terrestrial-based tipping buckets, which served as ground truth. Results indicate that the conventional R(Z)-Convective algorithm performs best in terms of mean absolute error, in addition to predicting the greatest number of hits and least number of misses, compared to other dual-polarized algorithms, including R(Z,ZDR), R(KDP), and R(ZDR,KDP) equations. The R(Z,ZDR) algorithm, however, recorded the fewest of false alarms. Algorithms containing the specific differential phase shift (KDP) performed poorly overall, excessively recording large amounts of missed precipitation, leading to large overall errors. Quantitative analyses, such as the current study, are important for determining the sources of error from radar rain rate estimations. The current study provides new information to the hydrometeorological community over a long-period of time such that the overall performance of radars, especially at large distances, is presented.

Introduction

One of the most necessary parameters for hydrologic simulations is that of quantitative precipitation estimates (QPE) (Wang and Chandrasekar, 2010). Accurate measurements of rainfall data are the primary input to hydrologic models as precipitation serves as the largest portion of input of water to the vast majority of watersheds throughout the world, especially for urban environments (Schilling, 1991; Vieux and Bedient, 2004; Habib et al., 2008a, 2008b). For most modeling scenarios, precipitation input comes from terrestrial based precipitation gauges (e.g., tipping-buckets) which, typically, are sparsely spaced within a watershed. In fact, for many regions, no gauges are known to exist (Berne and Krajewski, 2013). This presents a problem as point measurements of precipitation, few and far in-between many areas, are unavailable as observed precipitation measurements necessary for calibrating hydrologic models (Ogden et al., 2000; Yang et al., 2004).

Within the past few years, implementation of weather radar has been utilized as a potential remedy to the lack of terrestrial-based precipitation gauges for a particular region (e.g., Ogden et al., 2000; Gourley et al., 2010). Weather radars (hereafter, simply radars) exhibit superior spatial and temporal resolution when compared to rain gauges. For example, radars can cover areas extending beyond 200 km radially in all directions from the radar while most precipitation gauges exhibit a diameter for catching precipitation near 0.1 m, several orders of magnitude less than radar measurements. Furthermore, radars temporal resolution is on the order of 5-min, while rain gauge time resolutions are on the order of 30-min to 1-hr. Due to these significant resolution advantages, multiple researchers have utilized radar calculated variables including

reflectivity (Z) (Kitchen and Jackson, 1992; Smith et al., 1996; 2012) to estimate rainfall. By 2012, analyses by the National Severe Storms Laboratory (NSSL) provided sufficient evidence to upgrade the National Weather Service (NWS) Next Generation Radar (NEXRAD) network to dual-polarization technology. This allowed researchers to implement differential reflectivity (ZDR) and the specific differential phase shift (KDP) to estimate rainfall rates for some specified region (Ryzhkov et al., 2003, 2005; Cunha et al., 2013, 2015; Seo et al., 2015; Simpson et al., 2016). However, the assessment of radar rainfall estimates when compared to rain gauges has produced conflicting results since the upgrade (e.g., Ryzhkov et al., 2003; Cunha et al., 2015; Simpson et al., 2016).

One of the main reasons for the discrepancy in outcomes is that radars do not physically measure rain rates. When a radar sends out a pulse of electromagnetic radiation, the beam encounters hydrometeors in the atmosphere which absorb, diffract, and scatter the radiation. The radar measures the back-scattered radiation from each hydrometeor sampled (e.g., Goddard et al., 1982; Beard and Chuang, 1987), making calculations based on the average drop size distribution from each returned signal (e.g., Zhang et al., 2001; Bringi et al., 2003). Therefore, the rain rate is an assumption based on the electromagnetic properties for a given sample volume of objects encountered by the radar beam; there is no direct measurement of rainfall. This has prompted many researchers to conduct studies so as to produce an efficacious means of reliably converting the backscattered radiation amounts into rain rates through functions of Z, the returned power amount to the radar; ZDR, the average axial shape of the hydrometeors within a sample volume; and KDP, the degree phase shift difference of the radar beam between transmission and retrieval.

The errors associated with reliably measuring the backscattered radiation are compounded by the spatial resolution of the drop size distribution (Bringi et al., 1998; Chandrasekar et al., 2003), the inverse-squared deficit of power returned due to range from the radar (Kitchen and Jackson, 1992; Smith et al., 1996; Seo et al., 2000; Ryzhkov et al., 2003, Simpson et al., 2016), and effects from bright band contamination (Seo et al., 2000; Matrosov et al., 2007). Despite these numerous errors present for every radar scan, significant advances have been made throughout the past decade through dual-polarization technology to mitigate and, in some instances, resolve these issues. Therefore, rain rate calculations have been shown to be relatively accurate when compared to rain gauge measurements. However, the vast majority of the studies that have shown these results were for isolated cases, typically less than 10 hr of constant observations, over densely-instrumented (i.e., rain gauges) regions. Simpson et al. (2016) showed that for 100 hr of radar measurements 150 km from the radar, almost 1000 mm of precipitation, approximately 95% of the total yearly rainfall for central Missouri, were estimated by the radar but not measured by the ground-truthed precipitation gauges. Additionally, over 150 mm of precipitation was entirely missed by the radar, yet observed by the terrestrial-based rain gauges. Few studies have reported on the basic contingency table aspects of radar-gauge measurements (Cunha et al., 2015) and must be further analyzed to gain the true performance of radar rainfall estimation, especially over a region exceeding 100 km from the radar.

The overarching objective of this study (and subsequent papers) was to analyze one-year of radar data, from August 2015 – August 2016 from St. Louis, MO (KLSX) and Kansas City, MO (KEAX), over central Missouri (approximately 175-km from each

radar). The data were analyzed on an hourly basis such that 311 days were used for analysis, consisting of 7464 hours of data-points. An in-depth analysis of warm and cool seasons performance from an hourly perspective was also conducted in Part II of this series of papers. Previous studies have analyzed radar-gauge performances that observe hits, only (e.g., Ryzhkov et al., 2003, 2005; Gourley et al., 2010), whereas this study, among relatively few others (e.g., Cunha et al., 2013, 2015), include other contingency factors including false alarm ratios and probability of false detection values. Furthermore, this study includes quantitative error analyses including instances when the terrestrial based gauge (i.e., ground-truthed sensor) registered precipitation but the radar estimated nothing, the missed precipitation amount (MPA), and when the terrestrial based gauge did not register precipitation but the radar estimated precipitation to be present, the false precipitation amount (FPA).

Study site and methods

Study location and gauge data

Four separate precipitation gauges were utilized as the "ground-truth" observation of precipitation. All gauges were located in the Hinkson Creek Watershed (HCW), located in the Lower Missouri-Moreau River Basin in Boone county, Missouri (Figure 2B.1). Elevation ranges from 177 m at the Southern extent of the watershed (outlet) to 274 m at the Northern part of the watershed (headwaters) (Hubbart et al., 2014a, 2014b). The 30-year average of temperature and precipitation are approximately 14°C and 1082mm of precipitation, respectively (Hubbart and Zell, 2013). All tipping buckets were

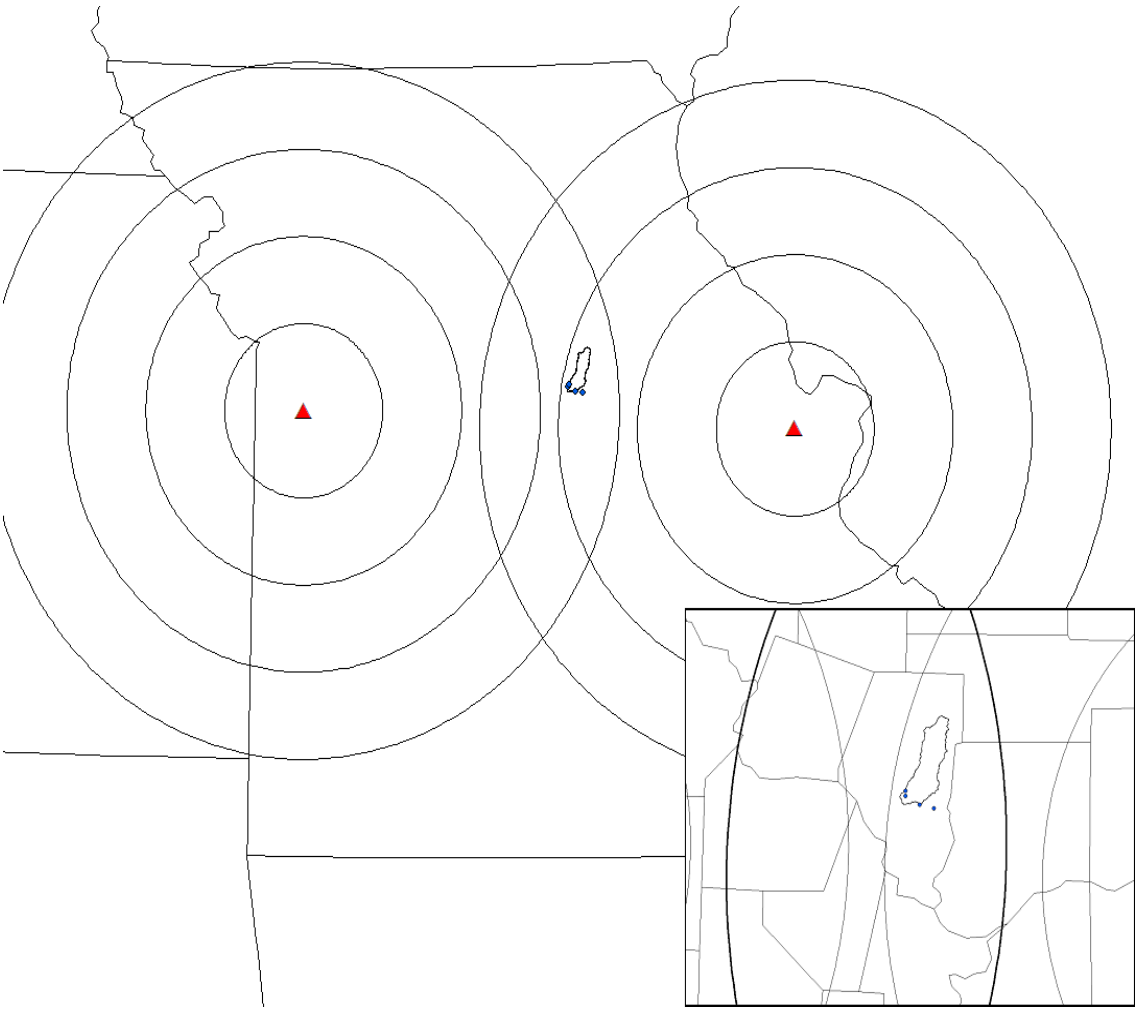

Figure 2B.1. Location of the two radars, St. Louis (KLSX) and Kansas City (KEAX), in addition to the area of study, the vicinity of the Hinkson Creek watershed, located in central Boone County, MO with the four terrestrial-based precipitation gauges which served as ground-truth. Radar 50-, 100-, 150-, and 200-km range rings are also displayed from each radar.

manufactured by Campbell Scientific, TE525MM series which registers 0.01 mm of precipitation to a balanced fulcrum device (i.e., the tipping bucket) via a 25.4-cm diameter orifice. All gauges were located, approximately, twice-to-three times the

distance of the height of the nearest building, compliant with the NWS's Cooperative Observer Program standards, in regions with properly maintained vegetation to mitigate any effects from turbulence (Habib et al., 1999; Villarini and Krajewski, 2010). The gauges were neither heated nor shielded and located, approximately, 1m above the surface. All data were recorded at hourly intervals with an accuracy of $\pm$ 1% at rainfall rates up to 25.4 $mmhr^{-1}$.

Precipitation data were gathered from the beginning of August 2015 through the end of August 2016. In general, the magnitude of precipitation was evenly distributed between warm (April – October) and cool (November – March) seasons, based from climatological monthly averages of temperature. However, near the end of 2016, there was a period of one week wherein the bulk of precipitation observed for the cool season was observed, whereas the warm season experienced multiple, short-lived stratiform events with a few isolated convective storms (Figure 2B.2). The average amount of precipitation from the four gauges were 829.75 mm.

Radar data

The dates chosen were from August 2015 through August 2016 to encompass an entire year's worth of data. However, due to radar maintenance and an incomplete 24-hr period for some days, only 311 days were used, for a total of 7,464 hours of data and, approximately, 87,000 radar scans. Furthermore, the data were selected such that both radars (KLSX and KEAX) were working and not undergoing maintenance.

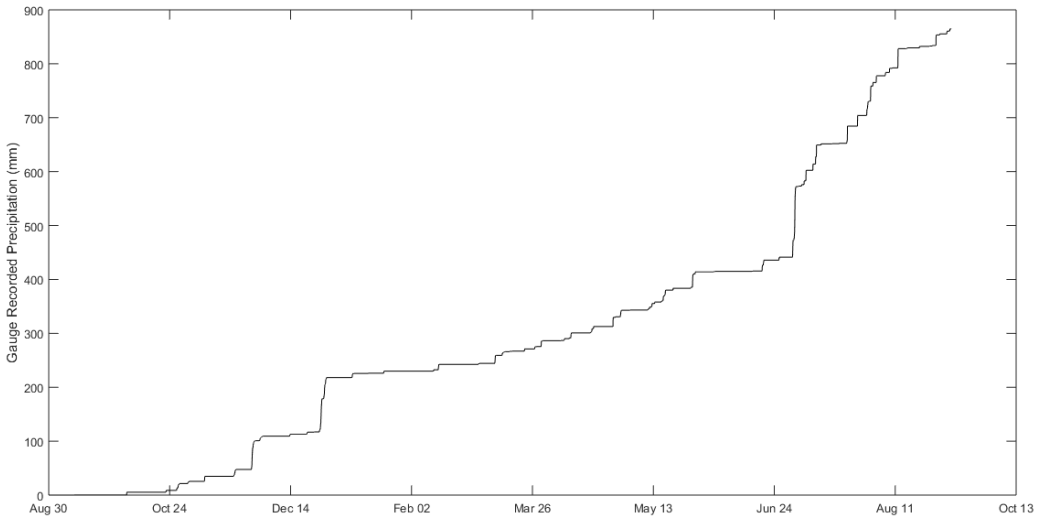

Figure 2B.2. Accumulation of precipitation for the study period based on the averages of the four terrestrial-based tipping buckets.

Radar data were retrieved from the National Climatic Data Center (NCDC) Hierarchical Data Storage System (HDSS) accessed via the National Centers for Environmental Information (NCEI) Archive Information Request System (AIRS). Level-II Next Generation Radar (NEXRAD) data were processed through the Weather Decision Support System-Integrated Information (WDSS-II) programme (Lakshmanan et al., 2007). Radar variables, including reflectivity (Z), differential reflectivity (ZDR), and the specific differential phase shift (KDP) were calculated in addition to KDP-filtered variables for reflectivity (DSMZ), ZDR (DZDR), and KDP (DKDP) (Ryzhkov et al., 2003). Lastly, a rain-rate echo classification (RREC) was developed (Kessinger et al., 2003).

Three-dimensional polar radar grids were converted to two-dimensional 256x256 1-km spacing Cartesian grids using WDSS-II, where the lowest elevation scan (0.5°) was used. The lowest elevation scan was utilized to mitigate turbulence, evaporation, and wind-drift effects, despite the radars sampling more than 1 km above the surface at the gauge locations in the HCW. Fifty-five different rain-rates were assessed, consisting of three R(Z) algorithms (Z-Stratiform, Z-Convective, and Z_Tropical) and their R(DSMZ) equivalents, six R(KDP) and R(DKDP), five R(Z,ZDR), R(Z,DZDR), R(DSMZ,ZDR), and R(DSMZ,DZDR), four R(ZDR,KDP), R(ZDR,DKDP), R(DZDR,KDP), and R(DZDR,DKDP), and one RREC algorithm were calculated (Table 2A.2), most of which may be found in Ryzhkov et al. (2003, 2005). The 55 separate rainfall algorithms were then aggregated over hourly time-steps to match the gauge data as closely as possible, whereby statistical analyses were then calculated based on the radar performance compared to the terrestrial-based gauges.

Statistical and quantitative analyses

Several statistical analyses were conducted to test the overall performance of the KLSX and KEAX radar rain rate estimates. These statistics consisted of one biased (bias; eq. 2A.1) and two unbiased measurements, the mean absolute error, eq. 2A.2 and normalized standard error:

$$NSE = \frac{\sum_{i=1}^{N} | R_i - G_i |}{\sum G_i} \qquad (2B.1)$$

where i, N, R, and G represent the ith iteration, N is the total number of samples, N = 7464 (i.e., 311 days times 24-hours), and R and G represent the radar estimated and gauge recorded precipitation amounts in mm, respectively. The normalized standard error (NSE) was included in this study such that it aims to normalize the data based on the amount of precipitation data measured by the gauges. In other words, the NSE measures the amount of total error compared to the actual amount of precipitation that was measured by the gauge. Therefore, the smaller the NSE (closer to 0.0) indicates smaller mean absolute error and, thus, better performance. A value greater than 1.0 (100%) indicates the amount of error was greater than the overall amount of precipitation observed by the tipping bucket.

Two other quantitative measurements were calculated, including the amount of precipitation estimated by the radar but not measured by the gauge, the false precipitation amount (FPA):

$$FPA = \sum_{i=1}^{N} R_i \bullet (G_i = 0) \tag{2B.2}$$

where the bullet (●) indicates the conditional "if" statement for the criterion in parenthesis. Conversely, the missed precipitation amount (MPA) calculates the amount of precipitation measured by the gauge but not estimated by the radar, and was presented as eq. 2A.5.

For all analyses, a single tip from the tipping bucket (i.e., rain gauge) was determined to be the lowest threshold at 0.254 mm. Therefore, for proper comparison, the lowest threshold for radar rainrate algorithms was also 0.254 mm. Equations (2B.1) and (2A.5) provide detail as to whether the overall error comes from the absolute error, or

when precipitation is falsely estimated (FPA) or missed (MPA). Qualitative performance indices, including the probability of detection (PoD) and probability of false detection (PoFD) were also calculated for each algorithm from each radar, and were presented as equations 2A.3 and 2A.4, respectively.

All analyses were conducted for each of the 55 algorithms used in the study from both KLSX and KEAX. The algorithms were then grouped between R(Z) and R(DSMZ); R(KDP) and R(DKDP); R(Z,ZDR), R(Z,DZDR), R(DSMZ,ZDR) R(DSMZ,DZDR); R(ZDR,KDP), R(ZDR,DKDP), R(DZDR,KDP), and R(DZDR,DKDP); and RREC to determine the best-performing equation from each group of algorithms. Therefore, five groups of algorithms spanning 55 equations were analyzed.

Instead of analyzing the statistics from each of the four gauges separately, the gauges with the lowest NSE from the radars were utilized such that any variability between the gauges would be due, at least in part, to the spatial heterogeneity of precipitation (Simpson et al., 2016). A 1-way Analysis of Variance (ANOVA) was run between all four gauges with an F-value of 0.11, mean-square-error of 0.82, and a p-value of 0.9562 indicating, with 95% confidence, that the gauges all share the same overall mean, and choosing one gauge over the other would be not be statistically different.

Results and discussion

Statistical analyses

The best-performing algorithms were consistent between both radars and groups of algorithms. For the R(Z) and R(DSMZ) calculations, R(Z)-Convective performed the best, while for the R(KDP) and R(DKDP), DKDP4 had the lowest bias, mean absolute

error (MAE) and normalized standard error (NSE). For the combinations of Z, DSMZ, ZDR, and DZDR variables, ZZDR5 performed best, while the combinations of KDP, DKDP, ZDR, and DZDR showed that ZDRDKDP3 performed best.

The statistical analyses conducted for this study included the bias, mean absolute error, and normalized standard error, encompassing a bias and two non-bias calculations. Overall, the dual-polarized ZZDR5 equation, had the lowest bias for both KLSX (0.0 mm) and KEAX (0.0 mm) (Table 2B.1), while the (National Weather Service's) standard R(Z)-Convective algorithm was the second-best (-0.2 mm and 0.2 mm for KLSX and KEAX, respectively). This indicates that, on average, the inclusion of the differential reflectivity aids in the overall accuracy of rainrates, such that there are no excessive over- or underestimated precipitation amounts (Giangrande and Ryzhkov, 2008). The only algorithm that displayed a negative bias was the KLSX R(Z)-Convective equation, possibly due, at least in part, to the radars' distance from the study area. However, this result is opposite to what have been previously reported for rainfall estimates at ranges in the proximity of 150 km (e.g., Ryzhkov et al., 2003; Simpson et al., 2016). This could be the result of the limited datasets in the previous studies, whereas the current study analyzed over an order of magnitude more hours.

For both radars, the combination of ZDR and KDP performed the weakest, with bias values of 0.3 mm and 0.6 mm for KLSX and KEAX, respectively. In contrast to observations from R(Z)-Convective and ZZDR5, the inclusion of the differential reflectivity to KDP estimates caused an overall increase in bias. For example, the best-performing KDP/DKDP algorithm for both radars, DKDP4, had a bias value of 0.3 mm and 0.6 mm, a 3 mm and 5 mm difference from the ZDRDKDP3 results, respectively.

Table 2B.1. Statistical measures including instances of hits, misses, false alarms, and correct negatives of bias, mean absolute error (MAE), and the normalized standard error (NSE) for the St Louis (KLSX) and Kansas City (KEAX), MO radars. The best-performing algorithm is reported for its respective grouping of equations, while RREC was the only algorithm calculated not in a group.

Statistics	KLSX	KEAX
Z / DSMZ	Bias: ZConvective (-0.2) MAE: ZConvective (1.5) NSE: ZConvective (1.3)	Bias: ZConvective (0.2) MAE: ZConvective (1.6) NSE: ZConvective (1.7)
KDP / DKDP	Bias: DKDP4 (0.3) MAE: DKDP4 (2.1) NSE: DKDP4 (2.0)	Bias: DKDP4 (0.6) MAE: DKDP4 (2.3) NSE: DKDP4 (2.2)
Z, ZDR	Bias: ZZDR5 (0.0) MAE: ZZDR5 (1.6) NSE: ZZDR5 (1.2)	Bias: ZZDR5 (0.0) MAE: ZZDR5 (1.8) NSE: ZZDR5 (1.6)
ZDR, KDP	Bias: ZDRDKDP3 (0.3) MAE: ZDRDKDP3 (2.1) NSE: ZDRDKDP3 (1.8)	Bias: ZDRDKDP3 (0.6) MAE: ZDRDKDP3 (2.3) NSE: ZDRDKDP3 (2.1)
RREC	Bias: 0.2 MAE: 2.0 NSE: 1.3	Bias: 0.5 MAE: 2.1 NSE: 1.6

Similarly, the difference between R(Z)-Convective and ZZDR5 for KLSX and KEAX were 0.2 mm and 0.2 mm, respectively.

The inclusion of the differential reflectivity improved bias calculations for the specific differential phase shift (KDP) but not reflectivity (Z), yet the KDP-smoothed measures of KDP (DKDP) performed better than the KDP-smoothed measure of reflectivity (DSMZ) (Figure 2B.3). For example, the sum of the total amount of precipitation from KLSX over the duration of the study were 729.2 mm (leading to the overall negative bias), while the sum of the KLSX R(DSMZ)-Convective algorithm was over 1000 mm: a 300 mm difference between the two variables. Similarly, for KEAX, the difference between R(Z)- and R(DSMZ)-Convective was, approximately, 200 mm.

However, for the KDP and DKDP comparisons, precipitation estimate differences were on the order of 1000 mm for both KLSX and KEAX. This could be due, at least in part, to the fact that KDP is heavily attenuated in areas of shallow, stratiform precipitation (Ryzhkov and Zrnic, 1995; Kumjian, 2013a; Seo et. Al., 2015). The areal smoothing of the KDP-field (DKDP) allowed for a more accurate representation of the observed rainfall that occurred.

The mean absolute error (MAE) calculated the average magnitude of error between the terrestrial-based precipitation sensor and the radar estimated rainfall amount. For both KLSX and KEAX, R(Z)-Convective performed best (MAE = 1.5 mm and 1.6, respectively). Furthermore, the KEAX R(Z)-Convective algorithm performed better than the second-best equation for KLSX: ZZDR5 (MAE = 1.6 mm). This indicates that, from an approximately years' worth of data, the R(Z)-Convective algorithm is the best-performing algorithm in terms of absolute error over any of the other dual-polarized equations, including RREC.

The DKDP and ZDRDKDP algorithms, much like the bias values, were highest among the grouping of equations. Similarly, the difference in the addition of the differential reflectivity for KDP rain rate estimates was smaller compared to the addition of ZDR to reflectivity measurements for KLSX. For example, the mean absolute error for the R(Z)-Convective equation for KLSX was 1.5 mm while the MAE for ZZDR5 was 1.60 mm, a 0.09 mm in difference; the MAE for DKDP for KLSX was 2.1 mm and the MAE for ZDRDKDP3 was 2.2 mm, a 0.1 mm difference. However, for KEAX, the addition of ZDR caused a greater difference for reflectivity measurements opposed to KDP measurements: the MAE for R(Z)-Convective (ZZDR5) was 1.6 mm (1.8 mm), a

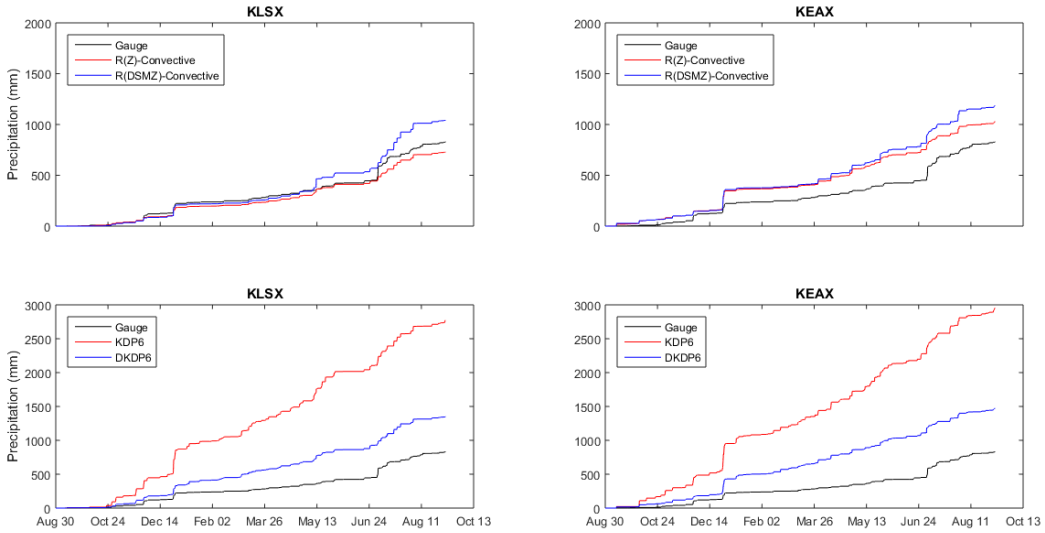

Figure 2B.3. Gauge accumulated precipitation in addition to precipitation amounts calculated by algorithms containing either reflectivity (Z) or the KDP-smoothed reflectivity (DSMZ) represented by the top two figures, and the specific differential phase shift (KDP) or the KDP-smoothed KDP field (DKDP) represented by the bottom two figures for St. Louis, MO (KLSX) and Kansas City, MO (KEAX).

0.2 mm difference, whereas the MAE for DKDP4 (2.3 mm) and ZDRDKDP3 (2.3 mm) was 0.1 mm.

The normalized standard error (NSE) divides the accumulated mean absolute error (MAE) throughout the course of the study by the total amount of observed precipitation. No algorithms had an NSE value less than 1.0, with several having double the amount of error than that measured by the terrestrial-based precipitation gauge.

The lowest normalized standard error (NSE) was 1.2, the NSSL ZZDR5 algorithm for KLSX, indicating that the magnitude of error between the radar estimated

precipitation using the ZZDR5 algorithm and the tipping-bucket rain gauge was +17%. Two more KLSX algorithms, R(Z)-Convective and RREC (NSE = 1.3 for both algorithms), yielded better results for the NSE than any other KEAX algorithm, for which the best-performing were the ZZDR5 and RREC (1.6). Two equations, DKDP4 and ZDRDKDP3, aggregated mean absolute errors exceeding twice the rain-gauge amount (829.8 mm).

All statistical analyses presented included instances of hits, misses, false alarms, and correct negatives. However, the number of correct negatives comprised over 90% of the total number of cases, resulting in relatively small bias and MAE values. Albeit useful for climatological studies, it is important to determine the overall performance of each equation and grouping of algorithms when precipitation is correctly assessed (i.e., assessment of hit performance). Table 2B.2 displays the overall performance of each algorithm during instances of hits, only.

Only algorithms from KLSX (R(Z)-Convective, DKDP6 and RREC) displayed overall negative biases, whereas equations containing differential reflectivity showed a positive bias. This may be explained such that the height of the beam encounters ice in the vertical extent of the cloud, decreasing the values of ZDR due to the nearly spherical shape of hail (Kumjian 2013a, 2013b). This results in a smaller denominator, ultimately resulting in a larger rain rate, which may be overestimating such that a positive bias is exhibited. Although the RREC relies upon several different R(Z,ZDR) algorithms, R(KDP) equations are sometimes implemented, particularly near the bright-band zone. This explains why the RREC has an overall negative number, indicating the utilization of R(KDP) algorithms were such that an overall negative bias resulted.

Table 2B.2. Statistical measures only including instances of hits to calculate bias and mean absolute error (MAE) for the St Louis (KLSX) and Kansas City (KEAX), MO radars. The best-performing algorithm is reported for its respective grouping of equations, while RREC was the only algorithm calculated not in a group.

Statistics	KLSX	KEAX
Z / DSMZ	Bias: ZConvective (-1.2) MAE: ZConvective (7.2)	Bias: ZConvective (1.2) MAE: ZConvective (9.8)
KDP / DKDP	Bias: DKDP4 (-2.2) MAE: DKDP4 (9.8)	Bias: DKDP4 (3.9) MAE: DKDP4 (13.0)
Z, ZDR	Bias: ZZDR5 (1.2) MAE: ZZDR5 (6.7)	Bias: ZZDR5 (0.54) MAE: ZZDR5 (9.5)
ZDR, KDP	Bias: ZDRDKDP3 (2.3) MAE: ZDRDKDP3 (10.5)	Bias: ZDRDKDP3 (5.9) MAE: ZDRDKDP3 (14.6)
RREC	Bias: -1.3 MAE: 7.3	Bias: 1.1 MAE: 9.7

The overall best performing algorithms for the St. Louis radar (KLSX) were R(Z)-Convective and ZZDR5 (-1.2 and 1.2 mm, respectively), with RREC (-1.3 mm) performing just as well. However, the best algorithm in terms of bias, overall, was the ZZDR5 equation for KEAX (0.54 mm), while the R(Z)-Convective equation performed similarly to KLSX (1.2 mm). Therefore, it may be concluded that the raindrop heterogeneity was similar enough that the differential reflectivity provided accurate results.

The small mean absolute errors (MAE) for both radars were, similarly, for the ZZDR5 algorithms (6.7 mm and 9.5 mm for KLSX and KEAX, respectively). Both equations which implement KDP performed the worst for both radars, with ZDRDKDP3 performing particularly inferior to the other algorithms (10.5 mm and 14.6 mm for KLSX and KEAX, respectively). The overall large bias and MAE values for algorithms containing KDP is due, mostly, to the poor performance of the specific differential phase

shift in ice (Kumjian, 2013b, 2013c; Cunha et al., 2015). Therefore, it may be concluded that the ZZDR5 algorithm performed best, overall, for both radars, whereas the algorithm performed particularly well for KEAX, similar to the results from Simpson et al. (2016).

Contingency analyses

From the 7464 hours utilized in the study, upwards of 90% of the time events recorded no precipitation (Table 2B.3). Therefore, the total number of hits, misses, and false alarms, comprise a small percentage of the total sample. Due to the thresholding imposed where a "hit" is designated such that precipitation measured by the gauge and radar were both above 0.254 mm, it was possible for algorithms within the same group to register differing number of hits, misses, and false alarms. Thus, the best performing algorithm from each group will be referenced hereafter such that R(Z) is the Z-Convective equation, and R(KDP), R(Z,ZDR) and R(ZDR,KDP) are algorithms DKDP4, ZZDR5, and ZDRDKDP3, respectively.

Overall, the KLSX algorithms registered the greatest number of hits when compared to KEAX. For KLSX, the R(Z) algorithm registered the greatest number of hits (213), with R(Z,ZDR) and R(ZDR,KDP) both registering 195 hits. Although R(KDP) and R(ZDR,KDP) had the largest bias, mean absolute error and normalized standard errors, the larger number of hits compared to the other algorithms (for KLSX) indicate that, at least in part, most the error was due to differences in magnitude errors. The RREC algorithm registered 189 hits, while R(Z,ZDR) calculated 186 hits, the lowest of any grouping of algorithms from KLSX.

Table 2B.3. Calculated contingency factors including hits, misses, false alarms (FA), and correct negatives (CN) for the St Louis (KLSX) and Kansas City (KEAX), MO radars. The calculated numbers were from the overall best-performing equations from each grouping of algorithms via Table 2B.2.

Contingency Values	KLSX		KEAX	
Z-Convective	Hits:	213	Hits:	176
	Misses:	272	Misses:	309
	FA:	190	FA:	398
	CN:	6789	CN:	6581
DKDP4	Hits:	195	Hits:	159
	Misses:	290	Misses:	326
	FA:	234	FA:	250
	CN:	6745	CN:	6729
ZZDR5	Hits:	186	Hits:	163
	Misses:	299	Misses:	322
	FA:	121	FA:	225
	CN:	6858	CN:	6754
ZDRDKDP3	Hits:	195	Hits:	159
	Misses:	290	Misses:	326
	FA:	237	FA:	249
	CN:	6742	CN:	6730
RREC	Hits:	189	Hits:	167
	Misses:	296	Misses:	318
	FA:	118	FA:	190
	CN:	6861	CN:	6789

Similar to KLSX, the Kansas City radar registered the most hits utilizing the NWS-standard R(Z) algorithm (176). However, RREC was the second-best performing algorithm in terms of the quantitative number of correct hits (167) with R(Z,ZDR) registering the next-best number of hits (163). For KEAX, R(KDP) and R(ZDR,KDP) calculated the least number of hits, possibly due to the radars' distance from the study site performing poorly during shallow, stratiform events.

Misses indicate scenarios when the terrestrial-based precipitation sensor measures precipitation such that 0.254 mm of precipitation has been collected, but the radar does

not estimate precipitation above this threshold. For many of the algorithms, apart from the number of correct negatives, the largest number of contingency factors were due to misses. This is due, at least in part, to the fact that the radars' distance from the study site is beyond 150-km. Previous studies (e.g., Kitchen and Jackson 1993; Smith et al. 1996; Ryzhkov et al. 2003) have reported the decreased detection of precipitation, particularly during the cool season, due to the primarily shallow vertical structure of clouds in comparison to the warm season. Therefore, the number of misses may be a result of the overshooting of the radar beam from such a large distance from the study area.

For the St. Louis radar, The NWS-standard R(Z) algorithm not only registered the most hits (213), but also the least number of misses (272). Conversely, R(Z,ZDR) registered the least number of hits (195), but the greatest number of misses (299) for all grouping of algorithms. This could be due to the fact that the bias for R(Z,ZDR) was approximately 0, indicating that the magnitude in precipitation estimates while utilizing R(Z,ZDR) were not large. The addition of the differential reflectivity to Z measurements may cause such a decrease in the precipitation amount, that the rain-rates become too small to account for correct hits or misses (Cunha et al., 2015). The opposite scenario may be observed for the addition of the differential reflectivity term to DKDP, whereby the number of hits and misses, for both KLSX and KEAX, remain the same. Thus, it may be concluded that ZDR has less of an effect on KDP than it does on reflectivity which may be due, at least in part, to the fact that reflectivity measurements perform better with ice at large ranges, whereas KDP has a weaker response to ice detected above the melting layer, especially during cool-season events.

The number of misses for all KEAX grouping of algorithms exceeded 300, with the lowest being the R(Z) equation (309). The RREC algorithm registered 318 misses, while R(Z,ZDR) registered 322, with the R(KDP) and R(ZDR,KDP) equations having the most number of misses (326). Similar to the KLSX equations, the addition of ZDR to reflectivity measurements cause an increase in the number of misses, and a decrease in the number of hits, while no differences were observed between R(KDP) and R(ZDR,KDP).

False alarms occur when the radar incorrectly estimates precipitation to be present, such that the ground-truthed gauge does not register any measurable rainfall. Therefore, bias may be introduced at low rainfall amounts, such that not enough precipitation has been collected to register a tip, a common error in tipping-buckets (Ciach and Krajewski, 1999; Ciach 2002). However, all radar calculated precipitation values below one tip (i.e., 0.254 mm of precipitation) were excluded from the analyses.

The least amount of false alarms, for both KLSX and KEAX were conducted by the RREC algorithm (118 and 190, respectively), with R(Z,ZDR) registering the second-least number of false alarms (121 and 225, respectively). With the number of hits, misses, and false alarms relatively close to one-another, it can be assumed that for most events, the RREC was utilizing some R(Z,ZDR) relationship. For KLSX, the R(Z) algorithm had 190 false alarms, and for KEAX the number of false alarms were the most of any algorithm for either of the radars at 398. This may be primarily due to the fact that at, approximately, 175 km from the radar, the electromagnetic radiation emitted is susceptible to the "bright-band" zone, such that reflectivity values, especially, are erroneously reported and excessively calculated (Kumjian 2013b). Therefore, the theory

that the addition of ZDR to reflectivity calculations lowers the overall rain-rate values is further verified by the 79 (149) decrease in the number of false alarms for KLSX (KEAX).

Conversely to what has been previously noted in that the addition of ZDR to KDP calculations has no effect on the contingency factors, the number of false alarms have been altered for both KLSX and KEAX. For example, the number of false alarms for KLSX for R(KDP) was 234, while for R(ZDR,KDP), was 237. Additionally, albeit by one count, the number of false alarms increased when ZDR was not included in DKDP equations for KEAX (249 in comparison to 250). Therefore, the number of correct negative decreases (increases) when ZDR is implemented into DKDP algorithms for KLSX (KEAX).

Two contingency factors have been calculated, the probability of detection (PoD) in addition to the probability of false detection (PoFD). For the St. Louis (KLSX) radar, the PoD did not exceed 0.45, indicating that no more than 45% of the precipitation events that the tipping bucket measured, was accurately estimated by the radar (Table 2B.5). The lowest probability of detection for KLSX was the R(Z,ZDR) algorithm (0.38), with the highest being R(Z) (0.44), indicating that the NWS-standard algorithm was capable of correctly detecting the greatest number of events. Algorithms R(KDP) and R(ZDR,KDP) were both equal at 0.40, and the RREC correctly detected 39% of precipitation that occurred.

For KEAX, no grouping of algorithms exceeded 0.40 for the probability of detection, indicating that, at a closer distance to the radar, KLSX correctly registered more hits than KEAX, albeit the algorithms were more consistent than KLSX. For

example, the largest PoD value for KLSX, R(Z) was 0.44, while the lowest was R(Z,ZDR) (0.38), a difference of 6%. For KEAX, the R(Z) algorithm registered 36% of correctly detected precipitation, with R(KDP) and R(ZDR,KDP) registering 33%, a 3% difference. Therefore, for the Kansas City radar (KEAX), a 3% difference in the probability of detection from R(Z) and R(ZDR,KDP) yielded an average MAE difference of 0.75 mm between the two equations, in addition to a 43% difference in the NSE.

For both KLSX and KEAX, no PoFD values exceeded 0.10, indicating that the radars could correctly assess when precipitation was not present for over 90% of the total events, or, a total of 6717 hours. Albeit the PoFD values appear to be significantly more accurate than the PoD, the PoFD calculations account for the large number of occurrences when precipitation was not measured, which accounted for, approximately, 90% of the time, whereas the PoD only accounts for instances when precipitation did occur, or, 10% of the time. Therefore, Table 2B.4 should be used in conjunction with Table 2B.3 to render a more accurate representation as to the relative number of hits, misses, false alarms, and correct negatives. However, it is important to diagnose the The correlation coefficient (CC) values describe the quantitative relationship between the time-series analysis of gauge-to-radar measurements of precipitation. A larger CC value indicates better correlation (i.e., a better agreement) between the gauge measured precipitation and the radar estimated rainfall amount. When the occurrences of false alarms and misses are included, no algorithm from either St. Louis or Kansas City had a CC value above 0.26 (Figure 2B.3). The overall difference between the CC values for KLSX and KEAX were, on average, 0.07, indicating the radar estimated precipitation from KLSX was better than for KEAX. Additionally, the best-performing algorithm was

Table 2B.4. Calculations of probability of detection (PoD) and probability of false detection (PoFD) for the St Louis (KLSX) and Kansas City (KEAX), MO radars. The calculated numbers were from the overall best-performing equations from each grouping of algorithms via Table 2B.3.

Contingency Factors	KLSX	KEAX
Z-Convective	PoD: 0.44 PoFD: 0.04	PoD: 0.36 PoFD: 0.05
DKDP4	PoD: 0.40 PoFD: 0.03	PoD: 0.33 PoFD: 0.06
ZZDR5	PoD: 0.38 PoFD: 0.02	PoD: 0.34 PoFD: 0.03
ZDRDKDP3	PoD: 0.40 PoFD: 0.03	PoD: 0.33 PoFD: 0.06
RREC	PoD: 0.39 PoFD: 0.02	PoD: 0.34 PoFD: 0.03

relative performance of the radar in accurately detecting precipitation when it did occur, and instances when the radar did not detect precipitation when the terrestrial-based sensor measured rainfall.

the R(Z) equation for both radars (0.26 and 0.17 for KLSX and KEAX, respectively), with R(KDP) performing the worst (0.24 and 0.15 for KLSX and KEAX, respectively), essentially indicating very little to no correlation exists between the radar and gauge.

When the occurrences of false alarms are excluded from the analyses, the CC values significantly ($p < 0.05$) increase for both KLSX and KEAX. In fact, for many of the algorithms, for either KLSX or KEAX, the CC values nearly double in value. The initial CC values, including both misses and false alarms for R(Z), R(KDP), R(Z,ZDR), R(ZDR,KDP), and RREC for KLSX were, respectively, 0.26, 0.24, 0.24, 0.25, and 0.24 while for KEAX, the CC values were, approximately, 0.17 0.15, 0.16, 0.15, and 0.17,

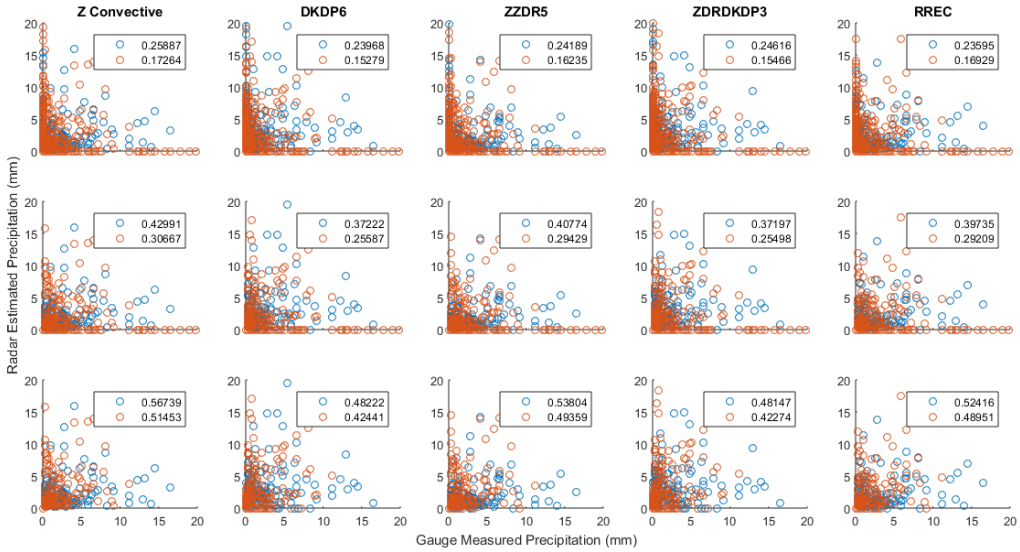

Figure 2B.4. Scatterplots of gauge estimated precipitation versus radar estimated precipitation for the five best-performing algorithms. Blue circles denote St. Louis, MO (KLSX) values while red circles indicate Kansas City, MO (KEAX) values, with correlation coefficient values recorded in the boxes of each graph. The first row of data represents all 7464 hours of data, with the second-row removing instances when the radar did not estimate precipitation but the gauge recorded rainfall, and the third row removing all instances when radar or gauge did not estimate or record precipitation.

respectively. When the false alarms were removed, the KLSX CC values increased to 0.43, 0.37, 0.41, 0.37, and 0.40, respectively, while KEAX showed an increase of CC values to 0.31, 0.26, 0.29, 0.25, and 0.29, respectively. correlation coefficient values recorded in the boxes of each graph. The first row of data represents all 7464 hours of data, with the second-row removing instances when the radar did not estimate

precipitation but the gauge recorded rainfall, and the third row removing all instances when radar or gauge did not estimate or record precipitation.

If the instances when the radar estimated no precipitation to be present but the gauge measured rainfall (i.e., misses) are further removed from the dataset, the CC values increase by an average of 0.16 for KLSX, and 0.20 for KEAX. Therefore, the last row in Figure 2B.4 represents instances when the gauge and radar both registered precipitation (hits). The best algorithm, in terms of correlation coefficient, was the R(Z) algorithm for both KLSX (0.57) and KEAX (0.51), while the worst-performing equations were R(ZDR,KDP) (0.48 and 0.42 for KLSX and KEAX, respectively). Although the difference in CC values when misses and false alarms were both included between each algorithm was relatively small, when only the hits are analyzed, the difference between the best and worst algorithms are, approximately, 10% in terms of correlation.

Quantitative analyses

Quantifying the amount of precipitation due to the number of misses (missed precipitation amount, MPA), false alarms (false precipitation amount, FPA), the overall magnitude of error (i.e., summing the mean absolute error; Error), and the amount of precipitation aggregated from each algorithm (Precip) allows for the insight into the true performance of each equation (Table 2B.5).

The missed precipitation amount correlates to the amount of precipitation due to the number of misses; the quantity reported aggregates the occurrences when the gauge recorded rainfall but the radar did not estimate precipitation. Overall, the MPA was lower

Table 2B.5. Quantitative measure of the missed precipitation amount (MPA), false precipitation amount (FPA), overall error (Error), and accumulated precipitation (Precip) for the St Louis (KLSX) and Kansas City (KEAX), MO radars. The calculated numbers were from the overall best-performing equations from each grouping of algorithms via Table 2B.2.

Quantitative Analyses	KLSX		KEAX	
R(Z)-Convective	MPA:	313.4	MPA:	459.8
	FPA:	330.9	FPA:	553.1
	Error:	1061.8	Error:	1412.5
	Precip:	729.2	Precip:	1028.8
DKDP4	MPA:	371.5	MPA:	495.3
	FPA:	703.0	FPA:	865.5
	Error:	1624.0	Error:	1859.3
	Precip:	1348.0	Precip:	1473.4
ZZDR5	MPA:	338.8	MPA:	478.2
	FPA:	235.1	FPA:	444.4
	Error:	969.6	Error:	1295.3
	Precip:	542.1	Precip:	868.4
ZDRDKDP3	MPA:	377.4	MPA:	499.9
	FPA:	634.3	FPA:	798.4
	Error:	1529.2	Error:	1764.6
	Precip:	1225.4	Precip:	1362.5
RREC	MPA:	343.9	MPA:	464.6
	FPA:	324.3	FPA:	489.4
	Error:	1088.3	Error:	1349.8
	Precip:	707.8	Precip:	962.5

for KLSX than KEAX for all algorithms by over 100 mm each. The largest differences between KLSX and KEAX were for R(Z) (146.4 mm) and R(Z,ZDR) (139.4 mm), whereas the smallest differences were from algorithms containing DKDP, potentially due to its non-degradation in quality with range (Ryzhkov and Zrnic 1995; Ryzhkov et al. 2003). For both KLSX and KEAX, the R(Z) algorithm reported the least amount of missed precipitation amount (313.4 mm and 459.8 mm, respectively), while the largest quantity of missed precipitation were for algorithms containing DKDP.

Although the number of misses for R(KDP) and R(ZDR,KDP) were more than the number of misses for R(Z,ZDR) for both KLSX, the overall magnitude in the MPA was lower for R(Z,ZDR) (338.8 mm) than for R(KDP) (371.5 mm) and R(ZDR,KDP) (377.4 mm). This indicates that, on average, for scenarios when the R(Z,ZDR) did not correctly assess precipitation were for less convective (i.e., less magnitude in rainfall) precipitation than instances when R(KDP) and R(ZDR,KDP) missed the precipitation.

For all algorithms except for KLSX RREC and both radar's R(Z,ZDR), the quantity of precipitation falsely assessed (FPA) exceeded the missed precipitation amount. For example, the R(Z) MPA for KLSX and KEAX were 313.4 mm and 459.8 mm, respectively, while the FPA were 330.9 mm and 553.1 mm, respectively. However, the R(Z,ZDR) MPA for KLSX and KEAX were, respectively, 338.84 mm and 478.2 mm, while the FPA were 235.1 and 444.4, a 103.7 mm and 33.8 mm difference, respectively. This could be due, at least in part, to the observation that the inclusion of ZDR in reflectivity calculations causes an overall decrease in the amount of false alarms which, ultimately, would correlate to overall lower missed precipitation amounts. A similar analyses can be made for the RREC algorithm which, based off of the number of hits, misses, and false alarms, invoked more instances of a R(Z,ZDR) algorithm in comparison to other algorithms.

The R(KDP) and R(KDP,ZDR) equations exhibited, approximately, twice the amount of falsely reported precipitation in comparison to the amount of precipitation missed. The FPA for KEAX R(KDP) and R(ZDR,KDP) were 865.5 mm and 798.4 mm, while the MPA were 495.3 mm and 499.9 mm, respectively. This is due, at least in part, to the fact that the number of false alarms for KEAX for equations containing the specific

differential phase shift exceeded the number of misses. Similarly, the FPA (MPA) for KLSX for R(KDP) and R(Z,ZDR) were 703.0 mm (371.5 mm) and 634.29-mm (377.3 mm), respectively. However, the number of false alarms for DKDP-containing algorithms for KLSX were less than the number of misses. This indicates that, on average, the amount of precipitation that R(KDP) and R(ZDR,KDP) falsely assessed were larger in magnitude than for instances when the radar missed precipitation. This conclusion makes physical sense, such that, typically, the radar accumulated amount of missed precipitation should be, due to shallow stratiform precipitation (i.e., low rainfall amounts). Conversely, the amount of falsely reported precipitation could be due to instances including, but not limited to, significant impact from the bright-band, excessive evaporation of precipitation, and wind drift, causing the precipitation to blow horizontally out of the MATLAB-depicted pixel of rain-gauge comparisons.

The third row in Table 2B.5, Error, indicates the amount of error associated due not only from the MPA and FPA, but also for direct hits (i.e., MAE). Therefore, the accumulated amount of MAE from each grouping of algorithms from each radar may be calculated by subtracting MPA and FPA from Error. With the exception of the R(Z,ZDR) algorithm for KLSX, all equations had an Error value above 1000 mm, exceeding the average observed amount of precipitation collected over the four gauges. However, no algorithm's total error was less than the total amount of precipitation observed (829.8 mm), with R(Z,ZDR) being the closest (969.6 mm), a 139.8 mm difference. Conversely, R(KDP) for KEAX registered 1859 mm of Error precipitation, over twice the amount observed by the gauges (NSE = 2.2; Table 2B.2).

From each radar, R(KDP) registered the most amount of Error precipitation (1623.8 mm for KLSX, and 1859.3 mm for KEAX), while R(ZDR,KDP) registered the second-most (1529.2 mm for KLSX and 1764.6 mm for KEAX). Therefore, although algorithms containing DKDP calculated more (less) hits (misses) than R(Z,ZDR) and RREC for KLSX, the increase in false alarms (approximately 100 for DKDP-containing algorithms) causing the large amount of falsely reported precipitation (FPA) in addition to the large MAE contributed to the large amount of Error observed. However, R(KDP) and R(ZDR,KDP) registered less hits and more misses than both RREC and R(Z,ZDR) for KEAX, resulting in the, overall, largest Error values between the radars.

Precip, the fourth row in Table 2B.6, represents the overall summation of detected rainfall from each algorithm for each radar. Therefore, this quantitative measure may be analyzed as the average amount of precipitation reported by the radar over the course of the study. The only two algorithms that reported less overall precipitation than the observed amount were R(Z,ZDR) (542.1 mm), RREC (707.8 mm) and R(Z) (729.2 mm) for KLSX. This is observed via Figure 2B.5, such that the pink contour (sum of Precip) is less in overall magnitude at the end of the study than the gauge accumulation precipitation amount (black contour) for the three algorithms reported above.

Per the results presented in Table 2B.5, the overall magnitude in the MPA and FPA for the R(Z) equation calculated by the KLSX radar (313.4 mm and 330.9 mm, respectively) were, approximately, the same. Therefore, the amount of precipitation missed was nearly cancelled by the amount of precipitation falsely reported. This caused the overall prediction of precipitation (including error between radar and gauge) to be, overall, relatively close to the gauge amount (underpredicted by 100.6 mm).

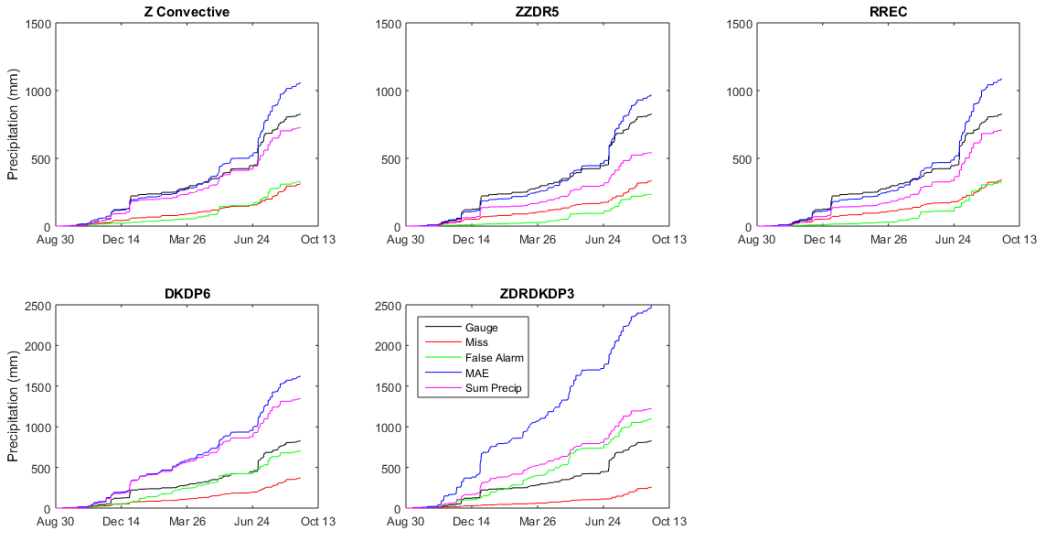

Figure 2B.5. Accumulation of the quantitative amount of precipitation based on the total number of misses (missed precipitation amount, MPA), number of false alarms (false precipitation amount, FPA), overall mean absolute error (MAE), and the overall accumulation of precipitation as recorded by the specified algorithm (Sum Precip) for St. Louis, MO (KLSX).

Similarly, the RREC for KLSX had a relatively approximate magnitude between the MPA and FPA, resulting in an overall accurate estimated accumulation of precipitation (707.8 mm), 122.0 mm less than the gauge. Due to the R(Z,ZDR) 5 KLSX algorithm registering less false alarms than R(Z) equation (121 compared to 190), the amount of missed precipitation amount (338.8 mm) exceeded the falsely reported precipitation amount (235.1 mm), causing a lower overall predicted rainfall amount, such that the overall accumulated precipitation from the radar was nearly 300-mm less than the gauge measured amount.

The algorithms containing R(KDP) for KLSX accumulated more precipitation, overall, compared to the gauge (1347.5 mm and 1225.4 mm, respectively). This is primarily due to the fact that both algorithms registered an excessive amount of error between the radar and gauge calculated, reaching MAE values in excess of 1500 mm (Figure 2B.5). Furthermore, the relatively large number of false alarms registered enough precipitation that the amount of rainfall falsely reported exceeded the gauge observed amount for R(ZDR,KDP), while R(KDP) was a few mm less than the total accumulated precipitation for RREC (703.0 mm) (Figure 2B.6).

For KEAX, all algorithms registered more accumulated rainfall than the observed gauge amount. However, the R(Z,ZDR) algorithm for KEAX calculated, overall, the most accurate precipitation amount (868.41 mm), despite having larger MPA than any other KLSX algorithm, and more FPA than R(Z), R(Z,ZDR), and RREC KLSX equations, in addition to more misses than any KLSX algorithm. Therefore, over time, the amount of error due to MPA and FPA may cancel one-another, leaving the MAE to be the main determinant of error from the radar. Due to the relatively low bias from KEAX (0.0 mm), and the fact that the accumulated precipitation amount was close to the observed amount, the MAE for KEAX R(Z,ZDR) (1.78 mm) primarily oscillated evenly between the positive and negative amounts, yielding an overall low accumulation of error over time. Therefore, depending on the purpose of one's study, one might conclude that the KEAX R(Z,ZDR) algorithm was, over the course of one year's worth of radar data, the best-performing. However, the excessive MPA and FPA, in addition to the relatively large Error values (Table 2B.5) indicates this equation may not be the best suited for daily analyses, whereas the R(Z) algorithm from KLSX, with the overall lowest MAE,

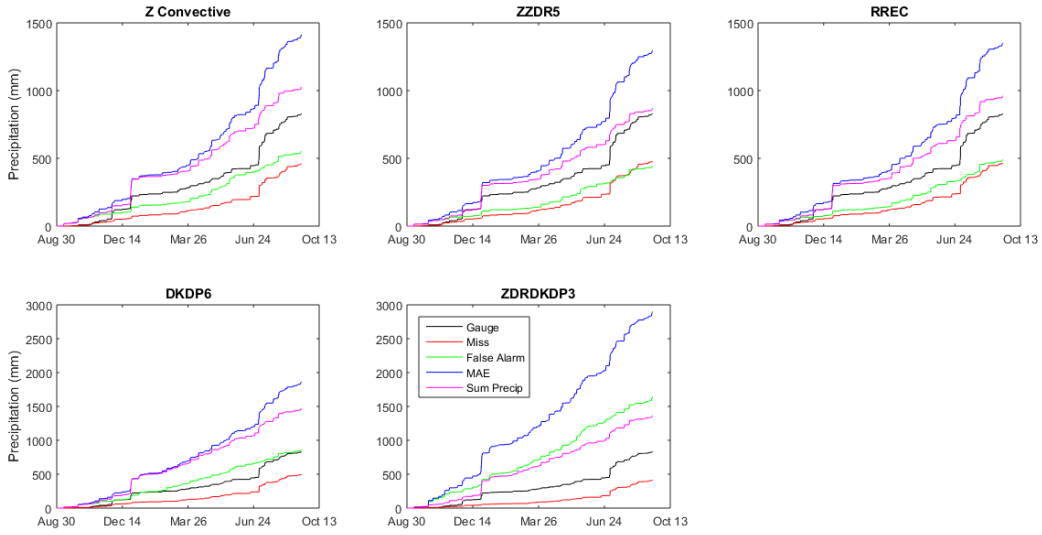

Figure 2B.6. Accumulation of the quantitative amount of precipitation based on the total number of misses (missed precipitation amount, MPA), number of false alarms (false precipitation amount, FPA), overall mean absolute error (MAE), and the overall accumulation of precipitation as recorded by the specified algorithm (Sum Precip) for Kansas City, MO (KEAX).

MPA, and Error amounts, may be more suitable. Therefore, caution is expressed depending on the overall "best" algorithm chosen for a study to be conducted, where emphasis based on the current study is to be placed on not choosing a single radar algorithm for analyses, unless a particularly best-fitting equation (either through least-linear-squared fitting or maximum likelihood regression analyses) has been derived for a particular region.

Conclusions

One years' worth of radar data has been analyzed to determine the overall performance of two National Weather Service S-band radars, St. Louis (KLSX), and Kansas City (KEAX), MO. Several measures were calculated to assess the strengths and limitations of the two radars through utilization of 55 different radar rain-rate estimation algorithms. The measures included one bias, and two unbiased statistical measurements, several contingency variables, including hits, misses, false alarms, and correct negatives, calculations of the probability of detection (PoD) and probability of false detection (PoFD), and multiple quantitative variables to determine the overall amount of precipitation missed and falsely assessed.

Overall, the conventional R(Z) algorithm was superior to other polarized algorithms in terms of the mean absolute error (MAE), but fell second-best to the R(Z,ZDR) algorithm in terms of the normalized standard error (NSE). The R(KDP) and R(ZDR,KDP) algorithms performed, overall, worst for both KLSX and KEAX, with mean absolute values above 2.0 mm. In general, it was found that the MAE and NSE both increased for KEAX, as it was further from the ground-truthed terrestrial-based precipitation gauges.

Similar to the statistical analyses, the R(Z) algorithm tended to perform superior to the other algorithms as it registered the most hits and least number of misses. However, R(Z,ZDR) calculated the least amount of false alarms for both KLSX and KEAX, while the R(Z) algorithm registered the most amount of false alarms for KEAX, potentially due to bright-banding. This, in turn, resulted in R(Z,ZDR) having the lowest PoD for KLSX, with R(KDP) and R(ZDR,KDP) having the lowest PoD values for

KEAX. Due to the relatively large sample size, the probability of false detections (PoFD) were overall low, as over 90% of the data were correct negatives for all algorithms.

The missed precipitation amount (MPA) constituted the majority of precipitation error for R(Z,ZDR) and RREC for KLSX, while only R(Z,ZDR) was larger in MPA than the false precipitation amount (FPA) for KEAX. These low FPA amounts for R(Z,ZDR) are a result of the low number of false alarms reported in the contingency analyses. Conversely, due to the relatively high number of false alarms reported by algorithms containing DKDP (e.g., DKDP6 and ZDRDKDP3), the FPA was often twice as large as the MPA. This lead to excessive overall errors and overall precipitation accumulation for these DKDP-containing algorithms.

The current study furthers understanding of the strengths and limitations of the utilization of dual-polarized algorithms versus the conventional equations overall. This information is important for the utilization of radar rain rate estimates to be ingested into hydrologic models to be utilized for flood forecasting, a field that is becoming a popular means of hydrologic analyses (Ogden et al., 2000; Gourley et al., 2010; Berne and Krajewski, 2013). In part II of this series of papers, in-depth analyses will determine whether any significant difference ($p < 0.05$) exist between algorithm performances during the warm or cool seasons. The implications in Part II will determine whether it is beneficial to switch between different algorithms based on the seasonality and, thus, main type of precipitation present to more accurately estimate precipitation amounts.

Acknowledgements

This material is based upon work supported by the National Science Foundation under Award Number IIA-1355406. Any opinions, findings, and conclusions or recommendations expressed in this material are those of the authors and do not necessarily reflect the views of the National Science Foundation.

Literature cited

Berne, A., and Krajewski, W.F., 2013: Radar for hydrology: Unfulfilled promise or unrecognized potential? *Adv. Water Resour.*, **51**, 357-366.

Beard, K.V., and Chuang, C., 1987: A new model for the equilibrium shape of raindrops. *J. Atmos. Sci.*, **44**, 1509-1524.

Chandrasekar, V., Bringi, V., Balakrishnan, N., and Zrnic, D.S., 1990: Error structure in multiparameter radar and surface measurements of rainfall. Part III: Specific differential phase. *J. Atmos. Oceanic Tech.*, **7**: 621-629.

Chandrasekar, V., Gorgucci, E., and Scarchilli, G., 1993: Optimization of multi-parameter radar estimates of rainfall. *J. Appl. Meteor.*, **32**: 1288-1293.

Chandrasekar, V., Meneghini, R., and Zawadzki, I., 2003: Global and local measurement of precipitation by radars. *Radar and Atmospheric Science: A Collection of Essays in Honor of David Atlas, Meteorology Monograms*, **30**: 215-236.

Ciach, G.J., and Krajewski, W.F., 1999: On the Estimation of Radar Rainfall Error Variance. *Adv. Water Res.*, **22**, 585-595.

Ciach, G.J., 2002: Local Random Errors in Tipping-Bucket Rain Gauge Measurements. *J. Atmos. Oceanic Technol*., **20**, 752-759.

Cifelli, R., Chandrasekar, V., Lim, S., Kennedy, P.C., Wang, Y., and Rutledge, S.A., 2010: A new dual-polarization radar rainfall algorithm: Application in Colorado precipitation events. *J. Atmos. Oceanic Tech.*, **28**: 352-364.

Cunha, L.K., Smith, J.A., Baeck, M.L., and Krajewski, W.F., 2013: An early performance of the NEXRAD dual-polarization radar rainfall estimates for urban flood applications. *Wea. Forecasting*, **28**, 1478-1497.

Cunha, L.K., Smith, J.A., Krajewski, W.F., Baeck, M.L., and Seo, B., 2015: NEXRAD NWS polarimetric precipitation product evaluation for IFloods. *J. Appl. Meteor.*, **16**, 1676-1699.

Giangrande, S.E. and Ryzhkov, A.V., 2008: Estimation of rainfall based on the results of polarimetric echo classification. *J. Appl. Meteor.*, **47**, 2445-2460.

Gourley, J.J., Giangrande, S.E., Hong, Y., Flamig. Z,, Schuur, T., and Vrugt, J., 2010: Impacts of polarimetric radar observations on hydrologic simulation. *J. Hydrometeorol.*, **11**: 781-796.

Habib, E., Krajewski, W.F., Nespor, V., and Kruger, A., 1999: Numerical simulation studies of rain gauge data correction due to wind effect. *J. Geophys. Res.*, **104**, 723–734.

Habib, E., Aduvala, A.V., and Meselhe, E.A. 2008a: Analysis of radar-rainfall error characteristics and implications for streamflow simulation uncertainty. *Hydrol. Sci. J.*, **53**: 568-587.

Habib, E., Malakpet, G., Tokay, A., and Kucera, P.A., 2008b: Sensitivity of streamflow simulations to temporal variations and estimation of Z-R relationships. *J. Hydrol. Eng.*, **13**: 1177-1186.

Hubbart, J.A., and Zell, C., 2013: Considering streamflow trend analyses uncertainty in urbanizing watersheds: A case study in the Central U.S. *Earth Interact.*, **17**: 1-28.

Hubbart, J.A., Kellner, E., and Freeman, G., 2014a: A case study considering the comparability of mass and volumetric suspended sediment data. *Environ. Earth Sci.*, **71**: 4051-4060.

Hubbart, J.A., Kellner, E., Hooper, L., Lupo, A.R., Market, P.S., Guinan, P.E., Stephan, K., Fox, N.I., and Svoma, B.M., 2014b: Localized Climate and Surface Energy Flux Alterations across an Urban Gradient in the Central U.S. *Energies*, ***7***: 1770-1791.

Kitchen, M. and Jackson, P.M., 1993: Weather radar performance at long range – simulated and observed. *J. Appl. Meteor.*, **32**, 975-985.

Kumjian, M.R., 2013a: Principles and applications of dual-poarization weather radar. Part 1: Description of the polarimetric radar variables. *J. Operational Meteor.*, **1**, 226-242.

Kumjian, M.R., 2013b: Principles and applications of dual-poarization weather radar. Part 2: Warm and cold season applications. *J. Operational Meteor.*, **1**, 243-264.

MATLAB and Statistics Toolbox Release 2016a, The MathWorks, Inc., Natick, Massachusetts, United States.

Ogden, F.L., Sharid, H.O., Senarath, S.U.S., Smith, J.A., Baeck, M.L., and Richardson, J.R., 2000: Hydrologic analysis of the Fort Collins, Colorado, flash floods of 1997. *J. Hydrol.*, **228**: 82-100.

Roebber, P.J., 2009: Visualizing multiple measures of forecast quality. *Wea. Forecasting*, **24:** 601–608.

Ryzhkov, A.V., Schuur, T., and Zrnic, D.S., 2001: Testing a polarimetric rainfall algorithm and comparison with a dense network of rain gauges. *Proceedings of the Fifth International Symposium of Hydrological Applications of Weather Radar*, Kyoto, Japan, 159-164.

Ryzhkov, A.V., Giangrande, S., and Schurr, T., 2003: Rainfall measurements with the polarimetric WSR-88D radar. National Severe Storms Laboratory Rep. Norman: OK, 98 pg.

Ryzhkov, A.V., Giangrande, S., and Schurr, T., 2005: Rainfall estimation with a polarimetric prototype of WSR-88D. *J. Appl. Meteor.*, **44**, 502–515.

Simpson, M.J., Hubbart, J.A., and Fox, N.I., 2016: Ground truthed performance of single and dual-polarized radar rain rates at large ranges. *Hydrol. Process.*, **30**, 3692-3703.

Sachidananda, M., and Zrnic, D.S., 1987: Rain-rate estimates from differential polarization measurements. *J. Atmos. Oceanic Tec*., **4**: 588-598.

Schilling, W., 1991: Rainfall data for urban hydrology: What do we need? *Atmos. Res.*, **27**: 5-21.

Seo, D.J., Breidenbach, J., Fulton, R., Miller, D., and O'Bannon, T., 2000: Real-time adjustment of range-dependent biases in WSR-88D rainfall estimates due to nonuniform vertical profile of reflectivity. *J. Hydrometeorol.*, **1:** 222 – 240.

Seo, B., Brenda, D., Krajewski, W.F., Rutledge, S.A., and Petersen, W., 2015: Comparison of Single- and Dual-polarization-based rainfall estimated using NEXRAD data for the NASA Iowa flood studies project. *J. Hydrometeorol.*, **16**: 1658-1675.

Stephenson, D.B., 2000: Use of the "odds ratio" for diagnosing forecast skill. *Wea. Forecasting*, **15**: 221-232.

Smith, J.A., Seo, D.J., Baeck, M.L., and Hudlow, M.D., 1996: An intercomparison study of NEXRAD precipitation estimates. *Water Resour. Res.*, **32**, 2035-2045.

Vieux, B.E., and Bedient, P.B., 2004: Assessing urban hydrologic prediction accuracy through event reconstruction. *J. Hydrol.*, **299**: 217-236.

Villarini, G., and Krajewski, W.F., 2010: Review of the different sources of uncertainty in single polarization radar-based estimates of rainfall. *Surv. Geophys.*, **31**: 107-129.

Wang, Y., and Chandrasekar, V., 2010: Quantitative precipitation estimation in the CASA X-band dual-polarization radar network. *J. Atmos. Oceanic Tech.*, **27**: 1665-1676.

Yang, D.W., Koike, T., and Tanizawa, H., 2004: Application of a distributed hydrological model and weather radar observations for flood management in the upper Tone River of Japan. *Hydrol. Process.*, **18**: 3119-3132.

Zrnic, D.S., and Ryzhkov, A.V., 1996: Advantages of rain measurements using specific differential phase. *J. Atmos. Oceanic Tech.*, **13**, 454-464.

YEARLY ANALYSES OF TWO DISTANT DUAL-POLARIZED RADAR PERFORMANCES PART II: SEASONAL ANALYSES

Abstract. The performance of S-band polarimetric radars have been well documented over the past decade. However, the long-term performance of such instruments has not been thoroughly investigated. Furthermore, seasonal analyses into the precision and accuracy of the Next Generation Radar system is virtually nonexistent. The current study assesses one year's worth of radar data from St. Louis (KLSX) and Kansas City (KEAX) to determine whether conventional and polarized radar algorithms perform preferentially during the warm or cool season. Data were separated nearly uniformly between the seasons, and were assessed by several tipping bucket gauges. Results indicate that the further radar from the study site, KEAX, by 25 km, was outperformed by KLSX in terms of statistical, contingency, and quantitative analyses. However, the cool season results tend to outperform the warm season results. This could be due, at least in part, to the relatively large missed and false precipitation amounts during the summer (i.e., larger variability), in addition to potential bright-banding effects. Furthermore, the cool season for this particular study was unseasonably warm, indicating deeper clouds and possible convection could have occurred, decreasing the number of misses and false alarms. In general, the conventional R(Z)-Convective equation outperformed all other algorithms, while an R(Z,ZDR) equation performed particularly well in the cool season, indicating a seasonal preference in algorithm choice may exist. R(KDP) and R(ZDR,KDP) algorithms tend to perform poorly overall. Results further understanding of the performance of the Weather Surveillance Doppler – 1988 radar system, especially in terms of precision and accuracy between different seasons.

Introduction

In the previous work of this dissertation (Simpson and Fox 2017a), 7464 hours of radar precipitation data were analyzed from St. Louis (KLSX) and Kansas City (KEAX) over the central Missouri region over the course of 311 days. Fifty-five algorithms, primarily from Ryzhkov et al. (2003, 2005) which consisted of three R(Z), six R(KDP), five R(Z,ZDR), and four R(ZDR,KDP) equations, several KDP-smoothed combinations of reflectivity (DSMZ), differential reflectivity (DZDR), and the specific differential phase shift (DKDP), in addition to a rain-rate echo classification (RREC) algorithm were implemented to estimate rainfall rates. The average gauge-measured rainfall amount equaled 818.64 mm, with no algorithm having a normalized standard error (NSE) value less than 60%. Furthermore, no algorithm from KEAX had an NSE value less than 100%, indicating that the overall error, including instances when the radar estimated precipitation but the gauge recorded none and when the radar estimated no rainfall but the gauge recorded rainfall, was more than the observed (i.e., terrestrial-based tipping bucket) amount.

Part II of this study will focus on separating the overall yearly analyses into seasons (warm and cool) for further investigation. Although many studies have been conducted on dual-polarization radars, relatively few studies have investigated the warm and cool season differences between quantitative precipitation estimates (QPE). One of the earliest studies of seasonal radar analyses was conducted by Smith et al. (1996) in Oklahoma from the Twin Lakes (KTLX) and Tulsa (KINX) radars. It was discovered that underestimation of precipitation compared to rain gauges occurred beyond 150 km (100 km) from the radar during the warm (cool) season due to incomplete beam filling in

addition to overshooting of the radar beam. The warm season range was larger than the cool season since convection is more likely during the summer, extending the vertical structure of storm systems and, thus, increasing the range at which the radars can detect precipitation. Overall, for the warm season, the probability of detection (POD) was relatively constant up to the 230 km distance from the radar, whereas in the cool season POD decreased with range. However, anomalous propagation and bright-band contamination can cause overestimation of precipitation between 50-100 km from the radar, especially for the cool season (Seo et al., 2000). The overall analyses from the study determined that the Weather Surveillance Radar 1988-Doppler (WSR—88D) were far superior to the dense rain gauge network, such that large convective storms were not detected by the gauge-system.

Upgrading from single-polarized to dual-polarized radar technology, Ryzhkov et al. (2003) conducted a study of the Norman, OK (KOUN) radar to determine performance as a function of range in addition to seasonal effects. It was noted that the polarimetric algorithms outperform the conventional (i.e., single-polarized) algorithm, although the selected spring events were dominated by heavy rain, potentially skewing the results in favor of the polarimetric equations. Furthermore, these polarimetric algorithms tended to outperform the conventional algorithm in terms of root mean square error (RMSE) up to 200 km from the radar. The cool season, primarily associated with shallow stratiform events, revealed that the R(KDP) algorithm performed best, especially in instances when the bright band was located within the lowest elevation scan of the radar. Conversely, for the warm season, the synthetic R(Z,ZDR,KDP) algorithm performed best at all ranges. However, the performance of the R(KDP) algorithm was

inferior and underestimated precipitation which could be due, at least in part, to negative KDP values due to partial beam filling. For these instances, R(Z,ZDR) algorithms were shown to work better. The authors found that, overall, the polarimetric algorithms performed better than the conventional R(Z) equations within 125 km from the radar, while the results were increasingly nebulous as the distance increased beyond 125 km, and particularly beyond 200 km from the radar.

The main objective of the current study is to expand on Part I of this series of articles by analyzing the performance of one year of radar data, divided between warm and cool seasons, from the St. Louis (KLSX) and Kansas City (KEAX) radars over central Missouri, approximately 175 km from each radar. An assessment into whether a significant difference ($p < 0.1$) exists in the performance of the National Weather Service (NWS) Next Generation Radar (NEXRAD) system between the warm and cool seasons provides insight as to whether specific algorithms are superior during different times of the year. This has a potentially significant impact on the estimation of timing and intensity of storms, especially over regions that lie far from the NEXRAD radars.

Methodology

Study site and data

Many areas within the CONUS lie beyond 150 km of the nearest WSR-88D. One such location is Columbia, MO, residing, approximately, equidistance between Kansas City, MO, and St. Louis, MO. The WSR-88D's that exist at each location are KEAX, at Pleasant Hill, MO, and KLSX, at St. Louis, MO (Figure 1). The area of interest is within the vicinity of the Hinkson Creek watershed, located in the center of Boone County, MO.

The catchment and the surrounding areas are equipped with several Campbell Scientific tipping buckets, TE525M series, such that these rain gauges may serve as the ground-truth values of precipitation for the study. For a detailed discussion on the tipping bucket data, please refer to Figure 2B.1.

The TE525 series performs optimally in the range of temperatures between 0 and 50°C. Seventy-three days were recorded as having minimum temperatures below the optimal temperature threshold (i.e., 0°C) while no days exceeded 30°C, indicating the upper-bound of temperature was not breached. Therefore, a bias in tipping-bucket measurements may exist for the cool season, such that underrepresentation of precipitation due to poor performance from the gauges (Villarini and Krajewski, 2010). To mitigate this potential error, the average precipitation amount for each gauges were taken, such that, over the course of summer and winter, no significant difference existed between precipitation amount for each of gauges whereby a 1-way ANOVA was conducted with an F-value of 0.11, mean-square-error of 0.82, and p-value of 0.9562.

Radar data were acquired from the National Climatic Data Center (NCDC) Hierarchal Data Storage System (HDSS) accessed via the National Centers for Environmental Information (NCEI) Archive Information Request System (AIRS). Level-II NEXRAD data were obtained in .netcdf format, and processed with the Weather Decision Support System-Integrated Information (WDSS-II) programme (Lakshmanan et al., 2007). For a further detailed description of how the radar data were processed, please refer to the previous work, under the methodology section. Furthermore, three conventional algorithms (Z-Stratiform, Z-Convective, and Z-Tropical) were calculated, in addition to several R(KDP), R(Z,ZDR) and R(ZDR,KDP) algorithms, including all

combinations of DSMZ, DZDR, and DKDP. The radar data used herein is described in detail in the previous work It was shown that the following algorithms performed the best and are used for the remainder of this analysis:

$$R(Z) = 0.0033Z^{0.714} \tag{2C.1}$$

$$R(KDP) = 47.3 \mid KDP \mid^{0.791} \tag{2C.2}$$

$$R(Z, ZDR) = 144Z^{0.761}ZDR^{-1.51} \tag{2C.3}$$

$$R(ZDR, KDP) = 52.9 \mid KDP \mid^{0.852} \; ZDR^{-0.53} \tag{2C.4}$$

Warm and Cool Season Definition

Missouri has a continental type of climate, marked by strong seasonality. Due to its inland location and lack of proximity to large bodies of water, Missouri is subject to frequent changes in temperature. In terms of moisture, winter months are typically characterized by cool and humid, such that frequent snowfall and rainfall events are observed. Conversely, the summer months are, depending on La Niña or El Niño conditions, characterized by warm, moist air masses that produce copious convective events and, thus, heavy rainfall, or prolonged high pressures producing prolonged drought periods, respectively.

All of Missouri experiences freezing temperatures every year. In winter, there are an average of 110 days with temperatures below 0°C for the majority of state, whereas the number of freezing days reduces to, approximately, 70 in the southeast bootheel region. Therefore, the warm and cool seasons were defined from an agronomic perspective, such that phenology and freeze probabilities are considered over a 30-year

period for Missouri. From 1986 to 2016, the only month with a mean average temperature below 0°C was January, while February and December averages 0.83 and 0.55°C, respectively. Furthermore, March and November registered average temperatures of 6.5°C. Therefore, the months from 01 November 2015 through the 31 March 2016 were indicated as the "cool" season, while 01 August 2015 through 31 October 2015, and 01 April 2016 through 01 August 2016 were considered as the "warm" season. From the radar data collected, there were a total of 311 days (7464 hours), of which 162 and 149 days, or, 3888 and 3576 hours of data analyzed for the warm and cool seasons, respectively (Figure 2C.1).

Statistical analyses

The statistical analyses in this work follow those conducted via part I of this study. These include a statistical section (bias, mean absolute error (MAE), and normalized standard error (NSE), a contingency analysis (hits, misses, false alarms, probability of detection (PoD), and probability of false detection (PoFD)), in addition to a quantitative description of the performance of equations 2C.1 – 2C.4 which include the missed precipitation amount (MPA), false precipitation amount (FPA), and total precipitation error.

Results and discussion

Statistical analyses

The warm season data were separated into two periods, 01 August 2015 through 31 October 2015, and 01 April 2016 through 01 August 2016. In total, there was 547.1 mm

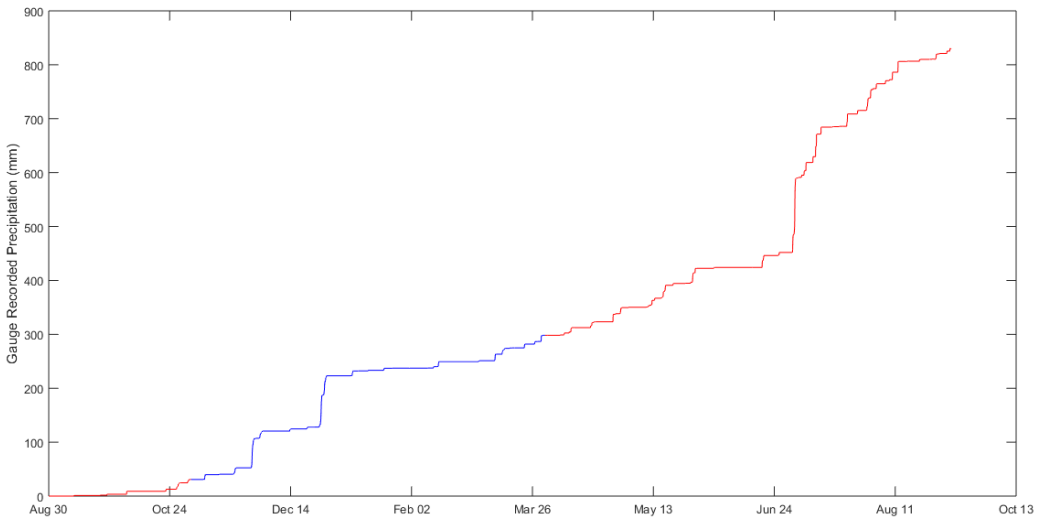

Figure 2C.1. Accumulation of precipitation for the study period based on the averages of the four terrestrial-based tipping buckets. The cool season is represented by the blue line, whereas the warm season is represented by the red line.

of precipitation recorded, with 3888 hours, or, 162 days analyzed. The best algorithms from each grouping were the R(Z)-Convective, DKDP4, ZZDR5, ZDRDKDP3, similar to those in Simpson and Fox (2017).

For the St. Louis (KLSX) data, the R(Z) algorithm tend to underestimate precipitation, with bias values of -0.4 and -0.2 mm for the summer and winter, respectively (Table 2C.1). Additionally, the R(Z,ZDR) algorithm underestimated the overall precipitation amount, but was more consistent between the warm and cool season (-0.1 mm for both warm and cool season). This contrast in bias values may be due, at least in part, to the differential reflectivity (ZDR) reducing the extremes of the reflectivity values (Kumjian, 2013a) in addition to the ability of ZDR to analyze the overall crystal

Table 2C.1. Statistical measures of bias, mean absolute error (MAE), and the normalized standard error (NSE) for the St Louis (KLSX) and Kansas City (KEAX), MO radars. The best-performing algorithm is reported for its respective grouping of equations, while RREC was the only algorithm calculated not in a group.

Algorithm	KLSX				KEAX			
	Warm Season		Cool Season		Warm Season		Cool Season	
ZConvective	Bias:	-0.4	Bias:	-0.2	Bias:	0.1	Bias:	0.5
	MAE:	2.1	MAE:	1.0	MAE:	2.2	MAE:	1.6
	NSE:	141.8	NSE:	100.0	NSE:	182.3	NSE:	172.2
DKDP6	Bias:	0.1	Bias:	0.5	Bias:	0.3	Bias:	1.3
	MAE:	3.2	MAE:	1.6	MAE:	3.1	MAE:	2.2
	NSE:	164.8	NSE:	161.0	NSE:	193.9	NSE:	255.7
ZZDR5	Bias:	-0.1	Bias:	-0.1	Bias:	0.2	Bias:	0.4
	MAE:	2.5	MAE:	1.1	MAE:	2.7	MAE:	1.7
	NSE:	127.4	NSE:	94.9	NSE:	160.9	NSE:	162.9
ZDRDKDP3	Bias:	0.1	Bias:	0.5	Bias:	0.4	Bias:	1.4
	MAE:	3.2	MAE:	1.7	MAE:	3.1	MAE:	2.3
	NSE:	163.3	NSE:	166.6	NSE:	196.2	NSE:	269.5
RREC	Bias:	0.5	Bias:	0.1	Bias:	0.5	Bias:	0.8
	MAE:	3.2	MAE:	1.3	MAE:	3.1	MAE:	2.0
	NSE:	182.0	NSE:	118.8	NSE:	194.1	NSE:	192.0

type (Vivekanandan et al., 1994; Ryzhkov et al., 1998; Wolfe and Snider 2012) which is a major source of uncertainty in QPE. The algorithms containing DKDP saw a sharp increase in bias when the cool season was analyzed while the opposite was observed for the RREC. Since the RREC tends to utilize more R(Z,ZDR) algorithms, the large convective events during the summer will cause the ZDR values to increase and, thus, promote larger rain rates. However, overestimation is apparent with the echo classification's utilization of the polarized-algorithm. Conversely, the increase in KDP and, therefore, DKDP, has been similarly observed to be sensitive to shallow, low precipitation events, especially during the cool season (Ryzhkov et al. 2003; Kumjian 2013a, b).

The Kansas City (KEAX) radar is, approximately, 25 km further from the gauge locations in comparison to the location of the St. Louis (KLSX) radar (Figure 2B.1). Therefore, the effects of range on radar performance should be amplified through the analyses. Opposed to the KLSX analyses, no algorithm reported a negative bias for either the warm or cool season (Table 2C.1). However, the values of bias for R(Z) and R(Z,ZDR), 0.1 mm and 0.2 mm, respectively, were close to zero, and were the smallest overall for KEAX. Similar to KLSX, the RREC registered the largest bias (0.5 mm), but the R(KDP) and R(ZDR,KDP) algorithms registered relatively high bias values (0.3 mm and 0.4 mm, respectively). However, the cool season bias values were largest between either radar or season. Furthermore, the R(ZDR,KDP) algorithm had a bias of 1.4 mm, while the R(ZDR,KDP) algorithm had a bias of 1.3 mm. Conversely, the smallest cool season bias for KEAX was R(Z,ZDR) (0.4 mm).

The largest warm season mean absolute errors were for RREC (3.2 mm), with R(KDP) and R(ZDR,KDP) with 3.2 mm and 3.2 mm, respectively. The lowest MAE for the warm season was the R(Z) equation (2.1 mm), which was also the lowest for the cool season (1.0 mm) for KLSX. However, the RREC was in the middle in terms of performance (1.3 mm), while R(ZDR,KDP) performed the worst, overall (1.7 mm). Mean absolute error (MAE) values, across all algorithms for KLSX, decreases by approximately 50% from warm to cool season. This could be due, at least in part, to the fact there was 58% less precipitation measured by the gauges in the cool season.

The only two algorithms calculated from the KEAX radar which outperformed rain rate estimates from KLSX were R(KDP) and RREC during the warm season (by 0.1 mm and 0.06 mm, respectively) in terms of the mean absolute error (MAE). Otherwise,

all algorithms performed worse for KEAX when comparing both warm and cool seasons to KLSX. For example, the MAE for KLSX (KEAX) for the warm and cool seasons were 2.1 mm (2.2 mm) and 1.0 mm (1.6 mm), respectively. There was a similar pattern to the St. Louis radar such that the cool season MAE values all outperformed the warm season MAE values. The largest difference between the seasonality in terms of mean absolute error was for RREC, calculating a 1.16 mm difference, whereas the smallest difference was R(Z) at 0.60 mm.

The normalized standard error aids in accounting for the discrepancy in precipitation amount between the seasons. The only algorithm calculated from the St. Louis data that had a higher NSE for the cool season was the R(ZDR,KDP) algorithm, increasing from 163.3% to 166.6%. Furthermore, R(KDP) also had a slight difference between warm and cool season NSE: 3.8%, with R(KDP) decreasing by 3.8% from the warm to cool seasons. Conversely, the other three algorithms (R(Z), R(Z,ZDR), and RREC) showed a significant ($p < 0.1$) difference between the warm and cool season NSE values. This indicates that the cool season R(Z,ZDR) algorithm (NSE = 94.9) was the most accurate in terms of least amount of overall error between the radar and gauge measurements.

Similar to KLSX, the NSE values were all smaller for the cool season opposed to the warm season. Furthermore, the difference between warm and cool season for R(Z), R(Z,ZDR), and RREC were relatively small, with values of 10.1, 1.9, and 2.1%, respectively. Conversely, the differences exhibited by R(KDP) and R(ZDR,KDP) were 61.8 and 73.3%, respectively. Overall, the largest NSE values were the KEAX cool

season R(ZDR,KDP) (269.5%) and R(KDP) (255.7%) algorithms, indicating that the performance of KDP (and, thus, DKDP) decreases as range from the radar increases.

Similar to chapter 2, the bias and mean absolute error values were calculated based on hits only, such that the overall performance of each algorithm relative to the gauge-recorded amount of precipitation was analyzed (Table 2C.2).

In general, algorithms containing the specific differential phase shift had the lowest bias for the warm season KLSX data (-0.2 and 0.5 mm for R(KDP) and R(ZDR,KDP), respectively), whereas R(KDP) and R(ZDR,KDP) were the worst performing algorithms for the warm (0.9 and 1.5 mm) and cool season for KEAX (3.2 and 4.2 mm, respectively). Despite the R(ZDR,KDP) algorithm performing worst in terms of bias for the cool KLSX data (2.2 mm), R(Z,ZDR) was the second-worst performing algorithm (-1.5 mm), while R(KDP) had a bias value of 1.3 mm. On average, the R(Z,ZDR) performed the worst in terms of bias for the St. Louis radar, but outperformed both R(KDP) and R(ZDR,KDP) in terms of the mean absolute error. For example, the MAE for R(KDP) and R(ZDR,KDP) for the warm season KLSX data were 4.1 and 4.3 mm, respectively, whereas the MAE for R(Z,ZDR) was 3.2, second-best only to the conventional R(Z) equation (3.0 mm). Similarly, for the cool season KLSX radar, R(KDP) and R(ZDR,KDP) bias values were 2.3 and 2.6 mm, while R(Z,ZDR) was 1.5 mm, slightly worse than both the R(Z) and RREC algorithm (both 1.4 mm). Therefore, it could be summarized that the precision of KDP values were best for the KLSX warm season (i.e., lowest bias of the five grouping of algorithms), but the accuracy suffered the worst (overall highest MAE).

Table 2C.2. Statistical measures of only including instances of hits to calculate bias and mean absolute error (MAE) for the St Louis (KLSX) and Kansas City (KEAX), MO radars. The best-performing algorithm is reported for its respective grouping of equations, while RREC was the only algorithm calculated not in a group.

Algorithm	KLSX				KEAX			
	Warm Season		Cool Season		Warm Season		Cool Season	
ZConvective	Bias:	-2.3	Bias:	-0.5	Bias:	-0.3	Bias:	1.7
	MAE:	3.0	MAE:	1.4	MAE:	2.8	MAE:	2.3
DKDP6	Bias:	-0.2	Bias:	1.3	Bias:	0.9	Bias:	3.2
	MAE:	4.1	MAE:	2.3	MAE:	3.8	MAE:	3.0
ZZDR5	Bias:	-3.5	Bias:	-1.5	Bias:	-0.5	Bias:	1.7
	MAE:	3.2	MAE:	1.5	MAE:	2.9	MAE:	2.4
ZDRDKDP3	Bias:	0.5	Bias:	2.2	Bias:	1.5	Bias:	4.2
	MAE:	4.3	MAE:	2.6	MAE:	4.0	MAE:	3.9
RREC	Bias:	-1.7	Bias:	-1.1	Bias:	0.9	Bias:	1.5
	MAE:	3.5	MAE:	1.4	MAE:	3.3	MAE:	2.2

The conventional R(Z) equation tended to display the lowest mean absolute error across both radars for the warm season (3.0 and 2.8 mm for KLSX and KEAX, respectively). Results coincide with Simpson et al. (2016) such that the KEAX data outperformed the KLSX data, but only for the warm season. Conversely, the cool season KLSX data was superior to the KEAX MAE values (1.4 and 2.3 mm, respectively). However, the RREC performed equally as well as the R(Z) equation cool season KLSX data in terms of MAE (1.4 mm), but its overall bias was -0.6 mm less than R(Z). Conversely, the RREC was the best performing algorithm for the cool season KEAX data in terms of bias (1.5 mm) and MAE (2.2 mm).

Contingency analyses

The four contingency variables calculated were hits, misses, false alarm (FA),

and correct negatives (CN). Across all grouping of algorithms, the number of hits were larger for the cool season rather the warm season (Table 2C3.). This could be due, at least in part, to the unseasonably warm winter that Missouri registered for the 2015-2016 year, such that the typical shallow stratiform snow bands were more vertical than normal, allowing for the radar to register more hits. The KLSX R(Z) equation and RREC registered the most amount of hits for the warm season (86 and 85, respectively), while the KLSX R(Z) equation registered 115 hits, the most for the cool season. Similarly, the conventional R(Z) algorithm had the most number of hits for KEAX (93), but R(KDP) and R(ZDR,KDP) (both 88) were relatively close to the number of hits calculated by R(Z,ZDR) (89). Overall, the two DKDP-containing algorithms had the least amount of hits (71 and 89 for both during the warm and cool season, respectively) for the St. Louis radar, while RREC registered the least amount of hits for KEAX (84). The range in the number of registered hits was lower for KEAX than KLSX, which may be an indication that at large distances from the radar (near 200 km), the overall performance of a particular rain rate algorithm is limited.

Conversely, the number of misses for the warm season were larger than the number of misses for the cool season for both radars. This indicates that the radars were more accurate in estimating cool season storms than the warm season, which could be due to the relatively small number of vertical convective storms normally observed during the summer months during 2016. Similar to the hit counts, the ZConvective and RREC registered the least number of misses (121 and 122, respectively), while the ZConvective had the least number of misses for the cool season (94) for St. Louis. Generally, the range of the cool season number of hits for KEAX were smaller than that

Table 2C.3. Calculated contingency factors including hits, misses, false alarms (FA), and correct negatives (CN) for the St Louis (KLSX) and Kansas City (KEAX), MO radars. The calculated numbers were from the overall best-performing equations from each grouping of algorithms.

Contingency Values	KLSX				KEAX			
	Warm Season		Cool Season		Warm Season		Cool Season	
R(Z)-Convective	Hits:	86	Hits:	115	Hits:	71	Hits:	93
	Misses:	121	Misses:	94	Misses:	136	Misses:	116
	FA:	164	FA:	113	FA:	221	FA:	129
	CN:	3517	CN:	3254	CN:	3460	CN:	3238
DKDP6	Hits:	71	Hits:	89	Hits:	56	Hits:	88
	Misses:	136	Misses:	120	Misses:	151	Misses:	121
	FA:	78	FA:	110	FA:	146	FA:	158
	CN:	3603	CN:	3257	CN:	3535	CN:	3209
ZZDR5	Hits:	75	Hits:	106	Hits:	61	Hits:	89
	Misses:	132	Misses:	103	Misses:	146	Misses:	120
	FA:	76	FA:	67	FA:	122	FA:	97
	CN:	3605	CN:	3300	CN:	3559	CN:	3270
ZDRDKDP3	Hits:	71	Hits:	89	Hits:	57	Hits:	88
	Misses:	136	Misses:	120	Misses:	150	Misses:	121
	FA:	77	FA:	111	FA:	147	FA:	158
	CN:	3604	CN:	3256	CN:	3534	CN:	3209
RREC	Hits:	85	Hits:	105	Hits:	66	Hits:	84
	Misses:	122	Misses:	104	Misses:	141	Misses:	125
	FA:	105	FA:	63	FA:	138	FA:	90
	CN:	3576	CN:	3304	CN:	3543	CN:	3277

of the number of misses for KLSX. For example, the largest (smallest) number of misses for KEAX and KLSX were RREC at 125 (R(Z) at 116) and R(KDP) and R(ZDR,KDP) at 120 (R(Z) at 94).

The R(Z,ZDR) algorithm registered the smallest number of false alarms for the warm season (76), similar to R(ZDR,KDP) (77) and R(KDP) (78) at KLSX. Despite these algorithms performing relatively poorly in terms of the number of hits and misses, polarized algorithms are beneficial for discriminating between false echoes as evidenced by the low false alarm count, especially for the warm season. The conventional R(Z)

algorithm had the most amount of false alarms (164 for KLSX and 221 for KEAX), potentially due to bright-band contamination, leading to overexaggerating reflectivity values and, thus, large amount of precipitation erroneously estimated (Elmore, 2011). The overall number of false alarms increased for the cool season for R(KDP) and R(ZDR,KDP) at both radars, potentially due to the sensitivity of KDP measurements during the cool season, and especially for shallow, stratiform precipitation (Seo et al., 2015). However, the RREC registered the least amount of false alarms for the cool season (63 at KLSX and 90 at KEAX), with R(Z,ZDR) performing second-best (67 at KLSX and 97 at KEAX). The similarity between the two algorithms' performance is due, at least in part, to the fact that the RREC primarily implements several different R(Z,ZDR) algorithms, especially during the cool season to account for precipitation shape.

Due to the relatively superior performance of the R(Z) and RREC algorithms during the warm season (e.g., large number of hits and low number of misses) at KLSX, the probability of detection (PoD) values were highest for these two algorithms during the warm season (0.42 and 0.41, respectively) (Table 2C.4). However, the PoD's are larger for the cool season than for the warm season, due to the larger number of hits and lower number of misses during the cool season (Table 2C.3). For example, PoD increased from 0.42 to 0.55 and 0.34 to 0.45 for the cool season for the R(Z) equation, while RREC increased from 0.41 to 0.5 and 0.3 to 0.40 at St. Louis and Kansas City, respectively. Similarly, R(Z,ZDR) increased from 0.4 to 0.51, second-best overall for the cool season, while R(KDP) and R(ZDR,KDP) performed, overall, the worst, increasing their Probability of detection values from 0.34 to 0.4 for KLSX. Therefore, at distances near 175 km, the detection of precipitation is superior for the cool season, opposed to the

Table 2C.4. Calculations of probability of detection (PoD) and probability of false detection (PoFD) for the St Louis (KLSX) and Kansas City (KEAX), MO radars. The calculated numbers were from the overall best-performing equations from each grouping of algorithms.

Contingency Factors	KLSX				KEAX			
	Warm Season		Cool Season		Warm Season		Cool Season	
R(Z)-Convective	PoD:	0.42	PoD:	0.55	PoD:	0.34	PoD:	0.45
	PoFD:	0.04	PoFD:	0.03	PoFD:	0.06	PoFD:	0.04
DKDP6	PoD:	0.34	PoD:	0.40	PoD:	0.27	PoD:	0.42
	PoFD:	0.02	PoFD:	0.03	PoFD:	0.04	PoFD:	0.10
ZZDR5	PoD:	0.40	PoD:	0.51	PoD:	0.30	PoD:	0.40
	PoFD:	0.02	PoFD:	0.02	PoFD:	0.03	PoFD:	0.03
ZDRDKDP3	PoD:	0.34	PoD:	0.40	PoD:	0.28	PoD:	0.42
	PoFD:	0.02	PoFD:	0.03	PoFD:	0.04	PoFD:	0.10
RREC	PoD:	0.41	PoD:	0.50	PoD:	0.30	PoD:	0.40
	PoFD:	0.02	PoFD:	0.02	PoFD:	0.03	PoFD:	0.03

warm season, opposite to what researchers have previously found (e.g., Smith et al., 1996; Ryzhkov et al., 2003, 2005). However, due to the relatively large amount of false alarms for R(Z) during the warm season (164), the probability of false detection (PoFD) was largest (0.04) whereas all other algorithms were 0.02. Similarly, the PoFD values for R(Z,ZDR) and RREC were lowest (0.02), while the three remaining algorithms PoFD values were 0.03 at KLSX. In general, the PoD and PoFD values were lower at KEAX than KLSX, indicating the poor performance of rain estimate detection at larger ranges.

Across the majority of algorithms, the correlation coefficient values comparing gauge measured precipitation versus radar estimated precipitation were largest for R(Z) for both radars during the warm season (Figure 2C.2). For example, the R^2 values for the R(Z) equation, including the accounts of misses and false alarms were 0.18 and 0.1 while the second-best correlation coefficient values were RREC, at 0.18 and 0.11 for KLSX and KEAX, respectively, the only occurrence of an algorithm outperforming R(Z) in

terms of R^2 values. The remaining three algorithms, R(Z,ZDR), R(DKP), and R(ZDR,KDP), all registered below 0.1 R^2 values for KEAX, but above 0.15 for KLSX. The overall weak performance of the gauge measured precipitation versus the radar estimated rainfall were due, primarily, to the large occurrences of missed and falsely alarmed precipitation. To ameliorate this issue, the accounts of misses were removed from the analyses, and the R^2 values were recalculated. This caused the correlation coefficient values to, at least, double, across all algorithms. Furthermore, the occurrence of false alarms were removed, resulting in all algorithms registering a further 0.22 increase in R^2 values across all algorithms. The largest correlation coefficient values, not accounting for the number of misses and false alarms, were 0.5 and 0.45 while the second-best performing algorithm, R(Z,ZDR), registered R^2 values of 0.51 and 0.4 for KLSX and KEAX, respectively.

The R^2 values for the cool season all outperformed those of the warm season for KLSX. In fact, the largest correlation coefficient values for the warm season, those that did not account for the misses and false alarms, were lower than the cool season R^2 values which included misses and false alarms (Figure 2C.3). For example, R^2 value for R(Z) (not including misses and false alarms) for the warm season was 0.5, but was 0.56 for the cool season. However, for Kansas City correlation coefficient values, the occurrences of misses were not included to increase the correlation coefficient values enough to outperform the warm season instances when misses and false alarms were not included. Overall, the cool season accounts of removing false alarms and misses performed the best for both radars. For KLSX, all R^2 values were above 0.62, while all R^2 values were above 0.59 for KEAX. The largest correlation values, overall, were R(Z) and RREC for KLSX

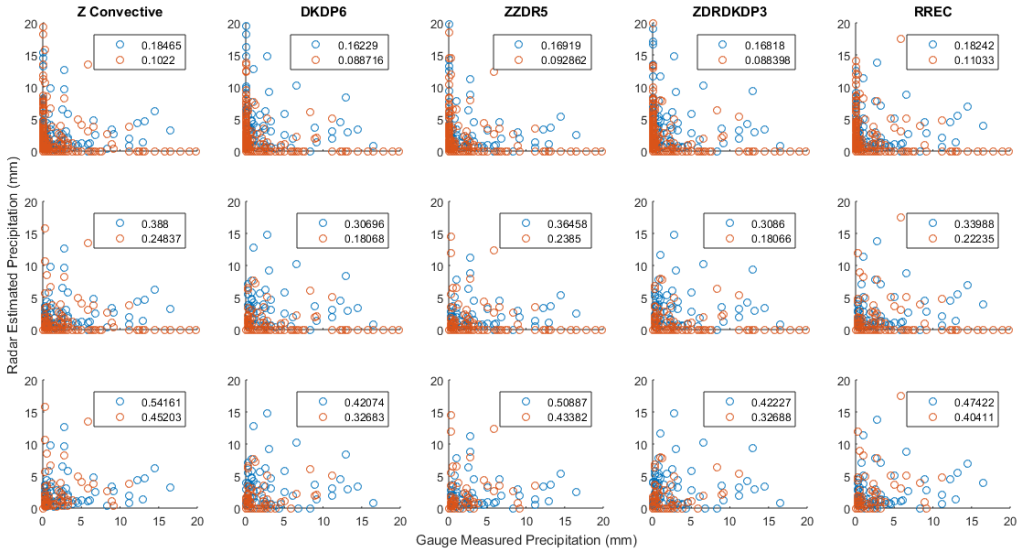

Figure 2C.2. Scatterplots of gauge estimated precipitation versus radar estimated precipitation for the five best-performing algorithms. Blue circles denote St. Louis, MO (KLSX) values while red circles indicate Kansas City, MO (KEAX) values, with correlation coefficient values recorded in the boxes of each graph. The first row of data represents all 3888 hours of data for the warm season, with the second-row removing instances when the radar did not estimate precipitation but the gauge recorded rainfall, and the third row removing all instances when radar or gauge did not estimate or record precipitation.

(0.66) and KEAX (0.66 and 0.65). The range of R^2 values were smaller for the cool season than they were for the warm season, providing evidence such that the overall performance of the algorithms degrade, overall, at distances beyond 175 km from the radar.

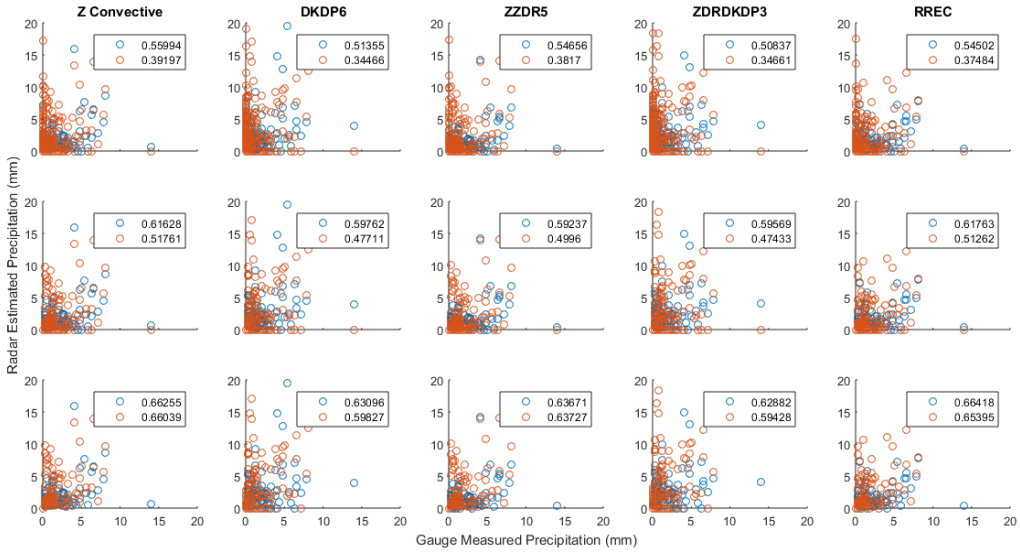

Figure 2C.3. Scatterplots of gauge estimated precipitation versus radar estimated precipitation for the five best-performing algorithms. Blue circles denote St. Louis, MO (KLSX) values while red circles indicate Kansas City, MO (KEAX) values, with correlation coefficient values recorded in the boxes of each graph. The first row of data represents all 3576 hours of data for the cool season, with the second-row removing instances when the radar did not estimate precipitation but the gauge recorded rainfall, and the third row removing all instances when radar or gauge did not estimate or record precipitation.

Quantitative analyses

The quantitative analyses accumulate the amount of precipitation due to the total number of misses (missed precipitation amount, FPA), falsely reported (false precipitation amount, FPA), and the overall absolute error (Error). Due to the less amount of precipitation registered by the gauges during the cool season (317.5 mm) compared to

the warm season (547.1 mm), the MPA, FPA, Error, and Precip values were relatively smaller, overall for both radars (Table 6). For example, the amount of precipitation missed by the KLSX R(Z) equation was 255.8 mm and 84.8 mm for the warm and cool season, respectively, while the MPA for R(Z,ZDR) was 276.9 mm and 93.2 mm for the warm and cool season, respectively (Figure 2C.4). Therefore, the percentage of precipitation missed compared to the overall gauge amounts were near 50% for both for the majority of the algorithm during the warm season, but only 30% for the cool season at KLSX. However, there were no algorithms calculated from the KEAX radar where the MPA and FPA were less than the gauge-accumulated precipitation amount (Figure 2C.5).

In general, the range for the false precipitation amount was larger than for the missed precipitation amount. For example, at KLSX, the largest FPA for the warm season was recorded by R(KDP), at 352.2 mm, while the smallest FPA was R(Z,ZDR) at 192.3 mm, but the largest and smallest values of MPA for the warm season were 287.8 and 255.8, respectively. Furthermore, the amount of false alarms during the warm (cool) season for R(Z,ZDR) and R(Z) were 76 (67) and 164 (113), but the FPA values were 192.3 mm (55.2 mm) and 259.0 mm (87.2 mm), respectively. Therefore, for the warm (cool) season, 88 (46) more false alarms registered by R(Z) resulted in 66.7 mm (32.1 mm) more falsely registered precipitation than R(Z,ZDR), contributing to the overall larger Error values observed for R(Z), 775.8 mm, than R(Z,ZDR), 708.5 mm from the St. Louis radar.

The amount of falsely reported precipitation was, overall, larger for KEAX than KLSX. Additionally, the range of values increased for KEAX when comparing the warm and cool seasons in comparison to the warm and cool season FPA for KLSX. Therefore, the amount of precipitation missed by the different algorithms at KEAX appears to be

Table 2C.5. Quantitative measure of the missed precipitation amount (MPA), false precipitation amount (FPA), overall error (Error), and accumulated precipitation (Precip) for the St Louis (KLSX) and Kansas City (KEAX), MO radars. The calculated numbers were from the overall best-performing equations from each grouping of algorithms.

Quantitative Analyses	KLSX				KEAX			
	Warm Season		Cool Season		Warm Season		Cool Season	
R(Z)-Convective	MPA:	255.8	MPA:	84.8	MPA:	364.2	MPA:	127.5
	FPA:	259.0	FPA:	87.2	FPA:	396.2	FPA:	213.2
	Error:	775.8	Error:	331.6	Error:	940.0	Error:	551.6
	Precip:	446.8	Precip:	290.8	Precip:	558.9	Precip:	504.6
DKDP6	MPA:	287.8	MPA:	113.5	MPA:	394.2	MPA:	146.6
	FPA:	352.2	FPA:	197.3	FPA:	476.7	FPA:	398.0
	Error:	901.6	Error:	511.3	Error:	1060.8	Error:	811.8
	Precip:	574.3	Precip:	466.8	Precip:	648.8	Precip:	778.6
ZZDR5	MPA:	276.9	MPA:	93.2	MPA:	381.8	MPA:	128.5
	FPA:	192.3	FPA:	55.2	FPA:	338.9	FPA:	181.2
	Error:	708.5	Error:	302.5	Error:	882.3	Error:	517.1
	Precip:	339.3	Precip:	215.4	Precip:	481.4	Precip:	450.3
ZDRDKDP3	MPA:	287.8	MPA:	114.3	MPA:	394.0	MPA:	146.1
	FPA:	317.6	FPA:	207.9	FPA:	487.1	FPA:	421.3
	Error:	893.2	Error:	529.1	Error:	1073.4	Error:	855.6
	Precip:	567.0	Precip:	488.7	Precip:	662.2	Precip:	826.4
RREC	MPA:	274.3	MPA:	94.7	MPA:	367.3	MPA:	136.9
	FPA:	241.7	FPA:	62.4	FPA:	370.1	FPA:	191.5
	Error:	777.9	Error:	306.4	Error:	910.9	Error:	517.2
	Precip:	447.5	Precip:	227.3	Precip:	551.0	Precip:	454.3

more a function of range, whereas the amount of falsely assess precipitation is a function of which polarimetric variables were implemented, whereby KDP (and, thus, DKDP) increases the overall FPA. Although this was observed for both radars, the difference was more pronounced for KEAX. There were a series of events shortly after 24 June 2016 such that a large amount of precipitation fell in a relatively short amount of time (Figure 2C.1). Although this even was associated with large mean absolute error values across both radars (Figures 2C.4 and 2C.5), there were few account of FA's registered by the accumulated graphs. Furthermore, this event allowed for the FPA to fall below the gauge accumulated rainfall amount at the end of the time period for DKDP6 at both radars.

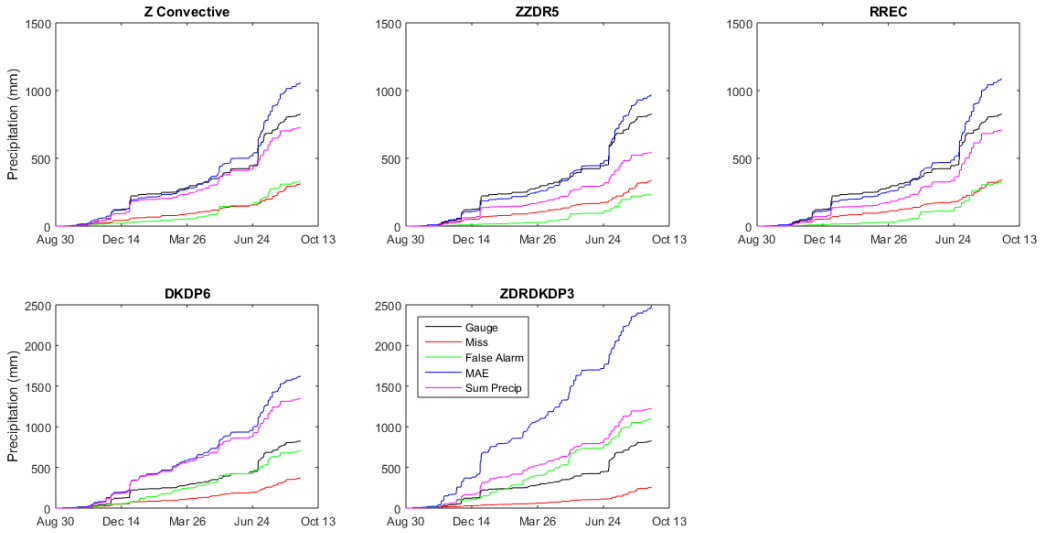

Figure 2C.4. Accumulation of the quantitative amount of precipitation based on the total number of misses (missed precipitation amount, MPA), number of false alarms (false precipitation amount, FPA), overall mean absolute error (MAE), and the overall accumulation of precipitation as recorded by the specified algorithm (Sum Precip) for St. Louis, MO (KLSX).

With the exception of R(KDP) and R(ZDR,KDP), most Error calculations decreased by more than 50% between the warm and cool season at KLSX whereas the error, typically, decreased by 30-40% for KEAX. For the St. Louis radar, the RREC registered near 800 mm of overall precipitation error for the warm season, whereas only 306.4 mm were registered for the cool season. Furthermore, only RREC (306.4 mm) and R(Z,ZDR) (302.5 mm) at KLSX registered less Error than the gauge-accumulated rainfall amount for either warm or cool season, across all algorithms. The largest Error values were produced by R(KDP) during the warm season (901.6 mm) for KLSX, and 1073.4

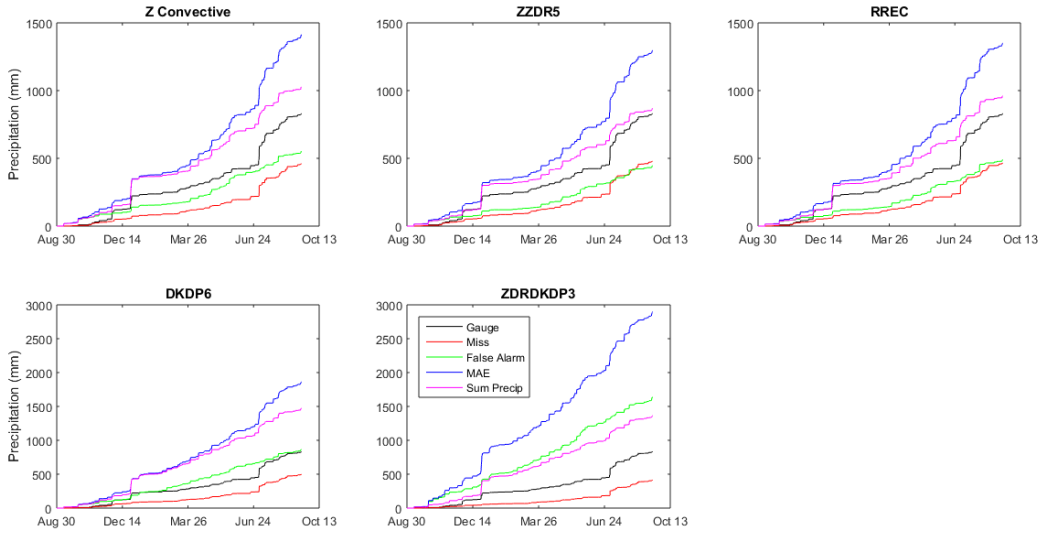

Figure 2C.5. Accumulation of the quantitative amount of precipitation based on the total number of misses (missed precipitation amount, MPA), number of false alarms (false precipitation amount, FPA), overall mean absolute error (MAE), and the overall accumulation of precipitation as recorded by the specified algorithm (Sum Precip) for Kansas City, MO (KEAX).

mm for KEAX. This indicates that, with an MPA of 287.8 mm and FPA of 352.2 mm, the error due to 71 discrepancies in the number of hits (Table 2C.3) was 261.6 mm of precipitation, or an average error of 3.68 mm of precipitation per hit by the St. Louis radar. The least amount of error calculated by the KEAX radar were for R(Z,ZDR) (517.1 mm) and the RREC (517.2 mm), further indicating that the RREC performed rain rate calculations primarily by the R(Z,ZDR) algorithm.

The last quantitative measure calculated for each algorithm was the accumulation of precipitation from each algorithm, Precip. Essentially, Precip is the normalized

standard error (equation 3) without the denominator (i.e., not accounting for the gauge accumulation precipitation amount), and is directly correlated to the NSE values via Table 2. Therefore, the closer NSE values are to 100%, the closer the Precip value was to the gauge-recorded precipitation amount over the course of the study. For example, at KLSX, R(Z) for the cool season had an NSE value of 100.0, such that the Precip value was 290.8, only 26.7 mm from the gauge-measured rainfall amount. Due to the RREC and R(Z,ZDR)'s relatively low false alarm counts for both radars, the accumulation by R(Z,ZDR) (Precip) was low compared to the gauge-measured precipitation amounts. Conversely, R(KDP) and R(ZDR,KDP) were the only algorithms that overestimated the gauge-measured amounts for both warm and cool season for KLSX, whereas every algorithm, for both warm and cool season, overestimated the gauge recorded precipitation amount.

Conclusions

Long-term analyses of two distant radars' performance on rain rate estimates is presented. One years' worth of radar data was separated into a warm and cool season, consisting of 162 and 149 days, or, 3888 and 3576 hours of data analyzed, respectively. The St. Louis (KLSX) and Kansas City (KEAX) radars were implemented to estimate rainfall from 55 different rain rate algorithms, including several conventional R(Z) equations, and multiple polarized algorithms. The 55 equations were grouped based on the radar variables implemented, including reflectivity, differential reflectivity, and the specific differential phase shift, including KDP-smoothed fields of the aforementioned variables. The area of study was, approximately, 175 km from the radars, consisting of

four terrestrial-based tipping buckets within the Hinkson Creek watershed in Central Missouri, which were averaged together to remove any errors that may have been attributed to the gauges.

The Kansas City radar (KEAX) was, approximately, 25 km further from the study site than The St. Louis radar (KLSX). Because of this, the overall errors associated with the KEAX radar were larger than KLSX, consistent with many previous findings. However, the cool season analyses, which would be primarily comprised of shallow, stratiform clouds and snowfall, outperformed many of the warm season statistical, contingency, and quantitative values that were calculated. Furthermore, the performance of the majority of the cool season rain rate estimates were superior to the warm season that the correlation coefficient values for the cool season were larger than those of the warm season which did not account for misses and false alarms. This could be due, at least in part, to the bright-banding that may have played a significant role in a particular series of events shortly after 24 June 2016, causing a large spike in the mean absolute error (MAE) for the warm season. Additionally, the cool season may have included several warm-season precipitation events, as the winter of 2015-2016 was unseasonably warm.

Overall, the conventional R(Z) algorithm outperformed the best-performing polarized algorithms. This was observed such that the R(Z) equation had the overall smallest mean absolute error and number of misses (and, thus, smallest missed precipitation amount) for both the warm and cool season for KLSX and KEAX, while registering the most number of hits and highest probability of detection for both seasons and radars. The R(Z,ZDR) and RREC algorithms performed best in terms of false

assessed precipitation, potentially due to the implementation of the differential reflectivity. Furthermore, R(Z,ZDR) and RREC outperformed R(Z) in the overall amount of error for both radars. However, the R(Z) equation, primarily, outperformed all other algorithms over the period of study, and, generally, accumulated the most accurate amount of precipitation relative to the average of the four terrestrial-based tipping bucket amount.

The current study provides one of, if not, the only long-term analyses of radar performance for the warm and cool season. Results indicate that the performance between R(Z) and R(Z,ZDR) may play a seasonal preference in terms of overall rain rate estimation, which has significant implications for hydrometeorological forecasts, especially for flood forecasting. Further analyses into the long-term performance of radars should be conducted over a domain with more densely covered rain gauges, in addition to ground-truthed sensors at a variety of ranges to assess performance as a function of range from the radar(s).

Acknowledgements

This material is based upon work supported by the National Science Foundation under Award Number IIA-1355406. Any opinions, findings, and conclusions or recommendations expressed in this material are those of the authors and do not necessarily reflect the views of the National Science Foundation.

Literature cited

Berne, A., and Krajewski, W.F., 2013: Radar for hydrology: Unfulfilled promise or unrecognized potential? *Adv. Water Resour.*, **51**, 357-366.

Ciach, G.J., and Krajewski, W.F., 1999: On the Estimation of Radar Rainfall Error Variance. *Adv. Water Res.*, **22**, 585-595.

Ciach, G.J., 2002: Local Random Errors in Tipping-Bucket Rain Gauge Measurements. *J. Atmos. Oceanic Technol*., **20**, 752-759.

Cunha, L.K., Smith, J.A., Baeck, M.L., and Krajewski, W.F., 2013: An early performance of the NEXRAD dual-polarization radar rainfall estimates for urban flood applications. *Wea. Forecasting*, **28**, 1478-1497.

Cunha, L.K., Smith, J.A., Krajewski, W.F., Baeck, M.L., and Seo, B., 2015: NEXRAD NWS polarimetric precipitation product evaluation for IFloods. *J. Appl. Meteor.*, **16**, 1676-1699.

Elmore, K.L., 2011: The NSSL hydrometeor classification algorithm in winter surface precipitation: Evaluation and future development. *Wea. Forecasting*, **26**, 756-765.

Gourley, J.J., Giangrande, S.E., Hong, Y., Flamig. Z,, Schuur, T., and Vrugt, J., 2010: Impacts of polarimetric radar observations on hydrologic simulation. *J. Hydrometeorol.*, **11**: 781-796.

Habib, E., Krajewski, W.F., Nespor, V., and Kruger, A., 1999: Numerical simulation studies of rain gauge data correction due to wind effect. *J. Geophys. Res.*, **104**, 723–734.

Kitchen, M. and Jackson, P.M., 1993: Weather radar performance at long range – simulated and observed. *J. Appl. Meteor.*, **32**, 975-985.

Kumjian, M.R., 2013a: Principles and applications of dual-poarization weather radar. Part 1: Description of the polarimetric radar variables. *J. Operational Meteor.*, **1**, 226-242.

Kumjian, M.R., 2013b: Principles and applications of dual-poarization weather radar. Part 2: Warm and cold season applications. *J. Operational Meteor.*, **1**, 243-264.

Ryzhkov, A.V., Zrnic, D.S., and Gordon, B.A., 1998: Polarimetric method for ice water content determination. *J. Appl. Meteor.*, **37**, 125-134.

Ryzhkov, A.V., Giangrande, S., and Schurr, T., 2003: Rainfall measurements with the polarimetric WSR-88D radar. National Severe Storms Laboratory Rep. Norman: OK, 98 pg.

Ryzhkov, A.V., Giangrande, S., and Schurr, T., 2005: Rainfall estimation with a polarimetric prototype of WSR-88D. *J. Appl. Meteor.*, **44**, 502–515.

Simpson, M.J., Hubbart, J.A., and Fox, N.I., 2016: Ground truthed performance of single and dual-polarized radar rain rates at large ranges. *Hydrol. Process.*, **30**, 3692-3703.

Seo, D.J., Breidenbach, J., Fulton, R., Miller, D., and O'Bannon, T., 2000: Real-time adjustment of range-dependent biases in WSR-88D rainfall estimates due to nonuniform vertical profile of reflectivity. *J. Hydrometeorol.*, **1:** 222 – 240.

Seo, B., Brenda, D., Krajewski, W.F., Rutledge, S.A., and Petersen, W., 2015: Comparison of Single- and Dual-polarization-based rainfall estimated using NEXRAD data for the NASA Iowa flood studies project. *J. Hydrometeorol.*, **16**: 1658-1675.

Smith, J.A., Seo, D.J., Baeck, M.L., and Hudlow, M.D., 1996: An intercomparison study of NEXRAD precipitation estimates. *Water Resour. Res.,* **32**, 2035-2045.

Villarini, G., and Krajewski, W.F., 2010: Review of the different sources of uncertainty in single polarization radar-based estimates of rainfall. *Surv. Geophys.*, **31**: 107-129.

Vivekanandan, J., Bringi, V.N., Hagen, M., and Meischner, P., 1994: Polarimetric radar studies of atmospheric ice particles. *IEEE Trans. Geosci. Remote Sens.*, **32**, 1-10.

Wolfe, J.P., and Snider, J.R., 2012: A relationship between reflectivity and snow rate for a high-altitude S-band radar. *J. Appl. Meteor. Climatol.*, **51**, 1111-1128.

Zrnic, D.S., and Ryzhkov, A.V., 1996: Advantages of rain measurements using specific differential phase. *J. Atmos. Oceanic Tech.*, **13**, 454-464.

CHAPTER III
X-BAND POLARIZED RADAR PERFORMANCE ANALYSES IN THE MIDWESTERN UNITED STATES.

Abstract. Over the past decade, polarized weather radars have been at the forefront of the search for a replacement of estimating precipitation over the spatially, and temporally inferior tipping buckets. However, many radar-coverage gaps exist within the Continental US (CONUS), proposing a dilemma in that radar rainfall estimate quality degrades with range. One possible solution is that of X-band weather radars. However, the literature as to their long-term performance is lacking. Therefore, the overarching objective of the current study was to analyze two year's worth of radar data from the X-band dual-polarimetric MZZU radar in central Missouri at four separate ranges from the radar, utilizing tipping-buckets as ground-truth precipitation data. The conventional R(Z)-Convective equation, in addition to several other polarized algorithms, consisting of some combinations of reflectivity (Z), differential reflectivity (ZDR), and the specific differential phase shift (KDP) were used to estimate rainfall. Results indicated that the performance of the algorithms containing ZDR were superior in terms of the normalized standard error (NSE), missed and false precipitation amounts, and the overall precipitation errors. Furthermore, the R(Z,ZDR) and R(ZDR,KDP) algorithms were the only ones which reported NSE values below 100%, whereas R(Z) and R(KDP) equations resulted in false precipitation amounts equal to or greater than 65% of the total gauge recorded rainfall amounts. The results show promise in the utilization of the smaller, more cost-effective X-band radars in terms of quantitative precipitation estimation at ranges from 30 to 80 km from the radar.

Introduction

Since the late 20th Century, weather radars have been at the forefront of multiple studies to determine their accuracy in determining precipitation estimation (e.g., Kitchen and Jackson, 1993; Smith et al., 1996; Ryzhkov et al., 2003; Cunha et al., 2013; Simpson et al., 2016). Multiple researchers have reported accurate measurements in radar rainfall estimates when compared to terrestrial-based precipitation gauges (e.g., tipping buckets). This has several important implications for multi-disciplinary fields which rely on highly spatialized and temporal precipitation data, which can be obtained from radar estimates compared to the spatially inferior rain gauges.

Most studies in the US have utilized the National Weather Service (NWS) Next Generation Radar (NEXRAD) system, comprised of Weather Surveillance Radar – 1988 Doppler (WSR-88D) series instruments, operating at S-band (approximately, 10 – 11 cm) wavelength for their analyses. However, the cost of installation and maintenance of these instruments are much larger in comparison to the smaller, lighter-weighted X-band radars, operating at, approximately, 3 cm wavelength (Matrosov 2010). Berne and Krajewski (2013) have stated that, primarily due to the sparse coverage of the WSR-88D S-band radar system, smaller, more frequently-placed X-band radars are a viable option for remediating radar rainfall errors that have been recorded at large distances (e.g., Smith et al., 1996; Ryzhkov et al., 2005; Simpson et al., 2016). However, due to the lack of literature from analyses conducted on X-band weather radars, primarily due to high attenuation effects (Matrosov et al., 2002; Park et al., 2005), conclusions based on their overall performance in different climatic regimes cannot be determined accurately.

Matrosov et al. (2002) conducted a study analyzing 15 separate rainfall events during an eight-week field campaign in Virginia while utilizing the National Oceanic and Atmospheric Administration's (NOAA) X-band dual-polarimetric radar. Several radar rainfall algorithms were implemented, including combinations of the equivalent reflectivity (Z_e), differential reflectivity (ZDR), and the specific differential phase-shift (KDP), an R(KDP) equation, and two R(Z_e) relations, over a region with three ground-truthed rain gauges. It was found that the combined polarimetric estimator (i.e., utilization of Z_e, KDP, and ZDR) resulted in the overall least standard deviation (22%), while the case-tuned R(Z_e) relation was slightly higher of 23%. It is noted that R(Z_e) measurements are derived from a priori knowledge of Z_e, KDP, and ZDR values, whereas the combined polarimetric estimator was not, implying the latter is superior for real-time use. However, the performance of the combined polarimetric estimator works best when rain rates exceeded 1.5 mm h^{-1}, while R(Z_e) algorithms were superior at lighter rain rates. Results from the R(KDP) algorithm reported an overall negative bias of 6-9% when compared to the gauge data, in addition to a standard deviation of 30%, primarily due to the sensitivity of KDP measurements while utilizing X-band radars.

Several years later, Matrosov (2010) conducted a similar study, evaluating X-band radar rain rates during the Hydrometeorology Testbed (HMT) West field campaigns in the Northern California and Sierra Nevada regions of California. Several radar rain rate algorithms were developed similar to Matrosov et al. (2002), with the addition of several R(Z_e, ZDR) algorithms. It was noted that, overall, R(KDP) algorithms performed the best, such that it displayed the lowest bias (ranging between -9 to 3% in addition to a standard deviation range of 17 - 23%. The three R(Z_e, ZDR) algorithms implemented in

the study displayed a wider range of bias values (-4 to 6%) in addition to larger overall relative standard deviations (20 – 32%). Therefore, similar results were obtained such that R(KDP) algorithms at X-band analyses are, generally, negative in bias while standard deviations range between 20-30%.

Expanding upon the literature of implemented R(KDP) algorithms through X-band radars, Wang and Chandrasekar (2010) assessed the performance of three separate R(KDP) algorithms from the Collaborative Adaptive Sensing of the Atmosphere (CASA) Engineering Research Center through the use of the distributed collaborative adaptive sensing (DCAS) network. The DCAS network, essentially, implements multiple radar networks within a relatively small spatial extent, all operating at different volume coverage patterns (VCP's) such that high spatiotemporal resolution data is achieved in addition to overall lower beam height over the area of interest (McLaughlin et al., 2009), mitigating effects that have been observed due to rain rate estimations at large ranges (Kitchen and Jackson, 1993; Ryzhkov et al., 2005; Simpson et al., 2016). The results indicated that through the use of several different R(KDP) algorithms from multiple different radars, radar Quantitative Precipitation Estimates (QPE) can be improved significantly. Furthermore, the R(KDP) algorithms exhibited similar bias values (between -6 and 8 %) that were reported by Matrosov (2002) and Matrosov et al. (2010). However, the normalized standard error (NSE) values ranged from, approximately, 16 to 54%, indicating that the overall error in R(KDP) rain rate estimates were less than half of the total amount of rain observed for the study.

Utilizing a subset of the same study area as Wang and Chandrasekar (2010), Vieux and Imgarten (2012) implemented X-band dual-polarimetric radar rainfall data into

a fully-distributed, physics-based hydrologic model, Vflo™ (Vieux, 2004) to determine the spatial errors associated with radar rainfall data and their impacts at relevant hydrologic scales. One of the main findings from the study was the effect of differences in runoff volume scale with the overall watershed area. It was found that the difference typically decreased as the watershed area increased, but random errors in the rainfall algorithms were averaged out as the watershed area increased. R(Z) and R(KDP) algorithms showed strong range dependencies, while R(KDP) estimators showed the best agreement between two separate radars implemented in the study, in addition to performing the best, overall in terms of runoff generation. It was eventually concluded that the errors associated with simulated hydrograph peaks from radar rainfall data were so pronounced that reliable hydrologic predictions could not be obtained. Furthermore, no predictable relationships were observed between hydrograph peaks and radar rainfall products.

A comparative study of several X-band radar rain rate algorithms was conducted by Koffi et al. (2014) in Benin, West Africa to determine the overall performance of estimators in estimating precipitation (i.e., QPE). Four algorithms were developed: R(Z), R(KDP), R(ZDR,KDP), and R(Z,ZDR,KDP) and were compared to ground-truthed rain gauges in addition to disdrometers located within the area of study. Overall, it was found that rain intensity was the biggest factor in determining performance. For example, at rain rates below 0.5 mm h^{-1}, root mean square error (RMSE) values exceeded 100% for R(KDP) analyses, whereas when rain rates exceeded 10 mm h^{-1}, RMSE values dropped below 40%. However, due to the climatic conditions of West-African, over 80% of the events were for rain rates exceeding 10 mm h^{-1}.

The overarching objective of the current study is to add to the relatively few articles on X-band dual-polarization radar rain rate performance. Authors have proposed (e.g., Berne and Krajewski 2013) that the capability of implementing more X-band radars in comparison to the relatively sparse and expensive S-band WSR-88D NEXRAD system to enhance precipitation estimation is a viable option (especially over the inter-mountain West), especially for hydrologic analyses, particularly flood forecasting. However, others (e.g., McLaughlin et al., 2009) suggest the sheer number of radars to achieve such a difference in radar rain rate estimation is impractical. Further justification for increasing, at least partially, the construction of X-band weather radars is necessary through analyses of those that already exist.

The current study analyzes two years of radar data from the newly-installed dual-polarimetric MZZU X-band radar located in Central Missouri. Over 100 different algorithms were implemented to test the performance of the radar while utilizing measurements of reflectivity (Z), differential reflectivity (ZDR), and the specific differential phase shift (KDP). Rain rates were calculated based on combinations of the aforementioned variables and compared to four separate tipping buckets, which served as ground-truth. To determine the performance of all algorithms, multiple statistical analyses were conducted, including the bias, mean absolute error, and normalized standard error. Additionally, several contingency factors were calculated, such as the overall number of hits, misses, false alarms, and correct negatives. Lastly, quantitative analyses, including the missed precipitation amount (MPA), false precipitation amount (FPA), and overall error were computed to determine the performance of the 108 algorithms. Analyses, such as the current study, are important for determining the

accuracy and limitations of dual-polarimetric radars such that their incorporation into hydrologic models may be correctly assessed (Ogden et al., 1997; Vieux, 2004; Vieux et al., 2004; Vieux and Bedient, 2004; Gourley et al., 2010; Cunha et al., 2015). Furthermore, studies analyzing the performance of X-band radars will allow further indications as to whether they should be installed in regions devoid of optimal NWS WSR-88D coverage.

Data and methodology

Study location and gauge data

The dates analyzed ranged from August 2015 to August 2017 which, when accounting for radar down time for maintenance and offline issues, yielded 608 days, or 14952 hours for analyses. The current study was conducted in Boone County, located in Central Missouri (Figure 3A.1), where the MZZU radar is located at 38.906°N and 92.269°W. Several Missouri Mesonet rain gauges lie within the domain of the MZZU radar, located in Versailles, Auxvasse, Williamsburg, and Vandalia, MO, located at, approximately, 75 km, 30 km, 45 km, and 80 km from the radar, respectively.

The TE525 rain gauge series performs optimally in temperature conditions between 0 and 50°C. Albeit no events recorded a daily maximum temperature above 50°C, 72 days in the cool season (e.g., January and February) recorded temperatures below 0°C. However, only 8 days that exhibited sub-freezing average daily temperatures registered precipitation. Thus, about 1% of the entire data, might be further unrepresentative

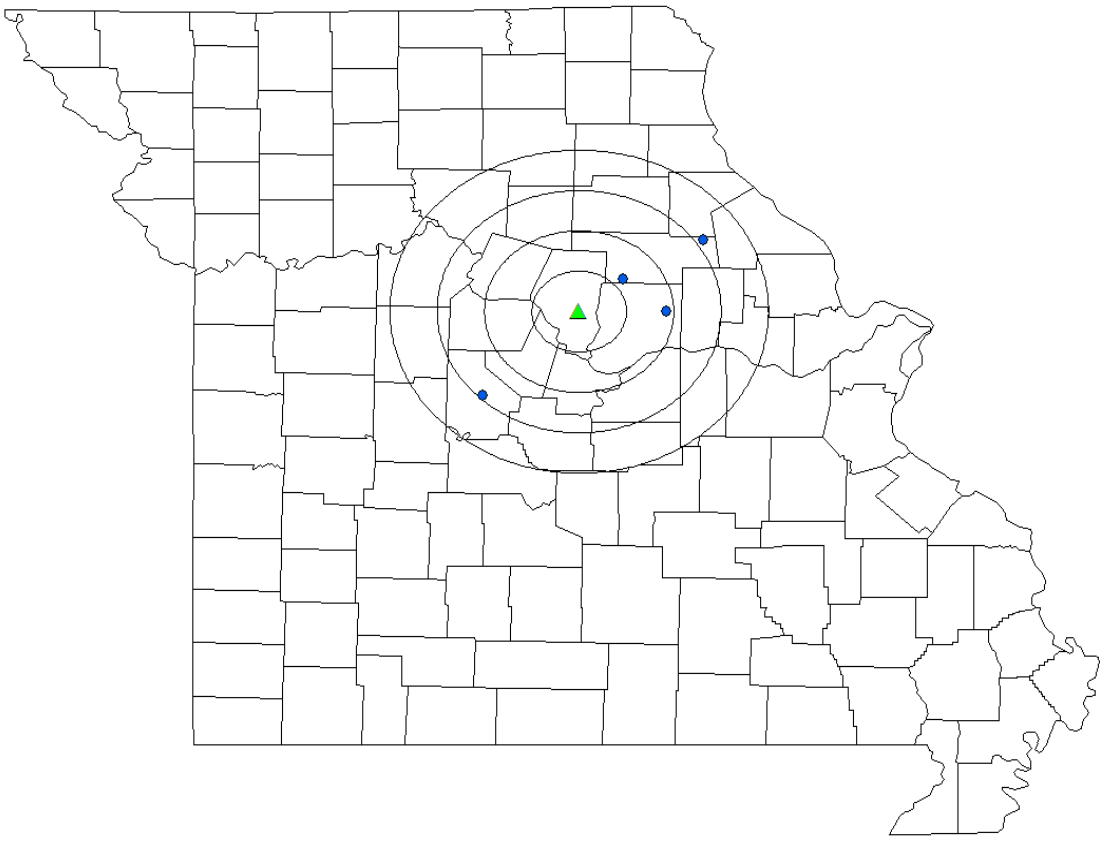

Figure 3A.1. Study location including to the four gauges utilized for the current study. From left-to-right, the gauges are Versailles, Auxvasse, Williamsburg, and Vandalia, MO. The MZZU X-band radar is plotted in addition to 25-, 50-, 75-, and 100-km range rings.

of the actual precipitation. For this study, it was assumed since the amount of precipitation recorded by the gauges during these events was below 5 mm in precipitation, no significant errors would affect the overall statistics. It is further assumed melting from frozen precipitation did not significantly impact the results.

Radar discussion and data

The radar for the current study is part of the Missouri Experimental Project to Stimulate Competitive Research (EPSCoR) program, primarily aimed at enhancing Missouri's modelling capacity of weather and climate on plants and communities at the local, and regional scale. The X-band radar (MZZU) was installed in the Summer of 2015, in which data acquisition became possible by the Fall of 2015 near the South Farm Research Center, located in central Boone County, MO (Figure 3A.1). The instrument is utilized, primarily, for research purposes, but is also quasi-operational. Specifics regarding the radar are detailed in Table 3A.1.

Algorithms were implemented based from previous X-band research to more closely resemble the sensitivity of the radars on KDP estimates. Six, three, and two R(KDP) algorithms were adopted from Matrosov (2009), Wang and Chandrasekar (2010), and Koffi et al. (2014), respectively. Additionally, two R(Z,ZDR) and two R(ZDR,KDP) algorithms were adopted from Matrosov (2009) and Koffi et al. (2014), respectively. Furthermore, as with the S-band algorithms, all measures of Z, ZDR, and KDP were tested with their KDP-smoothed derivatives, DSMZ, DZDR, and DKDP.

Algorithms were grouped based on the variables implemented to estimate rain rates. Collectively, three R(Z) algorithms were tested, R(Z)-Convective, R(Z)-Stratiform, and R(Z)-Tropical, in addition to the DSMZ counterparts. Additionally, five separate R(Z,ZDR) equations were implemented, including five R(Z,DZDR), five R(DSMZ,ZDR), and the five R(DSMZ,DZDR) combinations. These 26 equations encompassed the S-band equivalent algorithms to be tested on the X-band radar, to determine how versatile the equations are and are outlined via Table 2A.1.

Table 3A.1. MZZU X-band radar characteristics.

Variable	Value
Location (x,y)	38.906°N, 92.269°W
Altitude Above Ground Level	308 m
Dual Pulse Repetition Frequency	5:4 Stagger: 2,000 Hz – 124 kts
Radar Type	EWR Solid State: Parabolic prime focus composite reflector (Dish mounted radome cover)
Peak Power	1 kW standard
Frequency	9.35 GHz $\pm$ 50 MHz (User Selectable)
Pulse Width	1 – 80 μs
Antenna Diameter	1.82 m
Beamwidth	1.27°
Gain	42 dB
Sensitivity	(80 μs at 50 km range): -1.5 dBZ
Elevation Angle	-5° to 120°

Theoretically, theh relationship between R and Z for a well calibrated radar as controlled by the drop size distribution should be independent of radar wavelength. However, as the phase shift of the wave is a function of the ratio of wavelength to drop radius, the R(KDP) relationships are wavelength dependant. Thus, 38 X-band algorithms were tested for overall performance based on the MZZU radar estimates (Table 3A.2), with the addition of RREC, RKDP, and DRRZ, totaling 68 algorithms tested.

Results and discussion

From the four separate gauges, Auxvasse was the closest to the radar (approximately, 30 km) while Vandalia was the furthest (80 km), with Versailles slightly closer at 75 km (Figure 3A.1). Williamsburg lies 45 km from the radar, placing it near the middle of the group of gauges in terms of distance. The overall average amount of gauge recorded precipitation between the four sites was, approximately, 1650 mm (Figure

Table 3A.2. List of X-band polarimetric algorithms used for radar rainfall estimates.

$R(KDP) = aKDP^b$				
Algorithm number	a	b	c	References
1	17.0	0.73	-	Matrosov (2010)
2	16.5	0.71	-	Matrosov (2010)
3	16.6	0.82	-	Matrosov (2010)
4	14.4	0.71	-	Matrosov (2010)
5	16.4	0.80	-	Matrosov (2010)
6	14.9	0.79	-	Matrosov (2010)
7	47.3	0.79	-	WC (2010)
8	18.2	0.79	-	WC (2010)
9	19.6	0.82	-	WC (2010)
10	13.6	0.83	-	Koffi et al. (2014)
11	21.0	0.57	-	Koffi et al. (2014)
$R(ZDR, KDP) = aZDR^b KDP^c$				
Algorithm number				References
1	15.1	-0.29	0.94	Koffi et al. (2014)
2	20.9	-0.05	0.59	Koffi et al. (2014)

3A.2). Excluding the warm season (approximately from April – September), the amount of gauge-recorded rainfall was similar across the four gauges. The large variation in precipitation during the warm season were due, primarily, to several isolated convective

cells which were recorded at the certain gauges (e.g., Williamsburg), but missed at others (e.g., Versailles).

Statistical analyses

From the 68 algorithms overall, the best R(Z) and R(Z,ZDR) were similar to those in chapter 2. These were chosen to be the best overall algorithms from each grouping of equations due to their lowest MAE and NSE values (Table 3A.3). Furthermore, the best R(KDP) algorithm was from Matrosov (2010), while the best performing R(ZDR,KDP) equation was from Koffi et al., (2014), algorithms 6 and 11 from Table 3A.2, respectively. From the three fuzzy logic rain rate algorithms (RREC, RKDP, and DRRZ), RREC was considered to be the best.

With Auxvasse being the closest gauge to the radar (30 km), this location registered the least bias across all groups of algorithms, excluding RREC. In fact, the R(Z,ZDR) equation showed no bias, while R(KDP), R(ZDR,KDP), and RREC displayed slightly positive biases (0.3, 0.3, and 0.5 mm, respectively). Only the R(Z) equation registered a negative bias (-0.1 mm). Interestingly, the RREC registered less bias as distance from the radar increased (0.5, 0.2, 0.2, and 0.1 mm for distances of 30, 45, 75, and 80 km, respectively).

In general, Williamsburg, the second-nearest gauge from MZZU (45 km), registered the second-best bias with the notable exception of the R(Z) equation. For example, underestimation on the order of -0.3 mm was recorded at Williamsburg for R(Z), while -0.2 mm and -0.4 mm were registered at Versailles (75 km) and Vandalia 80 km), accordingly. Furthermore, Auxvasse was the only of the four gauges which did

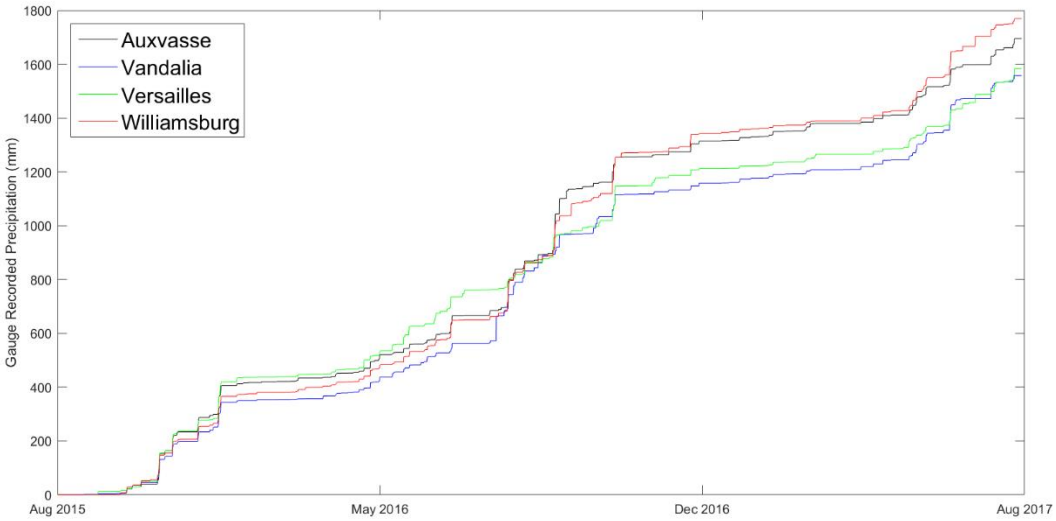

Figure 3A.2. Accumulated gauge-recorded precipitation from the beginning to the end of the study for the four-separate tipping buckets.

not register a negative bias for R(Z,ZDR). The largest biases were recorded by R(KDP) at the furthest location, Vandalia (0.6 mm), with R(KDP,ZDR) recording 0.5 mm of bias at the same location. No negative biases were registered for either of the KDP-containing equations, nor RREC. Similar to the pattern of increasing biases as distance from MZZU increased, the MAE increased for nearly all algorithms, with the exception of R(Z,ZDR). The mean absolute errors values recorded by the R(Z,ZDR) equation were 1.3, 1.4, 1.4, and 1.5 mm at distances of 30, 45, 75, and 80 km, respectively. Otherwise, the other four algorithms represented increasing error with increasing range from MZZU, with the lowest MAE being R(ZDR,KDP) with 1.2 mm, and the largest being RREC (1.7 mm).

At no locations for R(Z), R(KDP), or RREC, did the normalized standard error

Table 3A.3. Statistical analyses for the MZZU radar and the best algorithms from each grouping of equations with their respective distance from the radar.

Algorithm	**Auxvasse 30 km**	**Williamsburg 45 km**	**Versailles 75 km**	**Vandalia 80 km**
R(Z)	Bias: -0.1 MAE: 1.3 NSE: 102.6	Bias: -0.3 MAE: 1.4 NSE: 107.8	Bias: -0.2 MAE: 1.4 NSE: 119.9	Bias: -0.4 MAE: 1.5 NSE: 134.6
R(Z,ZDR)	Bias: 0.0 MAE: 1.3 NSE: 89.2	Bias: -0.2 MAE: 1.6 NSE: 99.0	Bias: -0.3 MAE: 1.6 NSE: 110.5	Bias: -0.2 MAE: 1.5 NSE: 106.9
R(KDP)	Bias: 0.3 MAE: 1.3 NSE: 119.1	Bias: 0.4 MAE: 1.3 NSE: 126.1	Bias: 0.5 MAE: 1.5 NSE: 142.5	Bias: 0.6 MAE: 1.6 NSE: 158.6
R(ZDR,KDP)	Bias: 0.3 MAE: 1.2 NSE: 84.7	Bias: 0.3 MAE: 1.3 NSE: 93.1	Bias: 0.5 MAE: 1.4 NSE: 104.7	Bias: 0.5 MAE: 1.5 NSE: 101.8
RREC	Bias: 0.5 MAE: 1.6 NSE: 103.1	Bias: 0.2 MAE: 1.7 NSE: 108.1	Bias: 0.2 MAE: 1.7 NSE: 120.0	Bias: 0.1 MAE: 1.7 NSE: 135.1

fall below 100%. Therefore, the two algorithms containing the differential reflectivity recorded NSE's less than 100%, in particular at the two closest gauge locations. The R(ZDR,KDP) registered 84.7 and 93.1% at Auxvasse and Williamsburg, whereas R(Z,ZDR) displayed NSE values of 89.2 and 99.0%, respectively. Furthermore, these two algorithms calculated less NSE at the furthest location (Vandalia) than at the third furthest location (Versailles), in spite of there being a 5 km difference in range between the two locations.

Contingency analyses

To determine where the bulk of errors implicit within the bias, mean absolute error, and normalized standard error originate from, contingency analyses were calculated, including hits, misses, and false alarms.

The number of tips recorded at Auxvasse, Vandalia, Versailles, and Williamsburg were 810, 725, 762, and 855, accordingly (Figure 3A.4). In terms of the number of hits, misses, and false alarms, an analysis of variance (ANOVA) table was constructed to determine whether any significant differences exist between the five algorithms. Results indicate that, with 99% confidence, the number of hits between the five algorithms, in addition to the number of misses and false alarms did not differ significantly from one algorithm to the next. Therefore, the results of contingency analyses will be conducted utilizing the R(ZDR,KDP) algorithm to reduce redundancies.

The number of hits were 688, 603, 647, and 736 at Auxvasse, Vandalia, Versailles, and Williamsburg, respectively, indicating that 85, 83, 85, and 86% of the precipitation events were correctly assessed by the radar. With 122, 122, 115, and 119 misses, only 15, 17, 15, and 14% of rainfall events were missed. However, the occurrences of false alarms were similar to the number of hits and, for Vandalia, exceeded the number of gauge tips. For example, Auxvasse, Williamsburg, Versailles, and Vandalia registered 7 more, 4 more, 9 less, and 135 more false alarms than the number of hits. Therefore, it may be concluded that the bulk of the errors in the QPE's were, primarily, due to false alarms.

In spite of the prevalent occurrences of the number of false alarms, the correlation coefficient values between the gauge recorded and radar estimated precipitation were as

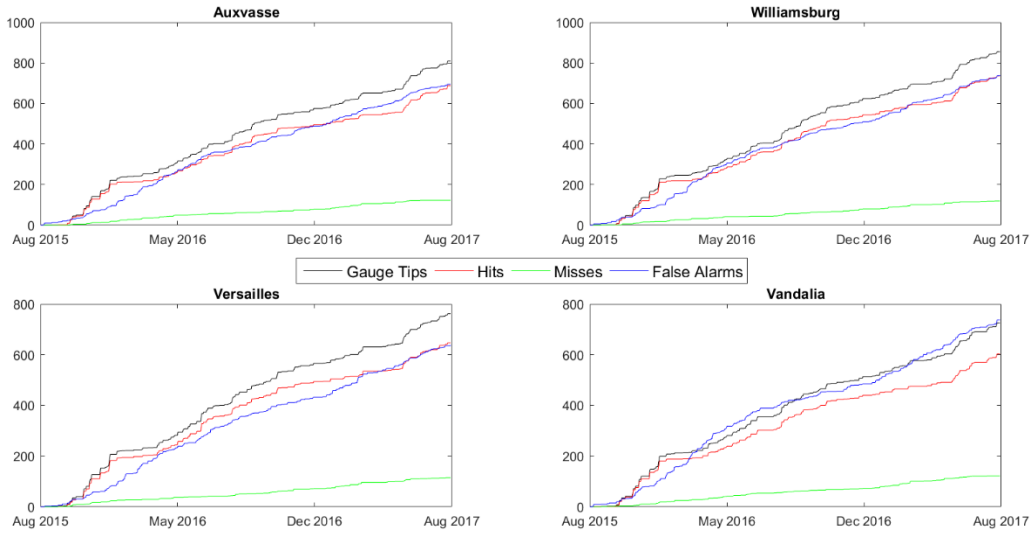

Figure 3A.3. Contingency analyses at each of the four gauges utilized for the current study, including the accumulated sum of the number of tipping bucket tips, hits, misses, and false alarms.

large as 0.70, particularly for the R(Z)-Convective and RREC algorithms (Figure 3A.4). Furthermore, these two algorithms had the same R^2 values for all of the four stations of 0.7, 0.68, 0.56, and 0.5 for Auxvasse, Williamsburg, Versailles, and Vandalia, respectively. The R(KDP) equation had similar values with the exception of Auxvasse, which was 0.69 (0.01 less).

The ZDR-containing algorithms have been shown to be superior to the other three equations in terms of NSE (Table 3A.3), yet produced the, overall, lowest R^2 values. The best values were 0.63 and 0.62 at Auxvasse for R(Z,ZDR) and R(ZDR,KDP), respectively, while the lowest values were 0.43 and 0.41 at Vandalia, accordingly. The reason for the findings may be due to the fact that the R(Z,ZDR) and R(ZDR,KDP)

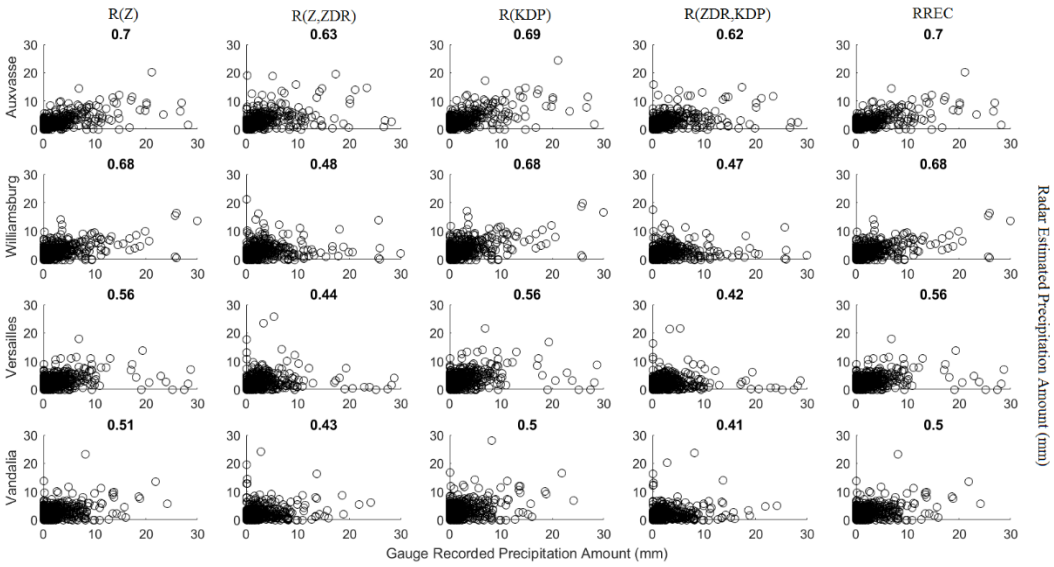

Figure 3A.4. Correlation coefficient values based on the comparison of the gauge recorded (abscissa) and radar estimated (ordinate) rainfall amounts for each of the five-best performing algorithms at each of the four gauges utilized.

algorithms showed more spread in the correlation data, particularly at Auxvasse. Although the RREC displayed spread in the data as well, the magnitudes of error were, typically, contained below 15 mm as estimated by the radar. Furthermore, the radar tended to underestimate precipitation for R(Z) and RREC, but showed larger radar estimated precipitation for R(KDP) and R(ZDR,KDP), correlating with the bias values found earlier (Table 3A.3).

Quantitative analyses

The quantitative analyses are the amount of precipitation associated with each miss, false alarm, or due to error overall. Additionally, the overall accumulation of

precipitation over the course of the study is presented to determine whether the errors cancel out over longer time periods.

Although it was found that 15, 17, 15, and 14% of rainfall events were missed, this accounted for 6.5, 5.6, 11.0, and 11.6% of the error relative to the gauge (Table 3A.4). This indicates that, on average, most of the missed precipitation events were for values less than 1.0 mm. For algorithms that did not contain ZDR, the furthest location (Vandalia) typically registered the largest MPA values, in addition to contributing the greatest quantity of MPA compared to the gauge accumulated total for any of the four locations. The largest MPA for R(Z) was at Vandalia (180.8 mm), which was 11.6 of the total gauge amount, where QPE's estimated at Williamsburg only recorded 99.4 mm of MPA (5.6% of total). Although Williamsburg (second-nearest gauge) recorded the least amount of MPA for R(Z), R(KDP) and RREC, the closest gauge (Auxvasse) registered the least amount of missed precipitation for R(Z,ZDR) (101.1 mm) and R(ZDR,KDP) (105.1 mm). Overall, the R(Z,ZDR) algorithm registered the least amount of missed precipitation overall at Auxvasse.

Conversely, the R(KDP) equation was calculated to have the lowest MPA (95.6) at Williamsburg, with R(Z) and RREC both recording 98.7 mm. This accounted for 5.4 and 5.6% of the total gauge recorded rainfall amount (1769.3 mm), while R(Z,ZDR) and R(ZDR,KDP)'s MPA percentages were 9.9 and 11.3%, accordingly. Therefore, algorithms containing ZDR tend to underestimate the rain rate at Williamsburg such that values less than 0.25 mm were registered and, ultimately, assumed no precipitation to be present. Larger magnitudes of ZDR were thus estimated by the radar, lowering the overall QPE for both R(Z,ZDR) and R(ZDR,KDP).

Table 3A.4. Quantitative analyses, including the missed precipitation amount (MPA), false precipitation amount (FPA), and total precipitation error (TPE). Percent indicates the relative error due to either MPA or FPA relative to the gauge accumulated precipitation amount (Gauge Precip row).

	Auxvasse	Williamsburg	Versailles	Vandalia
Gauge Precip	1695.7	1769.3	1583.7	1557.4
R(Z)	MPA: 110.3 Percent: 6.5 FPA: 634.0 Percent: 37.4 TPE: 1739.6	MPA: 99.4 Percent: 5.6 FPA: 633.9 Percent: 35.8 TPE: 1906.7	MPA: 174.4 Percent: 11.0 FPA: 674.23 Percent: 42.6 TPE: 1899.3	MPA: 180.8 Percent: 11.6 FPA: 811.3 Percent: 52.1 TPE: 2096.9
R(Z,ZDR)	MPA: 101.1 Percent: 6.0 FPA: 265.1 Percent: 15.6 TPE: 1512.0	MPA: 175.5 Percent: 9.9 FPA: 295.8 Percent: 16.7 TPE: 1751.0	MPA: 224.1 Percent: 14.2 FPA: 417.1 Percent: 26.3 TPE: 1750.2	MPA: 204.3 Percent: 13.1 FPA: 382.9 Percent: 24.6 TPE: 1664.3
R(KDP)	MPA: 107.6 Percent: 6.3 FPA: 794.7 Percent: 46.9 TPE: 2020.3	MPA: 95.6 Percent: 5.4 FPA: 797.7 Percent: 45.1 TPE: 2230.6	MPA: 172.1 Percent: 10.9 FPA: 840.6 Percent: 53.1 TPE: 2256.6	MPA: 171.9 Percent: 11.0 FPA: 1012.1 Percent: 65.0 TPE: 2470.4
R(ZDR,KDP)	MPA: 105.1 Percent: 6.2 FPA: 233.7 Percent: 13.8 TPE: 1436.5	MPA: 200.4 Percent: 11.3 FPA: 254.2 Percent: 14.4 TPE: 1647.1	MPA: 268.8 Percent: 17.0 FPA: 373.1 Percent: 23.6 TPE: 1657.3	MPA: 224.4 Percent: 14.4 FPA: 321.8 Percent: 20.7 TPE: 1586.0
RREC	MPA: 109.3	MPA: 98.7	MPA: 174.2	MPA: 180.8

	Percent: 6.4 FPA: 635.2 Percent: 37.5 TPE: 1748.0	Percent: 5.6 FPA: 635.2 Percent: 35.9 TPE: 1912.7	Percent: 11.0 FPA: 674.2 Percent: 42.6 TPE: 1899.9	Percent: 11.6 FPA: 811.3 Percent: 52.1 TPE: 2103.6

Due to the fact Versailles and Vandalia were 75 and 80 km from the MZZU radar, their differences in overall error were dependent upon the algorithm chosen. For example, similar to the instances when R(Z), R(KDP), and RREC were lower in MPA and the MPA percentage at Williamsburg than Auxvasse, these algorithms were more accurate at Versailles than Vandalia. This result demonstrates that the algorithms containing ZDR were superior at close (Auxvasse) and further (Vandalia) ranges from the MZZU radar, whereas the other three equations were best at intermediate distances (i.e., between 45 and 75 km).

As noted in the contingency analyses section, the number of false alarms outnumbered the counts of misses by more than six times, mirroring the number of hits, overall. Therefore, the false precipitation amount (FPA) is, unsurprisingly, approximately six times the MPA, particularly for the algorithms that did not contain ZDR. Conversely, R(Z,ZDR) and R(ZDR,KDP) recorded, approximately, twice the amount of FPA as MPA. For example, the FPA for R(Z,ZDR) at the gauge locations at increasing distances from the radar were 265.1, 295.8, 417.1, and 382.9 mm, whereas the MPA were 101.1, 175.5, 224.1, and 204.3 mm, respectively. This indicates that no MPA for R(Z,ZDR) was more than 15% of total precipitation measured at the gauge locations, whereas FPA did not exceed 27% (but was no lower than 15%). However, R(ZDR,KDP) displayed the

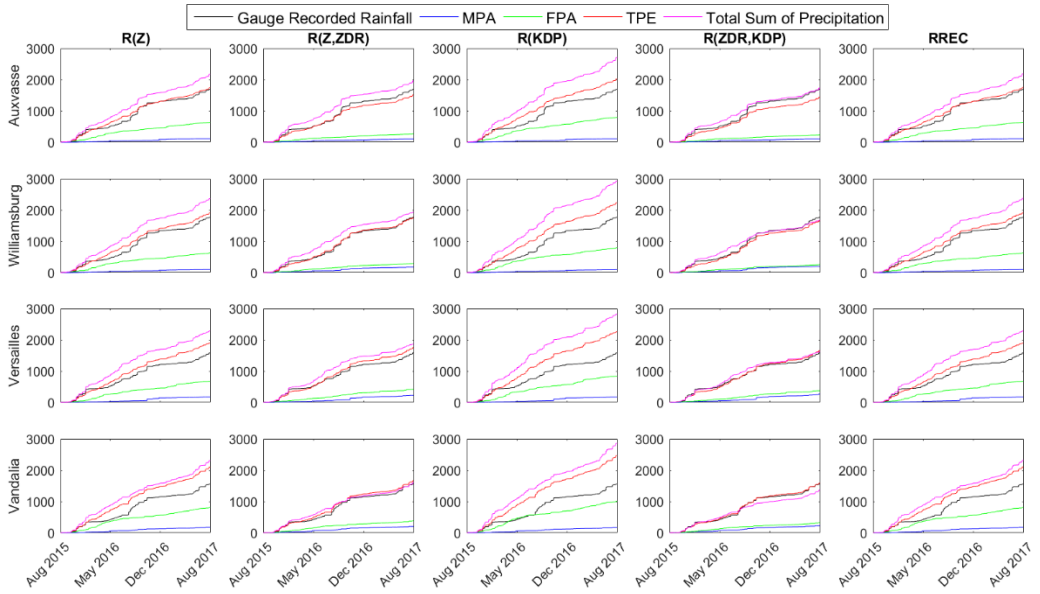

Figure 3A.5. Cumulative sum of the gauge recorded precipitation, missed precipitation amount (MPA), false precipitation amount (FPA), total precipitation error (TPE), and the overall accumulation of precipitation estimated by the specified radar QPE algorithm at each of the four gauge locations.

lowest FPA, overall, at each location such that it did not exceed 375 mm (373.1 mm at Versailles) nor did it register any less than 230 mm (233.7 mm at Auxvasse).

The sum of precipitation represents the amount of precipitation that would result if the direct accumulation of radar estimated QPE were conducted, such that missed precipitation were not included and false alarms were accounted for. Essentially, it acts as a long-term performance of the QPE from each algorithm at each site.

At all locations, the R(Z), R(KDP), and RREC overestimated the amount of total radar estimated QPE compared to the gauge recorded rainfall (Figure 3A.5). Furthermore,

the FPA tends to exceed the overall gauge recorded rainfall amount for these algorithms as well (Table 3A.4). The only algorithm which had a lower total accumulation of radar estimated QPE than the gauge recorded amount of rainfall was R(ZDR,KDP) at both Williamsburg and Vandalia. However, R(Z,ZDR) had more similar values (within 20 mm) at Vandalia than R(ZDR,KDP) than at Williamsburg.

From the quantitative analyses, it is seen that the ZDR-containing algorithms R(Z,ZDR) and R(ZDR,KDP) not only displayed the overall lowest MAE and NSE, but are more accurate with their overall accumulation of precipitation with respect to time. In other words, in spite of the relatively large FPA and MPA across all algorithms at each location, the ZDR-containing equations cancelled the FPA, MPA, and overall MAE over time, resulting in accurate gauge-accumulation precipitation amounts.

Conclusions

The current study analyzed two years' worth of X-band dual-polarimetric quantitative precipitation estimates (QPE) from Central Missouri. Four separate terrestrial-based precipitation gauges (i.e., tipping buckets) served as ground truth. Over 50 algorithms were tested, of which the analyses of the five best from each grouping of algorithms from R(Z), R(Z,ZDR), R(KDP), R(ZDR,KDP), and echo classifiers, were reported. Statistical, contingency, and overall quantitative analyses were reported to determine not only the best performing algorithms overall, but to determine the cause of the error.

The best equations were determined to be the R(Z)-Convective algorithm, an NSSL-derived R(Z,ZDR) equation from Ryzhkov et al., (2003, 2005), an R(KDP) equation from Matrosov (2009), an R(ZDR,KDP) equation from Koffi et al. (2014), and the rain rate echo classifier. Algorithms containing reflectivity typically exhibited negative biases, of which, the R(Z,ZDR) had the lowest bias values, overall. Conversely, the KDP-containing algorithms showed positive biases, with the R(KDP) being the largest, overall.

Overall, the R(Z,ZDR) and R(ZDR,KDP) equations performed the best. This was evidenced as these algorithms having the lowest MAE and NSE at nearly every gauge location. Furthermore, these were the only equations which exhibited NSE values below 100 %, particularly at the two closest gauge locations (30 and 45 km from the radar). However, these equations had the overall lowest correlation coefficient (R^2) values in comparison to the other algorithms. It is theorized that these low R^2 values were due, primarily, from an overall larger spread in the QPE's from these particular equations. The R(Z), R(KDP), and RREC algorithms exhibited correlation values as large as 0.70 at the closest gauge location, while values as low as 0.5 were reported at the furthest location (Vandalia, 80 km). A typical reduction in R^2 values were observed as range from the radar increased.

The majority of the error from the QPE's at each location were due to false alarms. In some instances, particularly for R(Z), R(KDP), and RREC, the false precipitation amounts were up to 65% of the total of the gauge accumulated rainfall amounts. Conversely, the ZDR-containing equations displayed not only the lowest missed and false precipitation amounts, but the overall accumulation of precipitation

from these two equations were most similar to the accumulated gauge rainfall amounts, thus indicating the robust performance of the utilization of ZDR in QPE estimates.

The results presented display the accuracy of X-band QPE estimates. It is noted that, however, algorithms used were those established previously by other radar systems. The results of the performance of the radar may be improved by not only comparing results to disdrometer data, but also from combinations of the algorithms at specific rain rates, much like the overall Joint Polarization (Ryzhkov et al., 2005; Giangrande and Ryzhkov 2008) and CSU-CHILL (Cifelli et al., 2011) algorithms. The promising results, particularly through the implementation of the differential reflectivity, further the considerations as to installing the devices as permanent, cost-effective solutions to the WSR-88D NEXRAD system, especially in regions where a gap in the radar coverage exists.

Acknowledgements

This material is based upon work supported by the National Science Foundation under Award Number IIA-1355406. Any opinions, findings, and conclusions or recommendations expressed in this material are those of the authors and do not necessarily reflect the views of the National Science Foundation.

Literature cited

Berne, A., and Krajewski, W.F., 2013: Radar for hydrology: Unfulfilled promise or unrecognized potential? *Adv. Water Resour.*, **51**, 357-366.

Cifelli, R., Chandrasekar, V., Lim, S., Kennedy, P.C., Wang, Y., and Rutledge, S.A., 2011: A new dual-polarization radar rainfall algorithm: Application in Colorado precipitation events. *J. Atmos. Oceanic Tech.*, **28**, 352-364.

Cunha, L.K., Smith, J.A., Baeck, M.L., and Krajewski, W.F., 2013: An early performance of the NEXRAD dual-polarization radar rainfall estimates for urban flood applications. *Wea. Forecasting*, **28**, 1478-1497.

Giangrande, S.E., and Ryzhkov, A.V., 2008: Estimation of rainfall based on the results of polarimetric echo classification. *J. Appl. Meteor. Climatol.*, **47**, 2445-2462.

Gourley, J.J., Giangrande, S.E., Hong, Y., Flamig. Z,, Schuur, T., and Vrugt, J., 2010: Impacts of polarimetric radar observations on hydrologic simulation. *J. Hydrometeorol.*, **11**: 781-796.

Kitchen, M. and Jackson, P.M., 1993: Weather radar performance at long range – simulated and observed. *J. Appl. Meteor.*, **32**, 975-985.

Koffi, A.K., Gosset, M., Zahiri, E.P., Ochou, A.D., Kacou, M., Cazenave, F., and Assamoi, P., 2014: Evaluation of X-band polarimetric radar estimation of rainfall and rain drop size distribution parameters in West Africa. *Atmos. Res.*, **143**, 438-461.

Matrosov, S.Y., Clark, K.A., Martner, B.E., and Tokay, A., 2002: X-band polarimetric radar measurements of rainfall. *J. Appl. Meteor.*, **41**, 941-952.

Matrosov, S.Y, 2010: Evaluating polarimetric X-band radar rainfall estimators during HMT. *J. Atmos. Oceanic Technol.*, **27**, 122-134.

McLaughlin, D., Pepyne, D., Chandrasekar, V., Phillips, B., Kurose, J., Zink, M., Droegemeier, K., Cruz-Pol, S., Junyent, F., Brotzge, J., Westbrook, D., Bharadwaj, N., Wang, Y., Lyons, E., Hondl, K., Liu, Y., Knapp, E., Xue, M., Hopf, A., Kloesel, K., Defonzo, A., Kollias, P., Brewster, K., Contreras, R., Dolan, B., Djaferis, T., Insanic, E., Frasier, S., and Carr, F., 2009: Short-wavelength technology and the potential for distributed networks of small radar systems. *Bull. Amer. Meteor. Soc.*, **90**, 1797-1817.

Ogden, F.L., Sharid, H.O., Senarath, S.U.S., Smith, J.A., Baeck, M.L., and Richardson, J.R., 2000: Hydrologic analysis of the Fort Collins, Colorado, flash floods of 1997. *J. Hydrol.*, **228**: 82-100.

Park, S.G., Maki, M., Iwanami, K., Bringi, V.N., and Chandrasekar, V., 2005: Correction of radar reflectivity and differential reflectivity for rain attenuation at X band. Part II: Evaluation and application. *J. Atmos. Oceanic Technol.*, **22**, 1633-1655.

Ryzhkov, A.V., Giangrande, S., and Schurr, T., 2003: Rainfall measurements with the polarimetric WSR-88D radar. National Severe Storms Laboratory Rep. Norman: OK, 98 pg.

Ryzhkov, A.V., Giangrande, S., and Schurr, T., 2005: Rainfall estimation with a polarimetric prototype of WSR-88D. *J. Appl. Meteor.*, **44**, 502–515.

Simpson, M.J., Hubbart, J.A., and Fox, N.I., 2016: Ground truthed performance of single and dual-polarized radar rain rates at large ranges. *Hydrol. Process.*, **30**, 3692-3703.

Smith, J.A., Seo, D.J., Baeck, M.L., and Hudlow, M.D., 1996: An intercomparison study of NEXRAD precipitation estimates. *Water Resour. Res.*, **32**, 2035-2045.

Vieux, B.E., 2004. Distributed hydrologic modeling using GIS, 2nd ed. Water Science Technology Series. Vol. 48. Kluwer Academic Publishers, Norwell, Massachusetts. ISBN 1-4020-2459-2.

Vieux, B.E., and Bedient, P.B., 2004: Hydrologic prediction accuracy assessment using radar rainfall. *World Water Congress*, **138**, 273.

Vieux, B.E., Cui, Z., and Guar, A., 2004: Evaluation of a physics-based distributed hydrologic model for flood forecasting. *J. Hydrol.*, **298**, 155-177.

Vieux, B.E., and Imgarten, J.M., 2012: On the scale-dependent propagation of hydrologic uncertainty using high-resolution X-band radar rainfall estimates. *Atmos. Res.*, **103**, 96-105.

Wang, Y., and Chandrasekar, V., 2010. Quantitative precipitation estimation in the CASA X-band dual-polarization radar network. *J. Atmos. Oceanic Technol.*, **27**, 1665-1676.

COMPARING NEARBY X-BAND RADAR RAINFALL ESTIMATES VERSUS DISTANT S-BAND RADAR RAINFALL ESTIMATES

Abstract. Accurate measurements in quantitative precipitation estimation (QPE) are essential for hydrometeorological studies. However, many areas in the Continental US (CONUS) reside further than 150 km from the nearest National Weather Service S-band radar, rendering the estimation of rain rates to be inferior to locations closer to the radar. One possible remediation technique is to install smaller, more cost-effective X-band radars intermittent of the National Weather Service radars. Although previous studies have shown superiority with densely populated X-band radars, few have diagnosed whether a single nearby X-band radar provides superior estimation of precipitation than distant S-band radars. The current study analyzed one year's worth of radar QPE data from a recently installed X-band radar (MZZU) compared to two distant S-band radars at St. Louis (KLSX) and Kansas City (KEAX). Results indicate that QPE estimates validated by ground-truthed gauges closest to the MZZU radar are significantly ($p < 0.10$) superior to those from the S-band radars. Conversely, gauges indicate that at distances beyond, approximately, 30 km from the X-band radar, the WSR-88D R(Z)-Convective algorithm was the most accurate, albeit by a non-significant ($p < 0.05$) margin. The majority of the QPE errors for the X-band radar were due to false alarms, whereas missed precipitation constituted the bulk of error for the S-band radars. The results presented demonstrate the importance of quality controlling radar data, especially for X-band dual-polarimetric data, as the performance is highly dependent upon the length of the time period analyzed.

Introduction

Quantitative precipitation estimation (QPE) is one of the most fundamental properties hydrologists and hydrometeorologists consider when undertaking hydrologic simulations. Rainfall provides the largest amount of water input to a watershed for many areas, which is mandatory for the water-mass balance equations necessary for modeling. Over the past few decades, multiple studies have been conducted to calculate rainfall rates estimated by weather radars through algorithms consisting of reflectivity (Z). Furthermore, with the advent of dual-polarization technology being upgraded to the National Weather Service (NWS) Next Generation Radar (NEXRAD) system, differential reflectivity (ZDR), and specific differential phase shift (KDP) have been incorporated into calculating rainfall rates (e.g., Ryzhkov et al., 2003; Matrosov 2010; Cunha et al., 2015).

One of the main benefits of implementing weather radars to estimate near real-time precipitation is the superior areal coverage when compared to terrestrial based precipitation sensors (i.e., rain gauges) which, essentially, are treated as "point" measurements of precipitation. For example, most rain gauges have an orifice diameter of, approximately, 0.2 m whereas S-band and X-band weather radars can cover areas as large as 2.5×10^5 and 3.0×10^4 km^2, respectively. This benefit of increased spatial coverage is compounded by the high temporal resolution of weather radars (on the order of 5 minutes) to cover vast regions of the CONUS at a nearly constant basis. Because of this, researchers have revealed that using radar data as precipitation input to hydrologic models show potential for estimating streamflow which, in turn, shows promise in flood forecasting (e.g., Ogden et al., 2000; Gourley et al., 2010). However, the degree of

improvement varies by study due to the myriad of errors associated with rainfall estimation (Berne and Krajewski, 2013).

The errors associated with radar rainfall estimations, which have been well documented, include inaccuracies in the representation of precipitation shape (Goddard et al., 1982; Beard and Chuang, 1987; Bringi et al., 1998; Gorgucci et al., 2000; Beard et al., 2010), drop size distribution (Zhang et al., 2001; Bringi et al., 2003), range effects on the sample volume (Smith et al., 1996; Seo et al., 2000; Ryzhkov et al., 2003; Cunha et al., 2013) and bright band detection and mitigation (Ryzhkov et al., 2005; Matrosov et al., 2007; Giangrande and Ryzhkov, 2008). Fortunately, significant advances have been made in ameliorating radar performance on precipitation estimates, especially for operationally-based Weather Surveillance Radar – 1988 Doppler (WSR-88D) S-band (10-cm wavelength) radars. However, advances in improving the aforementioned errors on smaller (e.g., X-band) radars haven been limited, primarily due to the effects of stronger attenuation at X-band which hinder rain rate estimates (Matrosov, 2010).

Albeit X-band radars seldom extend beyond 100 km, their relatively low cost and small size have caused a recent surge in studies using these instruments, especially in regions of limited WSR-88D coverage (Brewster et al., 2005, 2008). Because of the differences between Mie-scattering and Rayleigh-scattering of atmospheric hydrometeors at 3-cm and 10-cm wavelengths, respectively, several radar rainfall estimate algorithms have been developed specifically for X-band radars (e.g., Matrosov 2010; Wang and Chandrasekar 2010; Koffi et al., 2014) which differ from algorithms specifically designed for S-band radars (Ryzhkov et al., 2003). However, the amount of improvement of utilizing X-band radar rain rate algorithms to a nearby region which is sparsely

covered by the NEXRAD S-band system of radars has been limited in study. Quantitative analyses into whether improvement in radar rainfall estimates by a localized X-band radar versus a poorly (distant) covered S-band WSR-88D region would provide insight into the usefulness of further X-band radar installations.

The overarching objective of the current work was to determine whether a radar coverage gap region (approximately 150 km from the nearest WSR-88D), in the area of Columbia, MO, benefits from rainfall estimates from a newly-installed nearby X-band radar. One year of radar data were collected from August 2015 to August 2016, where four tipping bucket rain gauges served as ground-truthed data when compared to the rain rate algorithms calculated by the estimates made by the radar. Specific objectives included, (1) calculate the errors and compare the differences between rain rate algorithms from the WSR-88D S-band (St. Louis and Kansas City, MO; KLSX and KEAX, respectively) and the localized X-band (MZZU) radar, (2) calculate contingency table values for both radars, including hits, misses, false alarms, and correct negatives, (3) calculate accuracy, bias, probability of detection, false alarm ratio, probability of false detection, success ratio, threat score, and the equitable threat score from values obtained from (2), and (4) quantitatively calculate the total amount of precipitation correctly and incorrectly estimated by the radars when the terrestrial based gauges did or did not register precipitation.

Study site and data

Study location and precipitation gauge data

One-year of gauge data were collected between August 2015 and August 2016. Eight locations, in all, were utilized for the current study (Figure 3B.1). These locations were chosen based on their proximity to the MZZU X-band radar, such that any gauge maintained by the Missouri Mesonet, established by the Commercial Agriculture Program of University of Missouri Extension within a 90 km radius of the radar, were analyzed. All gauges were manufactured by Campbell Scientific, TE525MM series registering 0.01 mm of precipitation to a balanced fulcrum device (i.e., the tipping bucket) via a 25.4-cm diameter orifice. All gauges were located, approximately, twice-to-three times the distance of the height of the nearest building, compliant with the NWS's Cooperative Observer Program standards. Additionally, all sites were located in regions with properly maintained vegetation to mitigate any effects from turbulence (Habib et al., 1999; Villarini and Krajewski, 2010).

Four of the gauges were located in Central Boone County, MO. These represent the densest of gauge locations maintained by the Missouri Mesonet, which had accumulations of precipitation of 1165, 1095, 1087, and 1082 mm for an average of 1107 mm, overall, slightly larger than the 30-year climatological average for the region. An analysis of variance (ANOVA) table was constructed to determine whether a significant difference ($p < 0.05$) in precipitation existed between the four gauges. Furthermore, ANOVA tables in which different grouping of gauges were implemented to determine if any one gauge was unrepresentative of the rest. It was determined, similar to Simpson et al. (2016) that the gauges do not exhibit a significant difference ($p < 0.10$) in precipitation amounts for the current study period. Therefore, the four gauges (Bradford Farms, Capen Park, Jefferson Farms, and Sanborn Field) were averaged to produce a single-point

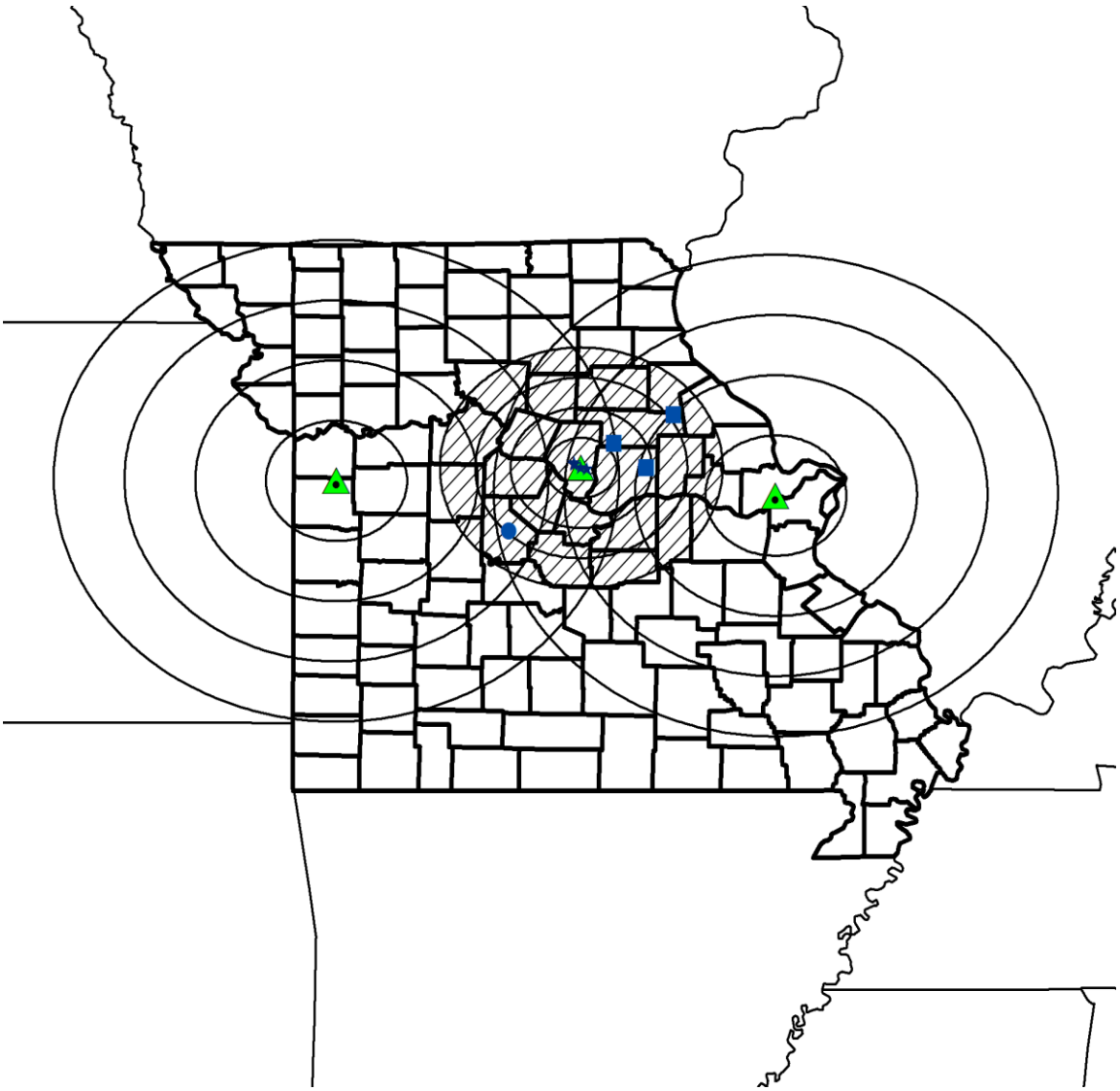

Figure 3B.1. Study site including the X-band (MZZU) radar (centered) with 25, 50, 75, and 100 km range rings (stippled), two S-band radars, Kansas City (KEAX, left) and St. Louis (KLSX, right) with 50, 100, 150, and 200 km range rings. Blocked gauges represent those analyzed by both MZZU and KLSX, starred gauges indicate the four locations analyzed by all three radars, and the circle gauge represents the location analyzed by both MZZU and KEAX.

calculation of rainfall, referred to hereafter, collectively, as Boone.

The other four gauges, Auxvasse, Vandalia, Versailles, and Williamsburg, produced accumulation of precipitation values of 931, 829, 766, and 887 mm, respectively. These locations were chosen due to their proximity to either the St. Louis (KLSX) or Kansas City (KEAX) radars. Furthermore, due to the decreased performance of radar rain rate estimations beyond, approximately, 180 km from the WSR-88D radar (Ryzhkov et al., 2003, 2005), only locations within this range were chosen. Therefore, MZZU analyzed all five gauges (including Boone: the average of the four gauges), whereas KLSX radar rainrates were compared to Boone, Auxvasse, Vandalia, and Williamsburg, and KEAX's performance was compared to the observed values from Boone and Versailles.

The current study is to determine the difference between the rain rate estimates from the S-band radars (KLSX and KEAX) and the X-band radar (MZZU). Therefore, MZZU and KLSX's rain rate estimates were compared to Auxvasse, Boone, Vandalia, and Williamsburg, whereas MZZU was compared with the performance of estimating rain rates from KEAX at Boone and Versailles. This indicates that four gauges served as ground-truth between MZZU and KLSX, and two gauges between MZZU and KEAX.

The radar data were processed in similar fashions to all previous chapters. However, the current study analyzed data from August 2015 through August 2016 from MZZU (X-band), KLSX (St. Louis), and KEAX (Kansas City). Furthermore, from previous studies (e.g., Simpson et al., 2016; Simpson and Fox, 2017), It was shown that the following algorithms performed the best for the S-band radars and are used for the remainder of this analysis:

$$R(Z) = 0.0033Z^{0.714} \quad \text{(3B.1)}$$

$$R(KDP) = 47.3 \mid DKDP \mid^{0.791} \quad \text{(3B.2)}$$

$$R(Z, ZDR) = 144Z^{0.761} ZDR^{-1.51} \quad \text{(3B.3)}$$

$$R(ZDR, KDP) = 52.9 \mid DKDP \mid^{0.852} ZDR^{-0.53} \quad \text{(3B.4)}$$

However, the X-band radar algorithms consisted of the 55 equations presented in Simpson et al. (2016) and Simpson and Fox (2017), in addition to previous X-band research. For example, six, three, and two R(KDP) algorithms were adopted from Matrosov (2009), Wang and Chandrasekar (2010), and Koffi et al. (2014), respectively, in addition to two R(Z,ZDR) and R(ZDR,KDP) algorithms which were adopted from Matrosov (2009) and Koffi et al. (2014), respectively. Furthermore, as with the S-band algorithms, all measures of Z, ZDR, and KDP were tested with their KDP-smoothed derivatives, DSMZ, DZDR, and DKDP, resulting in 108 algorithms tested for the X-band MZZU radar. It was found that the R(Z)-Convective (eq. 3B.1) and R(Z,ZDR) (eq. 3B.3) were the best performing equations from their respective grouping of algorithms, the same as the S-band equations. However, the best performing X-band equations were:

$$R(KDP) = 14.9 \mid DKDP \mid^{0.791} \quad \text{(3B.5)}$$

$$R(ZDR, KDP) = 15.13 \mid DKDP \mid^{0.94} ZDR^{-0.29} \quad \text{(3B.6)}$$

from Matrosov (2009) and Koffi et al. (2014), respectively. Therefore, when R(Z) and R(Z,ZDR) are referenced for either the S-band or X-band radar, equations (3B.1) and (3B.3) are implied. For R(KDP) and R(ZDR,KDP), equations (3B.2) and (3B.4) and equations (3B.5) and (3B.6) are referred to the S-band and X-band radars, respectively.

Results and discussion

Results were divided into overall and comparisons between the S-band and X-band results. The overall analyses encompass the effects of radar rain rate performance with range. Conversely, comparisons between S-band and X-band were divided between MZZU and KLSX (St. Louis), and MZZU and KEAX (Kansas City), such that four and two of the precipitation gauges utilized in the study served as ground truth, respectively. The four gauges (Auxvasse, Vandalia, Versailles, and Williamsburg) in addition to the average of the four co-located gauges (Boone) were assessed for total precipitation accumulation (Figure 3B.2). Auxvasse registered 931.3 mm of precipitation, with Boone, Vandalia, Versailles, and Williamsburg all recording 772.2, 829.2, 766.4, and 887.1 mm of rainfall, respectively. Although the majority of precipitation fell during the warm season, several convective storms passed through the state of Missouri on 27 November and the evening of 26 December, 2015, both registering over 50 mm of precipitation. Otherwise, the cool season precipitation was, primarily, marked by shallow stratiform snowfall, registering little precipitation.

Statistical Analyses

All five of the gauges were closest to MZZU (circled) in comparison to the two S-band radars up to a range of approximately 80 km, whereas the KLSX radar (starred) was 95, 100, 122, and 140 km from its respective gauges analyzed, and KEAX (square) was 130 and 173 km from its closest gauges.

The conventional R(Z) algorithm calculated by the MZZU radar tends to perform

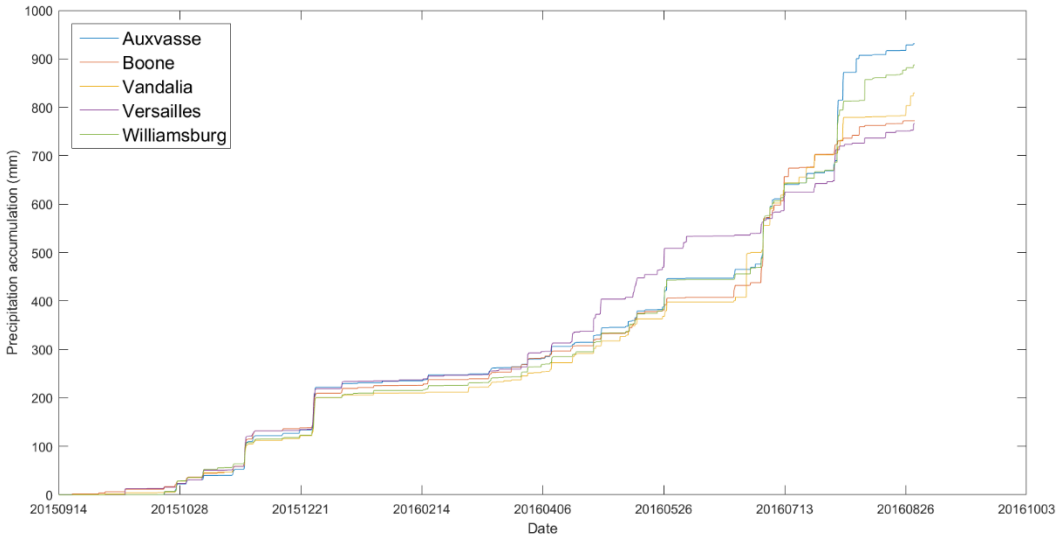

Figure 3B.2. Gauge accumulated precipitation from August 2015 to August 2016 with the five gauges utilized for the current study period.

the best in terms of bias, with the R(Z,ZDR) mirroring the overall performance, with an increase in magnitude towards positive bias (Figure 3B.3). The two X-band algorithms including KDP (eq's 3B.5 and 3B.6) resulted in a large bias to the closest gauge (Boone), eventually oscillating near 0.5 mm of precipitation for the rest of the gauges. Although there was a pronounced difference in the performance of the X-band R(Z) and R(Z,ZDR) algorithms in terms of bias, the KDP containing algorithms were relatively similar. Furthermore, the bias of the MZZU radar containing reflectivity estimates was, generally, slightly negative while R(Z,ZDR) had a slight positive bias. However, with the increased distance from the radar, the KLSX and KEAX biases were negative. Overall, all gauges analyzed by the St. Louis (KLSX) radar produced the most negative bias for algorithms containing reflectivity. For example, the biases recorded at the four KLSX gauges were -0.37, -0.31, -0.48, and -0.27 mm for R(Z) and -0.63, -0.51, -0.73, and -0.47

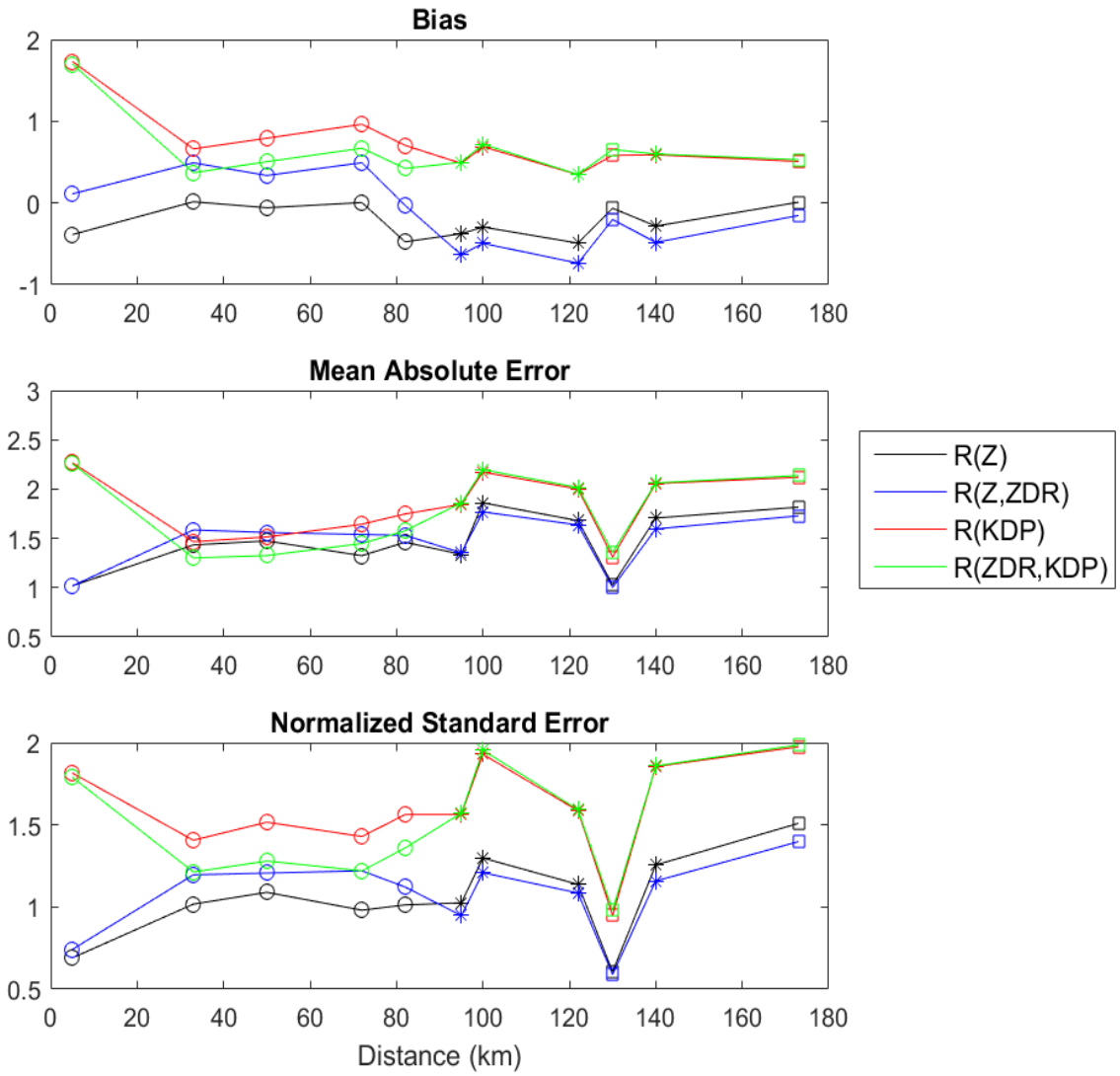

Figure 3B.3. Statistics for the MZZU X-band, St. Louis (KLSX) and Kansas City (KEAX) S-band radars with respect to range represented by circular, starred, and squared points, respectively. Statistics include bias (mm), mean absolute error (mm), and normalized standard error (%).

mm for R(Z,ZDR). Therefore, R(Z,ZDR) algorithms tend to produce more negative bias for S-band radars, whereas the conventional R(Z) equation registered more negative bias than R(Z,ZDR) for the X-band radar.

Typically, as distance from the radar increases, radar rain rate performance should decrease (Ryzhkov et al., 2013, 2015; Cunha et al., 2015). However, the results presented show an oscillatory pattern for the MZZU X-band data, with a general trend of increasing magnitude in error as distance increases for the two S-band radars. For example, the two closest gauges to MZZU (Boone and Auxvasse, 5 and 33 km from the radar, respectively) showed an increase in the MAE of, approximately, 1 mm for R(Z) and 1.5 mm for R(Z,ZDR). The third furthest gauge (Williamsburg at 50 km from the radar) had a slight decrease in the MAE, and the fourth furthest gauge (Versailles at 72 km from the radar) tended to perform equally well to the nearest gauge, Boone. However, the furthest gauge analyzed by the X-band radar saw an increase in the MAE from 1.0 mm, to 1.5 mm and 1.7 mm for R(Z) and R(Z,ZDR), respectively.

Algorithms containing KDP for MZZU analyses produced a decrease in the mean absolute error as distance increased until a distance of 81 km, which registered MAE values similar to those recorded by the majority of the S-band radars (2.2 mm). In general, R(KDP) had a higher MAE than R(ZDR,KDP) for MZZU of 0.25 mm. The R(ZDR,KDP) X-band equation was superior to all other algorithms for MZZU for the second and third gauges, while nearly all algorithms performed equally well at the furthest gauge (81 km).

For the St. Louis (KLSX) radar, the lowest mean absolute error was for the closest gauge (Williamsburg, 95 km from the radar), with R(Z) and R(Z,ZDR) performing the

best (1.3 mm). Thereafter, the next three gauges tended to display a slight decrease in MAE values for KLSX as distance from the radar increased. For example, the MAE for R(Z) at distances of 95, 100, 122, and 140 km registered values of 1.3, 1.9, 1.7, and 1.7 mm, respectively. Similarly, the R(ZDR,KDP) equation registered MAE values of 1.8, 2.2, 2.0, and 2.1 mm, respectively. The four KLSX gauges all had higher MAE's than Boone and Vandalia.

The Kansas City (KEAX) radar indicated that error increased with range such that the MAE at 130 km was 1.0 mm while the MAE at 173 km was 1.7 mm for both the R(Z) and R(Z,ZDR) equations. Conversely, the mean absolute error recorded by both the R(KDP) and R(ZDR,KDP) equations for KEAX were 1.35 and 2.2 mm, respectively, indicating algorithms containing reflectivity perform best for S-band radars, overall. The results presented coincide with those found by Simpson et al. (2016) such that the overall performance of KEAX tends to be superior to that of KLSX, despite the radar being further from the gauges analyzed.

The normalized standard error (NSE) remained near 100% (1.0) for the four gauges beyond the closest to the MZZU radar (Boone) using the R(Z)-Convective algorithm. In general, R(Z)-Convective outperformed the other three algorithms in terms of NSE, with that for R(Z,ZDR) typically being 10-15% more than the R(Z) equation. The three middle gauges for MZZU showed relatively similar comparisons in NSE values for both equations containing the differential reflectivity near 1.2. With the exception of the closest gauge from KEAX, the MZZU R(Z) equation tended to outperform the S-band locations in terms of NSE. Conversely, the R(KDP) and R(ZDR,KDP) both exhibited the largest NSE values, and were the only algorithms with above 1.5 NSE values.

In general, algorithms containing reflectivity (R(Z) and R(Z,ZDR)) outperformed algorithms containing KDP. Furthermore, only one location from each of MZZU (Boone, 5 km from the radar), KLSX (Williamsburg, 95 km from the radar), and KEAX (Versailles, 130 km from the radar) recorded an NSE below 1.0, all locations that were the closest gauge analyzed from each radar. None of the algorithms registered NSE values above 2.0.

Corresponding to Figure 3B.3, all conventional R(Z) bias values for MZZU and KLSX were negative with the exception of MZZU Vandalia and Williamsburg (Figure 3B.4). Conversely, all KLSX R(Z,ZDR) bias were negative whereas all MZZU R(Z,ZDR) biases were positive. The overall magnitude of R(Z) and R(Z,ZDR) bias registered by the MZZU radar was less than that by the KLSX radar. However, all R(KDP) and R(ZDR,KDP) equations resulted in a positive bias, with the MZZU R(KDP) producing larger biases than KLSX. The R(ZDR,KDP) X-band equation outperformed the S-band R(ZDR,KDP) algorithm at all locations with the notable exception of the closest gauge to MZZU (furthest from KLSX), Boone (1.8 mm for MZZU and 0.5 mm for KLSX, respectively).

The mean absolute error R(Z) and R(Z,ZDR) values were smaller for the S-band KLSX radar at all locations except the closest to the X-band radar (5 km for MZZU and 140 km for KLSX), indicating the robust performance of the S-band algorithms utilized by KLSX up to a distance of, approximately, 140 km. Conversely, the performance of the R(KDP) and R(ZDR,KDP) algorithms tended to perform equally well for the X-band and S-band radars. For example, the largest difference in MAE for any of the four gauges compared between KLSX and MZZU was at Boone (2.2 mm for MZZU and 2.0 mm for

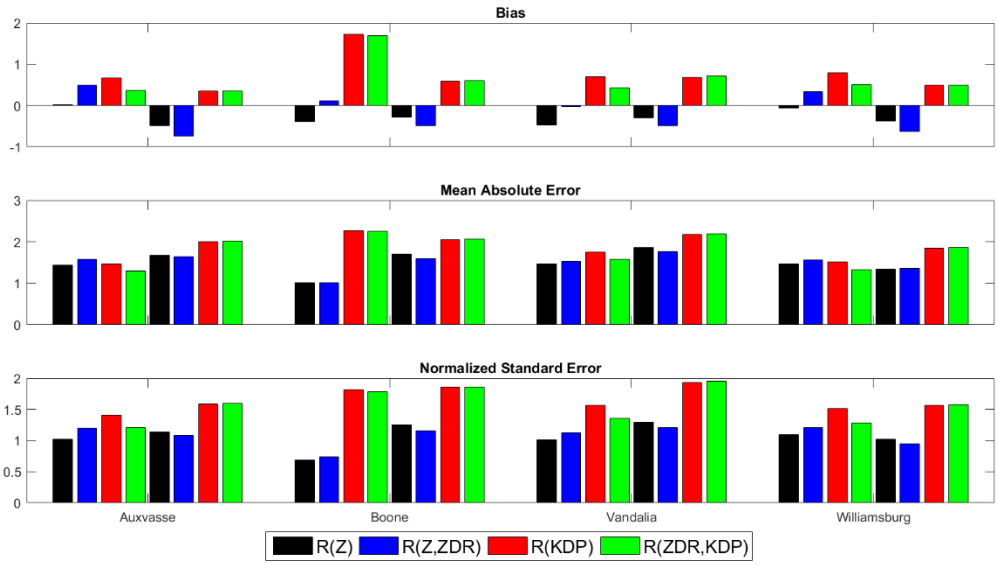

Figure 3B.4. Statistical comparisons between the MZZU X-band and St. Louis (KLSX) S-band radars including bias (mm), mean absolute error (mm), and normalized standard error (%). Distances from the Auxvasse, Boone, Vandalia, and Williamsburg sites were 33 and 122, 5 and 140, 81 and 100, and 50 and 95 km from MZZU and KLSX, respectively.

KLSX R(KDP)) due to, at least in part, to the large discrepancy in distance from the gauge of the two radars. This result demonstrates the independence of KDP on the effects of calibration between different wavelength radars, since the difference between R(Z) and, especially, R(Z,ZDR) MAE values were significantly ($p < 0.10$) different at all four locations, but were not significantly ($p < 0.01$) different between either of the KDP-containing algorithms.

In general, the NSE followed the same pattern of the MAE. The smallest NSE values were for MZZU R(Z) and R(Z,ZDR) at Boone (5 km) with values of 0.69 and 0.75 %, respectively. Similarly, the closest gauge to KLSX (Williamsburg, 95 km) registered

The four results to the left and right of each location represent results from, respectively, MZZU and KLSX.

NSE values of 1.03 and 0.95 % for R(Z) and R(Z,ZDR), respectively, representing the only locations and algorithms where the cumulative sum of the MAE did not exceed the gauge-recorded precipitation amount. The largest NSE values for MZZU were at the furthest location (Vandalia, 81 km) such that R(KDP) registered over 2.50% and R(ZDR,KDP) was 2.27 %. The KDP-containing algorithms also performed worst at this location as estimated by the KLSX radar, with NSE values of 1.94 % for R(KDP) and 1.97 % for R(ZDR,KDP). The only location whereby the NSE at MZZU was significantly ($p < 0.05$) less than at KLSX was for the R(Z) and R(Z,ZDR) equations at the closest location (Boone); KLSX outperformed MZZU at all other locations.

Similar to the results of MZZU and KLSX performance at the Boone location, MZZU outperformed KEAX at its closest location in terms of MAE and NSE (Figure 3B.5). However, the KEAX bias for the conventional R(Z) equation was slightly positive at 0.1 mm while the MZZU bias was -0.3 mm. The bias switched signs for the R(Z,ZDR) results, such that MZZU registered an average error of 0.2 mm and KEAX registered -0.2 mm for the bias. This indicates that the inclusion of ZDR to reflectivity measurements at large distances (140 km for KLSX and 173 km for KEAX) results in, overall, a decrease in the magnitude of precipitation. This is evidenced such that as distance increases, the radar beam samples a higher height level in the atmosphere, whereby larger droplets exist, causing the ZDR value to decrease (eq. 3B.3).

There were no significant ($p < 0.10$) differences between the MAE at Versailles between the two radars for any algorithm. However, similar to the MZZU and KLSX

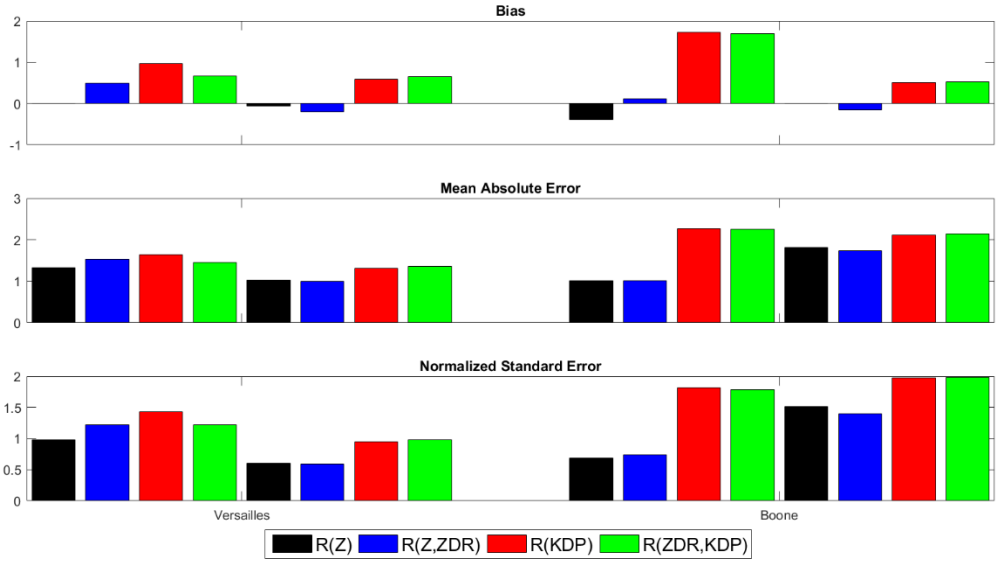

Figure 3B.5. Statistical comparisons between the MZZU X-band and Kansas City (KEAX) S-band radars including bias (mm), mean absolute error (mm), and normalized standard error (%). Distances from the Versailles and Boone sites were 72 and 130, and 5 and 173 km for MZZU and KEAX, respectively. The four results to the left and right of each location represent results from, respectively, MZZU and KEAX.

comparison, there was a significant difference ($p < 0.01$) in the MAE and NSE of R(Z) and R(Z,ZDR) between MZZU and KEAX. However, all algorithms estimated by the KEAX radar registered significantly ($p < 0.01$) lower NSE values than at the MZZU radar. Therefore, with the exception of the gauge that was 5 km from the MZZU radar (Boone), all other algorithms at each site location were superior when analyzed by the S-band radars based on the normalized standard error.

Contingency analyses

The contingency analyses include the number of hits, misses, and false alarms, indicating instances when the radar and gauge both recorded rainfall to be present, when the gauge recorded precipitation but the radar did not register rainfall, and when the radar estimated precipitation to be present but the gauge recorded no rainfall, respectively.

As distance from the gauges increased, the overall number of hits tended to decrease (Figure 3B.6). The largest number of hits was recorded at the closest gauge to the MZZU radar while utilizing the R(Z,ZDR) algorithm (374 hits), with the other three equations performing similarly (350 hits). Otherwise, the R(KDP), closely followed by the R(ZDR,KDP) equation, tended to register more hits than either the R(Z,ZDR) or R(Z) equations for MZZU. Furthermore, the number of hits was significantly more ($p < 0.10$) than any of the four locations analyzed by MZZU and the KLSX radar while utilizing the R(KDP)-containing algorithms. Conversely, the number of hits registered while implementing either R(Z) or R(Z,ZDR) was significantly different ($p < 0.10$) at Boone (5 km and 140 km for MZZU and KLSX, respectively) and Vandalia (81 km from MZZU and 100 km from KLSX).

The R(KDP) equation recorded 22 less hits than the R(Z,ZDR) at Boone, but registered 25, 47, 30, and 31 more hits at the next four furthest locations, respectively. Conversely, the R(Z) and R(Z,ZDR) equations showed superiority in registering hits for the S-band radars with the exception of the furthest location from KLSX (Boone; 234 for R(KDP) and R(ZDR,KDP) and 230 hits for R(Z,ZDR)). This may be due to an implicit bias with the specific differential phase shift in relatively low rain rates (Zrnic and Ryzhkov, 1996). Additionally, the overall spread in the performance between KDP-

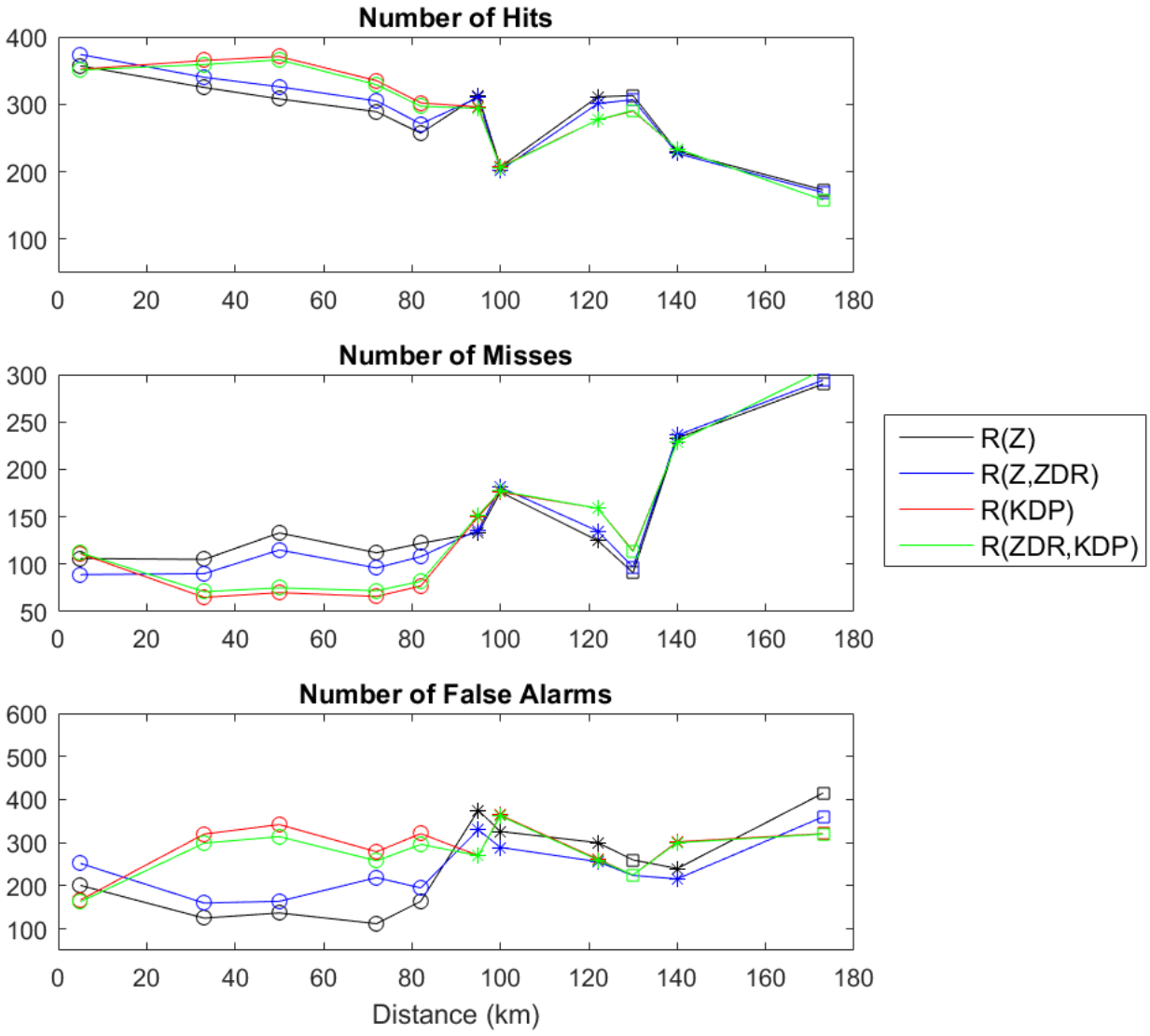

Figure 3B.6. Contingency analyses for the MZZU X-band, St. Louis (KLSX) and Kansas City (KEAX) S-band radars with respect to range represented by circular, starred, and squared points, respectively.

containing and Z-containing algorithms were more pronounced for the X-band radar than the S-band radars, providing evidence of the sensitivity of shorter wavelengths on KDP QPE estimates (Wang and Chandrasekar, 2010; Kumjian 2013a, 2013b).

The lowest number of hits were recorded at the furthest gauge location, Boone, by the KEAX radar (173 km) with 173 for R(Z), 169 for R(Z,ZDR), and 158 for both R(KDP) and R(ZDR,KDP). The results presented show that as distance increases from the radar, the overall performance between each algorithm tends to become nebulous, contradicting the results of previous authors (e.g., Ryzhkov et al., 2003; Cunha et al., 2013) who describe the superiority of KDP at large distances. This may be due, at least in part, to the fact that QPE equations derived specifically for the KLSX or KEAX radars were not conducted, such that ZDR biases (Illingworth, 2004; Ryzhkov et al., 2005; Ice et al., 2013) and overall radar mis-calibrations (Hubbert and Bringi, 1995; Atlas, 2002; Williams et al., 2005) may result in similar QPE estimates.

The number of misses in general, displayed an increasing trend as distance from the radar increased, consistent with what others have found with QPE performance with range (Kitchen and Jackson, 1993; Smith et al., 1996; Ryzhkov et al., 2005). Similar to the results of the number of hits, the X-band R(Z,ZDR) algorithm performed best for the closest gauge to MZZU, with the R(KDP) and R(ZDR,KDP) equations outperforming both reflectivity-containing algorithms for the rest of the four MZZU gauges analyzed. Furthermore, the number of misses registered by the four furthest gauges from MZZU were only 65, 70, 66, and 77, and 71, 75, 72, and 82 for R(KDP) and R(ZDR,KDP), respectively, out of the 7075 hours of data analyzed, outperforming all gauge comparisons to the S-band radars.

The greatest number of misses were registered at the furthest two locations from KLSX and KEAX, both at Boone (140 and 173 km, respectively), with values of, approximately, 250 and 300, respectively. Similar to the accounts of hits, the closest

location to KEAX, Versailles (130 km) outperformed the four furthest gauges from MZZU, especially when utilizing either R(Z) or R(Z,ZDR) (97 and 115, respectively).

The number of false alarms displayed the most variability between algorithm choice for all three radars. Furthermore, the R(Z) and R(Z,ZDR) equations tended to perform similarly, with R(Z,ZDR), overall, registering a smaller number of false alarms for the S-band radars and R(Z) registered fewer false alarms than R(Z,ZDR) for the X-band radar. The differences between performances may be due to the lack of ZDR calibration (Atlas, 2002; Gourley et al., 2009) and potential noise in the transmitting/receiving chains of the radar, resulting in the high false alarm count for R(KDP) and R(ZDR,KDP) (Hubbert and Bringi, 1995; Wang and Chandrasekar, 2009) for the MZZU radar. However, the smallest number of false alarms at the closest gauge to the MZZU radar were the KDP-containing equations, indicating that noise increases as distance from the radar increases.

The overall lowest false alarm rate was at the middle three gauges from MZZU (Auxvasse: 33 km; Williamsburg: 50 km, and Versailles: 72 km) with values of 125, 137, and 112, respectively. Conversely, the largest false alarms (415) were utilized by the R(Z)-Convective algorithm by KEAX (173 km).

The results indicate that the differential reflectivity has a larger impact on reflectivity estimates than on KDP estimates. For example, the average difference between R(Z) and R(Z,ZDR) hits, misses, and false alarms were 50, 73, and 82, respectively, whereas the average difference in the counts of hits, misses, and false alarms between R(KDP) and R(ZDR,KDP) were 10, 9, and 20, respectively.

When comparing the X-band and S-band contingency analyses, all accounts of hits and misses across all four algorithms were superior for the MZZU radar in comparison to the KLSX radar (Figure 3B.7). For example, the largest number of hits at Auxvasse, 33 km from MZZU and 122 from KLSX, were 365 and 311, respectively. Similarly, at Boone (5 and 140 km), Vandalia (72 and 100 km), and Williamsburg (50 and 95 km), the largest number of hits were 374 and 234, 302 and 207, and 371 and 313 for MZZU and KLSX, respectively. As previously discussed, the R(KDP) algorithm tend to register the greatest number of hits for MZZU (excluding the closest gauge, Boone), while the R(Z) equation performed best in terms of hit count for KLSX. Only at Boone and Vandalia were the maximum number of hits significantly ($p < 0.10$) different.

Conversely, all locations analyzed by the MZZU radar displayed significantly fewer misses than the KLSX radar ($p < 0.05$). The X-band R(KDP) registered 111 misses at Boone (second to the R(Z) with 106 misses), while KLSX R(KDP) counted 229 misses. The lowest number of misses at Auxvasse, Vandalia, and Williamsburg for the MZZU and KLSX were 65 and 125, 77 and 176, and 70 and 133, respectively. Similar to the occurrences of hits, the R(KDP) performed best for MZZU while R(Z) tended to outperform the other S-band algorithm for KLSX.

The results for the false alarms were less clear than for the hits and misses. For example, while all four of the algorithms for MZZU tended to outperform those at the same gauge as KLSX, the superiority was highly dependent upon the location analyzed. At Boone, the R(Z), R(KDP), and R(ZDR,KDP) registered 201, 167, and 163 false alarms, respectively, whereas R(Z,ZDR) registered 252 false alarms. The St. Louis R(Z) and R(Z,ZDR) outperformed the MZZU R(Z,ZDR) algorithm with 240 and 216,

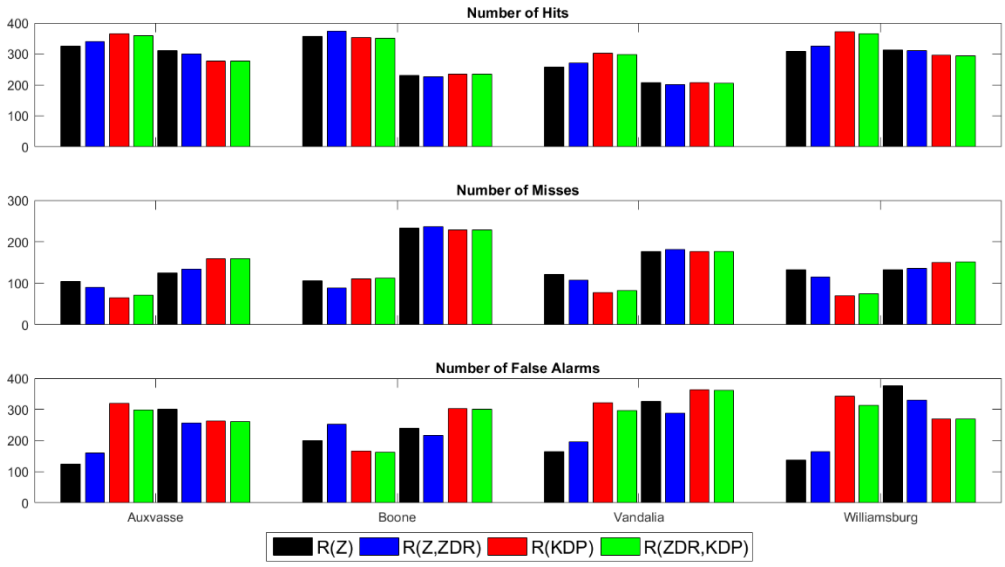

Figure 3B.7. Contingency analyses between the MZZU X-band and St. Louis (KLSX) S-band radars. Distances from the Auxvasse, Boone, Vandalia, and Williamsburg sites were 33 and 122, 5 and 140, 81 and 100, 50 and 95 km from MZZU and KLSX, respectively. The four results to the left and right of each location represent results from, respectively, MZZU and KLSX.

respectively. Conversely, at Auxvasse (33 km from MZZU), the R(Z) and R(Z,ZDR) were significantly ($p < 0.05$) superior to any of the algorithms at KLSX, whereas the X-band R(KDP) was the worst, overall. In spite of the varied performance of each algorithm at the four gauge locations, The R(Z)-Convective tended to outperform the other algorithms for MZZU, while the R(Z,ZDR) was superior for the KLSX radar in terms of lowest false alarms.

When comparing the MZZU and KEAX radars, MZZU performed significantly ($p < 0.05$) better than KEAX at Boone for the number of hits, misses, and false alarms,

whereas the differences were minimal when the results of Versailles were analyzed. For example, the number of hits at MZZU for Boone was 374 for the R(Z,ZDR) equation, but the maximum number of hits analyzed by KEAX was 173 for R(Z), 169 for R(Z,ZDR), and 158 for R(KDP) and R(ZDR,KDP), over twice as many hits (Figure 3B.8). Similarly, the number of misses were over 3 times less for MZZU than at KEAX, and the number of false alarms were twice as less. However, the results were more even for Versailles.

At 72 km from MZZU and 130 km from the KEAX radar, the best algorithms in terms of greatest number of hits were the R(KDP) and R(Z)-Convective equations, respectively, with values of 335 and 313. Similarly, the R(KDP) and R(Z) performed best in terms of the least number of misses (66 for MZZU and 91 for KEAX). However, the least number of false alarms at Versailles were for the R(Z)-Convective equation at MZZU (112) and the R(Z,ZDR), R(KDP), and R(ZDR,KDP) algorithms all registering 225 false alarms. This indicates that the number of false alarms for the MZZU radar, typically, is more sensitive to dual-polarized variables (i.e., ZDR and KDP), whereas the implementation of ZDR and/or KDP to the S-band radars reduces the number of false alarms.

Quantitative analyses

Four different quantitative analyses were computed, including the missed precipitation amount (MPA), the false precipitation amount (FPA), total precipitation error (TPE), and the overall accumulation of precipitation. This will reveal where the bulk of the error of each algorithm from each radar originates from when contributed to the bias, mean absolute error, and normalized standard error.

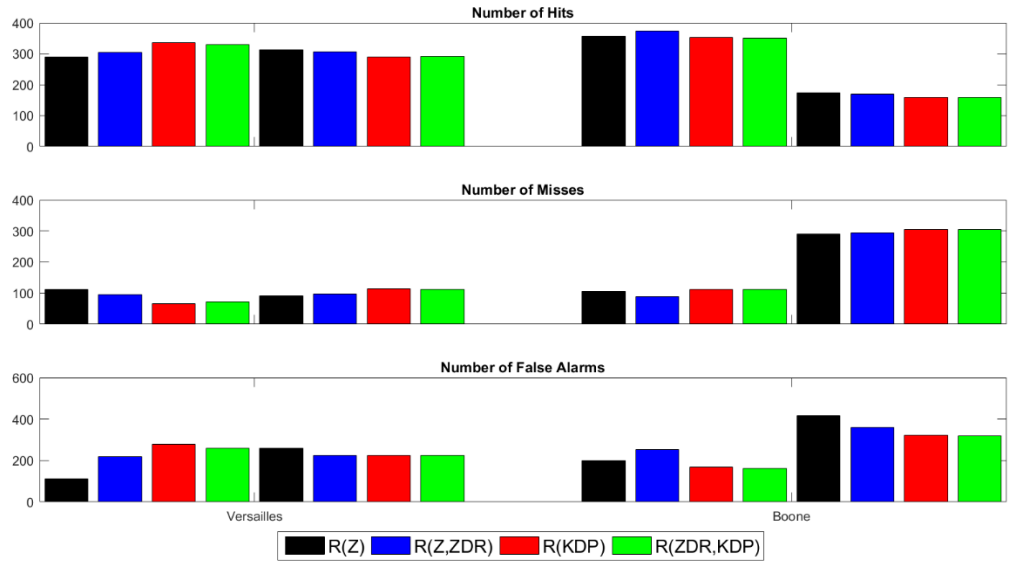

Figure 3B.8. Contingency analyses between the MZZU X-band and Kansas City (KEAX) S-band radars. Distances from the Versailles and Boone sites were 72 and 130, and 5 and 173 km for MZZU and KEAX, respectively. The four results to the left and right of each location represent results from, respectively, MZZU and KEAX.

When one of the gauges records precipitation but the radar does not estimate rainfall to be present, a miss has occurred. Furthermore, quantifying the total amount of precipitation results in the missed precipitation amount (MPA, Figure 3B.9). Results indicate that, in spite of the R(Z,ZDR) equation having the fewest number of misses at the closest gauge to MZZU (Boone), the R(KDP) and R(ZDR,KDP) equations registered the least amount of MPA (66.7 and 68.3 mm of precipitation, respectively) whereas R(Z,ZDR) registered 80.1 mm of missed rainfall.

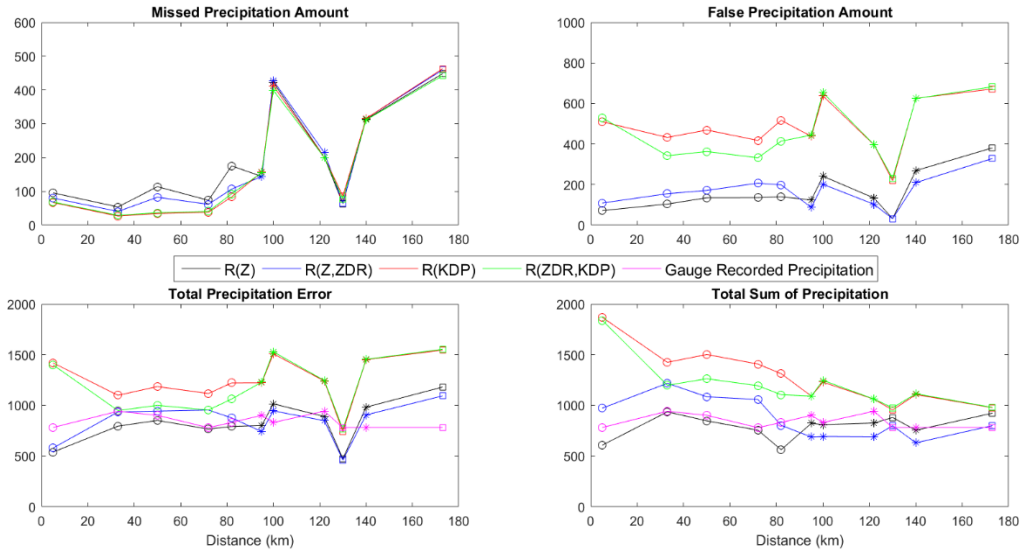

Figure 3B.9. Quantitative analyses including the missed precipitation amount (MPA), false precipitation amount (FPA), total precipitation error (TPE), and the total accumulation of precipitation for the MZZU X-band, St. Louis (KLSX) and Kansas City (KEAX) S-band radars with respect to range represented by circular, starred, and squared points, respectively.

The overall lowest MPA was for the second-closest gauge to MZZU (Auxvasse, 33 km) with 26.7 mm and 29.0 mm of rainfall for R(KDP) and R(ZDR,KDP), respectively. The third and fourth furthest gauges, Williamsburg and Vandalia, also registered less MPA than the least amount from any of the S-band radars. The closest location to KEAX, Versailles (130 km), registered 63.5 and 64.0 mm of MPA for R(Z) and R(Z,ZDR), respectively. The next best-performing gauge was for the closest to KLSX (Williamsburg at 95 km) with an MPA of, approximately, 150 mm across all four algorithms.

The R(Z)-Convective algorithm registered the greatest amount of MPA for the X-band radar, whereas the R(Z,ZDR) and R(KDP) tend to have the greatest MPA for KLSX and KEAX, respectively. The most MPA was for the furthest location (KEAX), with an MPA of 462.8, 459.2, 447.8, and 442.0 mm of rainfall for R(KDP), R(Z,ZDR), R(Z), and R(ZDR,KDP), respectively.

Not only did the R(KDP) algorithms for MZZU register the least amount of overall MPA, they also contributed the least to the overall gauge accumulated precipitation amount (Table 3B.1). For example, of the 772.2 mm recorded at Boone, the R(KDP) equation at MZZU missed 8.6% of the total rainfall. Similarly, 2.9%, 3.9%, 5.0%, and 10.1% were missed at increasing distances from MZZU. In general, the R(KDP,ZDR) equation contributed, at most, 2% more MPA to the total gauge amount of rainfall at any of the sites.

The algorithm which contributed the least to the gauge reported rainfall amount over the course of the current study for the S-band radars was unclear. For example, the performance of each of the algorithms yielded minor differences in the total MPA, with differences no larger than 30 mm. Furthermore, there was no clear distinction between whether reflectivity-containing algorithms, or KDP-containing algorithms were superior than the other for either KLSX or KEAX.

The false precipitation amount (FPA) is the opposite of the missed precipitation amount. However, the results indicate that the bulk of the error in QPE is due to the FPA for the R(KDP) and R(ZDR,KDP) equations for all three radars. This directly correlates to the large positive biases for both R(KDP) and R(ZDR,KDP) for all of the gauges analyzed (Figures 3B.4 and 3B.5). Furthermore, the R(KDP) equation tend to

Table 3B.1. Gauge accumulated precipitation for each of the five stations including the Missed Precipitation Amount (MPA) and its overall percentage relative to the gauge accumulated precipitation amount as analyzed by each radar.

Site / Equation	R(Z)	R(Z,ZDR)	R(KDP)	R(ZDR,KDP)
Boone	772.2	772.2	772.2	772.2
MZZU: 5km	95.3 / 12.3%	80.1 / 10.4%	66.7 / 8.6%	68.3 / 8.8%
KLSX: 140km	313.2 / 40.6%	315.7 / 40.9%	315.5 / 40.9%	311.4 / 40.3%
KEAX: 173km	447.8 / 58.0%	459.2 / 59.5%	462.8 / 59.9%	442.0 / 57.2%
Auxvasse	931.1	931.1	931.1	931.1
MZZU: 33km	53.8 / 5.8%	40.4 / 4.3%	26.7 / 2.9%	29.0 / 3.1%
KLSX: 122km	200.4 / 21.5%	214.4 / 23.0%	200.4 / 21.5%	199.6 / 21.4%
Williamsburg	887.1	887.1	887.1	887.1
MZZU: 50km	113.7 / 12.8%	82.5 / 9.3%	34.4 / 3.9%	36.6 / 4.1%
KLSX: 95km	144.0 / 16.3%	143.8 / 16.2%	156.5 / 17.6%	155.2 / 17.5%
Versailles	766.4	766.4	766.4	766.4
MZZU: 72km	73.4 / 9.6%	61.5 / 8.0%	38.0 / 5.0%	40.7 / 5.3%
KEAX: 130km	63.5 / 8.3%	64.0 / 8.4%	85.6 / 11.2%	76.7 / 10.0%
Vandalia	829.2	829.2	829.2	829.2
MZZU: 81km	175.3 / 21.1%	106.7 / 12.9%	83.4 / 10.1%	92.6 / 11.2%
KLSX: 100km	422.4 / 50.9%	427.5 / 51.6%	411.7 / 49.7%	398.8 / 48.1%

register more false precipitation amount than the R(ZDR,KDP) for the MZZU radar, whereas the opposite was true for the S-band radars. In a similar manner, the R(Z,ZDR)

outperformed the R(Z)-Convective for the S-band radars, whereas the opposite were true for the X-band radar.

The lowest FPA were for the R(Z) and R(Z,ZDR) equations at the closest location to KEAX (31.9 mm and 30.4 mm, respectively). The overall performance of the Kansas City (KEAX) radar has been shown to be superior to the KLSX radar, especially at larger ranges (Simpson et al., 2016; Simpson and Fox 2017). Conversely, the most FPA was registered at the furthest location from KEAX (Boone), with 328.5 mm and 447.8 mm for R(Z,ZDR) and R(Z), respectively, and 671.5 mm for R(KDP) and 682.1 mm for R(ZDR,KDP).

The total precipitation error (TPE) accounts for the MPA, FPA, and overall error (i.e., MAE) and is, essentially, the quantitative error that is due to the normalized standard error (NSE). For example, the graph of the TPE directly mirrors the NSE, but gives a quantitative value to the total error. All of the gauges analyzed by the MZZU R(Z) equation registered NSE values less than 1.0, indicating that the total precipitation error were less than the gauge accumulated precipitation amount. Conversely, the closest and third-furthest gauge from KLSX, and the closest gauge from KEAX both analyzed by R(Z) and R(Z,ZDR) had NSE values less than 1.0 and, thus, recorded less TPE than the gauge accumulated amount. With the exception of the Versailles gauge analyzed by KEAX, there were no instances of either the R(KDP) or R(ZDR,KDP) equations registering less precipitation than that accumulated by the gauge. As indicated by the large FPA values, the positive bias and relatively large MAE values contribute to the excessive errors.

The total sum of precipitation is the quantitative sum of precipitation throughout the event. In other words, it is the sum of what the radar estimated the precipitation amount to be. Given the previous results, it is unsurprising that the R(KDP) and R(ZDR,KDP) overestimated the gauge recorded precipitation amounts for any of the gauges from either of the three radars. Similarly, the overall FPA results tend to mirror the overall total sum of precipitation, since this tend to contribute the largest overall errors for each of the radars. Furthermore, the R(Z,ZDR) and R(Z) equations estimated more and less precipitation than the gauge recorded amount for MZZU, respectively.

In spite of the large errors that were determined to be due to either the MPA or FPA, the overall total sum of precipitation values (particularly for the R(Z) equations) were close in value to the gauge recorded precipitation amount. Therefore, over a year's worth of time, the errors due to the MPA, FPA, and overall error (i.e., MAE) cancelled to achieve an accurate representation of the total yearly gauge accumulated precipitation amount. Thus, the total sum of precipitation could also be considered as the long-term performance of the radar, depending on the time series analyzed. At shorter time-scales, the errors due to the radar's QPEs are more evident, but are smoothed out due to alternating MPA and FPA throughout the course of the year.

The amount of missed precipitation was significantly less ($p < 0.05$) for MZZU than any of the stations for KLSX (Figure 3B.10). In general, the least amount of MPA was the R(KDP) equation for MZZU, while the R(Z,ZDR) equation for KLSX tend to display the largest quantity of MPA (Table 3B.1). This correlates to what previous researchers have found, such that as distance from the radar increased, misses tend to

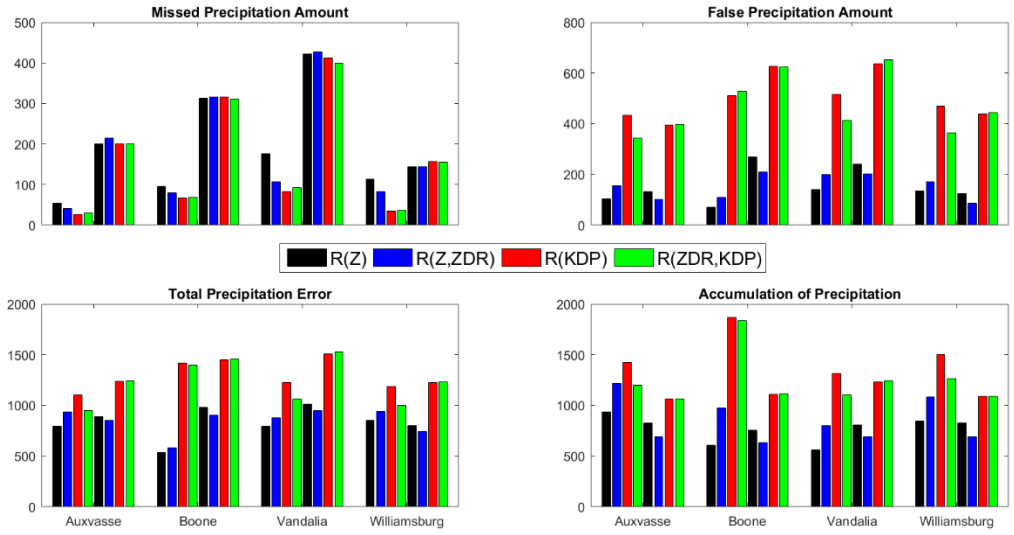

Figure 3B.10. Quantitative analyses between the MZZU X-band and St. Louis (KLSX) S-band radars. Distances from the Auxvasse, Boone, Vandalia, and Williamsburg sites were 33 and 122, 5 and 140, 81 and 100, 50 and 95 km from MZZU and KLSX, respectively. The four results to the left and right of each location represent results from, respectively, MZZU and KLSX.

increase due to overshooting of the beam, especially during the cool season (Ryzhkov et al., 2005; Cunha et al., 2015).

With the exception of the R(KDP) and R(ZDR,KDP) equations, the reflectivity-containing algorithms for MZZU outperformed those from KLSX. One notable exception was at Williamsburg, where KLSX outperformed MZZU (87.0 mm for the R(Z,ZDR) equation, and 134.8 mm for MZZU while utilizing R(Z)), while the KLSX R(Z,ZDR) equation performed equally as well as the MZZU R(Z)-Convective equation (103.8 mm) at Auxvasse. The X-band R(KDP) equations outperformed the KLSX R(KDP) equation

at Boone (5 and 140 km) and Vandalia (81 and 100 km), while the MZZU R(ZDR,KDP) outperformed all of the KLSX KDP-containing equations.

With the exception of Williamsburg, the MZZU radar registered less total precipitation error (TPE) than the other three locations analyzed by KLSX and MZZU, primarily due to the large number of hits registered by KLSX at this gauge, offsetting the highest number of false alarms registered by KLSX. In spite of the KDP-containing algorithms all producing TPE's greater than 1000 mm, MZZU was still superior than KLSX QPE's. As was observed via Figure 3B.6, the R(Z) and R(Z,ZDR) equations recorded the least amount of TPE for MZZU and KLSX, respectively.

The missed precipitation amount between MZZU and KLSX at Boone were significantly ($p < 0.05$) different, such that KEAX registered approximately five times as much than MZZU (Figure 3B.11). However, the MPA at Versailles were similar, evidenced by the 40.0 mm and 63.5 mm of precipitation missed by the MZZU R(KDP) and KLSX R(Z), respectively. Furthermore, no algorithm had an MPA greater than 100 mm at Versailles (72 km from MZZU and 130 km from KEAX).

Versailles was well analyzed by the Kansas City radar in terms of the false precipitation amount (Table 3B.2). For example, both the R(Z) and R(Z,ZDR) registered 31.9 and 31.5 mm of precipitation (4.2 and 4.1% of the gauge accumulated amount of rainfall, respectively) whereas the MZZU registered 135.5 and 207.1 mm of false precipitation (17.7 and 27.0 % of the gauge recorded precipitation amount, respectively). Conversely, the amount of FPA analyzed by the MZZU radar at Boone was 71.8 mm (9.3% of gauge total) and 109 mm (14.1% of gauge total) for R(Z) and R(Z,ZDR), accordingly. It

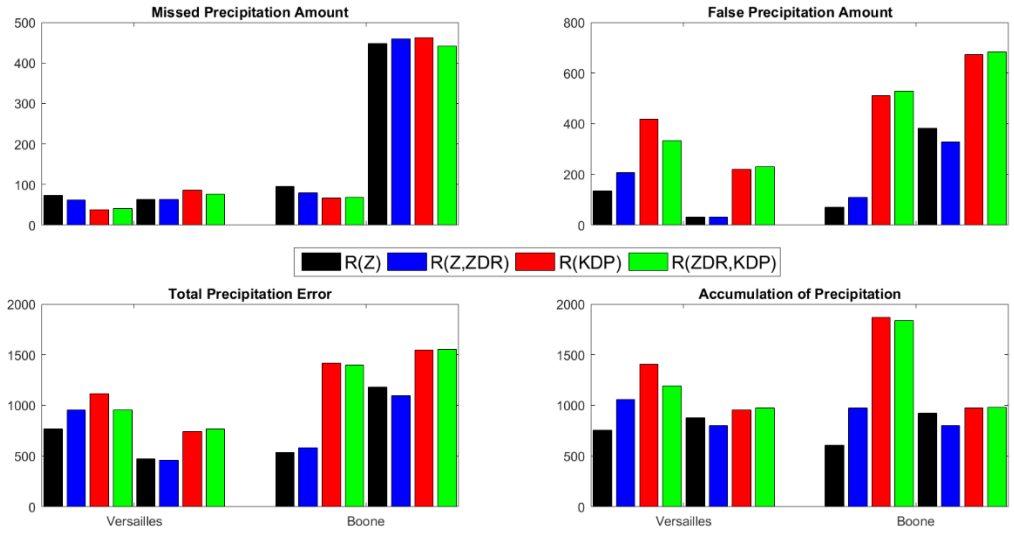

Figure 3B.11. Quantitative analyses between the MZZU X-band and Kansas City (KEAX) S-band radars. Distances from the Versailles and Boone sites were 72 and 130, and 5 and 173 km for MZZU and KEAX, respectively. The four results to the left and right of each location represent results from, respectively, MZZU and KEAX.

was also observed that the R(KDP) outperformed R(ZDR,KDP) for KEAX, while the opposite were true for the MZZU radar.

The largest contributions of the total precipitation error were due, primarily, from the FPA. This is evidenced that, for example, over 80% of the error in comparison to the Boone gauges were due to FPA by both of the KDP-containing algorithms for both of the S-band radars. Furthermore, no location had less than 50% of error contribution due to the FPA from KLSX, and none less than 25% from KEAX when R(KDP) or R(ZDR,KDP) were utilized.

Table 3B.2. Gauge accumulated precipitation for each of the five stations including the False Precipitation Amount (FPA) and its overall percentage relative to the gauge accumulated precipitation amount as analyzed by each radar.

Site / Equation	R(Z)	R(Z,ZDR)	R(KDP)	R(ZDR,KDP)
Boone	772.2	772.2	772.2	772.2
MZZU: 5km	71.8 / 9.3%	109.0 / 14.1%	509.5 / 66.0%	528.9 / 68.5%
KLSX: 140km	268.9 / 34.8%	209.5 / 27.1%	625.4 / 81.0%	624.0 / 80.8%
KEAX: 173km	381.1 / 49.4%	328.5 / 42.5%	671.5 / 87.0%	682.1 / 88.3%
Auxvasse	931.1	931.1	931.1	931.1
MZZU: 33km	103.8 / 11.2%	154.9 / 16.6%	432.4 / 46.4%	342.5 / 36.8%
KLSX: 122km	133.4 / 14.3%	102.6 / 11.0%	395.9 / 42.5%	396.7 / 42.6%
Williamsburg	887.1	887.1	887.1	887.1
MZZU: 50km	134.8 / 15.2%	171.2 / 19.3%	468.9 / 52.9%	362.8 / 40.9%
KLSX: 95km	124.0 / 14.0%	87.0 / 9.8%	437.5 / 49.3%	444.0 / 50.1%
Versailles	766.4	766.4	766.4	766.4
MZZU: 72km	135.5 / 17.7%	207.1 / 27.0%	417.6 / 54.5%	332.0 / 43.3%
KEAX: 130km	31.9 / 4.2%	31.5 / 4.1%	219.4 / 28.6%	230.2 / 30.0%
Vandalia	829.2	829.2	829.2	829.2
MZZU: 81km	139.8 / 16.9%	198.4 / 23.9%	517.0 / 62.4%	414.1 / 49.9%
KLSX: 100km	241.3 / 29.1%	201.4 / 24.3%	636.7 / 76.8%	652.7 / 78.7%

Due to the low MPA and particularly low FPA analyzed at Versailles by KEAX, the TPE was the lowest of any gauge by any radar (Figure 3B.9) with a total of 460.3 and

473.1 mm for R(Z,ZDR) and R(Z), accordingly. This, overall, resulted in the total sum of precipitation by KEAX at Versailles to be the most accurate to the gauge accumulated amount (Table 3B.1).

Conclusions

For the current study, one years' worth of radar data were analyzed from a nearby X-band dual-polarimetric radar (MZZU) and two distant WSR-88D's located in St. Louis (KLSX) and Kansas City (KEAX). The dates ranged from August 2015 – August 2016, with over 7000 hours assessed through means of statistical, contingency, and quantitative analyses to compare the performance of each radar's QPE's. The MZZU radar assessed a total of five gauges, whereas KLSX and KEAX provided QPE's to four and two of the same gauges as MZZU for comparison, respectively.

Results indicate that, in general, the R(Z)-Convective tend to underestimate at MZZU, whereas R(Z,ZDR), of the same magnitude as R(Z)-Convective, overestimated. Furthermore, the R(KDP) and R(ZDR,KDP) produced the largest bias values for all gauges analyzed by the MZZU, in particular, the closest to the radar (Boone, 5 km). The mean absolute error (MAE) provided evidence that the MZZU radar was most accurate when utilizing either R(Z) at the closest or furthest two gauges, with R(ZDR,KDP) providing the most accurate results otherwise. These MAE values were less than any of the locations for the S-band radars, with the notable exception of Versailles analyzed by KEAX (1.0 mm). This location also exhibited the lowest normalized standard error (0.6 mm), while the MZZU radar displayed the next lowest NSE values at the rest of the

locations. Typically, MAE and NSE increased as distance from the radar increased at both X-band and S-band.

Similarly, the number of hits increased, while the number of misses and false alarms decreased as distance from the radar increased. Therefore, the five gauges analyzed by MZZU exhibited the greatest number of hits, in addition to the least number of misses, typically when utilizing either R(KDP) or R(ZDR,KDP). However, the number of false alarms analyzed by the KDP-containing equations by MZZU were similar to those of the S-band radars. The R(Z)-Convective registered the least number of false alarms for MZZU, whereas algorithms containing the differential reflectivity typically were best for the S-band radars.

Due to the low number of misses, the R(KDP) and R(ZDR,KDP) equations registered the least amount of quantitative missed precipitation (MPA). It was noticed that the spread in the values of the MPA were larger for the closer gauges analyzed by MZZU than for those analyzed by either KLSX or KEAX, indicating the superiority of one algorithm over the other at larger distances is nebulous.

The large count of false alarms for the R(KDP) and R(ZDR,KDP) for both radars resulted in large FPA which contributed to the large biases for these algorithms, contributing to over 70% of overall error for KLSX and KEAX. Otherwise, the FPA were typically below 200 mm for MZZU, and below 400 mm for KLSX and KEAX, with the R(Z) providing the least for MZZU and R(Z,ZDR) being the least amount of FPA for the S-band radars.

No radars registered less than 500 mm of overall precipitation error with the notable exception of Versailles, analyzed by KEAX. This, in turn, made the radar most

accurate in terms of NSE and MAE. Furthermore, this provided the most accurate of measures in accumulating the radar estimated precipitation (total sum of precipitation). Otherwise, the MZZU R(Z) equation tended to match the gauge recorded precipitation amount over the course of the study the best.

The results presented indicate that over the short-term, the installation of an X-band radar for QPE in place of distance S-band radars is a viable option, with few caveats. For example, NSE values still approach 100%, with the bulk of error stemming from the false precipitation amount. It is noted that no active combination of algorithms for QPE estimates were conducted, which have been shown to be accurate for X-band radars (Wang and Chandrasekar, 2010). Additionally, disdrometers and, perhaps, more rain gauges are necessary to assure data and quality control of the observed data.

Acknowledgements

This material is based upon work supported by the National Science Foundation under Award Number IIA-1355406. Any opinions, findings, and conclusions or recommendations expressed in this material are those of the authors and do not necessarily reflect the views of the National Science Foundation.

Literature cited

Atlas, D., 2002: Radar calibration: Some simple approaches. *Bull. Am. Meteorol. Soc.*, **83**, 1313-1316.

Beard, K.V., and Chuang, C., 1987: A new model for the equilibrium shape of raindrops. *J. Atmos. Sci.*, **44**, 1509-1524.

Beard, K.V., Bringi, V.N., and Thurai, M., 2010: A new understanding of raindrop shape. *Atmos. Res.*, **97**, 396-415.

Berne, A., and Krajewski, W.F., 2013: Radar for hydrology: Unfulfilled promise or unrecognized potential? *Adv. Water Resour.*, **51**, 357-366.

Brewster, K., White, L, Johnson, B., and Brotzge, J., 2005: Selecting the sites for CASA NetRad, a collaborative radar network. *Preprints, Ninth Symp. on Integrated Observing and Assimilation Systems for the Atmosphere, Oceans, and Land Surface (IOAS-AOLS), San Diego, CA, Amer. Meteor. Soc.*, P3.4.

Brewster, K., Brotzge, J., Thomas, K, Wang, Y, Xue, M., Gao, J., and Weber, D., 2008: High resolution assimilation of CASA and NEXRAD radar data in near-real time: Results from spring 2007 and plans for spring of 2008. *Preprints, 12th Conf. on Integrated Observing and Assimilation Systems for the Atmosphere, Oceans, and Land Surface (IOAS-AOLS), New Orleans, LA, Amer. Meteor. Soc.*, 15B.7.

Bringi, V.N., Chandrasekar, V., and Xiao, R., 1998: Raindrop axis ratios and size distributions in Florida rainshafts: An assessment of multiparameter radar algorithms. *IEEE Trans. Geosci. Remote Sens.*, **36**, 703-715.

Bringi, V.N., Chandrasekar V., Hubbert, J., Gorgucci, E., Randeu, W.L., and Schoenhuber, M., 2003: Raindrop size distribution in different climatic regimes from disdrometer and dual-polarized radar analysis. *J. Atmos. Sci.*, **60**, 354-365.

Cunha, L.K., Smith, J.A., Baeck, M.L., and Krajewski, W.F., 2013: An early performance of the NEXRAD dual-polarization radar rainfall estimates for urban flood applications. *Wea. Forecasting*, **28**, 1478-1497.

Cunha, L.K., Smith, J.A., Krajewski, W.F., Baeck, M.L., and Seo, B., 2015: NEXRAD NWS polarimetric precipitation product evaluation for IFloods. *J. Appl. Meteor.*, **16**, 1676-1699.

Giangrande, S.E., and Ryzhkov, A.V., 2004: Polarimetric method for bright band detection. Preprints, 11th Conf. on Aviation, Range, and Aerospace Meteorology, Hyannis, MA, Amer. Meteor. Soc., CD-ROM, P5.8

Giangrande, S.E., and Ryzhkov, A.V., 2008: Estimation of rainfall based on the results of polarimetric echo classification. *J. Appl. Meteorol. Climate*, **47**, 2445-2462.

Goddard, J.W., Cherry, S.M., and Bringi, V.N., 1982: Comparison of dual-polarized radar measurements of rain with ground-based disdrometer measurements. *J. Appl. Meteor.*, **21**, 252-256.

Gorgucci, E., Scarchilli, G., Chandrasekar, V., and Bringi, V.N., 2000: Measurement of mean raindrop shape from polarimetric radar observations. *J. Atmos. Sci.*, **57**, 3406-3416.

Gourley, J.J., Illingworth, A.J., and Tabary, P., 2009: Absolute calibration of radar reflectivity using redundancy of the polarization observations and implied constraints on drop shapes. *J. Atmos. Oceanic Technol.*, **26**, 689-703.

Gourley, J.J., Giangrande, S.E., Hong, Y., Flamig. Z,, Schuur, T., and Vrugt, J., 2010: Impacts of polarimetric radar observations on hydrologic simulation. *J. Hydrometeorol.*, **11**: 781-796.

Habib, E., Krajewski, W.F., Nespor, V., and Kruger, A., 1999: Numerical simulation studies of rain gauge data correction due to wind effect. *J. Geophys. Res.*, **104**, 723–734.

Hubbert, J., and Bringi, V.N., 1995: An iterative filtering technique for the analysis of copular differential phase and dual-frequency polarimetric variables. *J. Atmos. Oceanic. Technol.*, **12**, 643-648.

Ice, R.L., Heck, A.K., and Cunningham, J.G., 2013: Polarimetric weather radar calibration – engineering challenges. *36th Conf. on Radar Meteorology, Albuquerque, NM, Amer. Meteor. Soc.*

Illingworth, A., 2004: Improved precipitation rates and data quality by using polarimetric measurements. *Weather Radar: Principles and Advanced Applications*. Springer, 130-166.

Kitchen, M. and Jackson, P.M., 1993: Weather radar performance at long range – simulated and observed. *J. Appl. Meteor.*, **32**, 975-985.

Koffi, A.K., Gosset, M., Zahiri, E.P., Ochou, A.D., Kacou, M., Cazenave, F., and Assamoi, P., 2014: Evaluation of X-band polarimetric radar estimation of rainfall and rain drop size distribution parameters in West Africa. *Atmos. Res.*, **143**, 438-461.

Kumjian, M.R., 2013a: Principles and applications of dual-poarization weather radar. Part 1: Description of the polarimetric radar variables. *J. Operational Meteor.*, **1**, 226-242.

Kumjian, M.R., 2013b: Principles and applications of dual-poarization weather radar. Part 2: Warm and cold season applications. *J. Operational Meteor.*, **1**, 243-264.

Matrosov, S.Y., Kingsmill, D.E., and Ralph, F.M., 2005: The utility of X-band polarimetric radar for quantitative estimates of rainfall parameters. *J. Hydrometeor.*, **6**, 248-262.

Matrosov, S.Y., Clark, K.A., and Kingsmill, D.E., 2007: A polarimetric radar approach to isentridy rain, melting-layer, and snow regions for applying correction to vertical profiles of reflectivity. *J. Appl. Meteorol. Climate*, **46**, 154-166.

Matrosov, S.Y., 2009: Radar rain-rate estimators and their variability due to rainfall type: An assessment based on hydrometeorology testbed data from the Southeastern United States. *J. Appl. Meteorol. Climate*, **55**, 1345-1358.

Matrosov, S.Y, 2010: Evaluating polarimetric X-band radar rainfall estimators during HMT. *J. Atmos. Oceanic Technol.*, **27**, 122-134.

Ogden, F.L., Sharid, H.O., Senarath, S.U.S., Smith, J.A., Baeck, M.L., and Richardson, J.R., 2000: Hydrologic analysis of the Fort Collins, Colorado, flash floods of 1997. *J. Hydrol.*, **228**: 82-100.

Ryzhkov, A.V., Giangrande, S., and Schurr, T., 2003: Rainfall measurements with the polarimetric WSR-88D radar. National Severe Storms Laboratory Rep. Norman: OK, 98 pg.

Ryzhkov, A.V., Giangrande, S., and Schurr, T., 2005: Rainfall estimation with a polarimetric prototype of WSR-88D. *J. Appl. Meteor.*, **44**, 502–515.

Seo, D.J., Breidenbach, J., Fulton, R., Miller, D., and O'Bannon, T., 2000: Real-time adjustment of range-dependent biases in WSR-88D rainfall estimates due to nonuniform vertical profile of reflectivity. *J. Hydrometeorol.*, **1:** 222 – 240.

Simpson, M.J., Hubbart, J.A., and Fox, N.I., 2016: Ground truthed performance of single and dual-polarized radar rain rates at large ranges. *Hydrol. Process.*, **30**, 3692-3703.

Simpson M.J., and Fox, N.I., 2017: Multi radar performance in the Midwestern United States at Large Ranges. *Submitted to Hydrol. Process.*

Smith, J.A., Seo, D.J., Baeck, M.L., and Hudlow, M.D., 1996: An intercomparison study of NEXRAD precipitation estimates. *Water Resour. Res.*, **32**, 2035-2045.

Villarini, G., and Krajewski, W.F., 2010: Review of the different sources of uncertainty in single polarization radar-based estimates of rainfall. *Surv. Geophys.*, **31**: 107-129.

Wang, Y., and Chandrasekar, V., 2009: Algorithm for estimation of the specific differential phase. *J. Atmos. Oceanic Technol.*, **12**, 643-648.

Wang, Y., and Chandrasekar, V., 2010: Quantitative precipitation estimation in the CASA X-band dual-polarization radar network. *J. Atmos. Oceanic Tech.*, **27**: 1665-1676.

Williams, C.R., Gage, K.S., Clark, W., and Kucera, P., 2005: Monitoring the reflectivity calibration of a scanning radar using a profiling radar and a disdrometer. *J. Atmos. Oceanic Technol.*, **22**, 1004-1018.

Zhang, G., Vivekanandan, J., and Brandes, E., 2001: A method for estimating rain rate and drop size distribution from polarimetric radar measurements. *IEEE Trans. Geosci. Remote Sens.*, **39**, 830-841.

Zrnic, D.S., and Ryzhkov, A.V., 1996: Advantages of rain measurements using specific differential phase. *J. Atmos. Oceanic Tech.*, **13**, 454-464.

CHAPTER IV

ASSESSING PERFORMANCE OF RAINFALL ESTIMATES FROM RAIN GAUGES AND LOCAL X-BAND AND DISTANT S-BAND RADARS FOR HYDROLOGIC SIMULATIONS

Abstract. Hydrologic simulations are essential for the understanding and prediction of flash flooding. However, these simulations need accurate and reliable precipitation input, as this is the primary source of water for many watersheds and varies over fine spatial and temporal scales. Within the past decade, the simulation of hydrographs have been conducted with the use of radar quantitative precipitation estimates (QPE's) due to the superior spatiotemporal coverage in comparison to rain gauges. However, many of these studies have been performed in well-calibrated, densely-instrumented watersheds that are close to the region of study. Therefore, the current study provides a novel approach of comparing hydrologic simulations while utilizing a physically-based model, Vflo, to estimate streamflow from an S-band National Weather Service radar at St. Louis (KLSX), over 140 km from the region of study. These simulations were compared against a locally-sited X-band dual-polarimetric radar (MZZU) in addition to several tipping buckets, some of which reside within, and just outside of the region of study. Results indicate that, during the calibration process, the amount of precipitation (i.e., bias) and initial saturation were the biggest factors in producing accurate hydrographs. Overall, the spatial average of gauge-recorded rainfall provided many instances of zero hydrograph response, particularly due to the localization of storms that did not encounter the gauges. The limiting differences between the performance of the radars were the accuracy, and timing of peak flow, for which the KLSX radar was superior. In spite of the calibration of the digital precipitation rate utilized for the KLSX radar, potential bright-banding resulted in several false responses of streamflow, which the MZZU radar

more accurately assessed. Overall, the superiority of one radar over the other was not significant, as the sensitivity of streamflow responses is dependent upon parameters not provided by high resolution data, in particular initial saturation.

Introduction

Measurements of rainfall can either be conducted as point-based measurements or in terms of areal measurements. Point-based measurements of precipitation are generally performed by automated rain gauges (i.e, tipping buckets) which records the cumulative depth of rainfall over a given time period. However, errors associated with rain gauges are well documented and include, but are not limited to, local random errors (Kitchen and Blackall, 1992; Ciach and Krajewski, 1999a; Habib et al., 2001), errors in counting of tips, especially at large rainfall rates (Ciach and Krajewski, 1999b; Ciach 2002), effects of turbulence (Habib et al., 1999) including wind (Sevruk and Hamon, 1984) and evaporation losses (Sevruk, 1982), and the mechanical error due to the water losses during the movement of the fulcrum device (Calder and Kidd, 1978; Marsalek, 1981; Yu et al., 1997). In spite of the wide range of errors associated with tipping buckets, they offer realistic estimates of rainfall and are much more cost-effective than weather radars.

Superior in terms of spatial coverage in comparison to terrestrial-based precipitation gauges, weather radars have been successfully utilized since the 1940's in precipitation estimates (e.g., Ryde 1941; Bent 1946; Marshall et al., 1947). For a more detailed explanation as to the history of weather radar technology, the reader is referred to the works of Bigler (1956, 1961, 1981), Hitschfeld (1986), Atlas et al. (1990), Rogers and Smith (1996), Whiton et al. (1998a) and Whiton et al. (1998b). However, the

documentation of the spatiotemporal errors associated with radar-estimated rainfall rates is also well-established, including uncertainties in the overall raindrop shape (Goddard et al., 1982; Beard and Chuang, 1987; Gorgucci et al., 2000, 2006; Brandes et al., 2002), uncertainties in the drop-size distribution of rainfall (Zhang et al., 2001; Bringi et al., 2003), hardware (mis)calibration (Hubbert and Bringi, 1995; Atlas, 2002; Williams et al., 2005; Gourley et al., 2009; Wang and Chandrasekar, 2009), beam propagation errors (Bringi et al., 1990; Delrieu et al., 1999; Berne and Uijlenhoet, 2005; Matrosov et al., 2005), and radar quality degradation arising from large range assessments from the radar (Kitchen and Jackson, 1993; Smith et al., 1996; Ryzhkov et al., 2003; Simpson et al., 2016). In spite of the wide range of errors associated with radar rain rate estimates, many studies have found significant agreement between observed (i.e., gauge) and radar estimates in terms of rainfall amounts (Villarini and Krajewski, 2010).

For regions devoid of adequate radar coverage (i.e., areas further than 150 km from the nearest radar), spatial interpolation of rain gauge data is often implemented for an area of interest, especially at the watershed scale (Shah et al., 1996; Brath et al., 2004; Smith et al., 2004; Dodov and Foufoula-Georgiou, 2005; Yu et al., 2011). However, the choice of interpolation method is important for accurate representations of rainfall (Yu et al., 2011). For example, Tabios and Salas (1985) stated that Kriging was superior to Inverse Distance Weighting (IDW), Thiessen Polygons, or polynomial trend surfaces in terms of interpolating point-based rainfall data. Several other studies (e.g., Laslett and McBratney, 1990; Weber and Englund 1994; Zimmerman et al., 1999) provide evidence that the Kriging method is superior to most other spatial interpolation methods. Furthermore, Sun et al. (2000) compared radar, rain gauge, and co-Kriging fields of

gauge and radar fields to determine that the co-Kriging of radar and three rain gauges yielded the most accurate representation of the areal extent of precipitation to a 1060 km^2 watershed. However, other studies have documented the superior capability of radar rainfall estimates as input to hydrologic models (e.g., Ogden et al., 2000; Yates et al., 2000; Vieux et al., 2005; Gourley et al., 2010) when long-term biases were identified and corrected for.

In spite of the conflicting results while utilizing radar or gauge data as precipitation input to hydrologic models, many studies tend to be for isolated cases with excessively calibrated models, making it difficult to determine whether errors are due to the spatial interpolation of gauge data, rainfall-runoff model structure, radar rain rate algorithm performance, overall model calibration, or some combination thereof (Berne and Krajewski, 2013). Thus, it can be stated that studies which assess the performance of gauge and radar (or some combination of both) performance over longer time periods (e.g., weeks-to-months) is essential to determining the true strengths and limitations of each method of precipitation input to hydrologic modeling.

The current study analyzes the performance of two month's worth of precipitation data from a locally-situated X-band dual-polarimetric and distant Next Generation Radar (NEXRAD) radar, in addition to several precipitation gauges in the vicinity of a small catchment located in central Missouri. Analyses are conducted at the daily, weekly, and monthly time scales to determine overall performance for each method of precipitation input to the physically-based hydrologic model, Vflo (Vieux et al., 2004; Vieux and Vieux, 2006). Biases in terms of storm-type and seasonal effects will also be addressed, in addition to the strengths and limitations between the standard National Weather

Service (NWS) radar rain rate algorithm (i.e., R(Z)-Convective) and dual-polarimetric algorithms.

Study site and methods

Study location

The current study analyzes the performance of two radars (one X-band and one S-band) on estimating rain rates which serve as precipitation input to the physically-based hydrologic model, Vflo. The Hinkson Creek Watershed (HCW), a small (233 km^2) mixed-land use catchment located in the Lower Missouri-Moreau River Basin, is located in Boone County, Missouri, with an elevation at the headwaters of 274 m and 177 m above mean sea level at the outlet (Hubbart et al., 2013) (Figure 4.1). The major land covers consist of forest (41%), grassland (35%), impervious cover (13%), and cropland (7%), whereby the upper half of the watershed is dominated by forest and cropland, and the lower half is predominately urbanized, developed land.

Soils in the upper half of the watershed are poorly drained with low permeability (hydrologic soil groups C and D) which are highly erodible and agriculturally active. The soil types in the HCW are primarily characterized by either Mississippian or Pennsylvanian sandstone, limestone, and shale. Crops include corn, soybeans, and wheat, whereas grassland is primarily utilized for grazing by cattle, horses, and sheep which constitute the primary livestock. Channel slope averages 1.86 m of fall per km, with the floodplain widths varying from 500 m at the north end of the watershed, to 300 m in the south. The upper reaches of the Hinkson Creek are classified as a Class C stream such

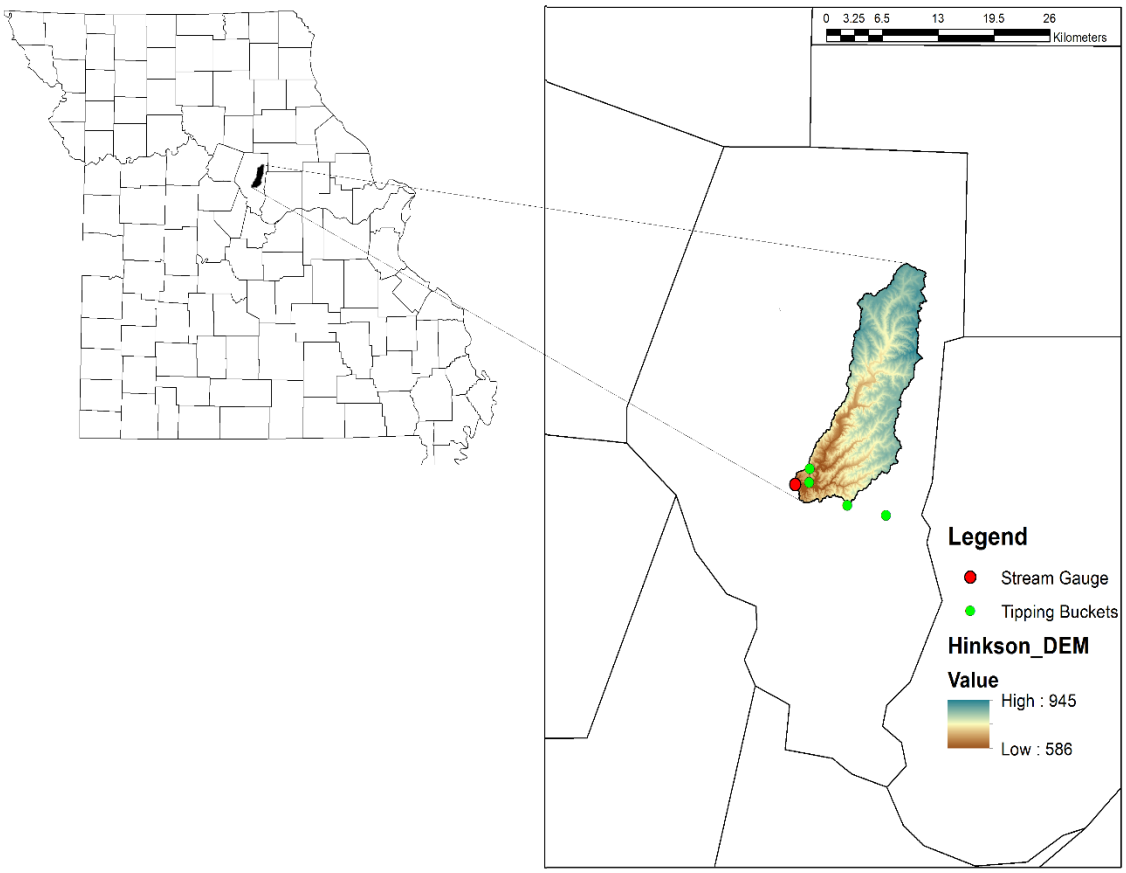

Figure 4.1 Study site for the current study including the Hinkson Creek Watershed, the four tipping buckets and their proximity to the catchment, and the United States Geologic Survey (USGS) operated stream gauge which serves as the observed streamflow.

that the stream may cease flowing in dry periods but maintains small ponding regions to support aquatic life. Conversely, the lower reaches of the stream are classified as a Class P stream, whereby the stream is capable of maintaining permanent flow even in drought periods.

A United States Geologic Survey (USGS) stream gauge is located in the lower third of the watershed, and has been operational since the end of 1987 (Figure 4.1). This gauge serves as the observed (i.e., truth) streamflow which is compared against

streamflow simulations generated by Vflo. One of the sources of precipitation input to Vflo is a set of a terrestrial-based precipitation sensors (tipping bucket), located in the central region of the watershed. The tipping bucket is manufactured by Campbell Scientific, with a 25.4-cm diameter orifice which introduces 0.254 mm of precipitation to a fulcrum device (i.e., the tipping bucket). The device is optimal between 0 and 50°C, with errors ranging between -1 to 1%, -3 to 0%, and -5 to 0% for precipitation up to 25.4 mm h^{-1}, 25.4 to 50.8 mm h^{-1}, and 50.8 to 76.2 mm h^{-1}, respectively. To mitigate these errors, the gauge is located 1 m above the ground with properly maintained vegetation, and positioned over three times the distance the height of the nearest building to mitigate any effects from turbulence (Habib et al., 1999; Villarini and Krajewski, 2010). Four separate rain gauges were utilized (Figure 4.1) to determine if there were significant differences ($p < 0.05$) in the proximity of the gauge to the catchment and performance of streamflow estimation.

Radar data

One of the other sources of precipitation data is that from the St. Louis S-band dual-polarization radar (KLSX). The performance of the device was studied extensively through chapter 2 and its subsections of this dissertation, revealing that QPE's were accurate in spite of being a distance of approximately 140 km from the radar (Simpson et al., 2016) The other radar is the locally-sited X-band dual-polarization radar (MZZU), on the southeast border of the Hinkson Creek Watershed (Figure 4.2). The performance of MZZU was examined throughout chapter 3, noting that comparisons between the distant

S-band radars (KEAX in Kansas City and KLSX in St. Louis) were relatively similar. Therefore, QPE's from KLSX and MZZU are utilized for the current study.

For chapter 2, the KLSX data were processed via the Weather Detection Support System – Integrated Information (WDSS-II) program. However, for this section, the KLSX QPE data is from the National Center for Environmental Information's (NCEI) radar data archive, specifically, the Digital Precipitation Rate (DPR). The DPR product is the instantaneous precipitation rate using the quality-controlled dual-polarization QPE algorithm, which is based on the Hydrometeor Classification Algorithm (HHC) which, in turn, depends on the Melting Layer (ML) algorithm (Park et al., 2005; Giangrande and Ryzhkov, 2008; Ryzhkov et al., 2011; Ryzhkov et al., 2013):

$$R(Z, ZDR) = 6.701^{-3} Z^{0.927} ZDR^{-3.43} \tag{4.1}$$

$$R(KDP) = 44 |KDP|^{-0.822} \, sign(KDP) \tag{4.2}$$

where eq. (4.1) is the default equation, and eq. (4.2) is utilized when hail is identified by the HHC. The data is ground-truthed from the Hydrometeorological Automated Data System (HADS; http://hads.ncep.noaa.gov/) and the Community Collaborative Rain, Hail, and Snow Network (CoCoRaHS; http://www.cocorahs.org/).

Hydrologic model

Vflo is a gridded, physics-based hydrologic model primarily utilized for

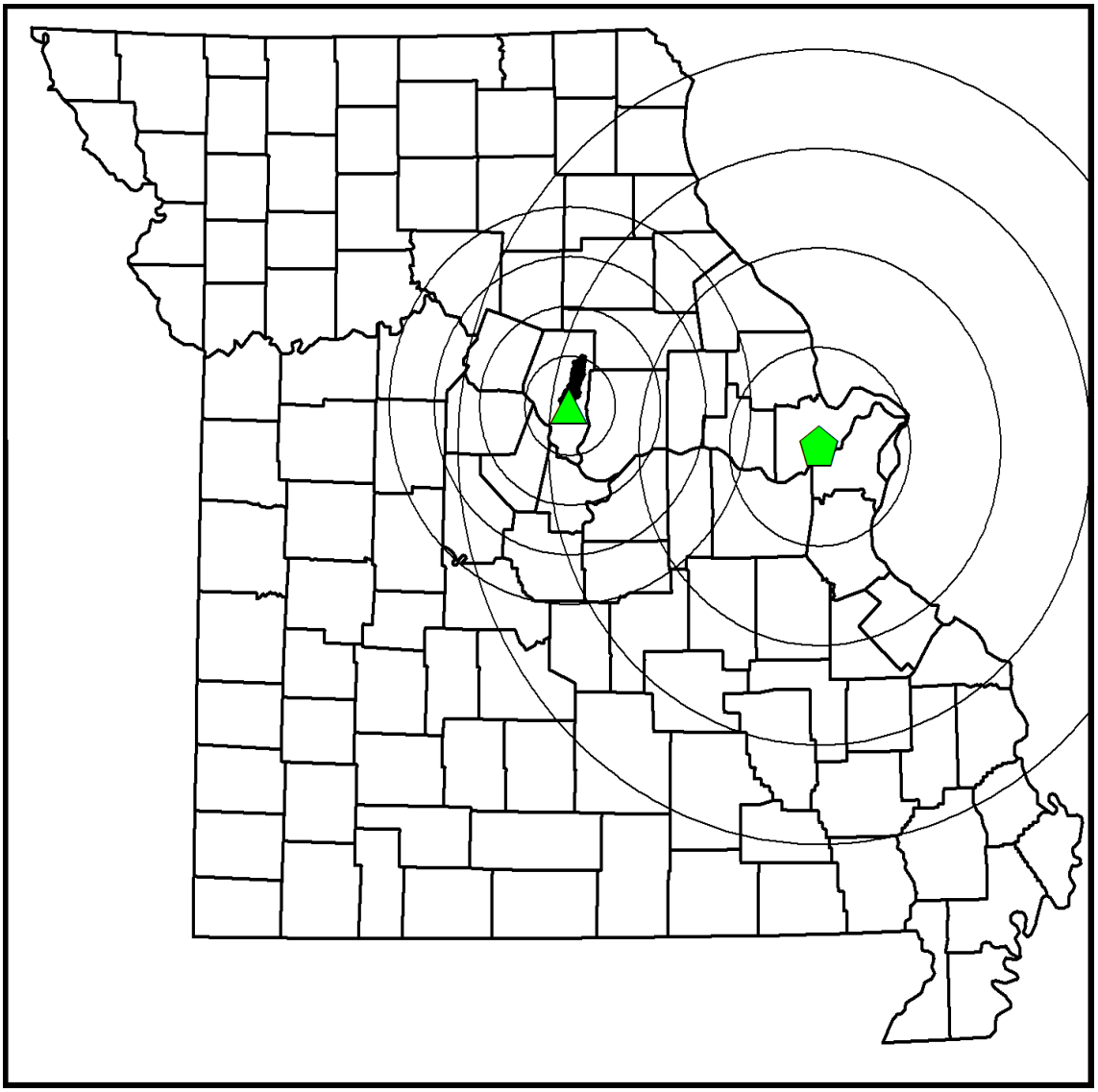

Figure 4.2. The X-band (MZZU) radar overlaid with 25-, 50-, 75-, and 100-km range rings with the St. Louis (KLSX) radar overlaid with 50-, 100-, 150-, and 200-km range rings. The Hinkson Creek Watershed is also displayed as the area of study.

simulating stormwater runoff from major river basins to small catchments based on geospatial data (Vieux et al., 2004). The numerical solution to solving the kinematic wave analogy (KWA) for overland and channel cells is performed in Vflo, such that finite element solutions in space and finite difference approximations in time are

conducted, respectively (Vieux et al., 1988). The principle gradient is the land surface slope to simplify the solutions of conservation of mass and momentum equations. These solutions differ from previous finite elemental solutions in that it represents parameters, such as roughness and slope, as nodal, opposed to elemental, parameters. This allows the watershed of study to be treated as a spatially variable surface in contrast to sub-areas or sub-basins.

The drainage network is created from a Digital Elevation Model (DEM) which, in turn, determines flow direction at each finite elemental and nodal slope value. The connectivity of the drainage network is used to develop the system of equations which provide the solution to the KWA, which has been shown to be an appropriate representation of the wave movement downstream (Chow et al., 1988). In addition to the DEM providing physically-based representation of the watershed, Vflo utilizes data including land use / land cover, Manning's roughness, Green and Ampt infiltration parameters (hydraulic conductivity, effective porosity, and wetting front suction), and channel cross sections which may be defined either by cross sections or rating curves. Baseflow, soil depth, soil type, initial saturation, initial abstraction, and impervious percentages are also utilized to represent the watershed.

Calibrating the hydrologic model

Model calibration is one of the first steps before any simulation is to be conducted. Therefore, the parameters that are available in Vflo, including overland and channel roughness, hydraulic conductivity, the wetting front, soil depth, initial saturation (I_{sat}), initial abstraction, channel width, rainfall (R), and imperviousness. The soil depth,

effective porosity, wetting front suction head, overland roughness, impervious cover, and saturated hydraulic conductivity were all obtained from the 2011 National Land Cover Database (NLCD). The remaining calibration factors, including abstraction, channel width and roughness, R, and I_{sat}, were calibrated using the first major precipitation event for July 2016.

The first calibration parameter tested was the initial saturation. If the soil is unsaturated, the effects of the soil depth, hydraulic conductivity, effective porosity, roughness, and overall imperviousness will determine the infiltration capacity of the soil and, thus, time to surface saturation. Furthermore, any precipitation that reaches the surface will eventually be infiltrated until field capacity (i.e., saturation) is achieved which, in turn, has an effect on when runoff begins and, ultimately, streamflow.

Over 100 mm of precipitation fell during the day of 03 July 2016, resulting in a 75 year storm event for the Hinkson Creek. To test the sensitivity of the model to initially saturated conditions, values of 95 – 99% saturation were chosen while holding all other variables constant (Figure 4.3). Not only does the shape of the hydrograph alter significantly ($p < 0.01$), the peak discharge is delayed, and reduced as initial saturation decreases. However, as saturation approaches 100%, initial small storms that began during the evening hours of 02 July 2016 are reported through the modeled hydrograph as large values of streamflow which were not observed. Therefore, the initial saturation value for the model was chosen to be 98% for the month of July.

One of the most important parameters for any hydrologic simulation is that of precipitation. Therefore, the sensitivity of the model to QPE from radar is important in determining the calibration of precipitation. Because the MZZU radar is not gauge-

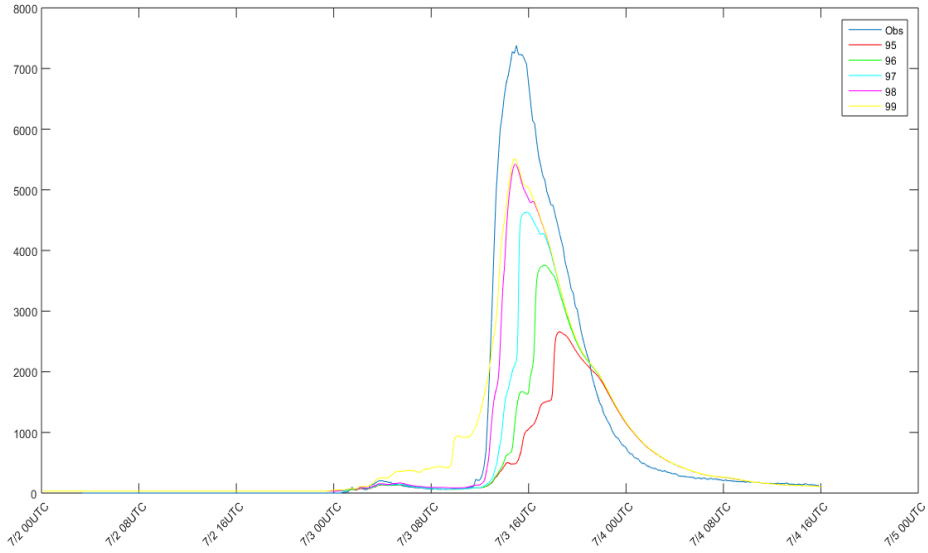

Figure 4.3. Example calibration effects of the initial saturation (in percent) on streamflow response while utilizing the R(Z)-Convective algorithm from MZZU.

corrected, the Vflo model serves as a streamflow-corrected QPE platform, whereas the DPR is derived from rigorous quality control techniques, including gauge, satellite, vertical temperature profiling, cloud detection, ground-clutter, and bright-band corrections.

While utilizing an initial saturation of 98%, the precipitation values were altered by adding 1, 2, 3, 4, 5, and 6 % of the total volume per radar scan (Figure 4.4). Unlike the initial saturation calibration (Figure 4.3), the change in precipitation amount has a more pronounced impact on the overall maximum of streamflow. As the increase of rainfall percentage changed from 0.01, 0.02, 0.03, 0.04, 0.05, and 0.06, the RMSE values decreased from 507.8, 404.5, 324.6, 279.0, 264.6, and 228.3 mm, respectively. Similarly, the Nash-Sutcliffe scores were 0.92, 0.95, 0.97, 0.98, 0.98, and 0.99. In spite of matching

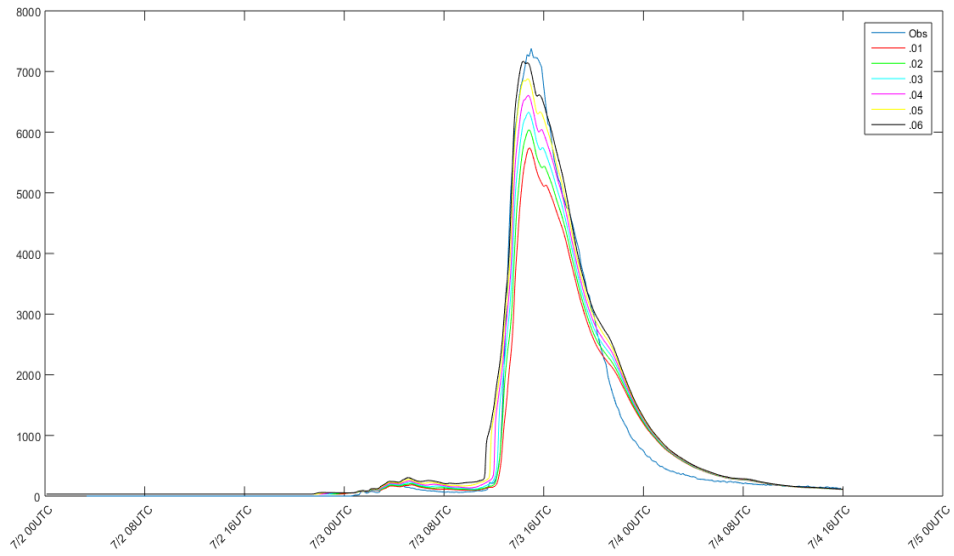

Figure 4.4. Example calibration effects of the precipitation (in percent) on streamflow response while utilizing the R(Z)-Convective algorithm from MZZU.

with the observed streamflow well, the errors are, primarily, due to the inexact match with the peak flow and the slower return to base flow.

Similar calibrations were conducted with the MZZU R(Z,ZDR) and KLSX DPR algorithms, in addition to the tipping bucket rain gauge (Table 4.1). In general, the roughness, hydraulic conductivity, wetting front, soil depth, and imperviousness were well calibrated through the NLCD. Conversely, the initial saturation and precipitation variables required the most calibration. For example, Figures 4.3 and 4.4 demonstrated the effect initial saturation and precipitation had on the shape of the simulated hydrographs, producing significantly ($p < 0.01$) different results. For the other variables, there were no significant changes in streamflow response without major alterations to the model, such that it would be rendered unrealistic.

Table 4.1. Calibrated variables and values for the Hinkson Creek Watershed.

Source of Precipitation	Initial Saturation (%)	Precipitation (%)
MZZU R(Z)-Convective	98	106
MZZU R(Z,ZDR)	97	105
KLSX DPR	99	105
Tipping Bucket	100	120

The precipitation percentages all had to be increased for the four sources of rainfall to the hydrologic model. In spite of the quality control that is conducted on the DPR, the effect of range on precipitation (Ryzhkov et al., 2003; Simpson et al., 2016) needed to be accounted for further. Similarly, the errors associated with tipping buckets (Habib et al., 1999; Ciach 2002), especially in tip-counting schemes, underestimates precipitation.

Results and discussion

The study period ranged from 01 – 31 July and 01 – 21 December 2016. These dates constitute a range of convective storms (e.g., 03 and 13 July) and stratiform events (e.g., 07 July, and 04 and 10 December) to determine the performance of the hydrologic model on streamflow simulation in addition to seasonal performance. The former of the months analyzed, July, contained two large storms that passed through Central Missouri on 03 and 13 July, producing 100 and 40 mm hr^{-1} of precipitation over the catchment, respectively. The latter of the months, December, exhibited typical shallow, stratiform frozen precipitation which produced small volumes of precipitation overall.

Results indicate there are significant ($p < 0.05$) differences between the KLSX Digital Precipitation Rate (DPR), the MZZU X-band algorithms, and the spatially-averaged tipping bucket rainfall data for the month of July (Figure 4.5). For example, from 06 to 09 July, the performance of each of the four sources of precipitation (X-band R(Z)-Convective and R(Z,ZDR), KLSX DPR, and spatially-averaged tipping bucket) resulted in significantly ($p < 0.01$) different hydrographs (Figure 4.6). These dates exhibit the importance of algorithm in addition to choice of radar for hydrologic simulations, such that both X-band algorithms underperformed, whereas the KLSX DPR overestimated streamflow. Furthermore, this particular quasi-linear convective system (QLCS) resulted in relatively localized storms in the northern portion of the catchment which were entirely missed by the spatially-averaged rain gauges to the south, resulting in a near-zero response in simulated streamflow.

The large response from the KLSX DPR during the storm of the evening of 06 July may be due, at least in part, to bright-banding, resulting in overestimation of precipitation and, thus, large discharge values (over 500%). Conversely, the X-band radar suffered from attenuation issues, which resulted in the underestimation of precipitation. The enhanced performance of the R(Z,ZDR) equation is likely due to the fact that the equation implements ZDR, accounting from drop-shape variability. Since the leading edge of the QLCS is dominated by convective precipitation with a trailing stratiform shield, the variability in the drop-size distribution (DSD) is better captured with this algorithm and, thus, better simulated for hydrologic simulations.

One of the other days with significant differences in simulated streamflow was from 15 to 17 July (Figure 4.7). This event was due to isolated convective cells that

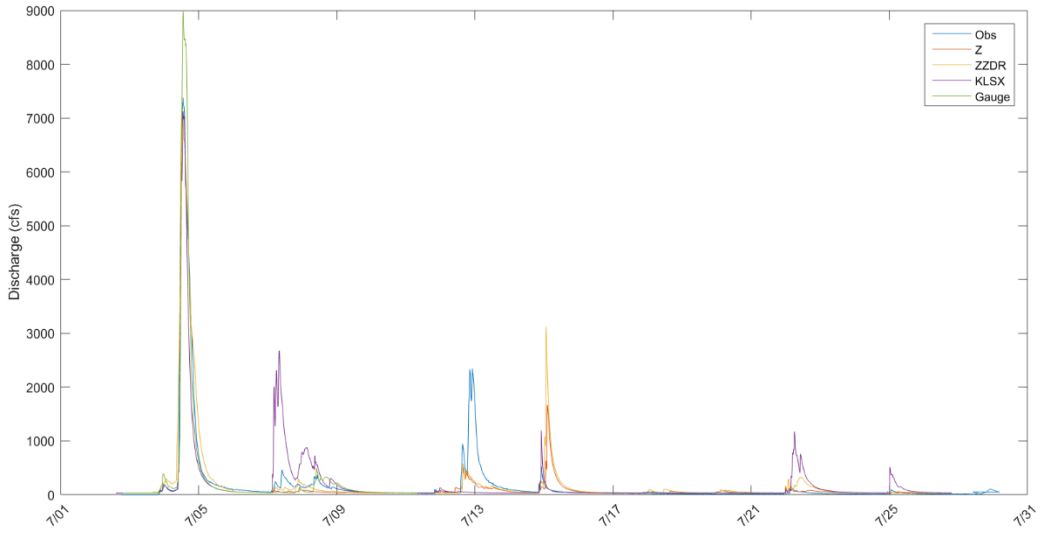

Figure 4.5. Observed streamflow (Obs) and simulations from the X-band (MZZU) R(Z)-Convective (Z) and R(Z,ZDR) algorithms, St. Louis Digital Precipitation Rate (KLSX), and spatially-averaged tipping bucket (Gauge) rainfall from 01 to 31 July, 2016.

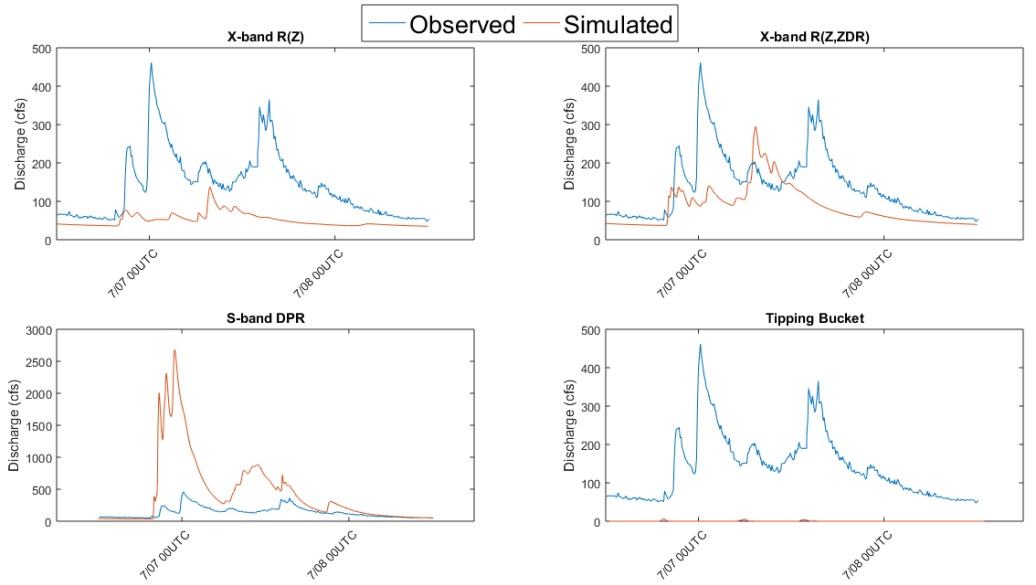

Figure 4.6. Simulated and observed discharge results from the Hinkson Creek Watershed from 06 to 09 July, 2016.

moved through the catchment, resulting in over 30 mm of precipitation throughout the evening of the 15th. However, the responses from each of the sources of precipitation were different, such that although the KLSX DPR matched the timing of the peak flow, the magnitude was larger than the observed value by three times, similar to the results of the 06 to 09 event (Figure 4.6). Although the storms passed through the range of the western-most tipping buckets (i.e., those within the catchment), hand-written records indicate these gauges became clogged and were not operational until after the storm had passed, rendering their ability to model the streamflow useless.

Similar to the issue with the MZZU radar from the events of 06 to 09 July, attenuation caused a delay in the response of the precipitation data during the evening of 15 July. Furthermore, major radome wetting resulted in a complete loss of signal from the radar, resulting in no precipitation to be present for several scans until after the storm had passed east of the radar. However, the pattern of the streamflow response was captured, yet delayed, with a significantly increased simulated peak flow. This may be due, at least in part, to the precipitation being incorrectly assessed as starting directly over the catchment due to the loss of signal. This results in a large amount of rainfall unable to be infiltrated, amounting to large values of runoff and, ultimately, discharge.

The evening of 12 July saw relatively large volumes of discharge with significantly less simulated streamflow response from any of those simulated. In spite of the large QLCS that moved through the area during 18Z of the 13th, a small hydrologic response was simulated by the MZZU and KLSX radars, in addition to the precipitation gauges for the peak flow of this event. It is theorized that streamflow from the upstream catchments may have played a significant role in the additional observed discharge.

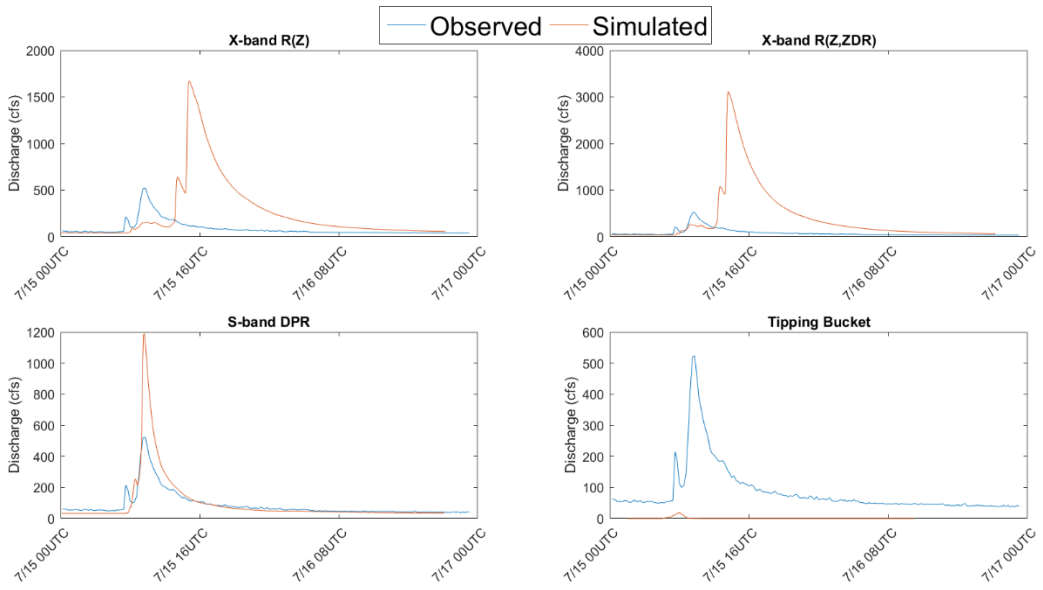

Figure 4.7. Simulated and observed discharge results from the Hinkson Creek Watershed from 15 to 17 July, 2016.

The largest event, during the evening of 03 July, can be assessed as a 75-year storm for Missouri. This was one of the few events which both radars were capable of analyzing well, in terms of the time and magnitude of peak flow. This indicates that the first few events are more readily simulated, as the initial saturation is better assessed. The effects of evapotranspiration, significant degree heating days (i.e., drying of soil), baseflow recession, and other variables which account for the (in)ability of infiltration are not carried through the simulation as well.

The simulations for the month of December displayed less agreement than for July (Figure 4.8). Furthermore, the end of December was not simulated such that due to a series of convective storms, no streamflow and/or KLSX data were available for this time period.

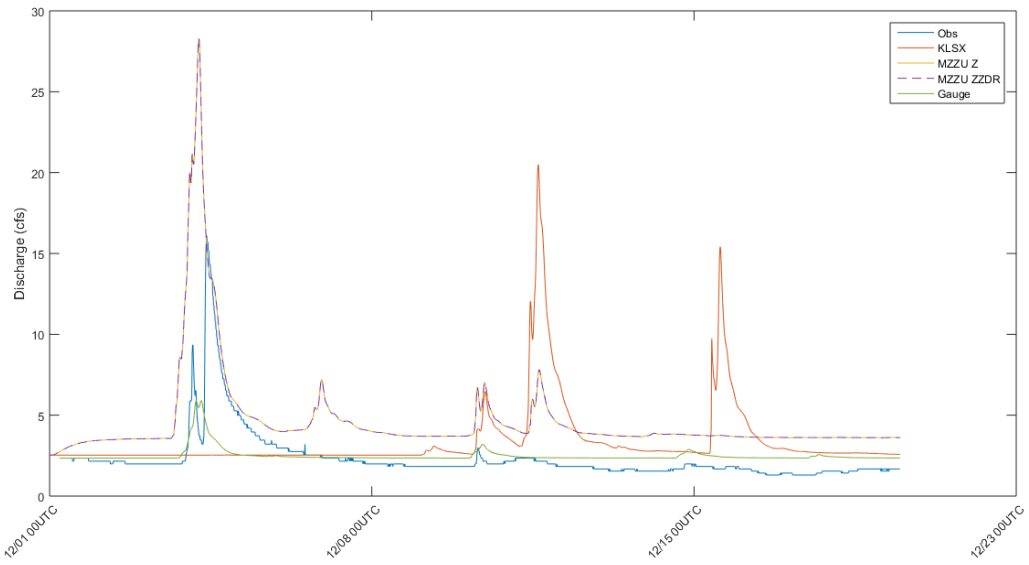

Figure 4.8. Observed streamflow (Obs) and simulations from the X-band (MZZU) R(Z)-Convective (Z) and R(Z,ZDR) algorithms, St. Louis Digital Precipitation Rate (KLSX), and spatially-averaged tipping bucket (Gauge) rainfall from 01 to 21 December, 2016.

Although the performance of the tipping buckets were inferior to the radars for the entirety of the month of July, the gauges were capable of assessing the beginning of the storm on the evening of 04 December well. However, the second peak in the observed streamflow was not well simulated. The shallow shield of frozen precipitation was such that the KLSX DPR did not register any precipitation, resulting in zero discharge (excluding baseflow). Conversely, the MZZU radar overpredicted the streamflow, perhaps due to the inability of the frozen precipitation to melt and become runoff and/or contribute to the overall streamflow.

Although the rest of the days analyzed in December (i.e., from 01 to 22 December) did not produce a large response in the observed streamflow, several days were marked by frozen precipitation events. For example, for 10 and 11 December, two broad shields of precipitation moved through the state of Missouri, resulting in meteorological echoes to be produced from MZZU and KLSX. However, since the vast majority of precipitation does not fall directly on the river, rather, on the land which did not melt, infiltrate, or runoff, no response was recorded by the USGS gauge.

The baseflow values for the MZZU radar were higher than that for either the KLSX DPR or tipping bucket. This is due to periodic ground clutter within the Hinkson Creek Watershed, particularly during the morning hours, producing false (albeit minor) responses in streamflow. The tipping bucket and KLSX DPR reach a baseflow of, approximately, 2.5 cfs, whereas the baseflow recession is, for winter, near 2.0 cfs.

Conclusions

The current study analyzed 2 months' of observed streamflow data to determine the performance of utilizing radar estimated QPE and spatially-averaged tipping bucket data as precipitation input to a physically-based hydrologic model. The radars consisted of a locally-sited X-band (MZZU) and distant (i.e., 140 km from the region of study) WSR-88D (KLSX) dual-polarimetric radars. After the calibration of each source of precipitation, it was observed that the simulated hydrographs were significantly ($p < 0.05$) different. Several examples were demonstrated, particularly at the beginning of July, that displayed the difference in responses. For example, possible bright-band contamination for the St. Louis radar resulted in a large streamflow response during the

afternoon of July 15, 2016. Furthermore, the storm caused attenuation, in addition to significant radome wetting at the MZZU radar, resulting in a complete loss of signal that delayed the response of streamflow.

From 07 to 08 July 2016, a quasi-linear convective system passed through the region of study. The KLSX radar, again, overpredicted the streamflow response, but was more accurate in terms of the timing of peak flow. The R(Z) equation for QPE's from the MZZU radar was not able to capture the variability and evolution of the drop-size distribution as well as the R(Z,ZDR) equation, but produced magnitudes of peakflow more accurate than that from KLSX. Due to clogging from the precipitation gauge, no streamflow response was recorded.

The first-half of the month of December was analyzed, and displayed that the rain gauges were accurate in the first portion of a storm that occurred during 03-04 December, yet resulting in little-to-no response afterwards. The KLSX radar provided multiple instances of false alarms of streamflow, potentially due to the fact the precipitation was frozen and unable to become runoff. This was also examined with the MZZU radar, but to a lesser extent. Furthermore, it was observed that the gauges and KLSX were more accurate in terms of baseflow, primarily due to random clutter echoes from the MZZU radar which produced slight responses in the hydrograph.

The results indicate that the superiority of one source of precipitation input to the other is inconclusive, although the precipitation gauges suffer from more errors than the radars (e.g., clogging, missing of storms, over-averaging of storms). Some hydrologic variables are unable to be captured from the radar, and need to be incorporated real time to the model. For example, one of the largest calibration factors was the initial saturation.

For more accurate hydrologic responses, particularly in the cool season and during extreme heating days, evapotranspiration, soil water holding capacity, and overall drying rates of the soil are necessary to determine more accurate runoff calculations and, thus, more accurate streamflow responses.

Acknowledgements

This material is based upon work supported by the National Science Foundation under Award Number IIA-1355406. Any opinions, findings, and conclusions or recommendations expressed in this material are those of the authors and do not necessarily reflect the views of the National Science Foundation.

Literature Cited

Atlas, D., 1990: Radar in Meteorology – Battan Memorial and 40th Anniversary Radar Meteorology Conference. Amer. Meteor. Soc. pp. 806.

Atlas, D., 2002: Radar calibration: Some simple approaches. *Bull. Am. Meteorol. Soc.*, **83**, 1313-1316.

Beard, K.V., and Chuang, C., 1987: A new model for the equilibrium shape of raindrops. *J. Atmos. Sci.*, **44**, 1509-1524.

Berne, A., and Uijenhoet, R., 2005: A stochastic model of range profiles of raindrop size distributions: Application to radar attenuation correction. *Geophys. Res. Lett.*, **32**: L10803.

Berne, A., and Krajewski, W.F., 2013: Radar for hydrology: Unfulfilled promise or unrecognized potential? *Adv. Water Resour.*, **51**, 357-366.

Bigler, S.G., 1956: A note on the successful identification and tracking of a tornado by radar. *Weatherwise*, **9**, 198-201.

Bigler, S.G., 1961: Status of the radar program of the U.S. Weather Bureau. *Proc. 9th Conf. on Weather Radar, Kansas City, MO*, Amer. Meteor. Soc., 428-431.

Bigler, S.G., 1981: Radar: A short history. *Weatherwise*, **34**, 158-163.

Brandes, E.A., Zhang, G., and Vivekanandan, J., 2002: Experiments in rainfall estimation with a polarimetric radar in a subtropical environment. *J. Appl. Meteor.*, **41**, 674–685.

Brath, A., Montanari, A., and Toth, E., 2004: Analysis of the effects of different scenarios of historical data availability on the calibration of a spatially-distributed hydrologic model. *J. Hydrol.*, **291**, 232-253.

Bringi, V.N., Chandrasekar, V., Balakrashnan, N, and Zrnic, D.S., 1990: An examination of propagation effects in rainfall on radar measurements at microwave frequencies. *J. Atmos. Oceanic Technol.*, **7**, 829-840.

Bringi, V.N., Chandrasekar V., Hubbert, J., Gorgucci, E., Randeu, W.L., and Schoenhuber, M., 2003: Raindrop size distribution in different climatic regimes from disdrometer and dual-polarized radar analysis. *J. Atmos. Sci.*, **60**, 354-365.

Calder, I.R., and Kidd, C.H.R., 1978: A note on the dynamic calibration of tipping-bucket gauges. *J. Hydrology*, **39**, 383-386.

Chow, V.T., Maidment, D.R., and Mays, L.W., 1988: Applied Hydrology. McGraw-Hill, New York.

Ciach, G.J., and Krajewski, W.F., 1999a: On the Estimation of Radar Rainfall Error Variance. *Adv. Water Res.*, **22**, 585-595.

Ciach, G.J. and Krajewski, W.F. 1999b: Radar-raingage comparisons under observational uncertainties. *J. Appl. Meteor.*, **38**, 1519-1525.

Ciach, G.J., 2002: Local Random Errors in Tipping-Bucket Rain Gauge Measurements. *J. Atmos. Oceanic Technol.*, **20**, 752-759.

Delrieu, G., Serrar, S., Huardo, E., and Creutin, J.D., 1999: Rain measurement in hilly terrain with X-band weather radar systems: accuracy of path-integrated attenuation estimates derived from mountain returns. *J. Atmos. Oceanic Technol.*, **16**, 405-415.

Dodov, B., and Foufoula-Georgiou, E., 2005: Incorporating the spatiotemporal distribution of rainfall and basin geomorphology into nonlinear analyses of streamflow dynamics. *Adv. Water Resour.*, **28**, 711-728.

Giangrande, S.E., and Ryzhkov, A.V., 2008: Estimation of rainfall based on the results of polarimetric echo classification. *J. Appl. Meteor. Climatol.*, **47**, 2445-2462.

Goddard, J.W., Cherry, S.M., and Bringi, V.N., 1982: Comparison of dual-polarized radar measurements of rain with ground-based disdrometer measurements. *J. Appl. Meteor.*, **21**, 252-256.

Gorgucci, E., Scarchilli, G., Chandrasekar, V., and Bringi, V.N., 2000: Measurement of mean raindrop shape from polarimetric radar observations. *J. Atmos. Sci.*, **57**, 3406-3416.

Gorgucci, E., Baldini, L., and Chandrasekar, V., 2006: What is the shape of a raindrop? An answer from radar measurements. *J. Atmos. Sci.*, **63**, 3033-3044.

Gourley, J.J., Illingworth, A.J., and Tabary, P., 2009: Absolute calibration of radar reflectivity using redundancy of the polarization observations and implied constraints on drop shapes. *J. Atmos. Oceanic Technol.*, **26**, 689-703.

Gourley, J.J., Giangrande, S.E., Hong, Y., Flamig, Z., Schuur, T., and Vrugt, J., 2010: Impacts of polarimetric radar observations on hydrologic simulation. *J. Hydrometeorol.*, **11**, 781-796.

Habib, E., Krajewski, W.F., Nespor, V., and Kruger, A., 1999: Numerical simulation studies of rain gauge data correction due to wind effect. *J. Geophys. Res.*, **104**, 723–734.

Habib, E., Krajewski, W.F., and Kruger, A., 2001: Sampling errors of Tipping-Bucket Rain Gauge Measurements. *J. Hydrol. Eng.*, **6**, 159-166.

Hitschfield, W.F., 1986: The invention of radar meteorology. *Bull. Amer. Meteor. Soc.*, **67**, 33-37.

Hubbart, J.A., Kellner, E., and Freeman, G., 2013: A case study considering the comparability of mass and volumetric suspended sediment data. *Env. Earth Sci.*, **71**, 4051-4060.

Hubbert, J., and Bringi, V.N., 1995: An iterative filtering technique for the analysis of copular differential phase and dual-frequency polarimetric variables. *J. Atmos. Oceanic. Technol.*, **12**, 643-648.

Kitchen, M. and Blackall, M., 1992: Representativeness errors in comparisons between radar and gauge measurements of rainfall. *J. Hydrol.*, **134**, 13–33.

Kitchen, M. and Jackson, P.M., 1993: Weather radar performance at long range – simulated and observed. *J. Appl. Meteor.*, **32**, 975-985.

Laslett, G.M., and McBratney, A.B., 1990: Further comparison of spatial methods for predicting soil pH. *Soil Sci.*, **54**, 1553-1558.

Matrosov, S.Y., Kingsmill, D.E., Martner, B.E., and Ralph, F.M., 2005: The utility of X-band polarimetric radar for quantitative estimates of rainfall parameters. *J. Hydrometeorol.*, **6**, 248-262.

Marsalek, J., 1981: Calibration of the tipping bucket raingage. *J. Hydrology*, **53**, 343-354.

Ogden, F.L., Sharid, H.O., Senarath, S.U.S., Smith, J.A., Baeck, M.L., and Richardson, J.R., 2000: Hydrologic analysis of the Fort Collins, Colorado, flash floods of 1997. *J. Hydrol.*, **228**: 82-100.

Park, S.G., Maki, M., Iwanami, K., Bringi, V.N., and Chandrasekar, V., 2005: Correction of radar reflectivity and differential reflectivity for rain attenuation at X band. Part II: Evaluation and application. *J. Atmos. Oceanic Technol.*, **22**, 1633-1655.

Rogers, R.R., and Smith, P.L., 1996: The attenuation and radar echoes produced at centimeter wave-length by various meteorological phenomena. *Meteorological Factors in Radio-Wave Propagation*, Phys. Soc. London, 169-188.

Ryde, J.W., 1941: Echo intensities and attenuation due to clouds, rain, hail, sand and dust storms. *Rep. No. 7831*. General Electric Co. Ltd. Res. Lab., Wembley. pp. 48.

Ryzhkov, A.V., Giangrande, S., and Schurr, T., 2003: Rainfall measurements with the polarimetric WSR-88D radar. National Severe Storms Laboratory Rep. Norman: OK, 98 pg.

Ryzhkov, A.V., Pinsky, M., Pokrovsky, A., and Khain, A., 2011: Polarimetric radar observation operator for a cloud model with spectral microphysics. *J. Appl. Meteor. Climatol.*, **50**, 873-894.

Ryzhkov, A.V., Kumjian, M.R., Ganson, S.M., and Khain, A., 2013: Polarimetric radar characteristics of melting hail. Part I: Theoretical simulations using spectral microphysical modeling. *J. Appl. Meteor. Climatol.*, **52**, 2849-2870.

Sevruk, B., 1982: Methods of correction for systematic error in point precipitation measurement for operation use. *Operational Hydrology Report No. 21, WMO*, 589, pp. 91.

Sevruk, B., and Harmon, W.R., 1984: International Comparison of National Precipitation Gauges with a Reference Pit Gauge, Instruments and Observing Methods. *Rep. No. 17*, WMO, Geneva.

Shah, S.M.S., O'Connell, P.E., and Hosking, J.R.M., 1996: Modelling the effects of spatial variability in rainfall on catchment response. 1. Formulation and calibration of a stochastic rainfall field and model. *J. Hydrol.*, **175**, 67-88.

Simpson, M.J., Hubbart, J.A., and Fox, N.I., 2016: Ground truthed performance of single and dual-polarized radar rain rates at large ranges. *Hydrol. Process.*, **30**, 3692-3703.

Smith, J.A., Seo, D.J., Baeck, M.L., and Hudlow, M.D., 1996: An intercomparison study of NEXRAD precipitation estimates. *Water Resour. Res.*, **32**, 2035-2045.

Smith, M., Koren, V., Zhang, Z., Reed, S., Pan, J., and Moreda, F., 2004: Runoff response to spatial variability in precipitation: An analysis of observed data. *J. Hydrol.*, **298**, 267-286.

Sun, X., Mein, R.G., Keenan, T.D., and Elliot, J.F., 2000: Flood estimation using radar and raingauge data. *J. Hydrol.*, **239**, 4-18.

Tabios, G.Q., and Sala, J.D., 1985: A comparative analysis of techniques for spatial interpolation of precipitation. *Water Resources Bull.*, **21**, 365-380.

Vieux, B.E., Cui, Z., and Guar, A., 2004: Evaluation of a physics-based distributed hydrologic model for flood forecasting. *J. Hydrol.*, **298**, 155-177.

Vieux, B.E., Bedient, P.B., and Mazroi, E., 2005: Real-time urban runoff simulation using radar rainfall and phsyics-based distributed modeling for site-specific forecasts. *10th Int. Conf. on Urban Drainage, Copenhagen, Denmark*, 1-3.

Vieux, B.E., and Vieux, J.E., 2006: Continuous distributed modeling for evaluation of stormwater quality impacts from urban development. *Computational Hydraulics Internation, Toronto, Canada*.

Villarini, G., and Krajewski, W.F., 2010: Review of the different sources of uncertainty in single polarization radar-based estimates of rainfall. *Surv. Geophys.*, **31**: 107-129.

Wang, Y., and Chandrasekar, V., 2009: Algorithm for estimation of the specific differential phase. *J. Atmos. Oceanic Technol.*, **12**, 643-648.

Weber, D.D., and Englund, E.J., 1994: Evaluation and comparison of spatial interpolators, II. *Math Geology*, **24**, 381-391.

Whiton, R.C., Smith, P.L., Bigler, S.G., Wilk, K.E., and Harbuck, A.C., 1998: History of operational use of weather radar by U.S. Weather services. Part I: The pre-NEXRAD era. *Wea. Forecast.*, **13**, 219-243.

Whiton, R.C., Smith, P.L., Bigler, S.G., Wilk, K.E., and Harbuck, A.C., 1998: History of operartional use of weather radar by U.S. Weather services. Part II: Development of operational Doppler weather radars. *Wea. Forecast.*, **13**, 244-252.

Williams, C.R., Gage, K.S., Clark, W., and Kucera, P., 2005: Monitoring the reflectivity calibration of a scanning radar using a profiling radar and a disdrometer. *J. Atmos. Oceanic Technol.*, **22**, 1004-1018.

Yates, D.N., Warner, T.T., and Leavesley, G.H., 2000: Prediction of a flash flood in complex terrain. Part II: A comparison of flood discharge simulation using rainfall input from a radar, a dynamic model, and an automated algorithmic system. *J. Appl. Meteor.*, **39**, 815-825.

Yu, B., Ciesiolka, C.A.A., Rose, C.W., and Coughlan, K.J., 1997: A note on sampling errors in the rainfall and runoff data collected using tipping bucket technology. *Trans. ASAE*, **40**, 1305-1309.

Yu, B., Chen, X., Li, L., Bao, A., and Jean de la Paix, M., 2011: Streamflow simulation by SWAT using different precipitation sources in large arid basins with scares raingauges. *Ware Resour. Manage.*, **25**, 2669-2681.

Zhang, G., Vivekanandan, J., and Brandes, E.A., 2001: A method for estimating rain rate and drop size distribution from polarimetric radar measurements. *IEEE Trans. Geosci. Remote Sens.*, **39**, 830-841.

Zimmerman, D.L., Pavlik, C., Ruggles, A., and Armstrong, M., 1999: Experimental comparison of ordinary and universal Krigin and inverse distance weighting. *Math Geology*, **31**, 375-390.

CHAPTER V

CONCLUSIONS AND SYNTHESIS

Summary

Though radar meteorology has existed since the 1950's, it has not only been since the turn of the 21st century and, in particular, through the technology of dual-polarization, that quantitative precipitation estimates have become an extensively studied field. Many researchers have found that the addition of dual-polarization variables significantly improve rain rate estimates (Hogan, 2007; Giangrande and Ryzhkov, 2008; Cifelli et al., 2011) through advantages in echo classification (e.g., Straka et al., 2000; Gourley et al., 2007; Dolan and Rutledge, 2009), identifying and characterizing the microphysical processes in precipitation and clouds (e.g., Gorgucci et al., 2000, 2006; Cifelli et al., 2002; Medina and Houze, 2003), and better estimates of the drop size distribution and its evolution in storms (e.g., Waldvogel, 1974; Atlas et al., 1999; Zhang et al., 2001; Bringi et al., 2003; Brandes et al., 2004; Anagnostou et al., 2008). Therefore, its application is far reaching in the realms of hydrometeorology, yet some authors have argued its implementation to hydrological studies is not as extensive as one could expect (e.g., Berne and Krajewski, 2013).

The current research reviews the strengths and limitations of the current state of dual-polarization technology in chapter 1. Furthermore, it is discussed that although many studies have focused on radar rainfall rates, few have rigorously assessed the effects range have on QPE's (e.g., Smith et al., 1993; Kitchen and Jackson 1996). Furthermore, these studies are even fewer for analyzing the question as to whether dual-

polarized technology is superior to the conventional rain rate equation (i.e., only using reflectivity) at extended ranges (e.g., Ryzhkov et al., 2003, 2005).

X-band dual-polarimetric radars have been proposed to be a cost-effective alternative to the bulkier and permanent S-band WSR-88D's (Chandrasekar et al., 2004; McLaughlin et al., 2009). Also, many authors have reported good results in rain rate estimates from X-band, particularly through the utilization of the specific differential phase shift (KDP) (e.g., Wang and Chandrasekar, 2010; Matrosov et al., 2002; Matrosov, 2010; Koffi et al., 2014). However, it is noted that the literature is still lacking as to whether the performance of X-band radars do, in fact, provide superiority over S-band radars, especially at larger ranges; the majority of studies assess the overall performance of X-band radars without comparing to S-band counterparts.

Hydrologic simulations require accurate and high-resolution datasets, both spatially and temporally, to capture the rapid evolution of storms (Gourley et al., 2010). Weather radars provide a solution to this data inquiry, in which many researchers have found conflicting results as to the performance (or lack thereof) single- and dual-polarization radar QPE's for hydrologic simulations (Yates et al., 2000; Ogden et al., 2000; Vieux et al., 2005; Gourley et al., 2010; Vieux and Imgarten, 2012; Looper and Vieux, 2013). Furthermore, it has been discussed that from experiments including the Distributed Model Intercomparison Project, or DMIP (Reed et al., 2004), lumped models still tend to outperform distributed models (Berne and Krajewski, 2013). Based on these results, it was noted that few studies have determined whether the error from hydrologic simulations while utilizing QPE's from radar are moreso due to the model, or the uncertainties in radar rainfall, overall.

Based on the discussion, this dissertation was divided into three chapters to address the overall objectives:

Objective 1: Determine the relative error in using Kansas City (KEAX) and St. Louis (KLSX) radars on localized rain rates using ground-truthed tipping buckets within the state of Missouri.

Objective 2: Analyze whether the implementation of a dual-polarized X-band radar within Columbia MO will be better at estimating rainfall rates as opposed to KEAX and/or KLSX.

Objective 3: Model streamflow in the Hinkson Creek Watershed using a physically based hydrologic model, Vflo, to determine comparisons between observed streamflow and precipitation-gauge, X-band, and S-band radar rainfall data.

Objectives 1, 2, and 3 were assessed through chapters 2, 3, and 4, accordingly. The main results from each of the objectives are detailed below.

Objective 1: Determine the relative error in using Kansas City (KEAX) and St. Louis (KLSX) radars on localized rain rates using ground-truthed tipping buckets within the state of Missouri.

Objective 1 was conducted through three sub-sections in chapter 2. This first of which analyzed the QPE performance of three separate radars, St. Louis (KLSX), Kansas City (KEAX), and Springfield (KSGF), MO. Over 1000 hours were assessed, with 15 terrestrial-based precipitation gauges utilized, of which 8, 9, and 5 of the gauges were

ground-truthed by QPE's from KLSX, KEAX, and KSGF, respectively. Over 50 dual-polarized rain rate algorithms were tested, including combinations of R(Z), R(Z,ZDR), R(KDP), and R(ZDR,KDP).

Results indicate that the majority of precipitation errors were due to false precipitation echoes, the maximum of which (60%) were from gauges furthest from the radar, while up to 20% of the error were due to precipitation missed by the radar. In general, an NSSL R(Z,ZDR) algorithm performed the best, while a similar NSSL equation utilizing KDP and ZDR (i.e., R(ZDR,KDP)) typically performed the worst, particularly at large ranges. These results contradict those found by Ryzhkov et al. (2003, 2005) such that equations containing KDP tend to perform better at large ranges, due to the fact the variable is immune to radar calibration issues, beam blockage, and does not degrade in quality with range (Zrnic and Ryzhkov, 1996, 1999).

The data were separated into warm and cool seasons, and was found that the cool season tend to perform better in terms of correlation coefficient values than the warm season for KEAX and KSGF, but not KLSX. The largest R^2 value when utilizing the radar's best-performing equation (based on bias, mean absolute error, and normalized standard error values) was 0.36 for the warm season QPE's analyzed by KLSX, with the lowest value being the warm season KEAX and KSGF (0.25). Therefore, the quality of rain rate estimates from the radars were not only a function of the particular algorithm, but distance, and seasonality. The superiority of one radar over the other was inconclusive, as the statistics at similar distances from KLSX and KEAX were different, including combinations of KLSX and KSGF, and KEAX and KSGF.

More hours could be analyzed to provide a more robust dataset. Similarly, the warm and cool season definitions may need to be changed, or perhaps dynamically controlled. For example, December of 2015 exhibited many convective storms, unrepresentative of winter-time precipitation, thus rendering the month to be more akin to summer-time precipitation. This theory displays the importance of incorporating vertical profiles of temperature, such that cool and warm season precipitation can be correctly classified and, furthermore, the melting layer may be identified and quality controlled for.

The second and third part of chapter 2 analyzed the performance of one years' worth of WSR-88D QPE's from KLSX and KEAX from four areal-averaged precipitation gauges in Boone County (140 km from KLSX, and 170 km from KEAX). The second section of chapter 2 assessed the data overall, whereas the third section analyzed the same dataset, separated into seasons (warm and cool).

Similar to chapter 2, the NSSL R(Z,ZDR) algorithm performed best in terms of fewest false alarms, overall. However, the conventional R(Z)-Convective equation recorded the lowest mean absolute error (1.5 and 1.6 mm) while simultaneously predicting the greatest number of hits (213 and 176) and fewest number of misses (272 and 309) for KLSX and KEAX, respectively. However, when only the number of hits were assessed, statistically, the R(Z,ZDR) recorded the lowest MAE for KLSX (6.7) and KEAX (9.5). Additionally, the R(Z,ZDR) algorithm registered the least amount of overall precipitation error (969.6 and 1295.3 mm for KLSX and KEAX, accordingly).

In general, being further from the study area, the KEAX radar performed worse than the St. Louis radar. Mean absolute error and normalized standard error values were, typically, 0.2 mm and 30% larger, with the number of hits (misses) being, approximately,

20% less (more). The superiority of the algorithms containing KDP in terms of false alarm detection was apparent, as the values were minimal (i.e., less than 20) between the two radars, in spite of the equations performing the worst, overall for both radars.

Interestingly, the cool season statistics tend to outperform the warm season statistics for both KLSX and KEAX, as outlined in the third section of chapter 2. Furthermore, the MAE and NSE values were less, particularly for non-KDP containing algorithms. The statistics were also recalculated for instances of hits, only, and found that the MAE for the warm season was higher as well, particularly due to the errors inherent in the tipping buckets at relatively high rain rates. Without instances of misses or false alarms, R^2 values were as large as 0.54 for KLSX during the warm season, but increased to 0.66 for the cool season. These errors are due, primarily, to the fact that the cool season precipitation amounts are much less than the summertime.

Objective 2: Analyze whether the implementation of a dual-polarized X-band radar within Columbia MO will be better at estimating rainfall rates as opposed to KEAX and/or KLSX.

The third chapter assessed the performance of an X-band dual-polarimetric radar (MZZU) which was installed during the fall of 2015. chapter 3 analyzed the overall performance of the radar through two years' worth of data, ranging from August 2015 to August 2017. Four gauges served as ground truth, ranging from 30, to 45, 75, and 80 km from the radar. It was discovered that algorithms containing differential reflectivity, R(Z,ZDR) and R(ZDR,KDP) were superior in QPE's compared to the conventional R(Z) equation in addition to an R(KDP) algorithm. This was evidenced such that they

contained the lowest MAE values at each of the four gauges, and were the only algorithms which recorded NSE values below 100%.

The superiority of the ZDR-containing algorithms is attributed to the capability of the variable, ZDR, to accurately represent precipitation shape and, thus, scale the rain rate to an appropriate value. This shows the importance of utilizing a proper rain rate equation to each radar, as the R(KDP) equation registered as much as 65% error due to false alarms, alone, whereas R(Z,ZDR) and R(ZDR,KDP) registered as little as 15%.

Future work includes the implementation of a radar-derived algorithm specifically for MZZU. Additionally, seasonal analyses will be conducted, similar to the second and third sections of Chapter 2, to determine the performance of the radar between the warm and cool seasons.

The second section of chapter 3 compared the performance of MZZU to KLSX and KEAX QPE's at the same four gauges analyzed in the first part of chapter 3, including the areal-averaged gauges near MZZU. For this study, only one years' worth of data were analyzed between the three radars. It was found that the rain rates analyzed by MZZU were significantly ($p < 0.10$) better than either KLSX or KEAX at the areal-averaged Boone County gauges. Beyond the closest gauges to MZZU (i.e., beyond 5 km), the R(Z) equation, typically, dominated in terms of lowest overall bias, and lowest MAE and NSE, although followed closely by the R(Z,ZDR) equation. Unlike in chapter the first part of 3, the R(ZDR,KDP) equation typically performed the worst of the algorithms analyzed by MZZU, with similar errors to the R(KDP) equation. The reason for this discrepancy in performance between the two sections in chapter 3 is unresolved, but is being conducted.

Similar to most rain rate studies, the number of hits decreased while the number misses and false alarms decreased as range from the radar increased. However, the closest gauge analyzed by KEAX (Versailles, 130 km) displayed the lowest overall false precipitation amount (FPA, 31.9 mm) and overall total precipitation error (450 mm). The superiority in rain rate estimates by the KEAX radar was also observed in Simpson et al. (2016), such that, in spite of KEAX being further from Boone than KLSX (by approximately 30 km), performed better. Therefore, not only is algorithm preference important in QPE's, but the particular radar may serve an advantage, even if it is further from the region of study.

Objective 3: Model streamflow in the Hinkson Creek Watershed using a physically based hydrologic model, Vflo, to determine comparisons between observed streamflow and precipitation-gauge, X-band, and S-band radar rainfall data.

The fourth and final chapter of data analyses of this dissertation compared the performance of hydrologic simulations based on the input of precipitation data. The MZZU R(Z) and R(Z,ZDR) equations, KLSX digital precipitation rate (DPR), and areal-averaged tipping buckets were utilized as precipitation input to a physically-based hydrologic model, Vflo (Vieux et al., 2004). Two months' of data were analyzed, including July and December of 2015.

Similar to the discussion present in Berne and Krajewski (2013), the superiority of one input of precipitation to the other was nebulous, with the exception of the precipitation gauges. It was shown that the gauges frequently missed the precipitation that occurred (July 06 – 09), or over-averaged the precipitation (July 03). In terms of the

performance of the radar's, KLSX matched the timing of the peak flow, but typically had a larger magnitude. Conversely, the MZZU radar produced similar magnitudes to the peak flows, but the timing was delayed either due to attenuation of the radar signal, or significant radome wetting which resulted in a complete loss of signal.

The most important factors within the hydrologic simulations were not only the input of precipitation, but also the antecedent soil moisture conditions. It was found that not only did this impact the magnitude of peak flow, but also the timing. Therefore, it is theorized that hydrologic models must incorporate this variable before accurate, long-term simulations are deemed accurate. At the current state of analyses, only simulations ran through a few days provide accurate hydrographs, as the hydrologic model is incapable of inputting extreme heating days (i.e., drying of soil rapidly), or other conditions that effect runoff and infiltration.

Literature cited

Anagnostou, M.N., Anagnostou, E.N., Vulpani, G., Montopoli, M., Marzano, F.S., and Vivekanandan, J., 2008: Evaluation of X-band polarimetric-radar estimates of drop-size distribution from coincident S-band polarimetric estimates and measured raindrop spectra. *IEEE Trans. Geosci. Remote Sens.*, **46**, 3067-3075.

Atlas, D., Ulbrich, C.W., Marks Jr., F.D., Amitai, E., and Williams, C.R., 1999: Systematic variation of drop size and radar-rainfall relations. *J. Geophys. Res*., **104**, 6155–6169.

Berne, A., and Krajewski, W.F., 2013: Radar for hydrology: Unfulfilled promise or unrecognized potential? *Adv. Water Resour.*, **51**, 357-366.

Brandes, E.A., Zhang, G., and Vivekanandan, J., 2004: Drop size distribution retrieval with polarimetric radar: model and application. *J. Appl. Meteor.*, **43**, 461-475.

Bringi, V.N., Chandrasekar, V., Hubbert, J., Gorgucci, E., Randeu, W., and Schoenhuber, M., 2003: Raindrop size Distribution in Different Climate Regimes from Disdrometer and Dual-Polarized Radar Analysis. *J. Atmos. Sci.,* **60,** 354–365.

Chandrasekar, V., Lim, S., Bharadwaj, N., Li, W., McLaughlin, D., Bringi, V.N., and Gorgucci, E., 2004: Principles of networked weather radar operation at attenuation frequencies. *Proc. Third European Conf. on Radar Meteorology, Visby, Sweden*, ERAD, 109-114.

Dolan, B., and Rutledge, S.A., 2009: A theory-based hydrometeor identification algorithm for X-band polarimetric radars. *J. Atmos. Oceanic Technol.*, **26**, 2071-2088.

Cifelli, R., Petersen, W.A., Carey, L.D., Rutledge, S.A., and Dias, M.A.F.D., 2002: Radar observations of the kinematic, microphysical, and precipitation characteristics of two MCSs in TRMM LBA. *J. Geophys. Res.*, **107**, 8077.

Cifelli, R., Chandrasekar, V., Lim, S., Kennedy, P.C., Wang, Y., and Rutledge, S.A., 2010: A new dual-polarization radar rainfall algorithm: Application in Colorado precipitation events. *J. Atmos. Oceanic Tech.*, **28**: 352-364.

Giangrande, S.E. and Ryzhkov, A.V., 2008: Estimation of rainfall based on the results of polarimetric echo classification. *J. Appl. Meteor*., **47**, 2445-2460.

Gorgucci, E., Scarschilli, G., Chandrasekar, V., and Bringi, V.N., 2000: Measurement of mean raindrop shape from polarimetric radar observations. *J. Atmos. Sci.*, **57**, 3406-3413.

Gorgucci, E., Baldini, L., and Chandrasekar, V., 2006: What is the shape of a raindrop? An answer from radar measurements. *J. Atmos. Sci.*, **63**, 3033-3044.

Gourley, J.J., Tabary, P., and Parent-du Chatelet, J., 2007: A fuzzy logic algorithm for the separation of precipitation from nonprecipitating echoes using polarimetric radar observations. *J. Atmos. Oceanic Technol.*, **24**, 1439-1451.

Gourley, J.J., Giangrande, S.E., Hong, Y., Flamig, Z., Schuur, T., and Vrugt, J., 2010: Impacts of polarimetric radar observations on hydrologic simulation. *J. Hydrometeorol.*, **11**, 781-796.

Hogan, R.J., 2007: A variational scheme for retrieving rainfall rate and hail reflectivity fraction from polarization radar. *J. Appl. Meteorol. Climate*, **46**, 1544-1564.

Kitchen, M. and Jackson, P.M., 1993: Weather radar performance at long range – simulated and observed. *J. Appl. Meteor.*, **32**, 975-985.

Koffi, A.K., Gosset, M., Zahiri, E.P., Ochou, A.D., Kacou, M., Cazenave, F., and Assamoi, P., 2014: Evaluation of X-band polarimetric radar estimation of rainfall and rain drop size distribution parameters in West Africa. *Atmos. Res.*, **143**, 438-461.

Looper, J.P., and Vieux, B.E., 2013: Distributed hydrologic forecast reliability using Next-Generation radar. *J. Hydrol. Eng.*, **18**, 260-268.

Matrosov, S.Y., Clark, K.A., Martner, B.E., and Tokay, A., 2002: X-band polarimetric radar measurements of rainfall. *J. Appl. Meteor.*, **41**, 941-952.

Matrosov, S.Y, 2010: Evaluating polarimetric X-band radar rainfall estimators during HMT. *J. Atmos. Oceanic Technol.*, **27**, 122-134.

McLaughlin, D., and Coauthorrs, 2009: Short-wavelength technology and the potential for distributed networks of small radar systems. *Bull. Amer. Meteor. Soc.*, **90**, 1797-1817.

Medina, S., and Houze, R.A., 2003: Air motions and precipitation growth in alpine storms. *Quart. J. Roy. Meteorol. Soc.*, **129**, http://dx.doi.org/10.1029/2000JD000264.

Ogden, H.L., Sharif, H.O., Senarath, S.U.S., Smith, J.A., Baeck, M.L., and Richardson, J.R., 2000: Hydrologic analysis of the Fort Collins, Colorado, flash flood of 1997. *J. Hydrol.*, **228**, 82-100.

Reed, S., and Coauthors, 2004: Overall distributed model intercomparison project results. *J. hydrol.*, **298**, 27-60.

Ryzhkov, A.V., Giangrande, S., and Schurr, T., 2003: Rainfall measurements with the polarimetric WSR-88D radar. National Severe Storms Laboratory Rep. Norman: OK, 98 pg.

Ryzhkov, A.V., Giangrande, S., and Schurr, T., 2005: Rainfall estimation with a polarimetric prototype of WSR-88D. *J. Appl. Meteor.*, **44**, 502–515.

Simpson, M.J., Hubbart, J.A., and Fox, N.I., 2016: Ground truthed performance of single and dual-polarized radar rain rates at large ranges. *Hydrol. Process.*, **30**, 3692-3703.

Smith, J.A., Seo, D.J., Baeck, M.L., and Hudlow, M.D., 1996: An Intercomparison Study of NEXRAD Precipitation Estimates. *Water Resour. Res.*, **32**, 2035-2045.

Straka, J.M., Zrnic, D.S., and Ryzhkov, A.V., 2000: Bulk hydrometeor classification and quantification using polarimetric radar data: Synthesis of relations. *J. Appl. Meteorol.*, **39**, 1341-1272.

Vieux, B.E., Cui, Z., and Guar, A., 2004: Evaluation of a physics-based distributed hydrologic model for flood forecasting. *J. Hydrol.*, **298**, 155-177.

Vieux, B.E., Bedient, P.B., and Mazroi, E., 2005: Real-time urban runoff simulation using radar rainfall and phsyics-based distributed modeling for site-specific forecasts. *10th Int. Conf. on Urban Drainage, Copenhagen, Denmark*, 1-3.

Vieux, B.E., and Imgarten, J.M., 2012: On the scale-dependent propagation of hydrologic uncertainty using high-resolution radar rainfall estimates. *Atmos. Res.*, **103**, 96-105.

Waldvogel, A., 1974: The N_0 jump of raindrop spectra. *J. Atmos. Sci.*, **31**, 1067-1078.

Wang, Y., and Chandrasekar, V., 2010: Quantitative precipitation estimation in the CASA X-band dual-polarization radar network. *J. Atmos. Oceanic Tech.*, **27**: 1665-1676.

Yates, D.N., Warner, T.T., and Leavesley, G.H., 2000: Prediction of a flash flood in complex terrain. Part II: A comparison of flood discharge simulation using rainfall input from a radar, a dynamic model, and an automated algorithmic system. *J. Appl. Meteor.*, **39**, 815-825.

Zhang, G., Vivekanandan, J., and Brandes, E.A., 2001: A method for estimating rain rate and drop size distribution from polarimetric radar measurements. *IEEE Trans. Geosci. Remote Sens.*, **39**, 830-841.

Zrnic, D.S., and Ryzhkov, A.V., 1996: Advantages of rain measurements using specific differential phase. *J. Atmos. Oceanic Tech.*, **13**, 454-464.

Zrnic, D.S., and Ryzhkov, A.V., 1999: Polarimetry for weather surveillance radars. *Bull. Amer. Meteor. Soc.*, **80**, 389-406.

VITA

Micheal Simpson was born in Rochester, NY and attended the Monroe Community College for two years, receiving Associate's credits. In the Fall of 2008, he was accepted into the Atmospheric Science program at the State University of New York – The College at Brockport until he graduated in the Spring of 2012.

Thereafter, he was accepted as a Master's student at the University of Missouri for meteorology, under guidance from Dr. Patrick Market. His thesis was entitled "A new method of calculating vertical motion in isentropic space". He successfully defended his thesis and received his M.S. in 2014.

In the spring of 2015, Micheal was awarded a Graduate Research Assistantship (GRA) via the Missouri Experimental Project to Stimulate Competitive Research (EPSCoR), an NSF funded program where he analyzed radar data from a newly installed X-band dual-polarimetric radar, which comprised the bulk of his dissertation which was successfully defended in the fall of 2017.

Micheal currently works at the Cooperative Institute for Mesoscale Meteorological Studies (CIMMS) and the National Severe Storms Laboratory at the University of Oklahoma, improving quantitative precipitation estimates from the Multi-Radar Multi-Sensor (MRMS) system.